



Dipl.-Ing. Lukas Tribuser, BSc.

Synthesis of Fluoroionophores and its Application for Optical Ion Sensors

Dissertation

Zur Erlangung des akademischen Grades

Doktor der technischen Wissenschaften

eingereicht an der

Technischen Universität Graz

Betreuer:

Univ.-Prof. Dipl.-Chem. Dr.rer.nat. Ingo Klimant

Institut für Analytische Chemie und Lebensmittelchemie

Graz, 2. Juni 2020

**“Man merkt nie,
was schon getan wurde;
man sieht immer nur das,
was noch zu tun bleibt.”**

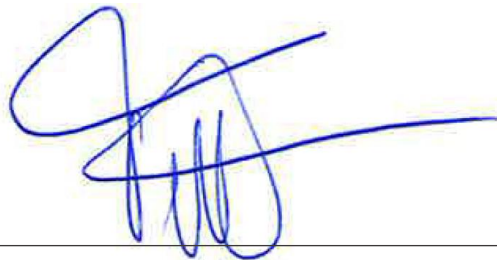
Marie Curie

Eidesstattliche Erklärung

Ich erkläre an Eides statt, dass ich die vorliegende Arbeit selbstständig verfasst, andere als die angegebenen Quellen / Hilfsmittel nicht benutzt, und die den benutzten Quellen wörtlich und inhaltlich entnommenen Stellen als solche kenntlich gemacht habe. Das im TUGrazonline hochgeladene Textdokument ist mit der vorliegenden Dissertation identisch.

2. Juni 2020

Datum



Unterschrift

Statutory Declaration

I declare that I have authored this thesis independently, that I have not used other than the declared sources / resources, and that I have explicitly marked all material which has been quoted either literally or by content from the used sources.

2 June 2020

Date



Signature

Danksagung

Es ist jetzt wirklich passiert, ich bin fertig. Jetzt, wo alles niedergeschrieben ist will ich mich natürlich noch bei einigen Leuten bedanken, nicht nur weil sie mich durch mein Studium begleitet haben, sondern auch bei einigen ohne die dieses Studium gar nicht möglich gewesen wäre. Durch eure Unterstützung wäre ich niemals so erfolgreich und weit gekommen. Ihr habt mich geformt, gepusht, motiviert, aber auch von meinem hohen Ross runtergeholt (wenn nötig) und in schwierigen Zeiten wieder aufgebaut. Durch euren Einsatz konnte ich meine Ziele weiterverfolgen. Ihr seid der Grund warum ich mich mit großer Freude bedanken möchte, denn ohne euch wären mir viele Türen verschlossen geblieben.

Danke Ingo, ohne deine Unterstützung, lehrreichen Diskussionen, Besprechungen sowie Ideen könnte ich jetzt nicht mit so einem guten Gefühl in die Arbeitswelt „entlassen“ werden. Danke, dass ich während meines Studiums genügend Freiheiten hatte, meine eigenen Ideen zu verwirklichen und zahlreiche Ideen im Labor umsetzen zu dürfen.

Danke Sergey, ohne deinem Know-how wären so manche Sachen noch unvollständig in irgendeinem Kasten im Labor. Deine Unterstützung während meiner Zeit am Institut kann man vermutlich nicht mit Gold aufwiegen. Ich weiß dein Engagement sehr zu schätzen.

Auch möchte ich mich bei meiner Studien-Gang den Dumpfbacken bedanken. Mit euch konnte ich die Zeit auf der Uni so richtig genießen. Nicht nur da wir gemeinsam unsere Lehrveranstaltungen etc. gemeinsam bewältigt haben, sondern auch die gemütlichen Bierlis und Gespräche abseits des Uni-Alltags. Alle Dumpfis die diesen Text bis hierhin lesen werden sich vermutlich gerade denken was das wieder für ein „Schaß“ ist was da Luki da schreibt und ihr habt auch ein wenig recht, den jetzt kommt erst das wichtigste: Ich glaube, da wir auch jetzt nach unseren abgeschlossenen Studien noch nahezu wöchentlich auf einem Grätzel zusammen picken und Sachen unternehmen, ist vermutlich Beweis genug warum ihr einer der größten Stützpfiler meines Lebens seid. Danke Leitls.

An dieser Stelle möchte ich mich auch bei meiner Freundin Nici bedanken. Du hast dir während der letzten Jahre so einiges mit mir miterleben müssen. Denn nicht immer ist alles Gold was glänzt und du musstest dir nach so manch harten Labortagen einiges von mir anhören. Danke, dass du mir immer wieder Mut gibst und mich weiter motivierst meine (sowie auch unsere) Ziele zu verfolgen. Die letzten Wochen waren ja eine wirkliche Herausforderung für uns beide. Aber wenn ich so zurückdenke, war es das gar nicht, denn jeder Tag an deiner Seite ist eine Bereicherung für mich und ich freue mich schon auf

unseren weiteren Weg. Danke das du mir jeden Tag das Gefühl gibst alles erreichen zu können, du bist mein Motor.

Danke Sandi, ich bin dankbar dich nicht nur meinen Bürokollegen, sondern auch sehr guten Freund nennen zu dürfen. Die unzähligen Gespräche im Büro, sowie den Spaß und Blödsinn den wir während unserer gemeinsamen Zeit auf der Uni erlebt haben, weiß ich sehr zu schätzen. Danke. Auch möchte ich mich bei David und Tobi bedanken, ihr habt mir gezeigt, dass es wichtigere Dinge im Leben gibt, als so manch „Problemchen“ die während meiner Zeit auf der Uni aufgetaucht sind. Euer offenes Ohr, war und ist Balsam für die Seele.

Liebes gesamtes ACFC-Institut, es ist soweit, jetzt wird es ruhig am Institut. Danke, dass ich Teil des Besten Institutes sein durfte. Die zahlreichen Jahre mit euch konnte ich sehr genießen und ich werde die Zeit mit euch sicher vermissen. Danke, dass ich Teil dieses Teams sein durfte, jedoch ist es jetzt Zeit meine Koffer zu packen und weiter zu ziehen, aber man trifft sich ja zum Glück immer öfter im Leben.

Danke Mama und Papa. Ohne euch wäre ich erst recht nicht, wo ich jetzt bin. Durch eure Unterstützung wurde mir das alles erst ermöglicht und die Dankbarkeit die ich in mir trage kann ich vermutlich gar nicht in Worte fassen. Ihr könnt stolz sein. Auch bei meinen Brüdern möchte ich auch auf diesem Wege danken, ohne eure Unterstützung wäre mein Studium um einiges beschwerlicher gewesen.

Diese Arbeit widme ich meiner Familie und meiner Freundin Nici.

Abstract

In this thesis, novel ion sensors for cation sensing are presented. The sensors are based on fluoroionophores, which change their fluorescence intensity through analyte interactions due to the photo-induced electron transfer (PET). Such indicators consist of a receptor unit and a chromophore core, whereas the receptor acts as a host for target cations and the chromophore converts the information into measurable optical properties. Since both building blocks can be modified independently, this concept represents a modular strategy for the design of new ion sensors. Via immobilization of the indicators in water swellable polymers continuous and time-resolved measurements are systematically achieved.

In the first part a K^+ -selective fluoroionophore is used to investigate the influence of the polymer matrix on the sensing properties. The effects of polymer nature on the sensing characteristics like stability, sensitivity, fluorescence brightness and response time are investigated. A drastic increase in sensitivity upon addition of negatively-charged aliphatic sulfonates within the sensing layer ($K_d < 3$ mM) is achieved. Modification of a commercially available polyurethane hydrogel with sulfonate groups enables preparation of stable sensors with improved binding ability (K_d 11.1 mM).

The second part describes a new sensing strategy for amines using a NH_4^+ -selective fluoroionophore, fluorescein and an inorganic phosphor-reference is presented. The combination of both indicators enables the quantification of NH_3 and the determination of substituted amines. Comparison of spectral measurements with kinetic measurements revealed an accuracy of 94.3 ± 5.4 % for fluorescein and 98.1 ± 1.2 % for the fluoroionophore.

The third part is focused on the application of ion sensors for whole blood measurements. The center of attention for this work was on tackling the challenges for applying ion sensors for diagnostic applications. An improved DLR sensing system using fluoroionophores and phosphorescent reference particles is developed.

The last part contains the synthesis of new calcium indicators using BODIPY fluorophores. This study is mainly dedicated to the challenges of the behavior of charged fluoroionophores in solvents for Ca^{2+} sensing. Five new calcium fluoroionophores were successfully synthesized in their protected ester forms and their photophysical properties were analytically characterized. The behavior of the fluoroionophores was intensively studied in respect to their dependency of pH and the amount of organic solvent used for measurements.

Kurzfassung

Im Rahmen dieser Arbeit werden neuartige Sensoren für Kationenmessungen präsentiert. Diese Sensoren bestehen aus sogenannten Fluoroionophoren, welche ihre Fluoreszenzintensität aufgrund des Photoinduzierten Elektronen Transfers (PET) ändern. Solche Indikatoren bestehen aus einem Rezeptorteil und einem Farbstoffgrundgerüst, wobei der Rezeptorbaustein als Komplexierungseinheit für Kationen dient und der Farbstoff die Information als optische Eigenschaft wiedergibt. Dieses Sensorkonzept repräsentiert ein modulares System für die Entwicklung von Ionensensoren, da die beiden Bausteine (Rezeptor und Farbstoff) unabhängig voneinander synthetisiert und modifiziert werden können. Durch die gezielte Immobilisierung der Indikatoren in wasser-quellbare Polymere, sind zeitaufgelöste und kontinuierliche Messungen von Ionen möglich.

Im ersten Teil der Dissertation wird ein K^+ sensitives Fluoroionophor verwendet, um die Eigenschaften in verschiedenen Polymermatrizen zu untersuchen. Diese Studie verbindet die Polymerstruktur mit den Sensoreigenschaften wie zum Beispiel Stabilität, Sensitivität und Fluoreszenz-Helligkeit. Die Verwendung von negativen geladenen, aliphatischen Zusatzstoffen resultiert in einer deutlichen Absenkung der Dissoziationskonstante ($K_d < 3 \text{ mM}$). Die Anbringung von Sulfonatgruppen in einem Hydrogel resultiert in stabilen, reversiblen Sensoren mit verbesserten Bindungsstabilitäten ($K_d 11,1 \text{ mM}$).

Der zweite Teil beschreibt eine Messtechnik für Amine unter der Verwendung eines NH_4^+ -selektiven Fluoroionophores, Fluoreszein und einer Referenz (anorganischer Phosphor). Die Kombination beider Indikatoren ermöglicht die Quantifizierung von NH_3 sowie die Detektion von substituierten Aminen, mit einer Genauigkeit von $94.3 \pm 5.4 \%$ für das Fluoroionophore und für $98.1 \pm 1.2 \%$ Fluoreszein.

Der dritte Teil konzentriert sich auf die Applikation von Ionensensoren für die Blutanalytik. Das Hauptaugenmerk besteht darin, die Sensoren in Bezug auf ihre Sensitivität zu verbessern und ein Sensorsystem zu entwickeln welches für die medizinische Diagnostik verwendet werden kann. Ein DLR Sensorsystem mit immobilisiertem Fluoroionophor und einer Referenz wurde entwickelt und untersucht.

Der letzte Teil befasst sich mit der Synthese von Calcium Indikatoren. Es wurden fünf verschiedene Fluoroionophore hergestellt und auf ihre photophysikalischen Eigenschaften untersucht. Zusätzlich wurde das Verhalten in Lösung und die Abhängigkeit des pH-Wertes überprüft.

Content

Content.....	xiii
1. Scope and Outline of the Thesis.....	3
2. Theoretical background.....	5
2.1. Physiological Role of Ions in the human body.....	5
2.1.1. Sodium.....	7
2.1.2. Potassium.....	8
2.1.3. Chloride.....	9
2.1.4. Bicarbonate.....	9
2.1.5. Calcium.....	10
2.1.6. Phosphate.....	10
2.1.7. Magnesium.....	11
2.2. Host Guest Chemistry.....	12
2.2.1. Receptors for ion sensing.....	13
2.2.2. Fitting Concept.....	17
2.3. Fundamentals of Luminescence.....	19
2.4. Chemical Sensors.....	21
2.5. Types of Ion Sensors.....	22
2.5.1. Ion Selective Electrodes (ISE).....	22
2.5.2. Ionophore Based Optical Sensors (IBOS).....	23
2.5.3. Polarity Sensitive Dye Sensors (PSDS).....	25
2.5.4. Chromophore Based Optical Sensors.....	25
2.6. Optical Chemical Sensors.....	26
2.6.1. Photoinduced Electron Transfer.....	28
2.7. From Probe to Sensor.....	30
2.7.1. ICT based probes for sensors.....	30
2.7.2. PET based probes for sensors.....	31
2.7.3. Utilization of probes as sensors.....	32
2.8. BODIPY Dyes.....	34
3. Tuning the sensitivity of fluoroionophore-based K⁺ sensors via variation of polymer matrix: a comparative study.....	37
3.1. Preface for the Manuscript.....	38
3.2. Abstract.....	40
3.3. Introduction.....	40

3.4. Material and Methods	42
3.4.1. Materials	42
3.4.2. Sensor preparation.....	42
3.4.3. Hydrogel D4 modification	43
3.4.4. Fluorescence Measurements	43
3.4.5. Data evaluation.....	44
3.4.6. Quantum yields measurements.....	44
3.4.7. Response times.....	44
3.5. Results and Discussion.....	45
3.5.1. Response mechanism.....	45
3.5.2. Choice of materials.....	46
3.5.3. Polyurethane hydrogels.....	46
3.5.4. Effect of additional negatively-charged groups on binding constant in polyurethane hydrogels.....	50
3.5.5. Poly(2-hydroxyalkyl methacrylates) and their blends.....	55
3.6. Conclusion.....	57
3.7. Supporting Information	59
3.7.1. Glass Slide modification.....	59
3.7.2. Hydrogel modification.....	59
3.7.3. Determination of QY in solvents.....	60
3.7.4. Hydrogel blends.....	61
4. Ion Sensors for Whole Blood Analysis	69
4.1. Preface for the Manuscript.....	70
4.2. Abstract.....	72
4.3. Introduction	72
4.3.1. Dual Lifetime Referencing (DLR).....	74
4.4. Results and Discussion.....	76
4.4.1. Starting point	77
4.4.2. Composition dependency - Egyptian blue.....	78
4.4.3. Usage of Hydrophilic Phosphorescent pigments	79
4.4.4. Novel potassium fluoroionophore with enhanced hydrophilicity	82
4.4.5. Implementation of Cr-GAB with enhanced spectral properties.....	84
4.4.6. Sterilization tests for blood applications	90
4.4.7. Temperature influence and compensation.....	93
4.4.8. Additional investigations for whole blood ion sensors.....	97
4.4.9. Sodium fluoroionophores for blood measurements.....	104

5. Simultaneous sensing of ammonia and volatile amines with combination of a NH_4^+ fluoroionophore and a fluorescent pH indicator	109
5.1. Preface for the Manuscript.....	110
5.2. Abstract.....	111
5.3. Introduction	111
5.4. Material and Methods	113
5.4.1. Materials	113
5.4.2. pH calibration solutions.....	113
5.4.3. Ammonia and amine solutions	113
5.4.4. Fluorescence measurements.....	113
5.4.5. Synthesis of $\text{Bi}_2\text{Ga}_{3.9}\text{Cr}_{0.1}\text{O}_9$	114
5.4.6. Sensor preparation	114
5.5. Results and Discussion.....	114
5.5.1. Sensor composition and response mechanism.....	114
5.5.2. Sensor response to ammonia and amines.....	116
5.5.3. Mixtures of ammonia with substituted amines.....	118
5.6. Conclusion.....	121
5.7. Supporting Information.....	122
6. Calcium Fluoroionophores.....	125
6.1. Preface for the Manuscript	126
6.2. Abstract.....	127
6.3. Introduction.....	128
6.3.1. Indicators for Calcium	129
6.4. Materials and Methods	131
6.4.1. Chemicals.....	131
6.4.2. Calibration solutions	131
6.4.3. Fluorescence measurements.....	132
6.4.4. Settings for sensor foil calibration.....	132
6.4.5. Experimental.....	132
6.5. Results and Discussion	145
6.5.1. Synthesis of fluoroionophore esters.....	145
6.5.2. Properties of fluoroionophore esters.....	148
6.5.3. pH calibrations in solution	149
6.5.4. Behavior of fluoroionophores in solution.....	152
6.5.5. Calibrations in hydrogels.....	158
6.6. Conclusion.....	159
6.7. Outlook.....	160

6.8. Supporting Information.....	162
6.8.1. NMR and MS data.....	164
7. Summary and conclusion	203
8. References	206
9. Curriculum Vitae.....	220
10. List of Figures	222
11. List of Tables.....	228

Part I

Introduction

1. Scope and Outline of the Thesis

It is not a surprise that one of the main targets of sensor development focuses on ions, because of the ecological and physiological relevance of metal cations such as potassium (K^+), sodium (Na^+) and calcium (Ca^{2+}). Although ion selective electrodes (ISEs) and potentiometric sensors are well developed, fluorescent sensors provide various advantages related to multi-analyte sensing, miniaturization and their cost-effectiveness. Such sensors enable real-time imaging, which is one of the most important objectives in biomedical research. Several fluorescent indicators for cation sensing are reported in literature, but most of them lack in their performance as solid-state sensors and are not really applicable for industry or medical purposes. The majority of those indicators only represent probes and will never find their way to a practically orientated application. The goal of this thesis was the synthesis of new indicator dyes for cations and to further develop already existing sensor strategies, based on fluoroionophores. This thesis is written as cumulative work, whereas **Chapter 3** is already published and **Chapter 5** is prepared for submission to a peer-reviewed journal. Additionally, **Chapter 4** and **Chapter 6** provide fundamental research in sensor development for cation sensing and present a future prospect for follow up work. **Chapter 2** provides the necessary theoretical background about host guest chemistry, the importance of ions, luminescence and optical chemical sensors.

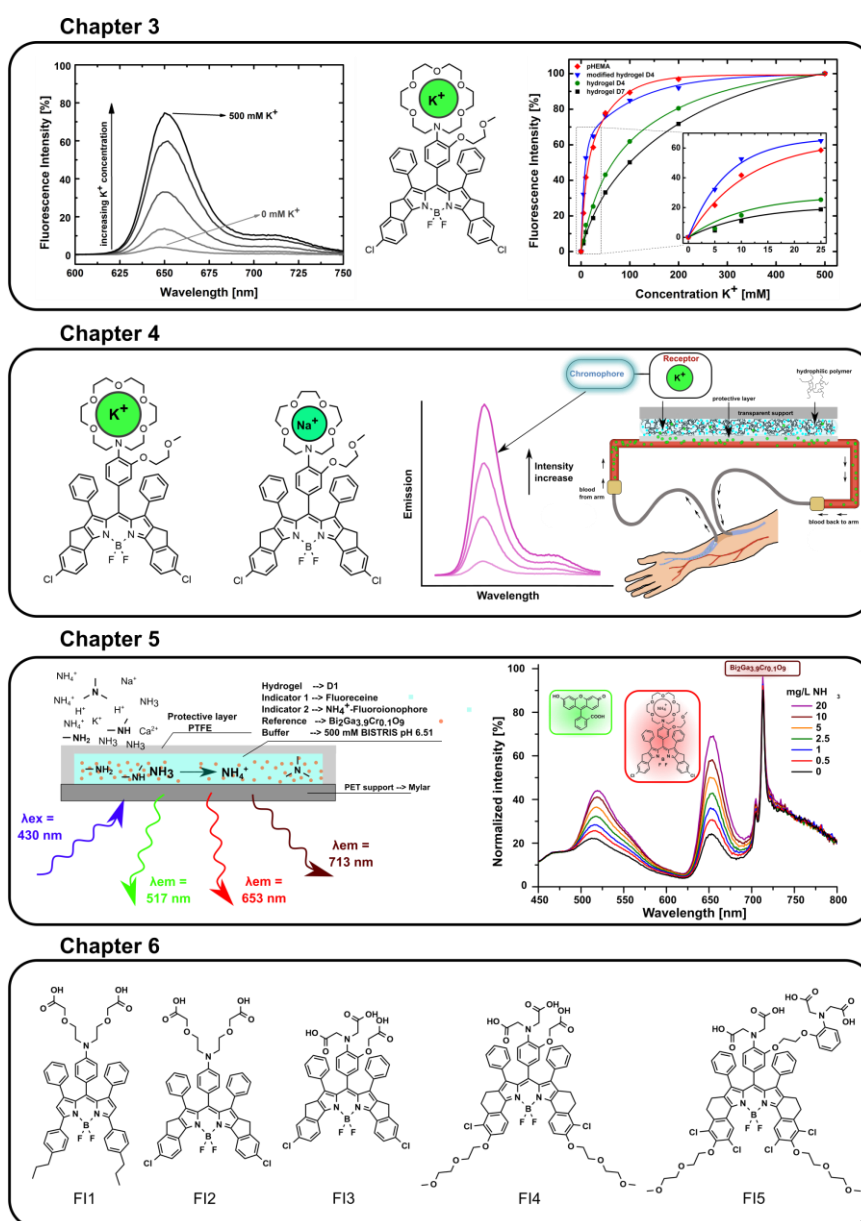
Chapter 3 (p. 37) presents the effects and influence of polymer nature on the sensing properties of a K^+ fluoroionophore, like stability, sensitivity, fluorescence brightness and response time. This study demonstrates the fundamental role of the polymer matrix on characteristics of the solid-state optical potassium sensors and provides the guidelines for the general design of ion sensors with improved characteristics. This research allows better understanding how the structure of the polymer affects the sensing properties of the resulting materials.

Chapter 4 (p.69) is focused on the application of ion sensors for whole blood measurements. The center of attention for this work was on tackling the challenges for applying ion sensors for medical diagnostic applications. An improved DLR sensing system using fluoroionophores and phosphorescent reference particles is developed.

Chapter 5 (p.109) describes a new sensing strategy for amines using a NH_4^+ selective fluoroionophore, fluorescein and a phosphor-reference is presented. The combination of

both indicators enables quantification of NH_3 and determination of substituted amines. This concept offers several new pathways for future amine sensing systems and might be a valuable tool for environmental applications and biotechnology.

Chapter 6 (p.125) contains the synthesis of new calcium indicators using BODIPY fluorophores. This study is mainly dedicated to the challenges of the behavior of charged fluoroionophores in solvents for calcium sensing. Five new calcium fluoroionophores were successfully synthesized in their protected ester forms and their photophysical properties were systematically characterized. The behavior of the fluoroionophores was intensively studied in respect to their dependency of pH and the amount of organic solvent used for measurements.



2. Theoretical background

2.1. Physiological Role of Ions in the human body

The human body requires a huge variety of ions, or electrolytes, which accomplish a diversity of functions. Some of them are needed for the transmission of electrical impulses along muscles, neurons and cell membranes.^{1,2} Others assist in the stabilization of protein structures in enzymes.^{3,4} Several others, are responsible for hormone release from endocrine glands.⁵ Ions found in the plasma are mostly connected and contributed to the osmotic balance⁶, controlling the transfer and movement of water between the human cells and their surrounding environment. The most important electrolytes for living systems include potassium, sodium, calcium, bicarbonate, chloride and phosphate.

These above-mentioned ions help in nerve excitability, membrane permeability, buffering body fluids, endocrine secretion and the transfer of fluids between different compartments.⁷ All of these ions are taken up by the body via the digestive tract. Over 90% of the phosphate and calcium taken up by the body is incorporated into teeth and bones, whereas the bones serve as a backup and reserve for these ion species. For example, in case of calcium or phosphate shortage, bone tissues metabolism can be broken down to serve as a supply for blood or other tissues using these ions. A fundamental component of nucleic acids is phosphate; hence, concentration levels of phosphate increase every time nucleic acids are broken down by the human body.^{7,8} In **Figure 2-1** an overview is given about the importance and function of the most relevant ions in the human body.

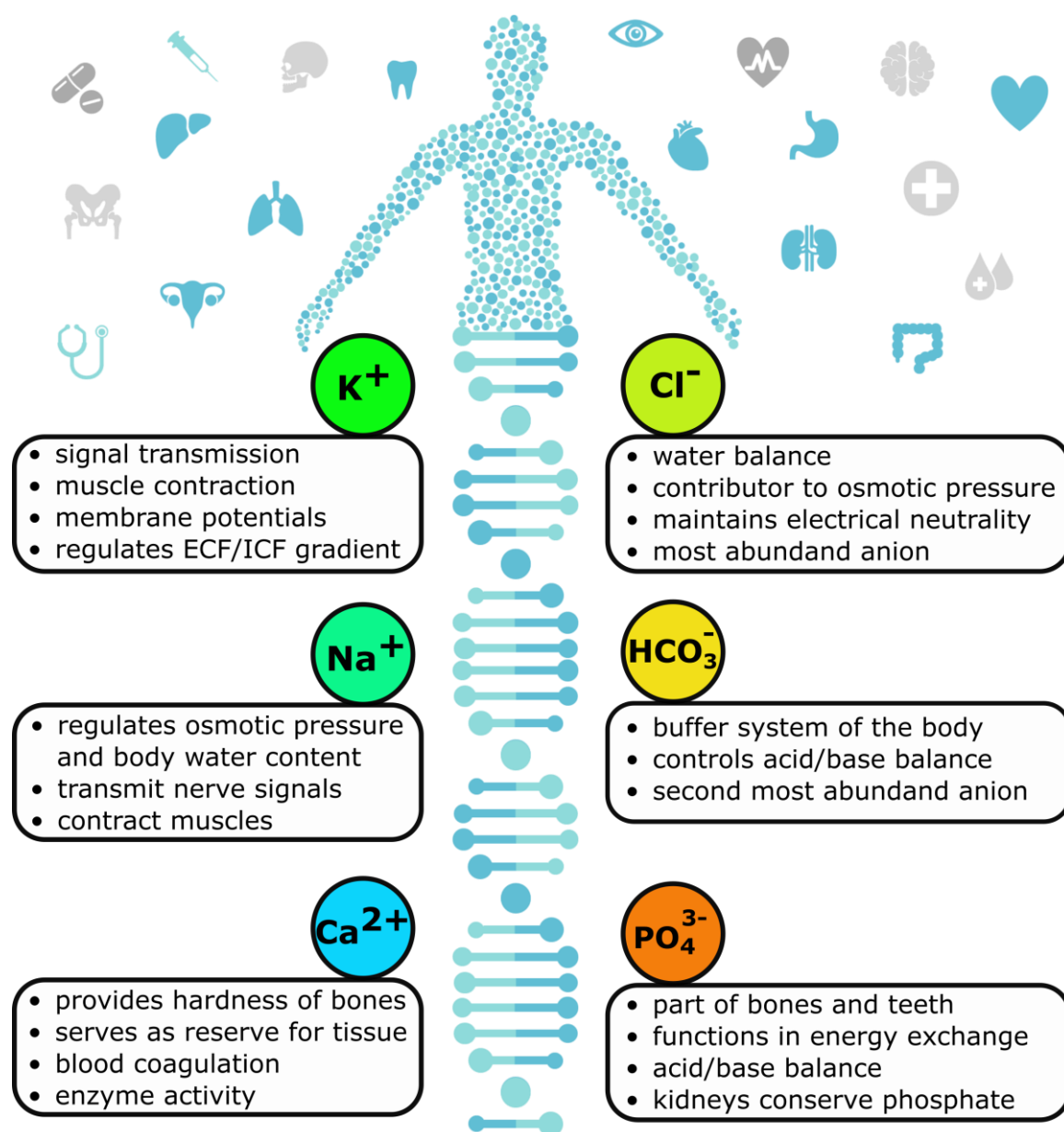


Figure 2-1: Most important ions for the human body with their main functions.

Excretion of ions mainly occurs across kidneys, and in smaller amounts by loss of sweat and feces.⁹⁻¹¹ In case of excessive sweating, a significant loss of sodium and chloride is caused. Diarrhea or vomiting may cause the loss of bicarbonate and chloride ions, whereas renal function and respiratory adjustments regulate the levels of these ions in the extracellular fluids (ECFs).¹²

In **Table 2-1** the concentration values of the six most important ions in plasma, cerebrospinal fluid (CSF) and urine, for the human body are shown. In typical clinical routine based analysis, sodium, potassium and chloride is analyzed via urine samples.¹³

Phosphate and calcium analysis requires a collection of urine samples over a period of 24 hours, because the excretion of those ions varies over the day.¹⁴ The only ion which is typically not excreted in urine is bicarbonate, because it is stored in kidneys, serving as a storage for the body's buffering system.

Table 2-1: Normal concentrations of ions in the human body in plasma, urine and cerebrospinal fluid (CSF).¹⁵

Ion name	Chemical symbol	Plasma	CSF	Urine
sodium	Na ⁺	136 - 146 [mM]	138.0 [mM]	40.0 - 220.0 [mM]
potassium	K ⁺	3.5 - 5.0 [mM]	0.35-3.50 [mM]	25.0 - 125.0 [mM]
chloride	Cl ⁻	98 - 107 [mM]	118.0 - 132.0 [mM]	110.0 - 250.0 [mM]
bicarbonate	HCO ₃ ⁻	22.0 - 29.0 [mM]		
calcium	Ca ²⁺	2.15 - 2.55 [mM/day]		Up to 7.49 [mM/day]
phosphate	HPO ₄ ²⁻	0.81 - 1.45 [mM/day]		12.90 - 42.00 [mM/day]

2.1.1. Sodium

Sodium, Na⁺, is the dominating cation in the extracellular fluid (ECF). Sodium is responsible for the osmotic pressure gradient between cells of the human body and the surrounding environment. Nutrition of typical Western diet contains high NaCl, which cause an uptake of 130 to 160 mM/day of sodium.¹⁶ But the human requirements on sodium is only 1 to 2 mM/day. Due to this excess, sodium is the main trigger causing hypertension (high blood pressure).¹⁷ Excretion of sodium is primary accomplished by kidneys, where the glomerular capillaries filter sodium in the Bowman's capsule. Much of the filtered sodium is reabsorbed by the proximal convoluted tubule, nevertheless some sodium remains in the filtrate and gets excreted by urine (**Figure 2-2**).¹⁸

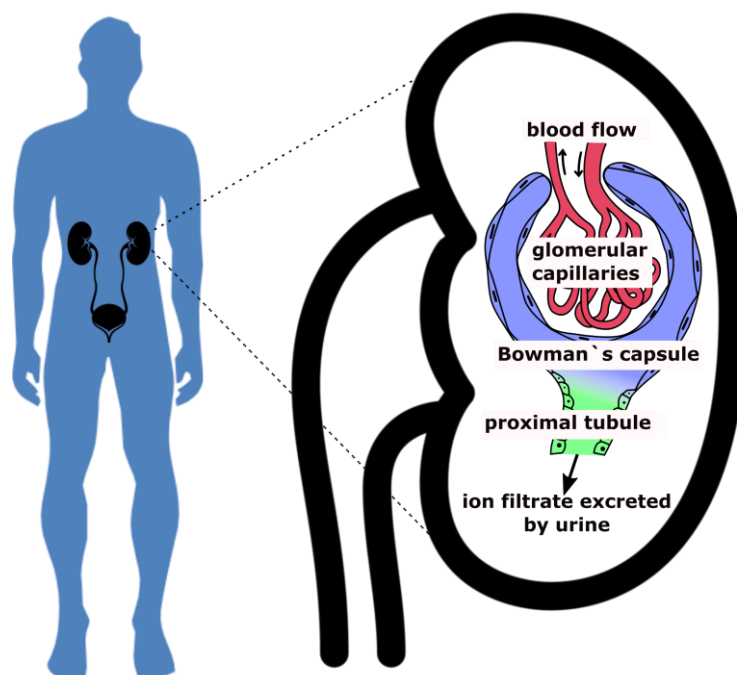


Figure 2-2: Location of kidneys in the human body with the connection to urinary bladder, for excess ion excretion. Additionally, the function of the Bowman's capsule is illustrated. Within these compartments, ion exchange from blood to urine takes place.

*Hyponatremia*¹⁹ is caused by a low sodium concentration, typically connected with excess water accumulation, which causes a dilution of sodium. *Hyponatremia* can result from several conditions like diarrhea, excessive sweating, vomiting, intake of diuretics, diabetes and acidosis.

*Hypernatremia*²⁰ is a higher-than-normal concentration of sodium. It results from water loss of the blood. *Hypernatremia* results in a hemoconcentration of all constituents in the blood.

2.1.2. Potassium

Potassium, K^+ , is the main cation for intracellular functions. It supports membrane potentials in muscles and neurons. 98% of the total body potassium is located in intracellular compartments, while 2% remain in the extracellular compartment. The ratio between extra- and intracellular potassium determines the resting membrane potential and has a pivotal role for normal functioning cells.²¹ Low potassium levels result from sodium-potassium pumps in cell membranes. These membranes typically maintain the normal gradients between extracellular fluids (ECF) and intracellular fluids (ICF).⁷ The recommended daily consumption of potassium is 4770 mg.¹⁶ Similar to sodium, potassium is excreted by renal tubules; any disturbance can either cause *Hypokalemia* or *Hyperkalemia*.

*Hypokalemia*²² is caused by low potassium blood levels. Similar to *Hyponatremia* the reduction of the ion concentration can occur due to decreased intake, often related to starvation, vomiting, diarrhea or alkalosis.

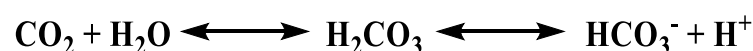
*Hyperkalemia*²³ describes elevated potassium blood levels and can affect functions of the nervous system, the heart and skeletal muscles. It results from an increased dietary intake, which leads in a high extracellular fluid concentration (ECF). This effect influences the skeletal muscle fibers, cardiac cells of the heart and neurons. This depolarization of the plasma effects the heart that it will not relax again after contraction and stop pumping blood, with fatal effects within minutes. Since *Hyperkalemia* also disturbs the nervous system, mental confusion, weakened respiratory muscles and numbness appear.

2.1.3. Chloride

The predominant extracellular anion is chloride, Cl⁻. It serves as the main contributor to the human osmotic pressure gradient between ECF and ICF, and is responsible to uphold proper hydration.²⁴ Chloride maintains electrical neutrality of the ECF, and the paths of secretion and excretion follow the paths of sodium and potassium ions. Lower-than-normal blood chloride levels are called *Hypochloremia*²⁵, and can occur from vomiting, metabolic acidosis and diarrhea. It occurs because of defective renal tubular absorption. *Hyperchloremia*²⁶, higher-than-normal blood chloride concentrations, occur because of dehydration, excessive NaCl uptake (e.g. drinking seawater), congestive heart failure, cystic fibrosis or chronic heart disease.

2.1.4. Bicarbonate

The second most relevant anion in the blood is bicarbonate, HCO₃⁻. It`s main function is to control the body`s acid-base balance, which is representing the buffer system of your body. Bicarbonate ions are formed by a chemical reaction, starting with carbon dioxide (CO₂) and water (H₂O). These two molecules appear at the end of the aerobic metabolism. Only small amounts of carbon dioxide can be dissolved in human body fluids, but over 90% of it is converted to bicarbonate.²⁷



CO₂ is produced in tissues that reveal high metabolic rates. In the cytoplasm, red blood cells convert the CO₂ in bicarbonate via an enzyme called carbonic anhydrase. The

produced bicarbonate is then transported via blood to the lung, where the reverse reaction takes place, and CO₂ can be exhaled as metabolic waste.²⁸

2.1.5. Calcium

Calcium, Ca²⁺, constitutes 1.5 to 2% human body mass. Calcium provides hardness of the bones and serves as a reserve for the rest of the tissue. A bit over 50% of the blood calcium is bound to proteins, whereas the rest is abundant in its ionized form. The function of calcium in our body stretches from muscle contraction, to blood coagulation and enzyme activity. Another very important function is, that calcium stabilizes cell membranes and is responsible for releasing hormones from glands and neurotransmitters from neurons. Providing a suitable supply of calcium is essential during pregnancy and child growth. An adequate nutrition can prevent osteoporosis in older people. Since calcium is absorbed by the intestine with the help of vitamin D, a depletion of vitamin D leads to a decrease of calcium stores and blood levels. Low calcium levels are called *Hypocalcemia*. *Hypercalcemia* instead, occur with high calcium levels causing hyperparathyroidism.

2.1.6. Phosphate

Phosphate appears in the human body in three different ionic forms, H₂PO₄⁻, HPO₄²⁻, and PO₄³⁻; and about 85% in form of calcium salts. Furthermore, it is found in phospholipids, cell membranes, ATP, nucleotides and buffers. *Hypophosphatemia*²⁹, low blood levels of phosphate, cause antacids during alcohol deprivation and malnourishment. Kidneys usually conserve phosphate, but starvation can impair this preservation. *Hyperphosphatemia*³⁰, high levels of phosphate in the blood, occur with decreasing renal function and acute lymphocytic leukemia. Since this ion is a fundamental component in the ICF, any damage of cells results in discarding phosphate in the ECF.

Within this thesis, receptors and optical ion sensors for cations were developed. With this research, reliable measurements for potassium are accomplished, **Chapter 3**. Further research on the application of ion sensors for blood analysis is given in **Chapter 4**. Furthermore, several indicators for calcium sensing were synthesized in **Chapter 5**. This research gives an insight in the necessities for the application of optical ion sensors for blood diagnostics.

2.1.7. Magnesium

Magnesium ions, Mg^{2+} , is an abundant mineral in the human body and mainly found in bones, similar like Ca^{2+} . Magnesium is one of the most important cofactors and more than 300 enzymes connected to magnesium regulate various biochemical functions in humans. Those functions include, protein synthesis, nerve and muscle function, blood-glucose control and it is responsible for blood pressure regulation.^{31,32} Furthermore, it is involved in energy production, glycolysis and oxidative phosphorylation. Additionally, Mg^{2+} controls the active transport of potassium and calcium in membranes, to name only a few functions of this important ion.³¹

Only 1% of the magnesium in our body is found in blood serum., whereas the levels are controlled between 0.75 and 0.95 mM.^{33,34} *Hypomagnesemia* occurs if a serum magnesium level lower than 0.75 mM is measured, whereas *Hypermagnesemia* if the concentration is above 0.95 mM.³⁵ Homeostasis is mainly controlled by kidney and in average 120 mg Mg^{2+} is excreted each day into the urine.³⁶ In *Hypermagnesemia* symptoms like confusion, decreased breathing rate and reflexes, weakness and in the worst case cardiac arrhythmia occurs. Nevertheless, if the concentration is too high or too low in our body, all the functions listed above might be influenced, since Mg^{2+} plays such an important role in our body.³⁷

2.2. Host Guest Chemistry

Application of fluoroionophores in optical ion sensors enables the utilization of a wide variability of receptors. The receptor represents the key component in ion sensing, which is well known described by the field of host-guest chemistry.³⁸⁻⁴⁰ This discipline focuses on noncovalent binding events between two molecules or a molecule and ions, which are held together. The binding force is dependent on the structure and nature of both components.⁴¹ The progress of the last decades has led to the nowadays well-known concept of molecular recognition. Today, this concept is positively employed in electronic devices, environmental analysis, sensors, medicine, functional materials and catalysis.⁴² The receptor is generally a molecule organic nature and has binding sites, often called cavity. The analyte or guest is the component which interacts or fits adequately in this cavity. This feature is important, since the guest interacts noncovalent with the host. Most hosts used as receptors for sensing are designed structurally in a certain way that they interact specifically to one specific guest molecule, which is in general a simple compound. Since the pioneering innovations in the host guest chemistry, a vast array of host molecules has been developed. Especially ion sensing was dominated by crown ethers⁴³, cyclodextrines⁴⁴, cyclophanes⁴⁵, calixarenes^{46,47} pillararenes⁴⁸ and cucurbiturils⁴⁹ (**Figure 2-3**).

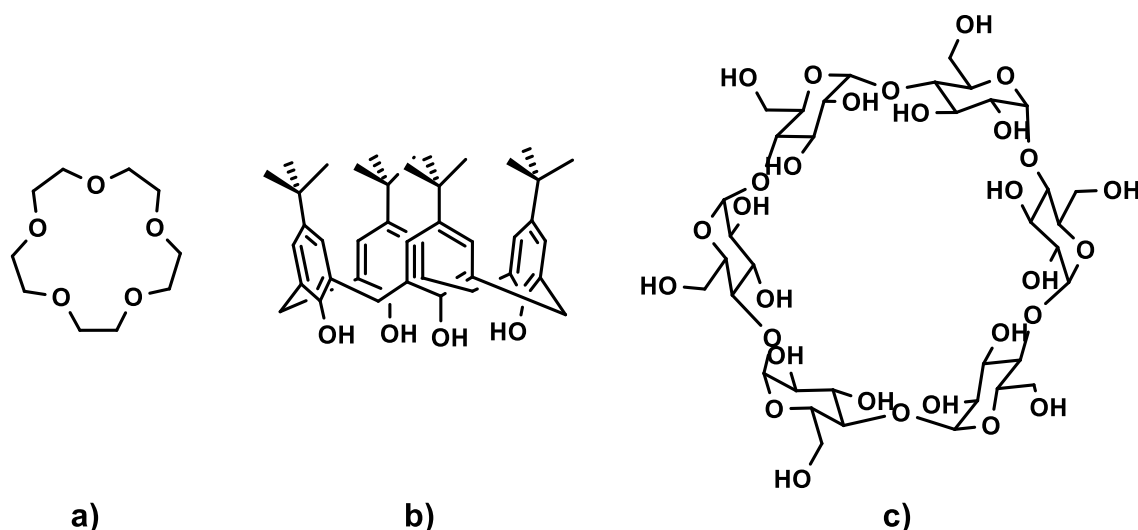
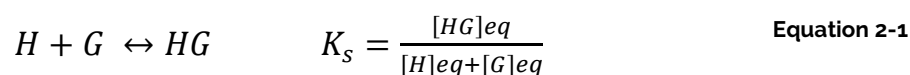


Figure 2-3: Examples of host molecules. **a)** crown ether **b)** calixarene **c)** cyclodextrin.

Since the complexation of target analytes is achieved via a non-covalent binding between the host and the guest, other interactions are needed to arrange a complex of high stability. On the one hand, such interactions can be coulomb interactions, if the guest has an ionic

nature. On the other hand, Van-der-Waals forces are necessary, for non-charged targets. Additionally, to all those interactions the solvophobic force plays a role. It describes the complexation between a host and a guest regarding the entropy and enthalpy. Target analytes are usually surrounded by molecules, meaning they are solvated. With the aim, to get complexed in the host, the analyte must get rid of those solvent molecules. Since this force is overwhelmed, the entropy ΔS_0 is increased, which supplies the free Gibbs energy. This energy is most effective in aqueous solutions. Therefore, host-guest complexation is usually lowered in polar solvents since the analytes are stronger solvated.⁵⁰

The stability of the complex is given as the stability constant (K_s), which describes the equilibrium between the receptor (host, H) and the analyte (guest, G), to form a complex (HG) (**Equation 2-1**).



In order to evaluate the binding constant, quantitative analysis of the complex formation is necessary. The easiest way to determine the stability constant (K_s) is done via titration of the guest with the host, or vice versa. Via concentration measurements of the complexed or uncomplexed molecules, the K_s can be determined. Furthermore, such experiments give suggestions about the binding stoichiometry. Several different techniques are known, whereas the measurement via NMR⁵¹, UV-VIS⁵², mass spectrometry⁵³ and of course electrochemical conductivity and their potential⁵⁴ are the most prominent ones. Complexation of analytes is always connected to energy changes, and therefore the temperature is affected. Because of that, the enthalpy and the K_s of the complexation event can be determined with the use of a calorimeter.⁵⁵

Binding constants are key parameters for the determination of ions in blood, and were intensively studied in **Chapter 3**, a study on the influence of sensing matrices and their properties.

2.2.1. Receptors for ion sensing

The simplest form of hosts are termed podands and were invented by Vögtle and Weber⁵⁶. Podands are neutral acyclic hosts which possess flexible binding sites, whereas the simplest forms are analogues of crown ethers. Penta ethylene glycol dimethyl ether or its diol are analogous to [18]-crown-6 (**Figure 2-4**). Podands in general exhibit a low cation affinity due to unfavorable entropic and enthalpic effects. Nevertheless, such hosts are able

to adopt wrapping conformations similar to crown ethers, if a suitable cation is present. Because of their neutral character and the aliphatic chains contribute to the lipophilicity of membranes like PVC, they possess a high membrane transport ability. An example of a Ca^{2+} podand carrier based on polar amide groups which is used as a transmembrane ionophore is shown in **Figure 2-4**.

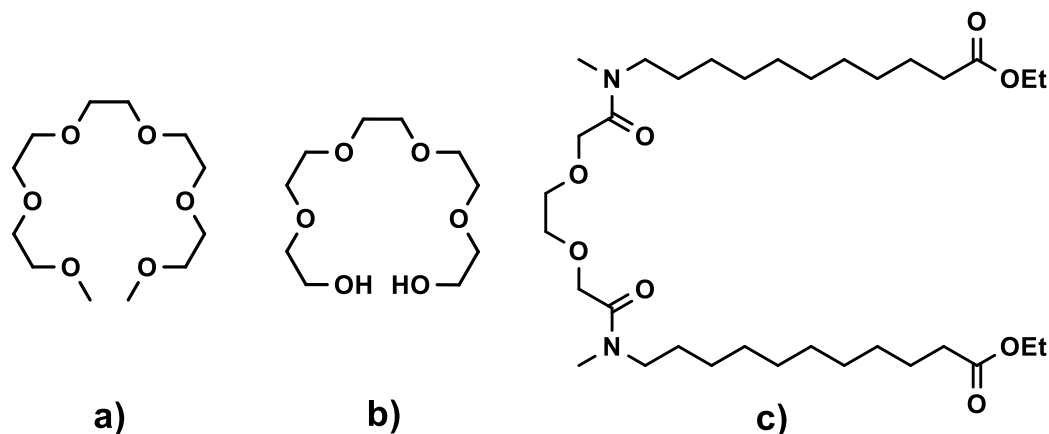


Figure 2-4: Penta ethylene glycol dimethyl ether (a) and its diol (b). Ca^{2+} ionophore used as a carrier in membranes (c).

From all known cyclic receptors, crown ethers represent the easiest form of hosts.⁵⁷ The structure of crown ethers typically has a repeating oxyethylene unit, which is connected in form of a ring. The ethylene groups have a hydrophobic, and the oxygen groups a hydrophilic character. Therefore, crown ethers behave like a fat droplet, in aqueous media and like a water droplet, in a lipophilic media (oil). The high hydrophilicity of the cavity fits perfectly for alkali cations, whereas depending on the number of repeating units (size of the crown), different ions can be complexed.⁵⁸ During complexation of alkali ions, the oxygen atoms are donating electron density to the electron deficient alkali cations. Over the last decades a huge variety of crown ethers has been developed.^{59–62} They do not just differ in their size, but also in their substitution pattern, where for example an oxygen atom is replaced by nitrogen or sulphur atoms. Those donor-heteroatoms enable the development of various new host molecules which can be seen in **Figure 2-5**.

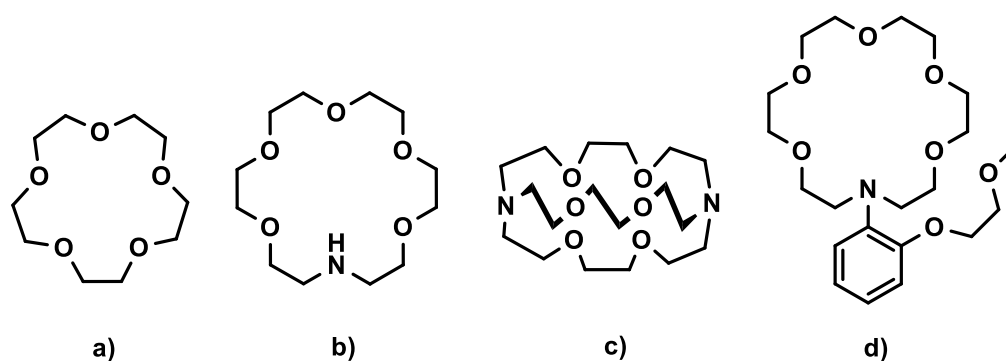


Figure 2-5: Examples of **a)** crown-ether **b)** aza-crown-ether **c)** cryptand **d)** (methoxyethoxyphenyl)aza-crown-ether.

The invention of aza-crown-ethers enabled the synthesis of three-dimensional complexing agents. Cryptands reveal better binding constants due to the additional oxyethylene units which are connected to the nitrogen of the crown ether, yielding in a bicyclic ligand. Lariat ethers can be seen as a blend of a crown ether and a cryptand, with an enhanced binding affinity compared to typical crown ethers. Due to the flexibility of the attached side arm, complexation is still fast, with additional electron donor to the macro ring for better ion complexation.

The development of hosts for polyvalent cations, like calcium, is by far more difficult since electronic densities of uncharged hosts do not supply sufficient attraction force. Therefore, almost all receptors for double charged cations have an open chain like structure, with charged moieties. The first reported receptor for calcium was published by Tsien.⁶³ The working group synthesized a EGTA (Ethylene glycol-bis(2-aminoethylether)-N,N,N,N-tetraacetic acid) derivative, which is known for selective complexation of calcium ions. The synthesized derivatives are shown in **Figure 2-6** and revealed a sensitivity in the μM range with good selectivity over other divalent ions. Tsien et al. set the starting point for the development of new receptors for calcium complexation events, and since then various indicators have been developed.⁶⁴⁻⁷⁰

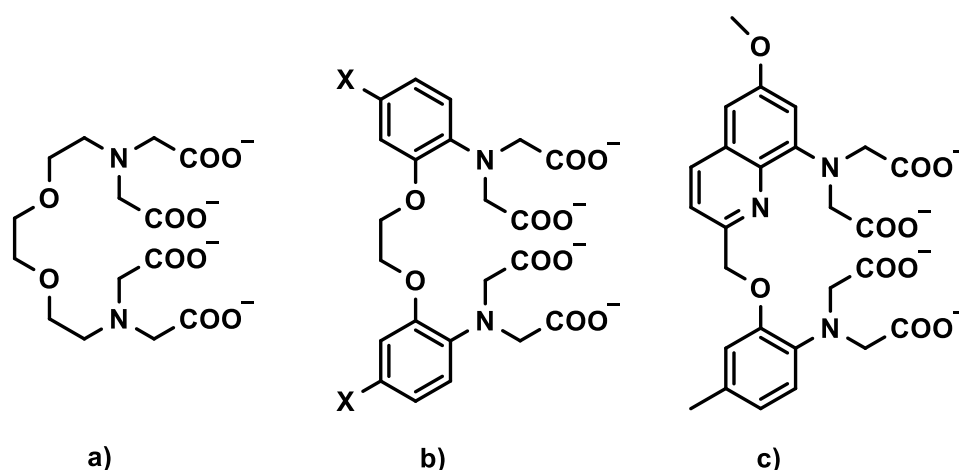


Figure 2-6: Structure of EGTA **a)** and the developed derivatives, **b)** and **c)** by Tsien and coworkers.⁶³

For the determination of calcium in blood the sensitivity of 1,2-bis(*o*-aminophenoxy)ethane-*N,N,N',N'*-tetraacetic acid (BAPTA) is not suitable, since it is in the μM range. *N*-phenyliminodiethoxyacetic acid (PIDA, **Figure 2-7**) on the other hand shows sensitivities in the mM range, and is therefore more applicable for measurements in whole blood. He et al.⁶⁴ synthesized a derivative of the receptor, mentioned beforehand. In aqueous solution, this receptor showed a dissociation constant in the range for blood measurements and K_d in the range of 0.3 to 2.2 mM was measured. The synthesized receptor is shown in **Figure 2-7**. It represents a perfect candidate for optical sensing, since it fulfills certain criteria. It contains a tertiary nitrogen, which performs as electron donating group during interaction with calcium (**section 2.6.1**). The receptor and the corresponding indicator should not be sensitive to any pH changes, to minimize any undesired pH interferences, and the receptor should be insensitive to other cations.

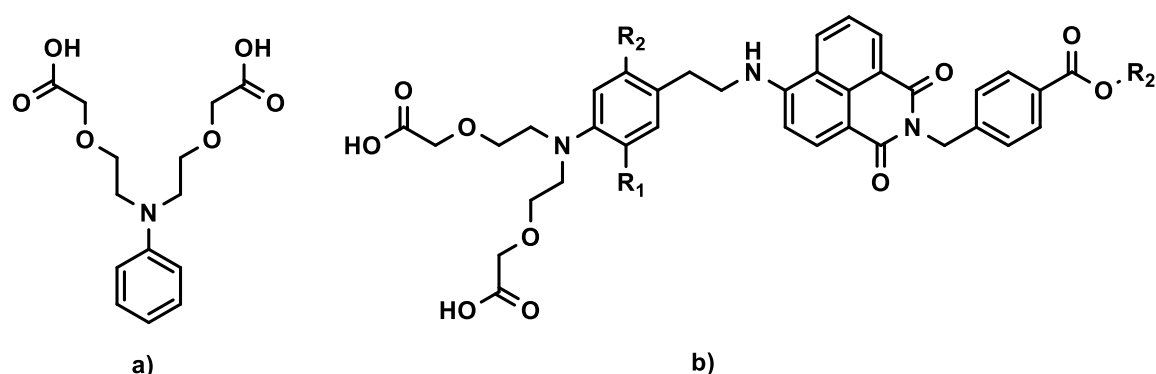


Figure 2-7: a) *N*-phenyliminodiethoxyacetic acid receptor for selective calcium complexation. b) fluoroionophore derivative of a, synthesized by He et al.⁶⁴

2.2.2. Fitting Concept

In host guest chemistry, the selectivity and sensitivity of the corresponding fluoroionophore is triggered by the size and type of the receptor, and moreover by the size and type of the cation. This theory is known as the hole-size fitting concept, which describes the interaction of a de-solvated cation with size and class of the receptor.⁴¹ The strength of interaction by the host with the guest is mainly caused by the size of the receptor and the cation. In case of optimum fitting, the electronic interactivity can exploit its full potential, if not, the interaction is energetically lowered. Therefore, the stability constant of the formed complex represent the relationship of the size and type as well as the strength of interaction.⁷¹ By comparing the diameter of a cation and the size of cavity diameters of different crown ethers, it can be easily estimated which receptors should be used for a certain ion (**Figure 2-8** and **Table 2-2**). Although such estimations are an easy and valuable tool, the specific interaction and electronic interaction cannot be fully explained with the fitting concept. Several other factors, influences and features of the host and guest are mentionable.⁷² For example, the possibility that one cation is complexed by two receptors revealing a 2:1 binding stoichiometry. This phenomenon can occur if the size of host and guest do not match perfectly.⁷³

From **Figure 2-8**, it can be seen that the sensitivity towards the cation of interest can be easily controlled via selection of the right host. This feature was successfully applied in **Chapter 4**, where sensors for blood measurements were developed. This chapter gives an insight how powerful and selective different fluoroionophores can measure ions for blood analysis. Additionally, in **Chapter 5** an NH_3 sensor was developed. It is demonstrated that ions of comparable diameter show a cross-sensitivity, but with specific usage of ion impermeable membranes, such cross-sensitivities can be overcome and selective measurements of NH_4^+ is enabled.

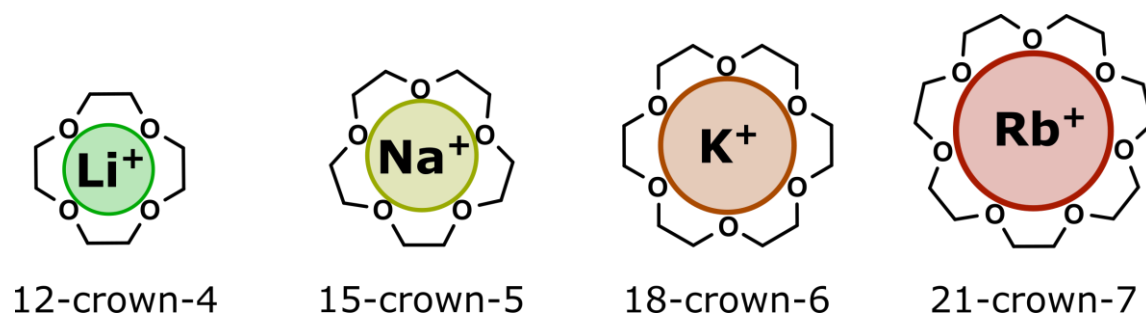


Figure 2-8: Crown-ethers for ion complexation.

Table 2-2: Size of ions and size of different substituted crown-ethers.^{57,74}

Cation	Diameter [Å]	Crown ether	Diameter [Å]
Li ⁺	1.36	12-crown-4	1.2 – 1.5
Na ⁺	1.90	15-crown-5	1.7 – 2.2
K ⁺	2.66	18-crown-6	2.6 – 3.2
NH ₄ ⁺	2.86	18-crown-6	2.6 – 3.2
Rb ⁺	2.94	21-crown-7	3.4 – 4.3

2.3. Fundamentals of Luminescence

Almost all optical sensors and sensing mechanisms are based on the concept of luminescence. Luminescence includes the excitation process of an electron and a de-excitation pathway. All possible phenomena are visualized in the Jablonski diagram (**Figure 2-9**). If a molecule absorbs light (energetically suitable wavelength), an electron can jump to an energetically higher level. The excited electron is then in the so-called excited singlet state (S_1). This state forms the basis of various following de-excitation pathways. Fluorescence occurs when the excited electron returns back to the ground state (S_0), via emission of photons. Fluorescence occurs in the nanosecond range, after absorption of light. Another effect which may occur is phosphorescence. It is a relaxation pathway from an excited triplet state (T_1) back to the ground state (S_0). During this mechanism the electron changes its spin, which is normally forbidden, but due to spin-orbit coupling it is possible. Due to the reason that intersystem crossing (ISC) is a rather slow process, the lifetime of the phosphorescence is between microseconds up to seconds. Another phenomenon which is possible is called delayed fluorescence. It describes the emission from the excited state (S_1) to the ground state (S_0) after the electron undergoes intersystem crossing (ISC) to the excited triplet state (T_1) and reverse intersystem crossing (RISC) back to the excited singlet state (S_1). Like fluorescence the emission takes place from S_1 . Therefore, the emission spectrum is the same for delayed fluorescence and fluorescence. The only difference between those effects can be seen in their lifetimes, since delayed fluorescence undergoes two times intersystem crossing. The lifetimes of delayed fluorescence are highly varying, depending on temperature, and therefore often used in temperature sensing.

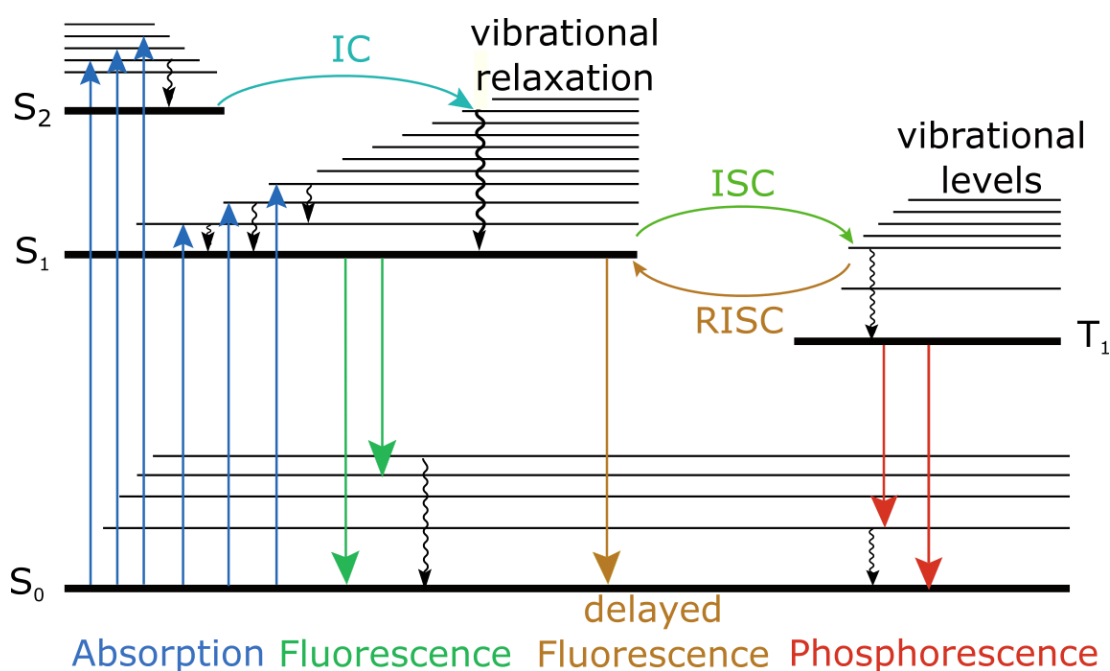


Figure 2-9: Jablonski diagram, describing the main phenomena, absorption, fluorescence, delayed fluorescence and phosphorescence. S_0 represents the ground state, S_1 the excited singlet state. T_1 exemplifies the excited triplet state. Intersystem crossing (ISC) describes the transition between excited singlet state S_1 and the triplet state T_1 .

One essential parameter, talking about luminescence, is the *luminescence brightness*. It combines the *quantum yield* (QY) with the capability of molecules to absorb light (*molar absorption coefficient*). The QY defines how effective molecules emit photons after excitation because luminescence participates with non-radiative de-excitation processes. If a population of fluorophores is in the excited state, the *luminescence lifetime* is the period it takes for the number of excited molecules to relax 38.2% of the original population. The difference between the absorption and emission maxima is called *Stokes shift*. If a molecule interacts with a molecule or with another molecule from the same origin, it is called *quenching*, which can influence any of these quoted properties. All of those properties are used for the evolution of optical sensors, since the optical characteristics of those parameters can be measured.^{75,76}

Optical based indicator dyes have gained more and more attention in the last decades. Depending on the concentration of the analyte, reversible changes in the luminescent properties like emission, lifetime or wavelength are detectable. The utilization of fluorescent and phosphorescent indicators is nowadays possible. For example, phosphorescent dyes are quenched by oxygen by collision, due to their long lifetime in the excited triplet state (T_1). Immobilization of such indicators into oxygen permeable matrices result in a stable reversible oxygen sensor. Other different interaction processes

for fluorescent indicators, also called fluoroionophores, will be discussed in the next sections.⁷⁷

2.4. Chemical Sensors

Chemical sensors are analytical instruments which are able to deliver on-line information of a specific analyte in a sample. Typically, a chemical sensor is based on a receptor (recognition unit) and a transducer unit. The receptor, specifically reacts or interacts to/with the analyte of choice. The transducer converts the gathered chemical information into either an optical or electrical signal. In the last decades, there has been an expanding interest and progress in the development and improvement of chemical sensors. Such devices, enable continuous reversible sensing of multiple analytes, in applications like environmental monitoring, industrial processes or medicine. Therefore, chemical sensors are of huge interest.⁷⁸

An ideal chemical sensor should accomplish a number of criteria:

- Response to changes of concentration must be reversible and fast
- The gathered information must be transduced to a measurable signal
- Response towards the analyte of interest has to be selective and sensitive
- The sensor should be stable during measurements and show a good shelf life
- The device should be small and low-cost
- The fabrication of the sensor should be simple and reproducible
- The utilization of the chemical sensor should be user-friendly

Typically, analytical chemistry includes the collection and selection of a sample, transport and the analysis in a research laboratory or test site. Such routine-based analysis is time intensive, expensive and requires trained personnel. The advantage of chemical sensors is that such devices can be transported right to the sample and field. This procedure enables immediate measurements of the analyte of interest. The use of a chemical sensor can prevent tedious sample preparation, enabling on-line and in-line monitoring. These features enable more control in industrial processes and environmental monitoring. Those benefits have led to a growing demand for chemical sensors in the last decades. Sensors in general, have a huge variety of measurement principles and are normally classified by the corresponding transduction method.

This thesis focusses on the development of optical sensors, which is dedicated to synthesis of fluoroionophores and their application in optical sensors for ions, as well as the characterization of new materials for optical ion sensing. An overview of other methods for ion sensing will additionally cover electrochemical sensors, since they represent the state-of-the-art technology for ion sensors.

2.5. Types of Ion Sensors

2.5.1. Ion Selective Electrodes (ISE)

Apart from all categories of ion sensors, the ion selective electrode is the most common used potentiometric sensor. The high effort in instrumental equipment is shown in **Figure 2-10**. Beside the selective electrode, a device for potential measurements and a reference electrode with a known potential is required.

The selective electrode interacts specifically with the cation, resulting in a potential difference within the membrane. A reference electrode is necessarily needed, for evaluating the potential difference between the electrodes. The ratio of the reference and the membrane potential yields in a net potential, which is proportional to the cation activity. With the use of the Nernst equation a connection of the electrode potential and the ion activity can be made (**Equation 2-2**).^{79,80}

$$E = E_0 - \frac{R \cdot T}{n \cdot F} * \ln (a_i) \quad \text{Equation 2-2}$$

For selective potential measurements, the membrane is the key part for ion selective electrodes. The selectivity of the electrode can be controlled via selection of different membranes, which are specific for different analytes. Three main varieties of membranes exist, the crystallin, the liquid (**Figure 2-10**) and the glass membrane.⁸¹

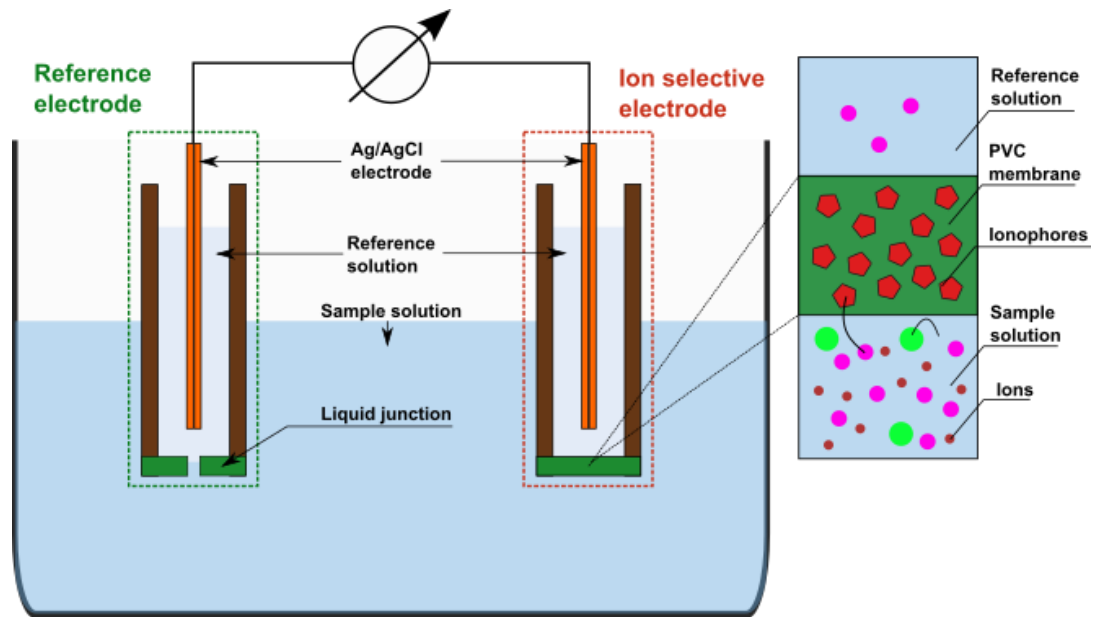


Figure 2-10: Working principle of ion selective electrodes (ISE). An Ag/AgCl reference electrode supplies a constant potential, whereas in this case a liquid membrane changes the potential depending on the activity of a specific target ion. Selectivity of the electrode can be controlled via the choice of ionophores used in the PVC membrane.

2.5.2. Ionophore Based Optical Sensors (IBOS)

Similar to the working principle of the ISE, the ionophore based optical sensors use a solid liquid phase membrane. This membrane, in most cases a PVC/DOS barrier, consists of incorporated ionophores, which enable a reversible and selective binding as well as the transport of the corresponding ion. Different to the ion selective electrode, the IBOS signal change is not induced due to the potential difference between the inner and outer sample solution. Concentration change is linked to a change in concentration within the PVC/DOS matrix (**Figure 2-11**). Molecular recognition is achieved with the use of ionophores, whereas an optical signal is generated with the usage of pH indicators. In order to obtain a stable sensing device, those indicators typically consist of lipophilic side chains, to prevent any leaching in the water phase. Binding of any target analytes is followed by an ion exchange or co-extraction. This feature is required, since electro-neutrality has to be ensured within the membrane. As a result of the ion exchange, the degree of protonation of the pH sensitive indicator is changed, leading to an optical signal depending on the current concentration. Therefore, the pH indicator acts as a transducer within the matrix leading to a change in absorption or fluorescence.⁸²

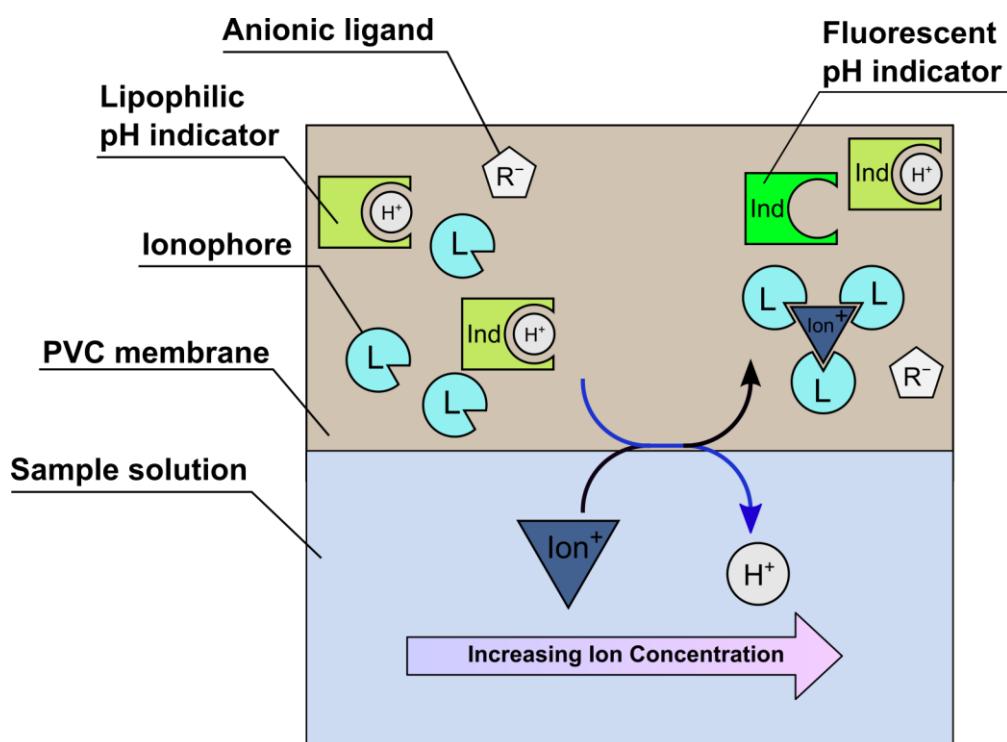


Figure 2-11: Principle of IBOS for ion sensing. The PVC sensing membrane is capable for extraction of ions with the use of anionic surfactants. The selective ionophores bind the target ions and promote a proton release to maintain charge neutrality. Since a pH indicator is used for sensing, and internal pH value is changed, e.g. fluorescence can be measured to determine the cation concentration in the sample.

Several different sensing setups are developed. This characteristic is needed, since the setup must be varied depending on the used pH indicator, ionophore and the charge and type of ions measured. It must always be ensured that electro-neutrality inside the matrix is guaranteed. Therefore, it is necessary to introduce and immobilize charged ionic groups (ionic liquids). Using this concept, enables a wide variety for ion sensing, since both, cation and anion sensing is possible. The large number of available indicators, ionophores and ionic surfactants make IBOS to a powerful tool for ion sensing.⁸³⁻⁸⁵ One of the main advantages is that IBOS do not need a reference electrode, and therefore sensing layers in the micro and nanoscale can be fabricated.⁸⁶ Beside all mentioned advantages, IBOS suffer from a severe drawback. Since pH indicators are used for sensing other ions, they suffer from their naturally given pH sensitivity, which converts in a pH cross-sensitivity if used in IBOS systems. Such cross-sensitivities can be compensated by additional simultaneous measurements of pH, which is of course accompanied with a more complex sensing system.

2.5.3. Polarity Sensitive Dye Sensors (PSDS)

Another group of sensors represent polarity-sensitive dyes (PSD). Those sensors have charged moieties acting as an catalyst capable extracting of ions out of aqueous solutions, forming a complex.⁸⁷ The formed complex changes its polarity, hence able to move into different locations of the sensing layer (e.g. plasticizer droplet) because of its lipophilicity. This causes a change of the micro-polarity of the dye, which results in an increase or decrease of the fluorescence or absorption of the PSD.⁸⁸ The potential sensitive dyes force a transport of ions from the aqueous media into the lipid membrane, whereas often neutral carriers are used to enable the transport inside a PVC membrane.⁸⁹ In **Figure 2-12** a schematic illustration of the working principle of PSD as a sensor is given. This model has to be seen as a simplified version of a sensor, since real PSD sensors are built up more complex. Depending on the choice of PSD and carrier for the desired ions it is possible to sense either anions or cations.⁸⁷⁻⁹²

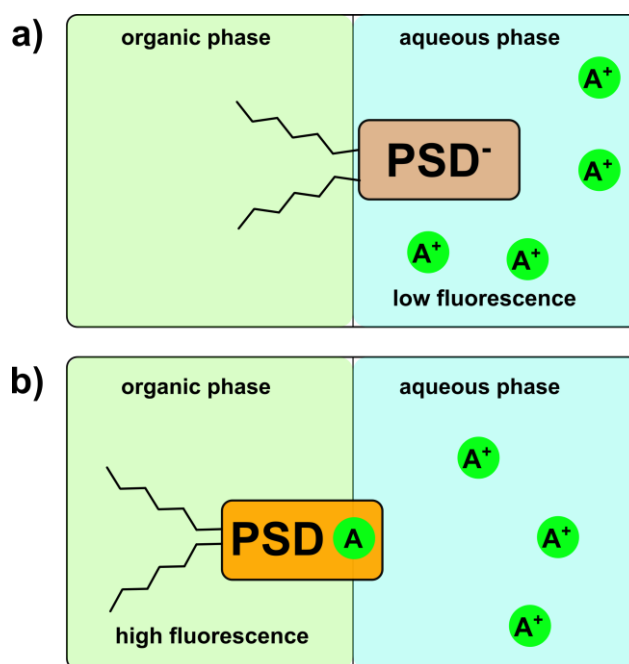


Figure 2-12: Simplified illustration of a polarity sensitive dye (PSD) and the effect of the microenvironment. **a)** Before complexation of the analyte the indicator is low in its fluorescence intensity. **b)** After interaction of the analyte the polarity of the complex changes and it can move into another location of the sensing layer. Due to the change in polarity of the surrounding environment the complex is fluorescent.

2.5.4. Chromophore Based Optical Sensors

Chromophores based optical sensors require just one single molecule for ion recognition. The so called fluoroionophores unite the transducer with the ionophore. Signal

transduction is achieved, either by photoinduced electron transfer (PET) if a molecular spacer is used between recognition unit and chromophore, or intramolecular charge transfer (ICT), if no spacer is used between transducer and ionophore. In second case, the chromophore and the ion receptor are directly coupled via covalent binding. The two compartments (fluorophore and receptor) of the fluoroionophore are not electronically separated, whereas in PET, the spacer causes an electrical separation between those units.^{93,94} Depending on the electrical environment, it is sometimes difficult to differentiate between ICT and PET. All synthesized and used indicators in this thesis are mainly PET sensors. For a better understanding, the difference is illustrated in **Figure 2-13**.

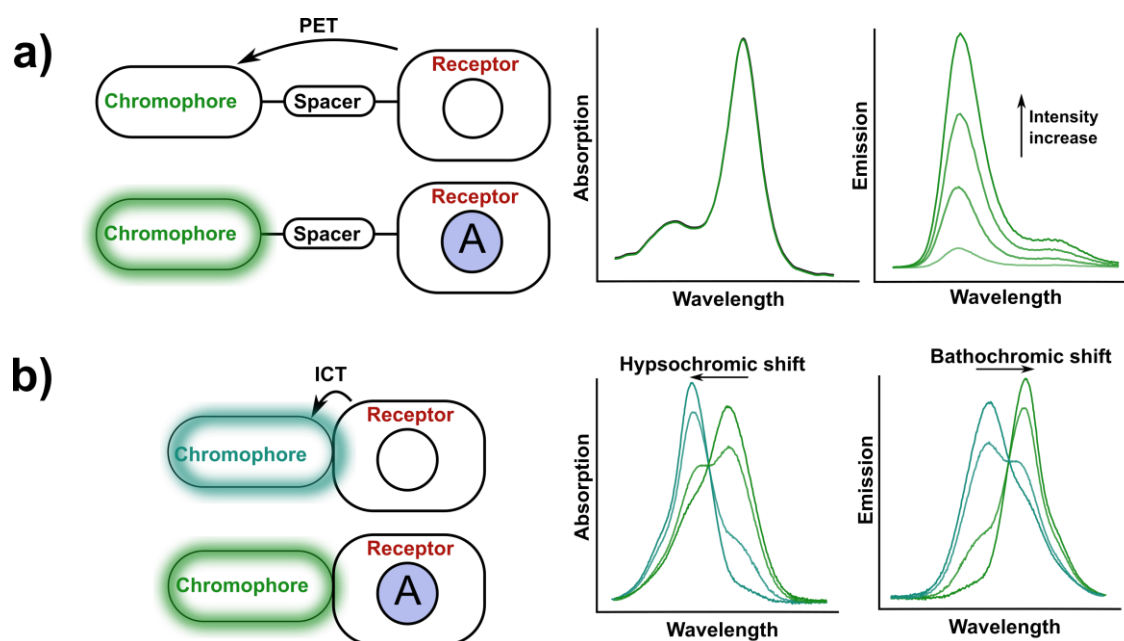


Figure 2-13: Visualization of PET and ICT upon complexation. **a)** In PET the absorption spectrum remains unchanged, whereas the emission intensity changes upon analyte interactions. **b)** In ICT the spectra upon complexation is changed.

2.6. Optical Chemical Sensors

An optical chemical sensor typically consists of a receptor and a transducer. The receptor part is responsible for analyte recognition, whereas the transducer converts the gathered information into a measurable signal. This conversion into optical properties can be based on the change of the absorption, refractive index, luminescence or Raman spectroscopy.⁹⁵⁻

103

For luminescent sensors, the device characteristically involves a light source, the sensing material and a photodiode as a detector for quantification of the received signal. Advanced

sensing systems, additionally contain filters and optical elements between the sensing material to provide specific light properties for the interaction with the sensing material. With the use of such components, wavelength`s can be adjusted and the background noise minimized.^{98,104}

The main benefit of optical chemical sensors over electrochemical and electrical sensors is that, there is no need of a reference electrode. They can be seen as self-referenced, turning them into a powerful tool against electromagnetic influences. The negligible reference electrode enables miniaturization of the entire sensing device. Consequently, such sensors can be manufactured in various formats, starting in the nanoscale¹⁰⁵ up to macroscale¹⁰⁶. In addition, it is not necessarily needed that the sensing unit is in direct contact with the read-out unit, since light is used for information transport. This enables sensing methods where the sensing unit is completely separated from the readout unit (e.g. measurements through glass). Physical separation yields in a less pronounced read-out setup because critical parameters like, pressure, temperature or chemical harmful environments do not play a role.

For sensor development some main parameters need to be considered:

- *Reversibility* is ensured if the analyte is not destroyed or consumed by the indicator or sensing material. The signal complies the current analyte concentration.
- *Selectivity* means that the produced transducer-signal is only generated by one specific compound. This can be controlled by the selection of proper receptors.
- *Response time* is typically given as t_{90} . This is the time when 90% of the corresponding signal intensity is reached. Quick response is decisive for real-time analysis.
- *Sensitivity* is describing the increase of signal intensity with rising analyte concentration. This important parameter can affect other characteristics such as *detection limit*, *dynamic range* or *resolution*.
- *Stability* is one of the main factors for long-term measurements. If the word drift is used, it is directly connected with stability. For example, if the signal intensity is increasing or decreasing over time although the analyte concentration remains the same, stability is not guaranteed.

2.6.1. Photoinduced Electron Transfer

Fluoroionophores can be quenched via two indicator-analyte interactions. The effects which can occur are photoinduced electron transfer (PET) and intramolecular charge transfer (ICT).^{107–110} The attachment of a PET-group on a fluorophore results in a redox capable indicator. The covalent connection of a receptor with a chromophore causes an electron transfer from the receptor-PET group to the dye moiety. This electron occupies the ground state S_0 of the chromophore. Since the ground state of the chromophore is filled with two electrons, no radiative emission via fluorescence can take place (**Figure 2-14 a**).

If the attached PET group interacts with certain analytes, the energy level of the PET group is lowered. In that case, the PET is inhibited and the fluorophore can emit fluorescence (**Figure 2-14 b**). Typically, PET is reductive, but some examples of an oxidative PET (e⁻ transfer from fluorophore to PET group) are reported.¹¹⁰

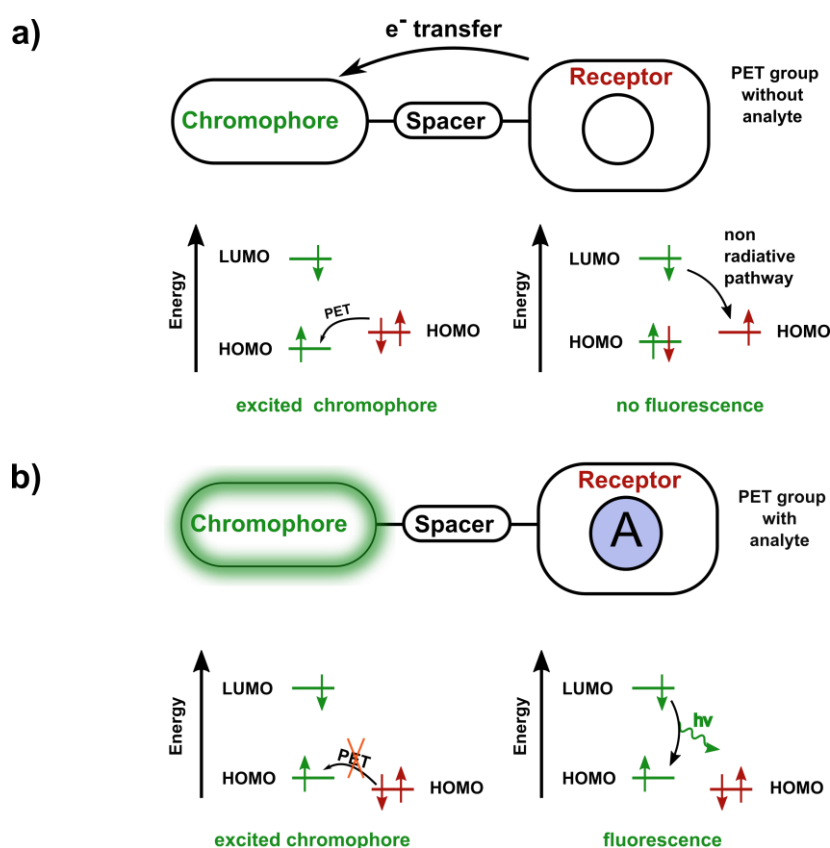


Figure 2-14: Illustration of PET. **a)** Classic photoinduced electron transfer (PET) **b)** PET-quenching upon complexation of the analyte of interest. Binding events cause a change in the molecular orbitals of the receptor. The indicator in this case is fluorescent.

Several functional groups, utilizing the PET are known, whereas the most groups used are phenolates¹¹¹ or carboxylates¹¹² and amines¹¹³. The combination of receptor and chromophore is decisive for the PET efficiency. The optimum quenching effect is achieved

by the combination of a good electron accepting group (fluorophore), with a strong electron donating group (receptor). Apart appropriate redox potentials, the PET is enhanced in polar environments (H_2O , EtOH, MeOH, etc.), enabling PET indicators for measurements under physiological and environmental conditions.⁹⁰

Utilization of the PET group as a pH indicator is the most common used sensing concept. Via (de-)protonation these chromophores show a high sensitivity to pH, near the pK_a value of the corresponding PET group.

The PET cannot just be inhibited by simple protonation or deprotonation. The usage of selected receptors cause interactions with the PET group, making such indicators responsive for multiple other analytes. Phenyl-aza-crown-ethers are applied successfully for sensing ions.^{58,114–119} Depending on the size of the aza-crown-ether, they are selective for certain ions. After recognition of the corresponding ion the PET converts the molecular recognition in a detectable luminescence signal.¹²⁰

Recognition units can be separated via a spacer from the chromophore or directly linked to it. If a spacer is incorporated in the chromophore, the PET groups are electronically separated from the dye moiety. The spacer bridge breaks the conjugation and the ground state as well as the excited state of the fluorophore is not affected by PET quenching. This only leads to a change in the fluorescence emission, if the analyte of interest interacts with the fluoroionophore. The shape of the emission and absorption spectrum as well as the shape of the absorption is not affected at all. Since only the emission intensity is influenced by analyte interaction, such indicators can be applied as turn-on-off fluoroionophores. Via immobilization in appropriate sensor matrices, reversible sensing is achieved.

In case of direct linkage of the recognition unit to the fluorophore, intramolecular charge transfer (ICT) is observed. The characteristics of this phenomenon is a change in the spectral properties (e.g. spectral shift), via interaction of the sensitive moiety with the analyte. Therefore, the HOMO-LUMO levels of the fluorophore is affected.

PET based indicators enable a huge playground for the usage in optical sensor systems. The combination of typically insensitive fluorescent dyes, with PET-able receptors, yields in new sensitive indicators, capable for sensing applications.¹⁰⁹ The utilization of the PET in fluorescence sensing offers a modular system, for the development of new indicators. The spectral properties can be adjusted by the fluorophore, whereas the selectivity and sensitivity can be controlled by the recognition unit. If different PET groups are attached

to the same dye, analogue spectral properties are expected, whereas the selectivity to different target analytes is controlled by different recognition building blocks. This enables a simplification for sensing devices, since optical filters and excitation LEDs do not have to be adjusted in the measurement devices. Furthermore, this concept enables multiparameter sensing via simple variation of chromophores with the same dye backbone.

This variety yields in a modular and tunable system. This thesis took advantage of this effects and shows the huge playground in the development of new fluoroionophores. Furthermore, the effect of the sensor matrix on the PET-effect was studied (**Chapter 3**). Additionally, calcium receptors for the use as PET sensors and probes was investigated, and give an insight in double charged cation sensing. It forms the basis for future divalent ion sensing developments (**Chapter 5**). Apart from this PET-receptors were successfully applied in potassium blood sensing systems, in combination with referenced long lifetime particles discussed in **Chapter 4**.

2.7. From Probe to Sensor

2.7.1. ICT based probes for sensors

ICT probes are usually named colorimetric dyes, or chromogenic dyes. This family represents systems, where the receptor is directly linked to a transducer. The complexation of ions causes a change in color, hence in the absorption spectrum (**Figure 2-15** and **Figure 2-13**). Interaction of ions with the receptor causes a destabilization of the excited state of the dye. As a result, the electron density is influenced, hence either a hypsochromic or bathochromic shift, of absorption bands can be obtained. Using ICT probes for sensors has one main advantage. Due to the shift in absorption, ratiometric dual wavelength measurements are enabled, in emission and absorption mode. Examples of ICT indicators are shown in **Figure 2-15**.

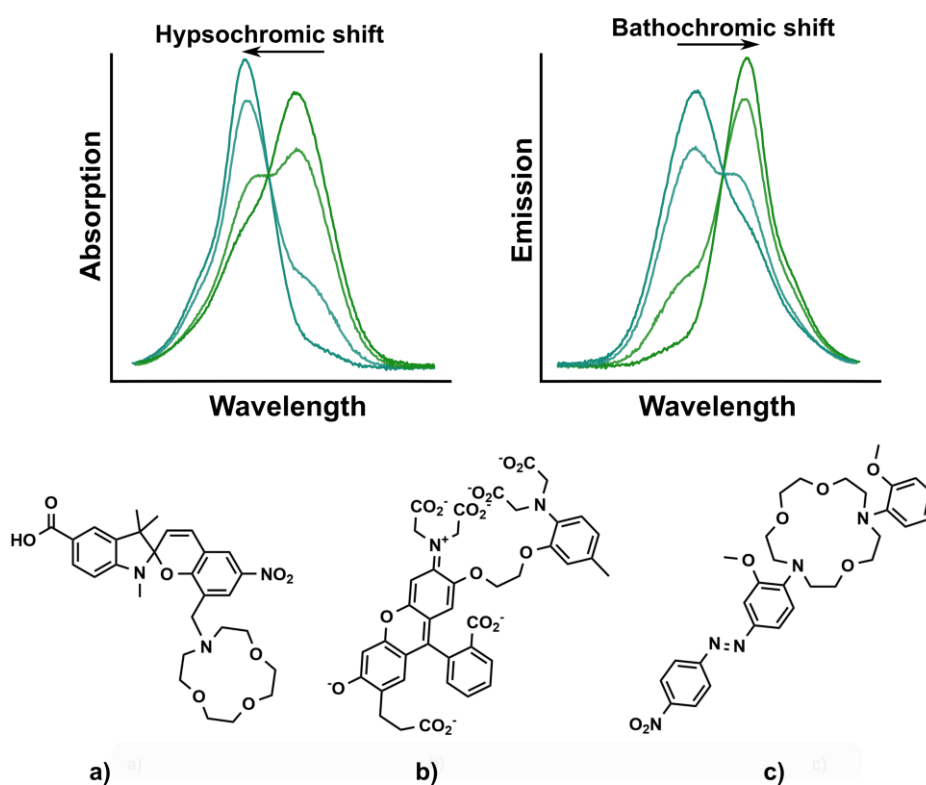


Figure 2-15: Examples of fluoroionophores **a)**¹²¹, **b)**⁷⁰, **c)**¹²² based on the ICT quenching mechanism for cation sensing.

2.7.2. PET based probes for sensors

The usage of PET probes involves receptors, which are mostly connected via a nitrogen to the spacer. The electron pair of the nitrogen is participating in ion complexation and is responsible for PET quenching. Upon complexation the absorption spectrum is not influenced and remains its shape and intensity, whereas the fluorescence emission intensity is affected. This effect can be either reductive or oxidative, causing either an OFF-ON or ON-OFF mechanism. In **Figure 2-16**, a selection of PET indicators is shown.

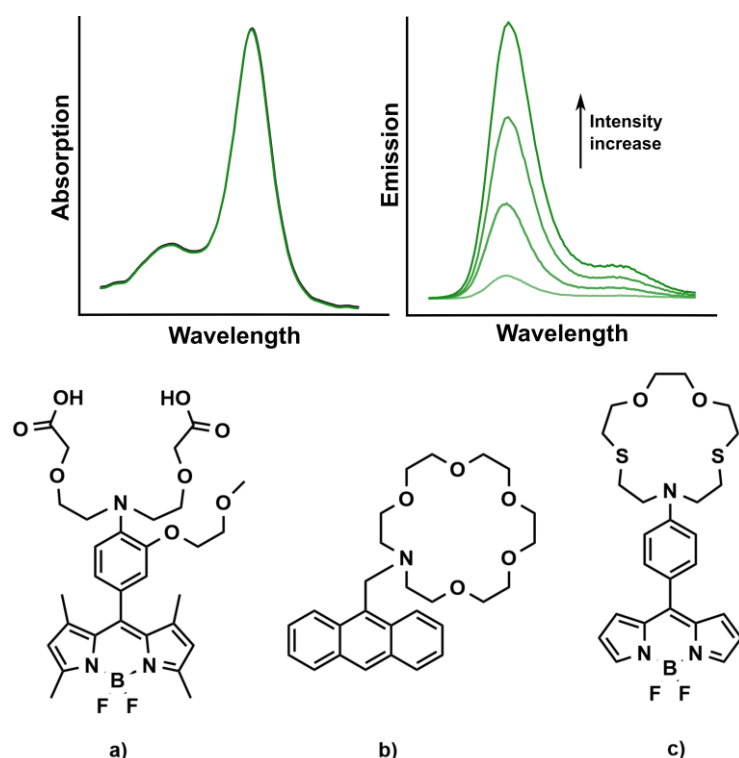


Figure 2-16: Examples of PET fluoroionophores **a)**¹²³, **b)**¹²⁴, **c)**¹²⁵. With increasing ion concentration, the emission intensity is increased, whereas the absorption spectrum remains unchanged.

2.7.3. Utilization of probes as sensors

Obtaining reversible sensors from ion indicators can be a challenging task. To ensure a continuous sensing setup, the fluoroionophores are usually immobilized in hydrophilic polymer matrices. Depending on the fluoroionophore the decisive goal is to discover the best suitable polymer, to obtain optimum sensing parameters (**Chapter 3**). The synergy between indicator and polymer matrices must fulfill some requirements. The fluoroionophore must be stable in the corresponding matrix, enabling a non-leaching environment for the dye, resulting in a permanent constant indicator concentration. Furthermore, the polymer must have a hydrophilic character to ensure ion mobility and permeability within the sensing layer. On the other hand, it should also have a hydrophobic character, since fluoroionophores sometimes tend to aggregate in hydrophilic environments. Because of those limiting requirements, hydrogels represent a good candidate for fluoroionophores as sensing matrices, since they vary in their hydrophilic and hydrophobic character. This was already shown for pH sensors.¹²⁶ The easiest way to accomplish a reversible sensor is by dissolving the fluoroionophore and the hydrogel in an organic solvent. After subsequent process steps, like spin coating or knife coating on a

transparent support, a planar sensing foil is obtained. Most of the sensors described in this thesis are prepared with the knife coating technique (**Figure 2-17**).

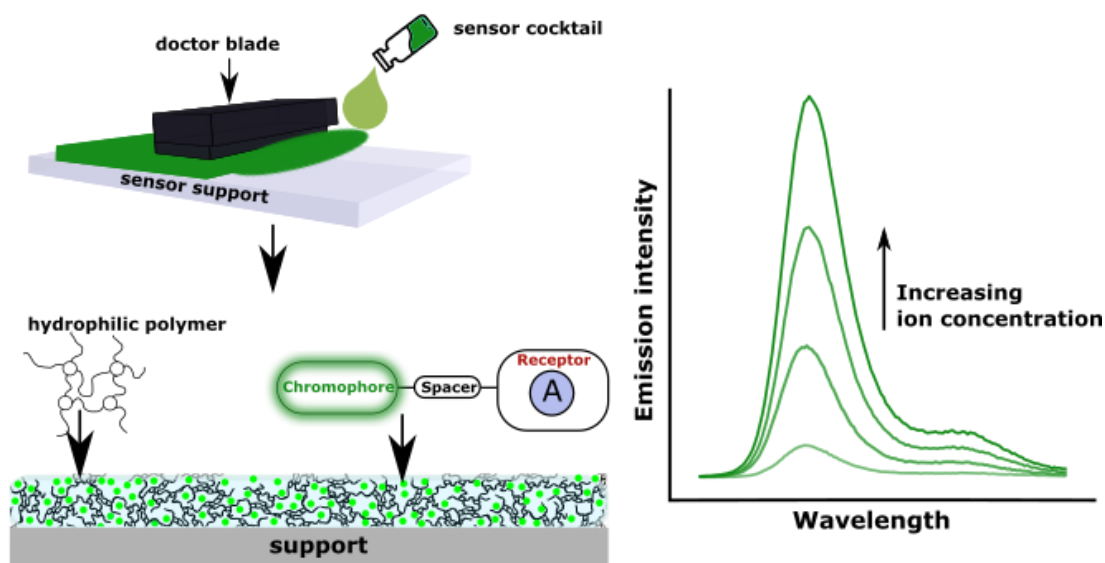


Figure 2-17: Knife coating illustration for a planar sensing foil. After the hydrogel and the indicator are dissolved in an organic solvent, the remaining sensor cocktail can be knife coated on a sensor support. Immediately after evaporation of the solvent the sensor can be used for measurements in aqueous solutions.

Nevertheless, several other techniques exist to achieve reversible sensing setups. Sensing fibers are fabricated by dip coating the corresponding sensor cocktail on an optical fiber.¹²⁷ Polymer nanoparticles are used as water dispersible nano-sensors, if the indicators are immobilized in such particles. This strategy is already successfully applied in biological applications, where such materials are taken up by cells.¹¹⁴

By now, the incorporation of fluoroionophores in hydrogels is not common, whereas the vast majority represents probes for ion detection. Still, there are reported ion sensors based on methacrylate hydrogels.^{128,129} The environmental circumstances of the polymer are the key factor for a reversible sensing platform. Polymers must be water swellable and the main goal is to find the balance between the perfect ion complexation conditions and a suitable stable sensing matrix. Best binding affinities are usually found in highly hydrophilic environments.¹³⁰ The effect of binding stabilities of a potassium fluoroionophore and the effect of different polymer matrices on the sensing properties is excessively studied in **Chapter 3**. This study also explains why nowadays a lack of solid-state materials exists, since the synergy between fluoroionophore, the analyte of interest and the polymeric matrices is highly complex.

2.8. BODIPY Dyes

From all existing fluorescent dyes, BODIPY dyes represent one of the highest potentials for future development and utilization in sensors. They are already invented by Treibs and Kreuzer in 1968 and it took two decades since they are used as indicators for sensing applications.¹³¹

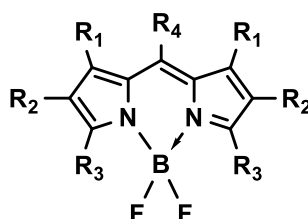


Figure 2-18: Structure of borondipyrromethene (BODIPY) dyes.

BODIPY dyes have certain characteristics, which explains why they achieved such high popularity:

- High chemical stability over a wide pH range
- High photostability
- High quantum yields and brightness
- Sharp emission and excitation spectra
- The photophysical and spectroscopic properties can be easily tuned
- They reveal a good solubility over several solvents
- Simple and versatile synthetic pathways

Due to these extraordinary properties, most of the synthesized and used indicators in this study are based on BODIPY dyes. Furthermore, due to their chemical robustness they allow modifications after complexation with BF_3OEt_2 . Nucleophilic substitution, reduction or oxidation of the dye itself does not cause troubles and enables further modification. The boron center of the dye can be used for the introduction of a variety of different substituents, making these dyes a promising candidate for tuning and adapting spectral properties.¹³²

The synthesis of meso-substituted BODIPY dyes is achieved by two different one-pot procedures. The first route (**Figure 2-19 a**) uses a Lewis acid (most common trifluoroacetic acid, TFA) as a catalyst for the condensation of a substituted pyrrole and an

aldehyde. Oxidation with p-chloraniline or DDQ, and subsequent base treatment (Hunigs base or Et_3N) as well as final complexation with BF_3OEt_2 yields to the corresponding BODIPY dye. The second route (**Figure 2-19 b**) uses an acid halide instead of an aldehyde. Again, subsequent treatment with a base and BF_3OEt_2 yield again to the corresponding dye.

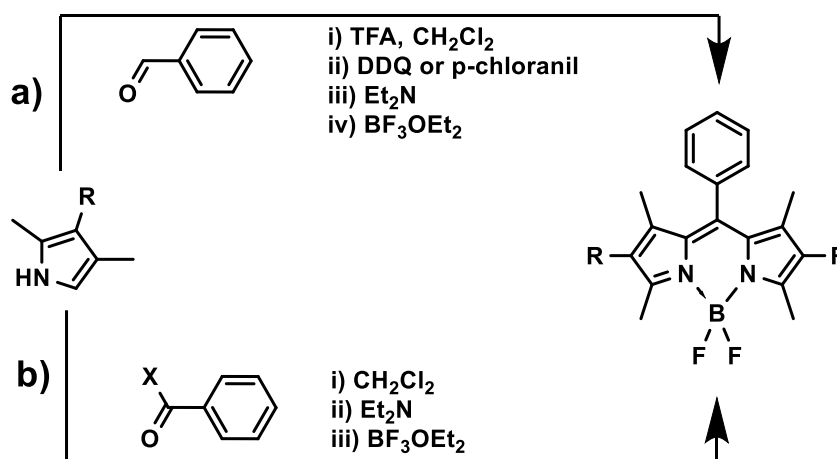


Figure 2-19: Synthesis of meso-substituted BODIPY-dyes via two different synthetic routes.

In general, the usage of acid chloride instead of aldehydes give better yields, but since the structural diversity, sensitivity to moisture and the availability of acid chlorides is limited, the synthetic route in **Figure 2-19 a** is more common. Important to note is that both approaches need to be carried out under inert conditions and require reaction times ranging from several hours to several days with moderate yields.

Another route for the synthesis of BODIPY dyes includes a simple one-pot condensation of pyrrole-carbaldehyde with the use of POCl_3 . Products formed via this synthetic route are usually obtained in high yields and little effort in purification is needed.

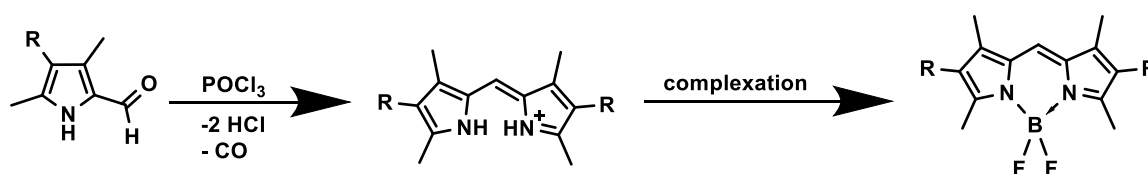


Figure 2-20: Condensation of pyrrole-carbaldehydes in a one-pot reaction yields to BODIPY dyes.

The chemical robustness of BODIPY dyes allows several modifications, ranging from reduction, oxidation and nucleophilic substitution reactions. Also the boron center can be

extended to a conjugated system which enables an enormous potential in structural design and tuning properties of BODIPY dyes.^{132,133}

In order to synthesize analyte sensitive dyes, two main synthetic routes are available and shown in **Figure 2-21**. The first strategy uses an aromatic aldehyde, which is already connected to a receptor unit. This strategy results in a PET sensitive chromoionophore.^{134,135} In another route an aromatic aldehyde is coupled onto a styrylated BODIPY dye, obtaining an ICT based chromoionophore.^{136,137}

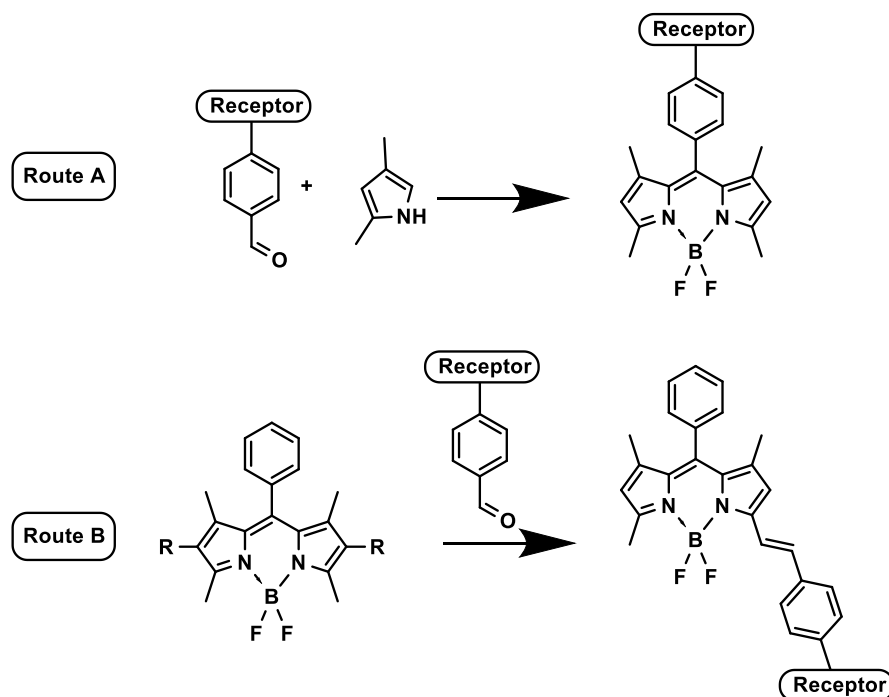
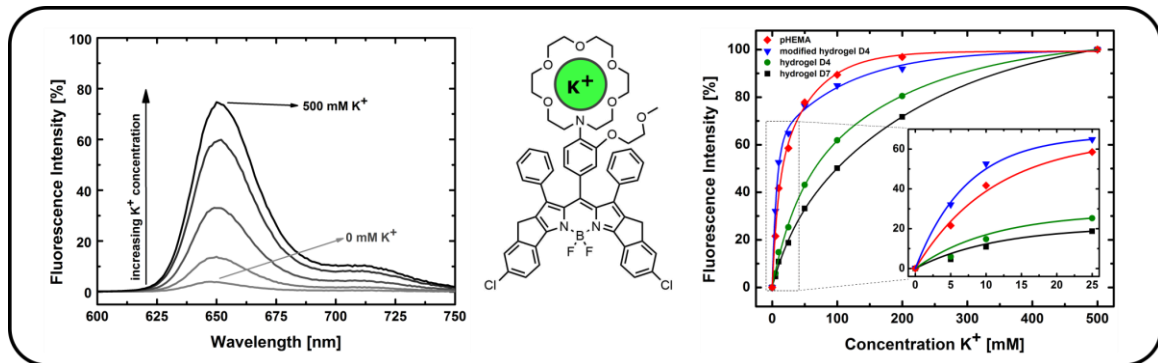


Figure 2-21: Possible synthetic routes for the introduction of analyte sensitive groups incorporated in BODIPY dyes. Route A results in a PET indicator, while route B yields in a ICT based dye.

BODIPYS are due to their beneficial properties (high chemical and photochemical stability, high brightness) and their versatile synthetic strategy an excellent candidate for the design of novel indicators. The synthetic playground of modifications for BODIPY indicators enables fine tuning of indicators and is the driving force for the development of new fluorescent cation indicators.

3. Tuning the sensitivity of fluoroionophore-based K^+ sensors via variation of polymer matrix: a comparative study



3.1. Preface for the Manuscript

This manuscript was published as Full Paper in *Sensors and Actuators B: Chemical* and focuses on the influence of the polymer matrix on the performance and sensitivity of optical potassium sensors.

In this manuscript, the effects of polymer nature on the sensing properties like stability, sensitivity, fluorescence brightness and response time are investigated (**Section 2.5**). On this purpose a previously reported FI3¹¹⁷ is used. It is composed of a highly selective phenylaza-[18]crown-6-lariat-ether receptor reported by Ast et al.¹¹⁵ and red-light emitting π -extended BODIPY fluorophore. It features high fluorescence brightness and good modulation of fluorescent properties by the receptor (**Chapter 2.8**). Additionally, its amphiphilic character allows non-covalent immobilization in hydrogels without leaching¹¹⁷, which is important for polymer screening studies.

The effects and influence of the polymer matrix (**Section 2.7.3**) on the sensing properties of the recently published “FI3”¹¹⁷ is investigated in this manuscript. Sensor foils were investigated according to their sensing dynamics (dissociation constant; K_d), response times (t_{90}), quantum yield (QY) in different polymer matrices including polyurethane hydrogels, pHEMA and hydrogels containing negatively-charged additives, which show how hydrophilicity of the materials and additional charges influence the K_d value. Additionally, hydrogel and pHEMA blends reveal that the K_d can be easily adjusted via the variation of different hydrogels and the amount of pHEMA within the foils.

This study demonstrates the fundamental role of the polymer matrix on characteristics of the solid-state optical potassium sensors and provides the guidelines for general design of ion sensors with improved characteristics.

Tuning the sensitivity of fluoroionophore-based K⁺ sensors via variation of polymer matrix: a comparative study

This manuscript was published as *Full Paper* in

Sensors and Actuators B: Chemical, 2020, 312, 127940.

doi: 10.1016/j.snb.2020.127940

Authors: Lukas Tribuser, Sergey M. Borisov, Ingo Klimant

Institute of Analytical Chemistry and Food Chemistry, Graz University of Technology, Stremayrgasse 9, 8010 Graz, Austria

***Corresponding author:** sergey.borisov@tugraz.at

Keywords: hydrogel, optical sensor, BODIPY, fluoroionophore, potassium, fluorescence

Highlights

- New fluorescent sensors for potassium are prepared and characterized.
- Systematic tuning of the sensitivity via variation of the matrix polymer and additives becomes possible.
- The sensitivity is enhanced in more hydrophilic polymers and polymers containing negatively-charged groups.
- Materials with improved sensitivity are promising for potassium monitoring in whole blood.

3.2. Abstract

Optical sensors are prepared via immobilization of K⁺ fluoroionophore (K⁺FI) into different hydrophilic polymers and their properties (luminescence brightness, stability, sensitivity, cross talk to sodium, dynamic range, response time) are investigated. Depending on the character of the used polymeric matrix, the fluorescence quantum yields for the K⁺-fluoroionophore complex (500 mM K⁺) span from 44% in commercial polyurethane hydrogel (D1) and 18% in poly(2-hydroxyethyl methacrylate). Dynamic intensity measurements show reversibility of the sensors and response times (t_{90}) below 1 min for most of the materials. Blending of poly(2-hydroxyethyl methacrylate) with polyurethane hydrogels is necessary to ensure compatibility of the indicator and the matrix. Comparison of dissociation constants (K_d) reveals moderate sensitivity enhancement in hydrophilic polymers such as polyurethane hydrogel (D1; K_d 51.8 mM) and poly(2-hydroxyethyl methacrylate) (K_d 15.4 mM) compared to previously used hydrogel D4 (K_d 60.4 mM) and drastic increase in the sensitivity upon addition of negatively-charged aliphatic sulfonates ($K_d < 3$ mM). In case of the latter, the enhancement in the sensitivity is significantly lower in presence of sodium ions. Modification of a commercially available polyurethane hydrogel with sulfonate groups enables preparation of stable sensors with improved binding ability (K_d 11.1 mM). This study demonstrates the fundamental role of the polymer matrix on characteristics of the solid-state optical potassium sensors and provides the guidelines for general design of ion sensors with improved characteristics.

3.3. Introduction

The field of optical chemical sensors is growing since decades. Many different sensing platforms, materials and techniques have been developed.^{98,104,126,138,139} and now optical sensors find numerous applications in areas like chemical industry, medicine, biotechnology, marine biology and environmental monitoring to mention only a few.¹⁴⁰ Despite that the word “sensor” became extremely popular to describe molecular probes, the true sensor is significantly more complex in design.¹⁴¹ To be reusable, the indicator has to be immobilized into a (polymeric) matrix, which may also contain additives to enable referenced sensing/imaging, eliminate interferences from ambient light and background fluorescence etc. Compatibility of such materials with compact and inexpensive read-out set-up is also of great importance for sensor design. Apart from the indicator, other

components of the sensing material play a pivotal role in terms of sensitivity, selectivity, response time and stability of the resulting sensor since numerous parameters can affect the sensing properties.¹²⁶

Sensing of K^+ is of highest importance in medicine and biology.^{142–144} Optodes represent a promising alternative to ion-selective electrodes.^{118,145} Most reported optodes are based on a combination of ionophores with pH indicators immobilized into hydrophobic polymers.^{146,147}

Fluoroionophores (FIs) combine the dual function of a selective receptor and a fluorescent reporter and therefore enable a significantly less complex design of a sensing material. Although a few fluoroionophores (FI) for K^+ have been reported, they have been mostly applied as molecular probes for intra- and extracellular sensing^{128,148}. Reversibly operating reusable materials for K^+ monitoring based on immobilized indicators are much rarer. For instance, He et al.¹⁴⁹ covalently immobilized a K^+ fluoroionophore on amino cellulose fibers that were further dispersed in hydrogel D4. Müller et al.¹¹⁷ reported K^+ sensors based on FIs immobilized into polyurethane hydrogel D4, whereas Ast et al.¹¹⁵ utilized a copolymer of acrylamide and acrylonitrile (Hypan) as a sensor matrix. Zhou et al.¹²⁸ investigated several hydrogels including poly(2-hydroxyethyl methacrylate) (pHEMA), its copolymers with acrylamide and copolymers additionally containing positively-charged quaternary ammonium groups and negatively-charged sulfo-groups. They showed increase and decrease of the K_a value in presence of the positively- and negatively-charged groups, respectively. Among these materials only the sensors reported by He et al.¹⁴⁹ and Zhou et al.¹²⁸ showed dynamic range optimal for K^+ monitoring in whole blood since the extracellular K^+ concentration in the human body is regulated between 3.5 and 5 mM¹⁵⁰. Therefore, new sensing materials that exhibit dissociation constants (K_a) within this range or at least approach it are still highly required. Unfortunately, the synthesis of the cryptand-based FI is extremely tedious (> 10 steps). On the other hand, preparation of crown-ether receptors and their combination with various fluorophores is more straightforward but the resulting sensing materials show strong response at significantly higher K^+ concentrations. Although several works were dedicated to correlation of the receptor structure and binding constant^{151,152}, to the best of our knowledge, only the study of Meldrum and co-workers¹²⁸ provides insights on the effect of sensor matrix on the sensing properties.

It should be mentioned that formats of optical ion sensors are not limited to planar optodes and such sensors have been applied successfully on the nanoscale in form of quantum dots¹⁵³, organosilica based particles^{154,155}, polymeric nanospheres^{114,156} etc. to name a few.

In this contribution, the effects of polymer nature on the sensing properties like stability, sensitivity, fluorescence brightness and response time are investigated. For this purpose a previously reported FI₃¹¹⁷ is used (**Figure 3-1**). It is composed of a highly selective phenylaza-[18]crown-6-lariat-ether receptor reported by Ast et al.¹¹⁵ and red-light emitting π -extended BODIPY fluorophore and features high fluorescence brightness and good modulation of fluorescent properties by the receptor. Additionally, its amphiphilic character allows non-covalent immobilization in hydrogels without leaching¹¹⁷, which is important for polymer screening studies. Herein we investigate the photophysical properties and K⁺ response of the FI in different matrices including polyurethane hydrogels, pHEMA and hydrogels containing negatively-charge additives and show how hydrophilicity of the materials and additional charges influence the K_a value.

3.4. Material and Methods

3.4.1. Materials

THF, cyclohexane, TRIS, NaCl, KCl and standard microscope slides were bought from Carl Roth GmbH (www.carlroth.com). Hydrogels (Hydromed D1, D2, D3, D4, D7) were obtained from AdvanSource biomaterials (www.advbiomaterials.com). NaH (60%), propanesultone, sodium 1-octadecanesulfonate, sodium dodecylbenzenesulfonate (hard type) were from TCI (www.tcichemicals.com). Poly(2-hydroxyethyl methacrylate) (pHEMA), poly(N-(2-hydroxypropyl)methacrylamide) (pHPMA), ethyl cellulose (EC49), chlorotrimethylsilane (TMSCl), polyvinylchloride (PVC), dioctyl sebacate (DOS) and sodium dodecylsulfate were purchased from Sigma Aldrich (www.sigmaaldrich.at). Fluoroionophore K⁺FI was prepared according to the literature procedure (“FI 3”)¹¹⁷.

3.4.2. Sensor preparation

A polymer was dissolved in tetrahydrofuran (THF) to obtain a 10 wt% solution. Stock solution of K⁺FI was added to obtain a “cocktail” with 0.2 wt% dye in respect to the polymer. The “cocktail” was vortexed and knife-coated (76 μ m wet film thickness), from BYK-Gardner (www.byk.com) on glass slides that were silanized with trimethylchlorosilane prior to use (see ESI). After evaporation of the solvent the thickness of the foils was measured with an “Inductive Digital Comparator Extramess 2000” from Mahr (www.mahr.com). In average the foils had a thickness of 7.6 \pm 0.2 μ m. Optional

additives were mixed in the sensor “cocktail” before knife-coating. For determination of absolute quantum yields, the same composition was coated on glass disks (\varnothing 8 mm, www.hilgenberg-gmbh.de).

3.4.3. Hydrogel D4 modification

5 g of hydrogel D4 were placed in a 500 mL flame-dried Schlenk tube. 250 mL of dry THF were added and the flask content was stirred for 30 minutes until polymer dissolution. 164 mg of NaH (60%; 4 mmol) were slowly added at room temperature and the solution was stirred for 20 minutes. The solution was heated to 60 °C, stirred at this temperature for 1 h and then cooled to room temperature. 500 mg of 1,3-propanesultone (4 mmol; Warning: extremely toxic!) were dissolved in 10 mL of dry THF and then added dropwise to the solution. The reaction was stirred for 22 h at room temperature. Excess of NaH and 1,3-propanesultone were destroyed by slow addition of 50 mL milliQ water and stirring the solution for another 2 h. The solution was added to 300 mL cyclohexane and the resulting polymer gum was stirred for 30 minutes to remove soluble impurities. The polymer gum was dried under vacuum, dissolved again in THF and precipitated in 300 mL cyclohexane. This washing step was repeated 3 times. The product was dried at 70 °C in the vacuum oven for 24 h. For storage, the hydrogel was stored in an oven at 60 °C to avoid water uptake. IR spectra (**Figure S1**) were recorded on an Alpha Fourier-transform infrared spectroscopy (FTIR) spectrometer (Bruker, www.bruker.com) using an ALPHA's single reflection diamond ATR module. Yield: 4.2 g

3.4.4. Fluorescence Measurements

The sensor slides were placed in a home-made flow through cell and buffer solutions (20 mM TRIS; pH 7.4) containing 0-500 mM K⁺ (0, 5, 10, 25, 50, 100, 200, 500 mM) with 0 or 150 mM Na⁺ background were pumped through the cell. The pumping speed was constant during the measurements (5 mL x min⁻¹). The fluorescence spectra and the kinetic mode measurements were done at RT (~ 23 °C) in front-face mode on a Fluorolog3 spectrofluorometer (Horiba Jobin Yvon). All measurements were performed with the same excitation ($\lambda_{\text{ex}}=580$ nm) and fixed emission wavelength ($\lambda_{\text{em}}=649$ nm), with the same excitation and emission slits. Standard deviation of the normalized fluorescence intensity did not exceed 5% of the value.

3.4.5. Data evaluation

In order to simulate physiologically relevant conditions, the sensors investigated in the range from 0 to 500 mM K⁺ in the absence of Na⁺ and in presence of 150 mM Na⁺ (NaCl) background. This comparison allows estimation of the cross sensitivity of the sensor materials to Na⁺. These values are representative for the corresponding polymer matrix to the K⁺FI. The dissociation constants (K_d) were calculated from the plot of $\log [(I - I_{\min}) / (I_{\max} - I)]$ (y-axis) vs. $\log [K^+]$ (x-axis). This double logarithmic plot gives an x-intercept that is the $\log (K_d)$ expressed in mM K⁺.

3.4.6. Quantum yields measurements

Absolute quantum yields for the immobilized K⁺FI were determined in presence of 0 and 500 mM K⁺ at pH 7.4 and in 0.1 M aqueous HCl. The sensor spots were placed into an integrating sphere from Horiba with the compartment under the spot filled with the corresponding buffer that was in direct contact with the sensing layer. Error in the determination of the quantum yields did not exceed 10% of the value.

3.4.7. Response times

Response times (t_{90}) are calculated between 0 and 5 mM K⁺ for measurements with 150 mM Na⁺ background.

3.5. Results and Discussion

3.5.1. Response mechanism

The fluoroionophore¹²⁷ used in this study is shown in Figure 3-1

Figure 3-1. The indicator is based on a N-phenylaza-18-crown-6-lariat-ether receptor, which is connected to a π -extended borondipyrromethene (BODIPY) chromophore. The sensing principle is fluorescence quenching in the absence of K^+ due to photoinduced electron transfer (PET) from the receptor to the chromophore (**Figure 3-1**). The ionophore bears a tertiary amine group that enables fluorescence enhancement due to the reduction of the PET upon complexation with K^+ ions.¹²⁰ Such fluoroionophores operate in aqueous solutions and in solvents and polymeric matrices containing some amount of water.^{117,128,157} Importantly, the aromatic character of the fluoroionophore results in comparably low pK_a value of 3.2¹¹⁷ so that the intrinsic pH sensitivity of the fluorophore does not interfere with potassium measurement in the whole blood.

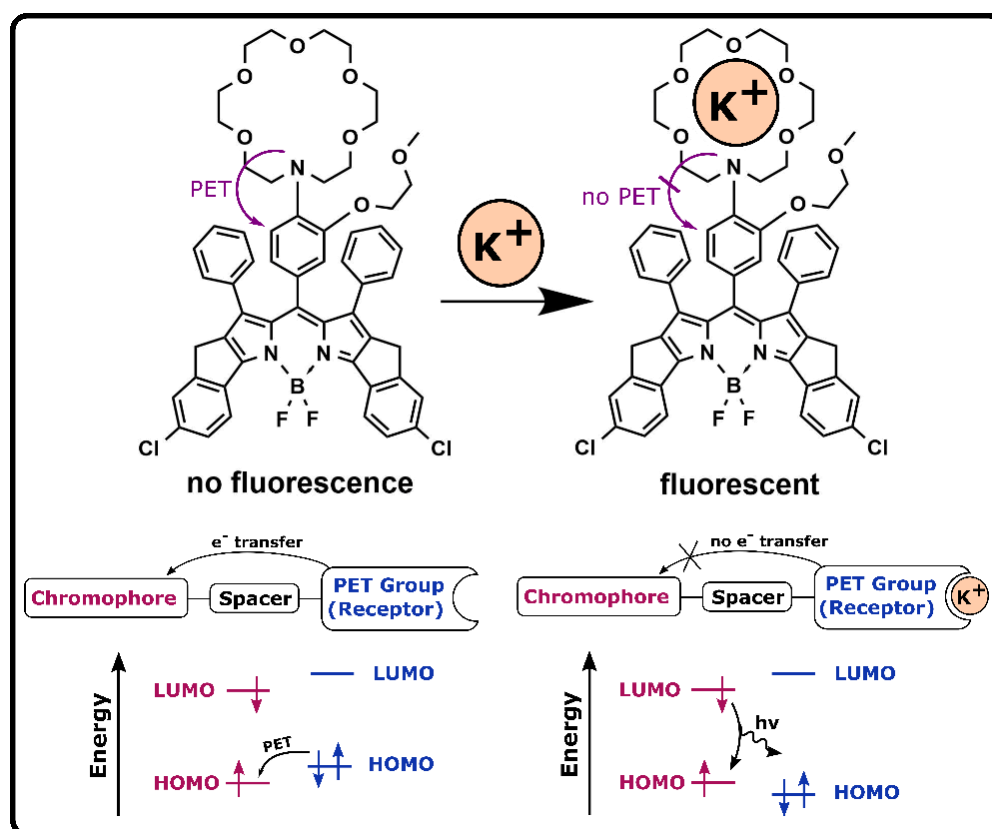


Figure 3-1: Chemical structure of the fluoroionophore and schematic illustration of the response mechanism. Via complexation of the analyte the HOMO of the receptor is energetically reduced which enhances the fluorescence emission.

3.5.2. Choice of materials

Immobilization of the indicator into a (polymer) matrix is essential for reusable character of the sensor. The matrix acts as a solvent and a support for the immobilized FI and should enable good diffusion of K⁺ for fast response. The hydrophilic polymers typically bear polar groups (e.g. carbamate, alcohol) that may weakly coordinate to the free/complexed ion and therefore affect the stability constant. Importantly, to ensure the stability of the sensing material, the polymer should be insoluble in water. This condition discards polymers like poly(vinyl alcohol), poly(vinyl pyrrolidone), non-cross-linked poly(acryl amide) etc. Therefore, the choice was limited to several homopolymers and copolymers, which form mechanically stable hydrogels in water. Among them polyurethane hydrogels and pHEMA represent widely established matrices for immobilization of pH indicators^{129,158–160} and were selected for this study as well. A classical plasticized poly(vinyl chloride) matrix was also used for referencing purposes.

3.5.3. Polyurethane hydrogels

Polyurethane hydrogel D4 is commercially available from AdvanSource biomaterials and has been widely applied for pH sensing.^{129,155,157–164} It was demonstrated to be a suitable matrix for immobilization of potassium^{150,153} and sodium^{118,146} fluoroionophores. The same company also offers other polyurethane hydrogels with varying water uptake and linear expansion (**Table 3-1**). Although the exact structure of the material is not disclosed, it is described as a combination of alternating blocks of hard and soft segments.^{165,166} The hydrophobic part is formed via the reaction of cycloaliphatic diisocyanate with a diol (butandiol or poly(tetrahydrofuran)) whereas the soft hydrophilic segments are built by poly(ethylene glycol) blocks. Due to their hard and soft alternating blocks, such polyurethanes are mechanically strong, tear resistant and show a good flex life. These properties make such hydrogels suitable as hydrophilic sensor matrices. Due to their physically cross-linked character, they are insoluble in water.

Fluorescence response of K⁺FI in hydrogel D4 is exemplified in **Figure 2-1 a**. By protonating the dye with 0.1 M HCl, a slight bathochromic shift is observed. This effect occurs because the receptor is not completely electronically decoupled from the fluorophore resulting in intramolecular charge transfer (ICT) from the amino group to the chromophore. **Figure 3-2 b** shows the corresponding kinetic measurement illustrating the fully reversible character of the response. In contrast, when the indicator is

immobilized into a classical hydrophobic matrix composed of poly(vinyl chloride) (PVC) plasticized with dioctyl sebacate (DOS, 1:1 w/w), hardly any response is observed (**Figure 3-2 b**). In fact, PET effect was inhibited in the apolar environment and the fluorescence was “switched on” already in the absence of the analyte. This observation correlates well with the highest difference between the fluorescence quantum yields of the neutral and protonated forms of the dye observed in polar solvents (particularly their mixtures with water, **Table 2-1**) although non-identical “switch on” mechanism (coordination of K^+ vs. protonation) makes the comparison more difficult. Overall, these data and the experiment with plasticized PVC indicate that operation principle of the fluoroionophore in hydrophilic matrices is significantly different from other ionophore-based optical sensors that relies on an ion exchange mechanism and pH sensitive indicators as transducers.^{85,147}

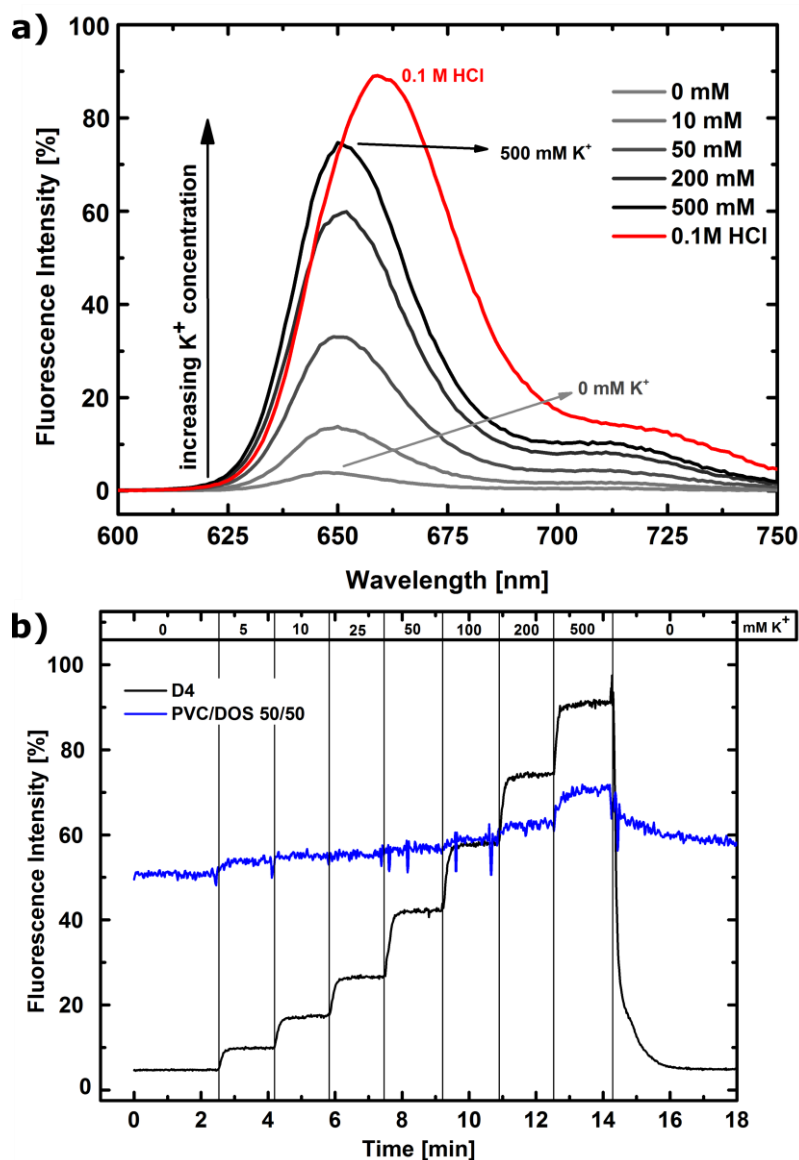


Figure 3-2: **a)** Emission Spectra of the K⁺FI in hydrogel (D4) at different K⁺ concentrations. Upon protonation with 0.1 M HCl K⁺FI is fully "switched on". **b)** Dynamic response of the indicator in polyurethane hydrogel D4 and PVC/DOS matrix.

Different hydrophilicity of commercially available polyurethane hydrogel is expected to influence the response characteristics of the FI in these matrices. The response in five polyurethane hydrogels is shown in **Figure 3-3**. Comparison of K_d values (**Table 3-1**) reveals better complexation in hydrogels with high water content and linear expansion: D1 ($K_d = 51.8$ mM) and D3 ($K_d = 54.5$ mM). The K_d rises with decreasing water amount, hydrogels D7 and D2 showing the worst binding affinity ($K_d = 92.0$ and 89.0 mM, respectively). Hydrogel D4 occupies intermediate position ($K_d = 60.4$ mM). Response times (t_{90}) are fast (<30 s). Hydrogel D1 (26 s) shows the slowest response time, whereas D7 (11 s) the fastest. This appears to be in contrast to the expectation of faster response in hydrogels with the highest water content due to faster diffusion of ions in polar media.

However, only the thickness of the dry sensing layers is identical for all the materials ($\sim 7.6 \mu\text{m}$). Due to different water uptake of the hydrogels the foils have a different layer thickness in the swollen state varying from about $11 \mu\text{m}$ in case of D7 to about $25 \mu\text{m}$ for D1, which explains the experimental results.

In case of hydrogels D1, D3 and D4 addition of 500 mM K^+ results in the fluorescence increase to about 55-58% of the maximum value achieved by protonation of the receptor in 0.1 M HCl . Whereas protonation of the receptor is expected to completely inhibit photoinduced electron transfer, the complexation with K^+ results only in partial inhibition. For hydrogels D2 and D7 in presence of 500 mM K^+ , the fluorescence is “switched on” only to about 32-35% of the maximum value which correlates well to higher K_a in these matrices. Interestingly, the fluorescence quantum yield in D2 in the protonated form is only 40% compared to about 75% in other hydrogels indicating that either partial aggregation of the dye takes place or it may localize in very hydrophobic domains of the hydrogel which have strongly reduced proton permeability. Despite some improvement achieved in hydrogel D1, the evaluated K_a values for commercial hydrogels are still too high for blood measurements since the extracellular K^+ concentration in the human body is regulated between 3.5 and 5 mM.

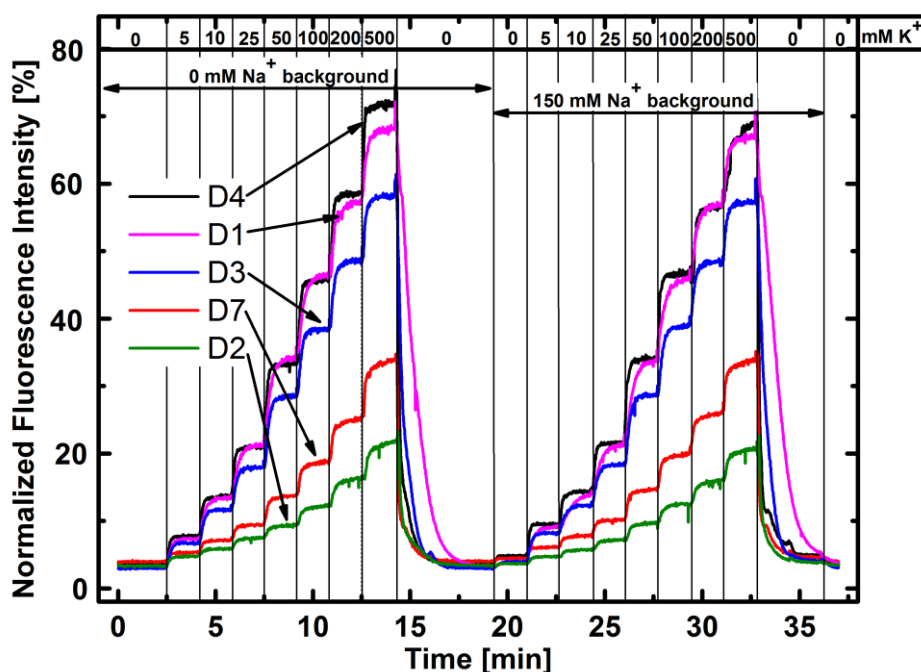


Figure 3-3: Dynamic response of hydrogel-immobilized K^+FI to K^+ in the absence of Na^+ background and with 150 mM Na^+ background.

Table 3-1: Sensing properties of the K⁺FI immobilized into different polyurethane hydrogels.

Hydrogel	D1	D2	D3	D4	D7
linear expansion [%] ^(a)	45	25	40	50	10
water content [%] ^(a)	70	55	60	50	30
QY at 0 mM K ⁺ [%]	< 3	< 3	< 3	< 3	< 3
QY at 500 mM K ⁺ [%]	44	14	42	42	24
QY at 0.1 M HCl [%]	76	40	73	77	76
t ₉₀ [s]	26	19	21	13	11
K _d [mM]	51.8	89.0	54.5	60.4	92.0
K _d with 150 mM Na ⁺ background	51.5	86.0	52.7	55.0	85.2

(a) Source: AdvanSource biomaterials

Since the K⁺FI shows different sensing properties in various hydrogels, their blends were tested in order to investigate if the K_d can be systematically varied. Since the hydrogels consist of different amounts of hydrophilic and hydrophobic compartments, the full miscibility is not guaranteed and the K_d trend for the hydrogels blends must not always show a linear behavior. For this reason, D1 and D7, which show the lowest and the highest K_d, respectively, were mixed in different ratios. The binding affinity excellently correlates with the water uptake of the corresponding hydrogels and mixtures (**Figure S 3-3 a**, **Table S 3.7-2**). The plot of the fluorescence intensity vs. K⁺ concentration reveals the highest slope (i.e. highest sensitivity) for K⁺FI immobilized in hydrogel D1 and the smallest slope for the hydrogel D7 whereas the blends occupy intermediate position. From 100% D1 to 100% D7 the K_d is rising gradually from 51.8 mM up to 92.0 mM (**Figure S 3-3 b**). A linear behavior indicates that the used hydrogels are fully miscible. In addition, the observed trend in the dynamic response time correlate very well with hydrogel composition (**Table S 3.7-2**) which can be again explained by increase in the thickness of the swollen films with lower content of D7.

3.5.4. Effect of additional negatively-charged groups on binding constant in polyurethane hydrogels

Various materials added into the sensing layer are widely used to modify the properties of optical sensors. For instance, gas and ion permeability of the polymers is modified by addition of plasticizers and addition of scattering particles such as TiO₂ particles is a common strategy to enhance sensor brightness,^{161,162} Zhou et al.¹²⁸ showed that negatively-charged sulfonic acid groups can enhance the binding stabilities for potassium in pHEMA

foils, making them more suitable for extracellular K^+ sensing. Since the complex of the fluoroionophore and K^+ is cationic, negatively charged additives are expected to favor the complexation whereas the positively charged additives should have an opposite effect. In fact, we have previously shown that the K_d value in positively-charged RL-100 polymer increases by about 3-fold compared to hydrogel D4.¹¹⁷

Here the effect of long chain aliphatic sulfonates, namely sodiumdodecylsulfate ($NaC_{12}H_{25}SO_4$), sodium dodecylbenzenesulfonate ($NaC_{18}H_{29}SO_3$) and sodium octadecanesulfonate ($NaC_{18}H_{37}SO_3$), on sensing properties of D4-immobilized K^+ FI was investigated (**Figure 3-4, Table 3-2**). These additives were added to the sensing layer in 99:1 molar ratio in respect to the K^+ FI. Without a sodium background, additives cause a tremendous increase in sensitivity compared to hydrogel D4 (**Figure S 3-4, Table S 3.7-3**). In fact, the K_d values of 2.6 and 2.7 were estimated for D4-doped with $C_{12}H_{25}SO_4^-$ and $C_{18}H_{37}SO_3^-$, respectively. Addition of $C_{18}H_{29}SO_3^-$ resulted in full sensor response already at 5 mM K^+ making calculation of K_d impossible (**Figure S 3-4b**). It is assumed that the additives (i) increase K^+ concentration in the foils via extraction and Na^+ exchange and (ii) promote stabilization of the resulting FI- K^+ complex via electrostatic interaction. The response times for the materials with additives are up to 5 times higher than for D4 foils indicating that the equilibrium state is reached slower. The complexation with K^+ results in formation of ion pair with the additive and may promote migration of the ion pair in different domains of the hydrogel.

Unfortunately, a dramatic increase of K_d is observed in presence of 150 mM Na^+ (**Table 3-2; Figure S 3-4 b**). Note that there is hardly any cross-sensitivity to Na^+ in case of D4 without additives. Nevertheless, in case of $C_{18}H_{29}SO_3^-$ additive and 150 mM Na^+ background the K_d value is still quite low (9.2 mM). Comparison of the fluorescence intensity without sodium background and in presence of 150 mM Na^+ allows quantification of this cross-talk recalculated for K^+ concentration (**Table S 3.7-3**). For instance, at 0 mM K^+ , the deviation is positive: 0.11 mM K^+ for D4 without additives, 0.2 mM K^+ for $C_{12}H_{25}SO_4^-$ and $C_{18}H_{29}SO_3^-$ and 0.13 mM for $C_{18}H_{37}SO_3^-$. At 5 mM K^+ and 150 mM Na^+ background the deviation is very high (-4.24 to -4.58 mM K^+) i.e. 0.76 mM K^+ would be measured instead of 5 mM K^+ with the same material if the calibration function established without Na^+ background is applied. On the other hand, such drastic changes are not observed if concentration of sodium ions is varied only minor (110 – 170 mM) which is the realistic range for fluctuations in whole blood (**Figure 3-4 b**). At

3. Tuning the sensitivity of fluoroionophore-based K⁺ sensors via variation of polymer matrix: a comparative study

0 mM K⁺ a slight increase in intensity with increasing Na⁺ concentration is observed. In presence of 5, 10 and 25 mM of K⁺ the effect is opposite and an increase of Na⁺ concentration results in decrease of the fluorescence intensity in case of materials containing C₁₈H₂₉SO₃⁻ and C₁₂H₂₅SO₄⁻ but not for C₁₈H₃₇SO₄⁻ (**Table S 3.7-4 d**). Although similar enhancement of sensitivity of K⁺ sensors in presence of negatively-charged groups has been demonstrated by Zhou et al.¹²⁸, the influence of interfering ions on the sensing properties was not studied.

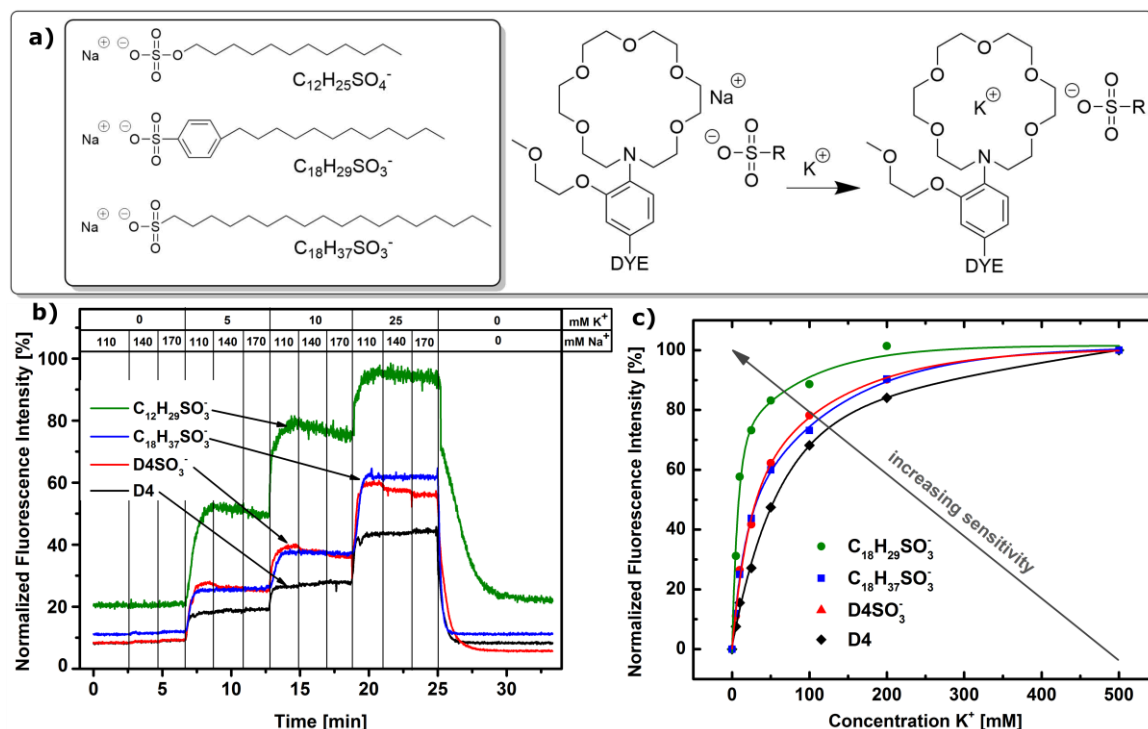


Figure 3-4: a) Chemical structures of the additives and schematic representation of the effect of negatively charged groups. b) Effect of sodium on the sensing properties at different K⁺ concentrations. c) Dependency of the fluorescence intensity of K⁺FI immobilized in D4 and modified D4 on C(K⁺).

Table 3-2: Effect of additives on the sensing properties of D4-immobilized K⁺FI.

Polymer	D4	C ₁₂ H ₂₅ SO ₄ ⁻	C ₁₈ H ₂₉ SO ₃ ⁻	C ₁₈ H ₃₇ SO ₃ ⁻	D4-SO ₃ ⁻
QY [0 mM K ⁺]	< 3	< 3	< 3	< 3	< 3
QY [500 mM K ⁺]	42	55	51	37	39
QY [0.1 M HCl]	77	76	76	74	62
t ₉₀ [s]	13	41	64	66	25
K _d [mM]	60.4	2.6	n.d.	2.7	11.1
K _d with 150 mM Na ⁺ background [mM]	55.0	38.9	9.2	31.4	30.2

The addition of negatively charged additives showed that the sensitivity of the sensors can be significantly improved. This approach is simple and straightforward but leaching of the amphiphilic additives out of the sensor foil cannot be excluded. Modification of the hydrogels with covalently attached negatively-charged groups (sulfonate or carboxylate) represents an interesting opportunity for further improvement. Here we investigate the modification of terminal hydroxyl groups present in the hydrogel via reaction with 1,3-propanesultone in presence of a strong base (NaH) at 60 °C resulting in the formation of terminal sulfonate groups.

As can be seen from **Figure 3-4** and **Figure S 3-5**, modification of the polymer indeed results in significant improvement of the sensitivity compared to unmodified D4. In fact, the K_d value for the modified material in the absence of Na^+ background was found to be 11.1 mM, which is about 6-fold smaller than for unmodified D4. Similar to the results obtained for the additives, K_d increases in presence of Na^+ (**Figure S 3-5 a**, **Table 3-2**, **Table S 3.7-4**). Nevertheless, at 150 mM Na^+ it is still about 2-fold smaller than in D4. The improvement in the sensitivity, however, comes at the cost of some cross talk to Na^+ (**Figure 3-4 b**). With increasing Na^+ concentration, the intensities for the modified material are decreasing, whereas unmodified hydrogel D4 shows an increase in the intensity, reflecting additional (weak) complexation of the FI by Na^+ (**Figure S 3-4 b**). It should be mentioned that since Na^+ concentration is routinely monitored in blood analysis, such cross talk can be potentially compensated for instance with help of FI bearing a different receptor.¹¹⁸ Importantly, the photophysical properties of K^+ FI in the modified hydrogel are almost identical to D4. The response times doubled but the response is still acceptably fast. The physical properties of the modified hydrogel are very similar to that of the D4 making preparation of homogeneous blends possible. In agreement with the decreased concentration of sulfonate groups in 1:1 (w/w) blend of the two polymers, the sensitivity of the resulting sensing material is between that of D4 and the modified hydrogel (**Table S 3.7-4**).

In conclusion, the investigations of negatively charged sulfonates showed that K_d can be significantly reduced. Measurements with the additive sodium dodecylbenzenesulfonate ($\text{NaC}_{18}\text{H}_{29}\text{SO}_3$) revealed a K_d of 9.2 mM (with 150 mM sodium background) which is already close to the optimum for blood analysis (3.5 to 5 mM K^+). Considering potential application for measurement in whole blood, additives should be treated with caution

3. Tuning the sensitivity of fluoroionophore-based K^+ sensors via variation of polymer matrix: a comparative study

since leaching effects cannot be excluded. Therefore, the modified hydrogel D4 enables a more trustful sensing matrix, albeit on the cost of significantly higher K_d value (30.2 mM).

3.5.5. Poly(2-hydroxyalkyl methacrylates) and their blends

18-crown-6 receptors are known to have good binding affinities in polar solvents like MeOH and EtOH.^{163,164} Consequently, polymers that possess alcohol groups are of much interest. Among them poly(2-hydroxyethyl methacrylate) (pHEMA) is of highest interest due to optimal water uptake of 40%. Since the polarity of the hydrogel may be comparable to solvents like MeOH and EtOH, we expected a relatively low K_d value for the immobilized K^+ FI. Therefore, a sensor material based solely on pHEMA, two materials utilizing blends of pHEMA and D4, and a material utilizing significantly more hydrophobic poly(2-hydroxypropyl methacrylate) (pHPMA) were prepared. The dynamic response of the sensors and the K_d plots are shown in **Figure 3-5** and the sensing properties of the materials are summarized in **Table 3-3**. As expected, a significant improvement (about 4-fold compared to D4) of the K_d is achieved in pHEMA. For pHPMA, the measurement without the sodium background indicated almost complete saturation of the signal at 5 mM K^+ (**Figure S 3-7**) so that the K_d cannot be estimated. Despite excellent binding affinity of K^+ FI in pHEMA and pHPMA, the overall performance of the sensors is far from being optimal. In fact, the fluorescence QYs at 500 mM K^+ were found to be only 18% and 21% for pHEMA and pHPMA, respectively, compared to 42% in D4. The QYs values for pHEMA and pHPMA are only a rough estimation since aggregation of the fluorophore is likely to occur in these polymers. In fact, QY increased only marginally in 0.1 M HCl (22 and 23% for pHEMA and pHPMA, respectively). Moreover, the emission spectra of K^+ FI are broader in pHEMA and pHPMA compared to D4 (**Figure S 3-8** and **Figure S 3-9**) and an increase in the turbidity of the foils was observed over the time (**Figure S 3-10** and **Figure S 3-11**) Modification of FI that allows improving the compatibility with these polymers (e.g. via introducing hydrophilic groups) is likely to represent a promising strategy to obtain materials combining high sensitivity and excellent photophysical properties and stability. Alternatively, covalent coupling of FI to pHEMA is likely to prevent the aggregation. Although strategies for integration of K^+ fluoroionophores into pHEMA are established¹²⁸ such modifications in case BODIPY-based FI are expected to significantly increase synthetic effort.

We found that synthetic modifications are not necessary if the FI is immobilized in blends of pHEMA and D4. In fact, K^+ FI retains high brightness even in the blend of 7:3 w:w of pHEMA:D4 (**Table 3-3**) indicating absence of dye aggregation in this matrix. The fluoroionophore embedded in the mixtures containing 30 and 70% wt. of pHEMA (**Figure**

3-5) in D4 shows K_d values of 43.9 and 28.2 mM, respectively, which are between those of pure pHEMA and pure D4 (15.4 and 60.4 mM, respectively). Due to lower K_d value this material is much better suited for K^+ monitoring in whole blood compared to the material based on D4 and D1 hydrogels. Similar behavior is observed for the materials based on the blends of D4 and pHPMA (**Figure S 3-8**). It can be concluded that blending a hydrophilic polymer, like pHEMA or pHPMA with a copolymer like D4, enables simple and versatile strategy to modify and adapt the sensing properties to the field of application. On the other hand, a K_d value of 28.5 mM (70w% pHEMA in D4) is not yet optimal for blood measurements (3.5 to 5 mM K^+), so that further improvement so that the materials based on pure pHEMA or pHPMA but with increased compatibility with the fluoroionophores remain of great interest.

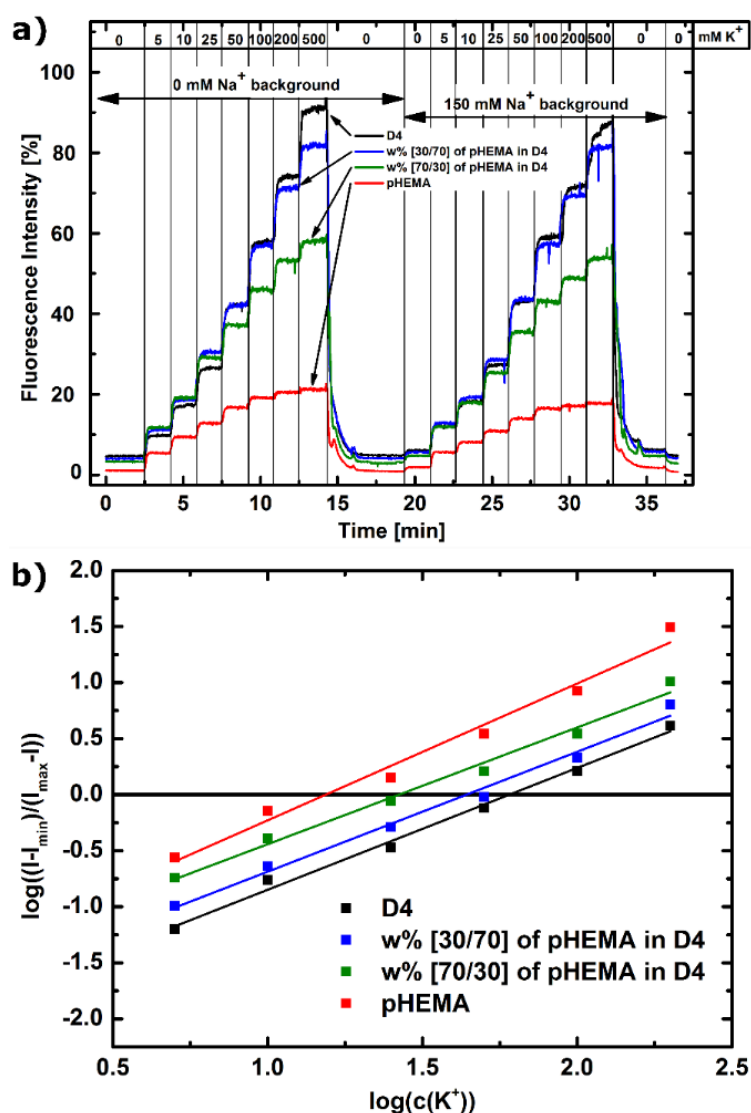


Figure 3-5: **a)** Dynamic response of K^+ FI immobilized in D4, pHEMA and their blends to K^+ in the absence of Na^+ background and with 150 mM Na^+ background. **b)** Double logarithmic plots of $(I-I_{min})/(I_{max}-I)$ vs $C(K^+)$ for the sensor materials for determination of K_d .

Table 3-3: Sensing properties for the K⁺FI immobilized into poly(2-hydroxyalkyl methacrylate) and their blends with hydrogel D4.

Polymer	D4	pHEMA	30w% pHEMA in D4	70w% pHEMA in D4	pHPMA
QY [0 mM K ⁺]	< 3	< 3	< 3	< 3	< 3
QY [500 mM K ⁺]	42	(18)	44	41	(21)
QY [0.1 M HCl]	77	(22)	73	65	(23)
t ₉₀ [s]	13	14	15	13	14
K _d [mM]	60.4	15.4	43.9	26.6	n.d.
K _d with 150 mM Na ⁺ background [mM]	55.0	14.9	46.2	28.5	9.5

3.6. Conclusion

In conclusion, investigation of different hydrophilic polymers as matrices for immobilization of K⁺ fluoroionophore allowed better understanding how the structure of the polymer affects the sensing properties of the resulting materials. We have shown that increasing hydrophilicity of the polyurethane hydrogels results in some improvement of the sensitivity. Introduction of negatively charged sulfonate groups either as an additive or via covalent modification of a polyurethane hydrogel results in a dramatic improvement of the sensitivity, albeit at the cost of strongly increased cross talk to Na⁺. Nevertheless, even at physiologically relevant sodium background, the sensitivity is still better compared to the unmodified hydrogels. Homogenous poly(2-hydroxyalkyl methacrylate) polymers enable very strong improvement in the sensitivity but are poorly compatible to the fluoroionophore that tends to aggregate in these matrices. On the other hand, blends of pHEMA and polyurethane hydrogels yield stable materials with improved sensitivity more adequate for blood measurements. Overall, this work makes it possible to shift the dynamic range of optical K⁺ sensors to the lower concentration range, making the materials better suitable for whole blood measurements without undergoing challenging and time-consuming modification of the receptor. The results are likely to be transferrable to other sensors that utilize fluoroionophores, for instance sensors for sodium, utilizing aza-15-crown-5 receptor.

3. Tuning the sensitivity of fluoroionophore-based K^+ sensors via variation of polymer matrix: a comparative study

3.7. Supporting Information

3.7.1. Glass Slide modification

Glass slides were modified with Chlorotrimethylsilane (TMSCl). Prior to the modification, the glass slides were dried with a heat gun for 5 minutes. After the slides cooled to room temperature, TMSCl was pipetted on the slide and stacked with another glass slide. After 30 minutes the slides were rinsed with EtOH three times and then with milliQ water. The slides were dried for one day at 70 °C. In order to check if the modification worked contact angle measurements were performed. Pictures with a USB-microscope from the company ELV (www.elv.com) were made and the contact angle calculated with an ImageJ software. For the unmodified glass slide, a contact angle of 29° and for the modified 79° was calculated (**Figure S 1a, b**).

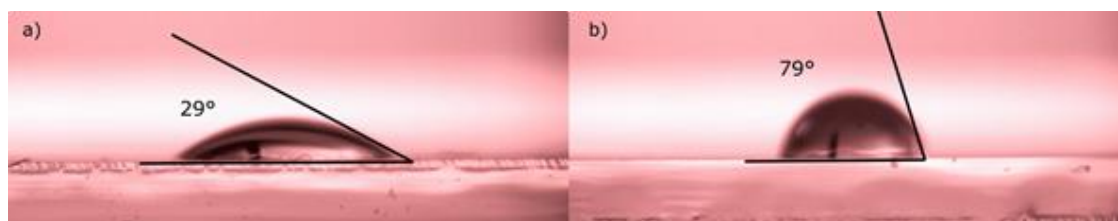


Figure S 3-1: contact angle pictures from an unmodified glass slide (a) and modified glass slide (b).

3.7.2. Hydrogel modification

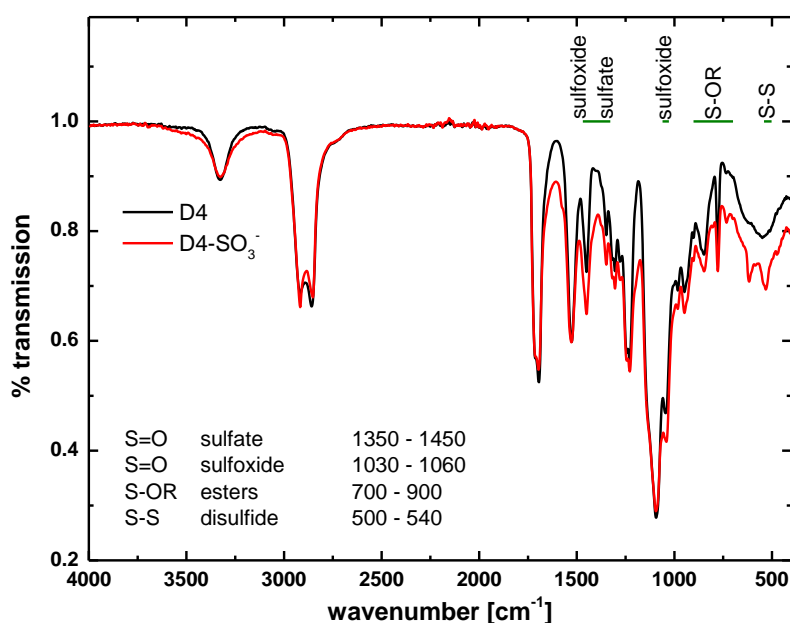


Figure S 3-2: FTIR spectrum of the modified and unmodified hydrogel.

3.7.3. Determination of QY in solvents

Absolute quantum yields for the indicator K⁺FI in different solvent was determined in the protonated and neutral state. Therefore, the indicator was dissolved in 2 mL of the corresponding solvent and the absorption was adjusted to 0.05. The cuvette was placed into an integrating sphere from Horiba and the quantum yield was determined. For characterization of the protonated indicator 3% v/v trifluoroacetic acid (TFA) was added. To ensure that there are no traces of acid in dichloromethane, a base (pyridine or N-ethyl-diisopropylamine DIPEA) was added. Note that the solvents were not dried over molecular sieve which may explain comparably high difference between the QYs in toluene. The error in determination of QYs does not exceed 10%.

Table S 3.7-1: measured absolute QY in different solvents.

Solvent	Additive	QY [%]
THF		5
THF	+ TFA	64
EtOH		7
EtOH	+ TFA	80
MeOH		7
MeOH	+ TFA	91
DCM		25
DCM	+ TFA	20
CHCl₃		15
CHCl₃	+ TFA	30
toluene		9
toluene	+ TFA	65
80% EtOH 20% H₂O		<3
80% EtOH 20% H₂O	+ TFA	86
50% EtOH 50% H₂O		<3
50% EtOH 50% H₂O	+ TFA	89
DCM	+ pyridine	26
DCM	+ DIPEA	22

3.7.4. Hydrogel blends

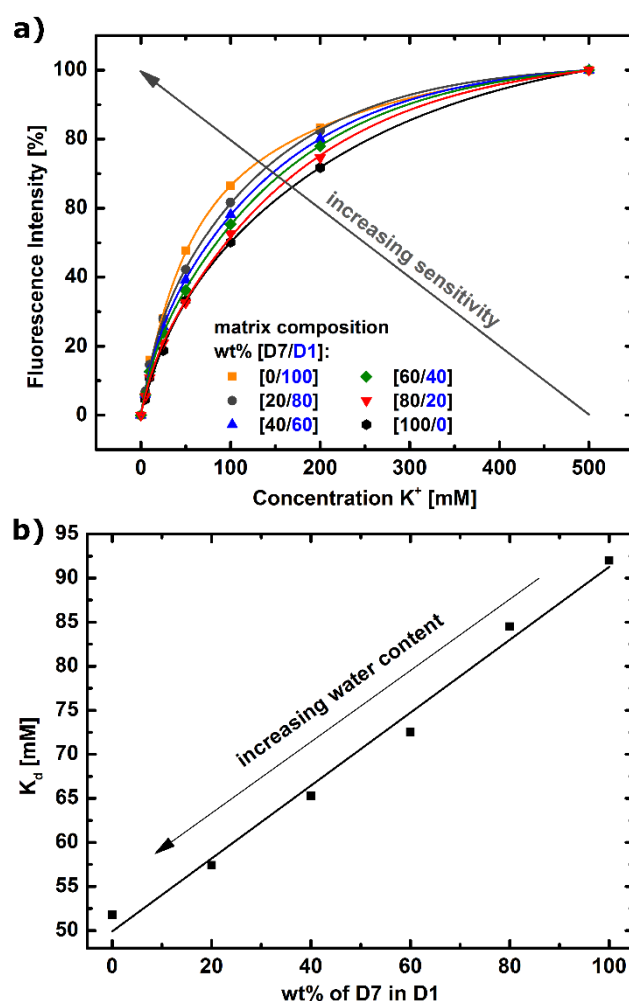


Figure S 3-3: a) Dependency of the fluorescence intensity of K^+ FI immobilized in hydrogel blends on $C(K^+)$. b) Dependency of the dissociation constant [K_d] on blend composition.

Table S 3.7-2: Sensing properties for the K^+ FI immobilized into blends of hydrogel D1 and D7.

Hydrogel	D1	20% D7 + 80% D1	40% D7 + 60% D1	60% D7 + 40% D1	80% D7 + 20% D1	D7
QY [0 mM K^+]	< 3	< 3	< 3	< 3	< 3	< 3
QY [500 mM K^+]	44	41	40	34	35	24
QY [0.1 M HCl]	76	78	82	78	79	76
t_{90} [s]	26	22	13	18	10	11
K_d [mM]	51.8	57.4	65.3	72.5	84.5	92.0
K_d with 150 mM Na^+ background	51.5	55.0	61.1	73.7	78.5	85.2

3. Tuning the sensitivity of fluoroionophore-based K⁺ sensors via variation of polymer matrix: a comparative study

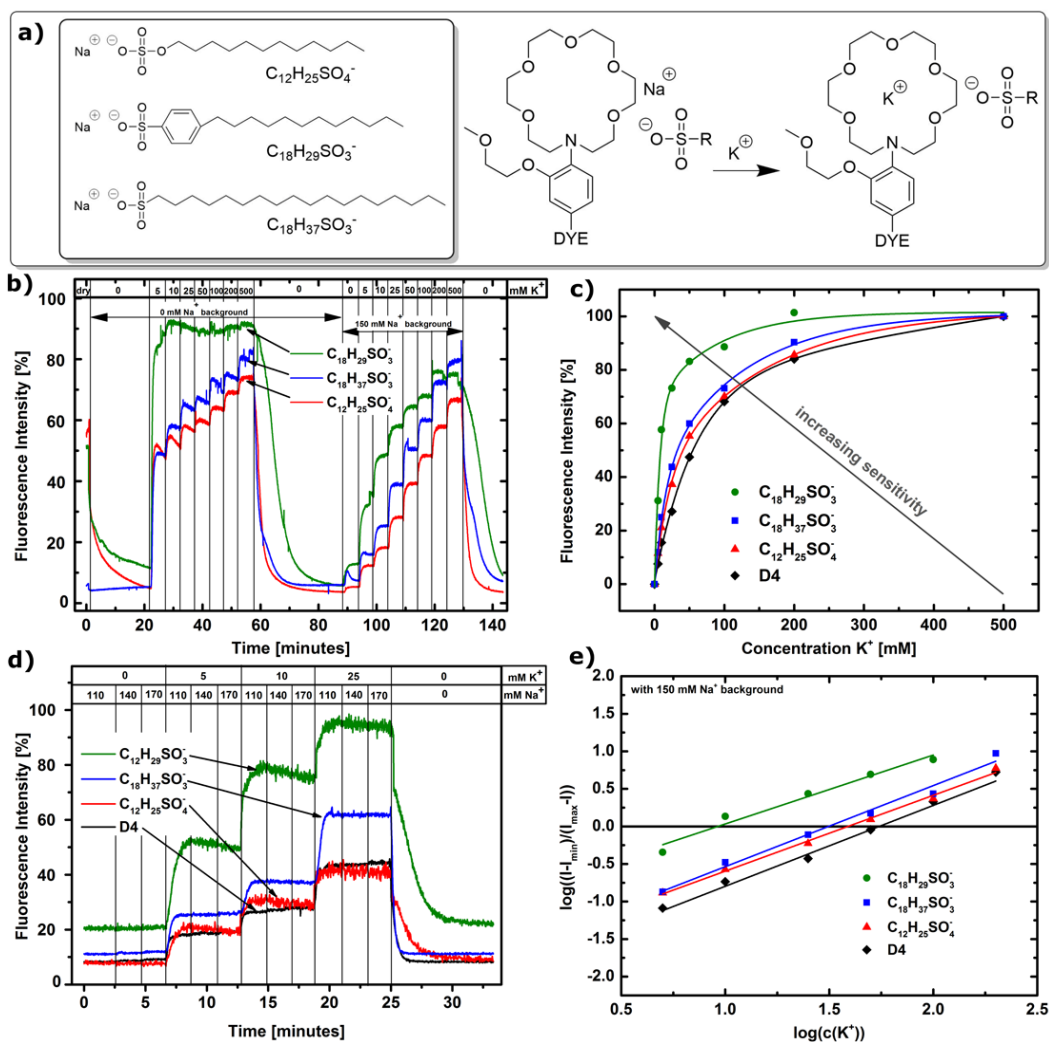


Figure S 3-4: a) Schematic representation of the effect of charged additives. b) Dynamic response of K⁺FI immobilized in D4 along with different long chain aliphatic sulfates and sulfonates to K⁺ in the absence of Na⁺ background and with 150 mM Na⁺ background. c) Dependency of the fluorescence intensity of K⁺FI immobilized in D4 with additives on C(K⁺). d) Effect of sodium on the sensing properties at different concentrations. e) Double logarithmic plots of $\log((I-I_{\min})/(I_{\max}-I))$ vs $\log(c(K^+))$ for the sensor materials for determination of K_d . Additive C₁₈H₂₉SO₃⁻ shows the highest binding affinity.

Table S 3.7-3: Effect of additives on the sensing properties of D4-immobilized K⁺FI.

Polymer	D4	C ₁₂ H ₂₅ SO ₄ ⁻	C ₁₈ H ₂₉ SO ₃ ⁻	C ₁₈ H ₃₇ SO ₃ ⁻
QY [0 mM K ⁺]	< 3	< 3	< 3	< 3
QY [500 mM K ⁺]	42	55	51	37
QY [0.1 M HCl]	77	76	76	74
t ₉₀ [s]	13	41	64	66
K _d [mM]	60.4	2.6	n.d.	2.7
K _d with 150 mM Na ⁺ background [mM]	55.0	38.9	9.2	31.4
error caused by 150 mM Na ⁺ at 0 mM K ⁺ [deviation in mM K ⁺]	0.11	0.02	0.02	0.13
error caused by 150 mM Na ⁺ at 5 mM K ⁺ [deviation in mM K ⁺]	0.80	-4.58	-4.57	-4.24

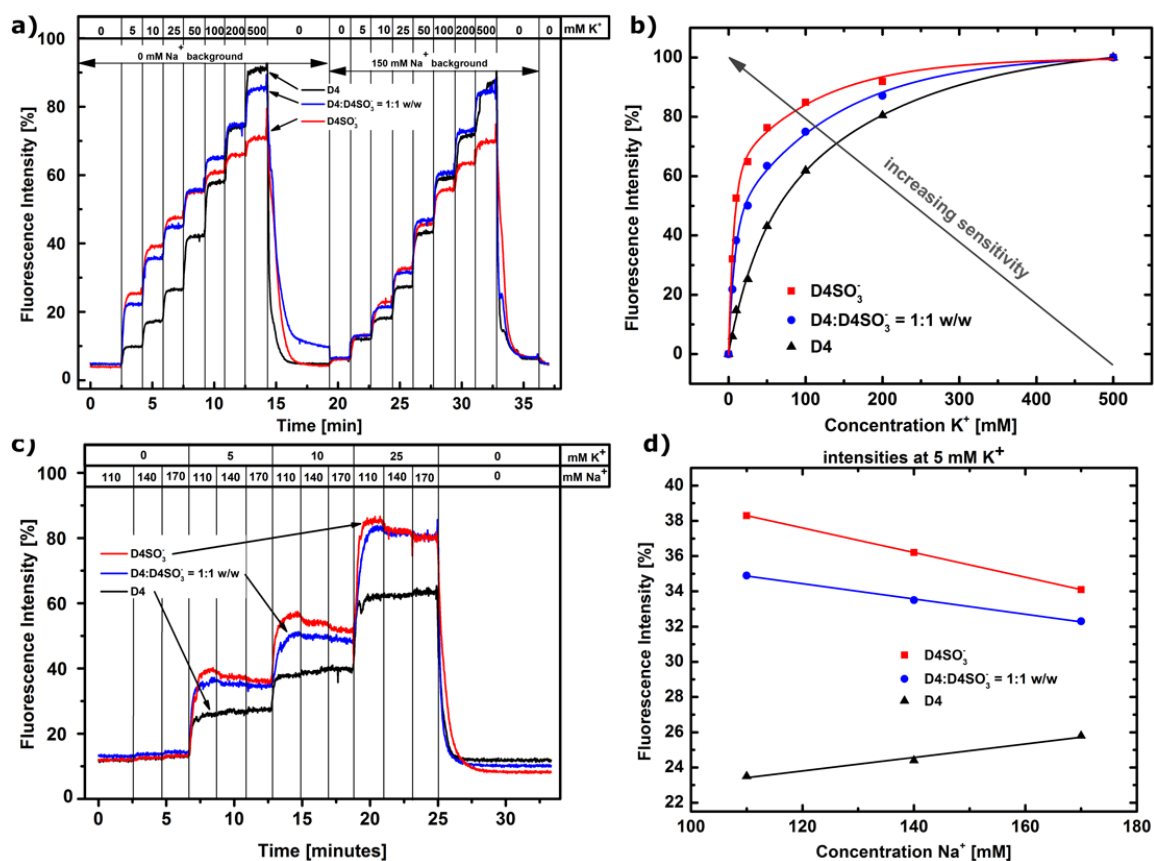


Figure S 3-5: **a)** Dynamic response of K⁺FI immobilized in D4, D4-SO₃⁻ and a 1:1 w/w blend to K⁺. **b)** Dependency of the fluorescence intensity of K⁺FI immobilized in D4 and D4-SO₃⁻ on C(K⁺). **c)** Influence of Na⁺ on the sensing properties at different concentrations. **d)** Intensities of K⁺FI in polyurethane hydrogels with and without negatively charged functionalities.

Table S 3.7-4: Sensing properties of the polyurethane hydrogel modified with SO₃⁻ groups, in comparison with the unmodified version.

Polymer	D4	D4-SO ₃ ⁻	50% D4-SO ₃ ⁻ + 50% D4
QY [0 mM K ⁺]	< 3	< 3	< 3
QY [500 mM K ⁺]	42	39	44
QY [0.1 M HCl]	77	62	76
t ₉₀ [s]	13	25	15
K _d [mM]	60.4	11.1	22.6
K _d with 150 mM Na ⁺ background [mM]	55.0	30.2	44.3
error caused by 150 mM Na ⁺ at 0 mM K ⁺ [deviation in mM K ⁺]	0.11	0.40	0.43
error caused by 150 mM Na ⁺ at 5 mM K ⁺ [deviation in mM K ⁺]	0.80	-3.33	-3.09

3. Tuning the sensitivity of fluoroionophore-based K^+ sensors via variation of polymer matrix: a comparative study

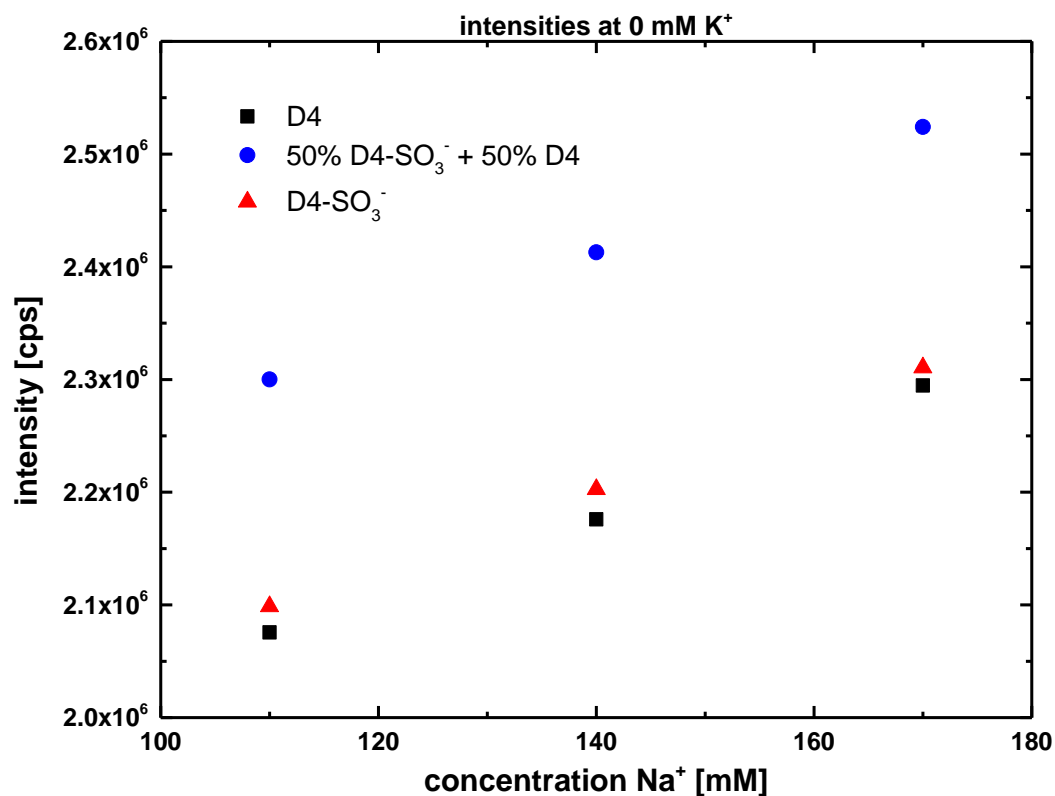


Figure S 3-6: Na^+ concentration [mM] vs. intensity at 0 mM K^+ for hydrogel D4, modified hydrogel D4- SO_3^- and the 1:1 blend. All polymers show an intensity increase with increasing Na^+ concentration.

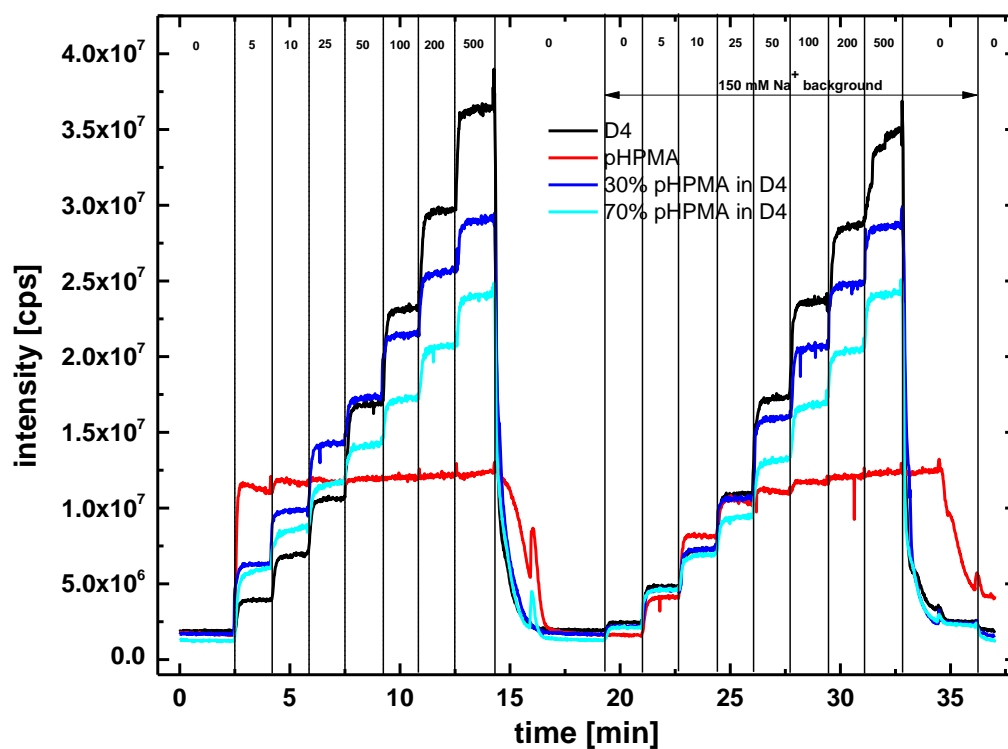


Figure S 3-7: Response of D4, pHPMA and mixtures to K^+ : pHPMA shows low intensities but good binding affinity towards K^+ . Blending of the highly hydrophilic polymer with a copolymer (D4) result in stable material

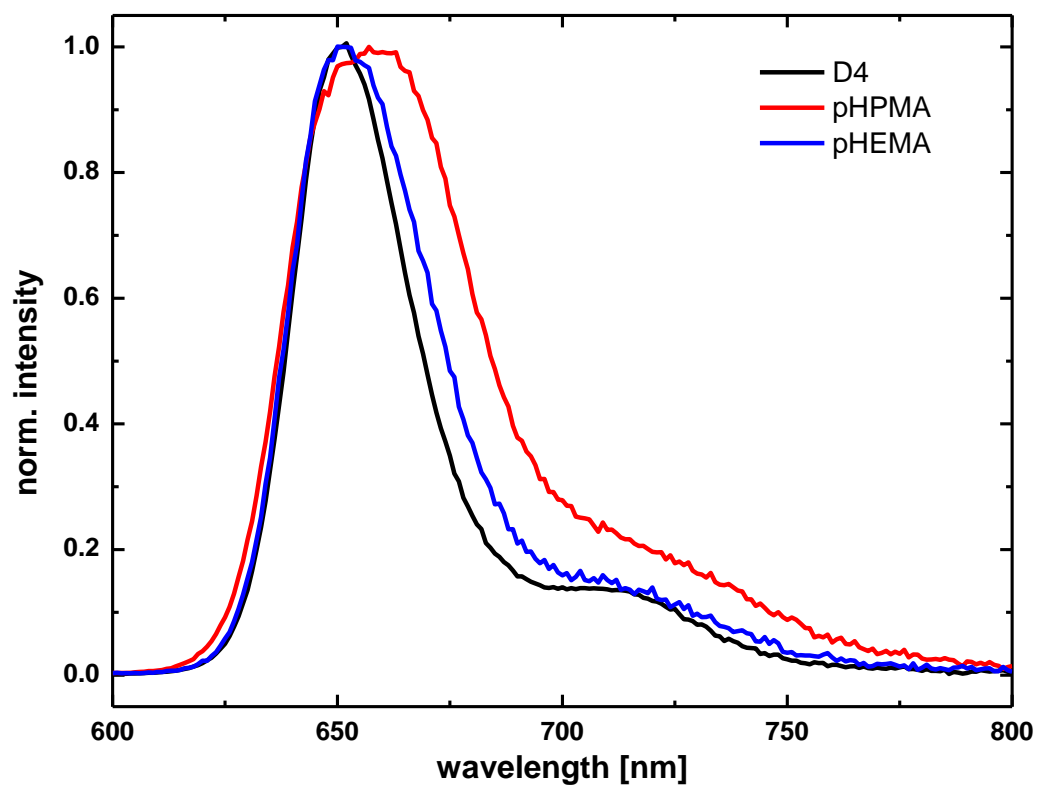


Figure S 3-8: normalized emission intensity of D4, pHPMA and pHEMA upon complexation with 500 mM K⁺. pHPMA shows aggregation phenomena visualized by the broader spectrum showing bathochromic shift.

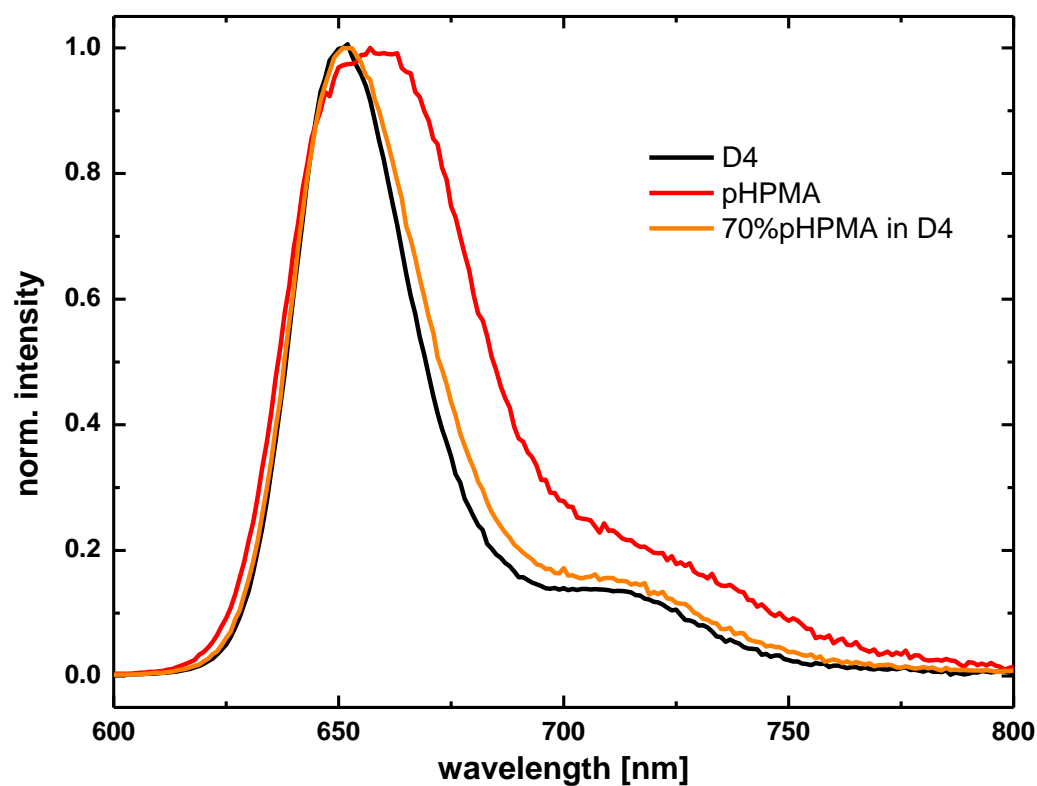


Figure S 3-9: normalized emission intensity of D4, pHPMA and 70% pHEMA in D4 upon complexation with 500 mM K⁺. Aggregation phenomena disappear in polymer blends with hydrogel D4.

3. Tuning the sensitivity of fluoroionophore-based K⁺ sensors via variation of polymer matrix: a comparative study

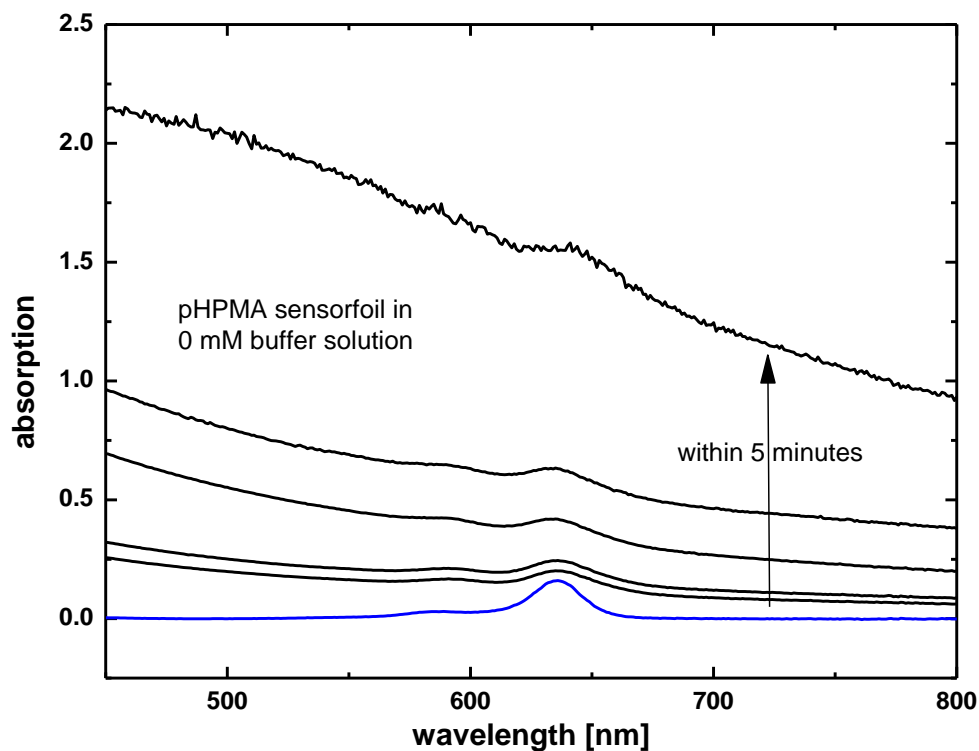


Figure S 3-10: pHPMA sensor layer in 0 mM buffer solution over 5 minutes. The sensor layer increases its turbidity within minutes. The aggregation phenomena seen by emission spectra cannot be visualized by UV/VIS spectrometry due to increasing turbidity.

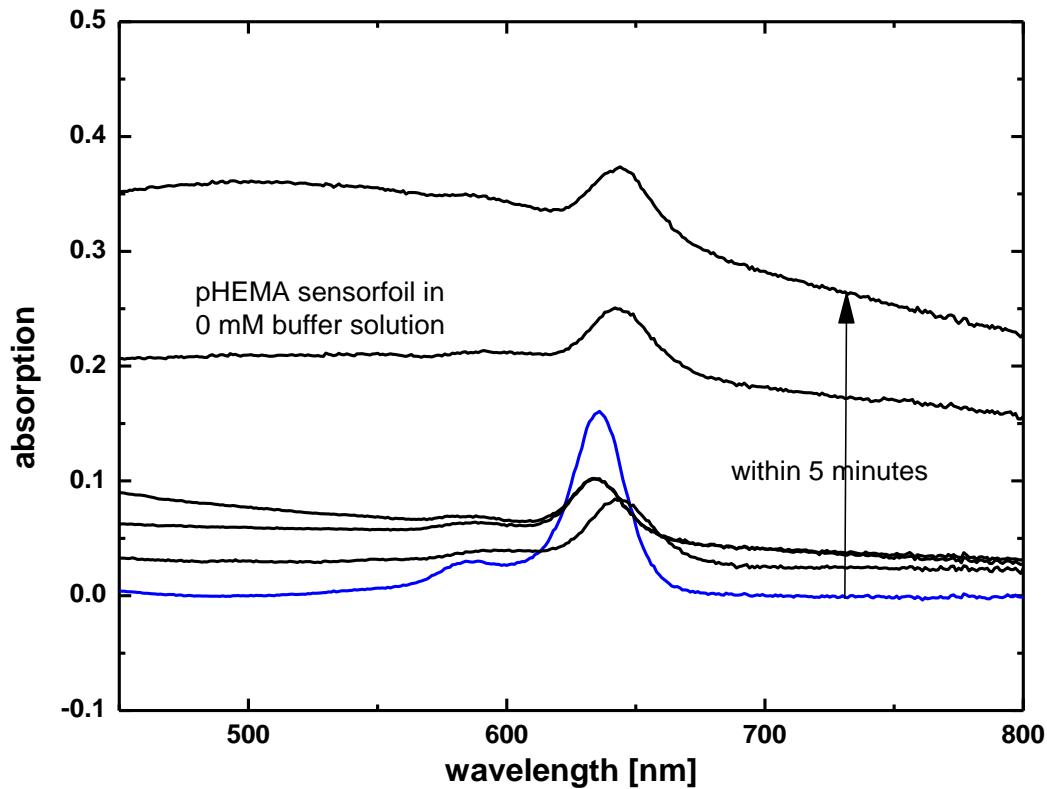
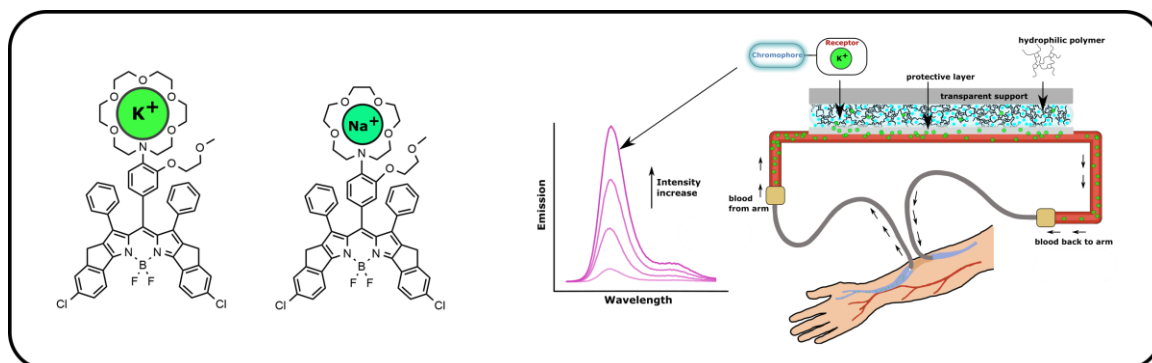


Figure S 3-11: pHEMA sensor layer in 0 mM buffer solution over 5 minutes. The sensor layer increases its turbidity within minutes.

4. Ion Sensors for Whole Blood Analysis



4.1. Preface for the Manuscript

This manuscript is focused on the application of ion sensors for whole blood measurements. The center of attention for this chapter was on tackling the challenges for applying ion sensors for diagnostic applications.

This part focuses on the development of a suitable DLR sensing system (**Chapter 4.3.1**) for ion sensors. The main properties of the BODIPY fluoroionophores are described in **Chapter 2.8**. Sub-sections of this chapter include the dependency and amount of reference used for the sensing system since type and amount of Egyptian blue and CrGAB drastically influence the resolution, in the physiological relevant concentration range. Concerning additives (references and TiO₂) in general, a hydrophilization technique (ARGET ATRP) was applied to achieve better homogenization of sensing cocktails, resulting in a better reproducibility for the production of ion sensors. For this project, a novel fluoroionophore with lipophilic chains on the dye moiety was synthesized. Previous investigations showed that pHEMA represents a perfect matrix for ion complexation (**Section 2.6.1**), but the BODIPY dyes tend to aggregate within this matrix due to their high hydrophobicity. Therefore, the aim was to synthesize a new fluoroionophore with a higher hydrophilicity that prevents aggregation in pHEMA. The indicator tended to be a better suited candidate but still showed some aggregation phenomena. Nevertheless, the indicator showed a better sensitivity in commercial hydrogels than previously used indicators. The usage of CrGAB as reference enabled the possibility to excite the sensing components in the blue visible spectrum, since BODIPY dyes also have an excitation band in the blue region. For an application in diagnostic areas, important parameters were checked to obtain a reliable sensing system for ions. Parameters like photostability, dynamics of the fluoroionophore, signal to noise ratios, storage capability, effect of modulation frequency and amount of referenced were optimized to an optimum.

Since fluoroionophores were used for this project and blood temperatures vary, the temperature effect of the indicators (**Chapter 2.2**) has to be compensated. After evaluation of the best sensing composition, temperature calibrations were performed to evaluate the temperature coefficients needed to obtain reliable ion concentrations, measured in the solutions.

Since the aim was to produce sensors for whole blood measurements, and the sensing layer is in direct contact with the media, sterilization tests were performed, to guarantee a non-

toxic sensor, which is applied in human body. Sterilization tests showed that during radiation sterilization the fluoroionophore gets partly destroyed. Therefore, ascorbic acid was added to the sensing layer, which acts as a scavenger for radicals, enabling a reproducible, reliable sensing system.

4.2. Abstract

Here, an improved DLR sensing system using fluoroionophores and phosphorescent pigments is developed. The phase angle difference for a potassium-DLR system at 37 °C was improved from 0.27° to 0.71°, within the physiological relevant concentration range (3-6 mM K⁺). The usage of the phosphorescent pigment CrGAB as a reference enabled the excitation with blue light with enhanced signal to noise ratios. Previous sensing setups used Egyptian Blue ($\lambda_{\text{ex}}=594$ nm) as a reference, revealing a signal to noise ratio of 1:42, whereas CrGAB ($\lambda_{\text{ex}}=430$ nm) a ratio of 1:100. Via a simple polymerization technique called activators regenerated by electron transfer atom transfer radical polymerization (ARGET ATRP) additives were modified, to obtain particles with a higher hydrophilicity. This modification enables better homogenization of sensor cocktails and enhanced the reproducibility. Calibrations were performed with different modulation frequencies, whereas with 0.2 w% fluoroionophore (FI) in respect to the amount hydrogel used, at 1917 Hz, a total phase shift of 4.32° was measured and at 4000 Hz a phase shift of 7.87°. An additional increase in the amount fluoroionophore immobilized in the sensing foil (0.4 w%), yields in a phase shift of 9.21°. Storage tests were performed for evaluation of the shelf life of the sensing foils and revealed stable and reversible sensing dynamics within 188 days. Photobleaching test, whereby the foil was permanently exposed to the excitation source for 5.5 hours, revealed a stable sensing system. A pulsing time of 100 ms corresponds to 200,000 measurement points. Temperature coefficients for sodium and potassium fluoroionophores were determined via calibrations from 32 to 39 °C. Radiative sterilization tests were performed with ascorbic acids, whereas a concentration of 10% of scavenger is needed, to guarantee stable sensing calibrations. Additionally, a novel hydrophilic fluoroionophore for potassium sensing was synthesized, revealing better sensitivities against potassium in commercially available hydrogels, D4 and D1.

4.3. Introduction

Potassium and sodium play a key role in human body. The function varies in signal transmission, muscle contraction, membrane potentials, osmotic pressure, transmission of nerve signals and they regulate the levels of ions in the extracellular and intracellular fluids (ECF/ICF gradient).¹² Sodium is the dominating cation in the ECF, whereas normal blood values are ranging from 136 to 146 mM. Abnormal values can cause hyponatremia¹⁹ or hypernatremia²⁰. Potassium is the main cation for intracellular functions, whereas

normal values in blood are ranging from 3.5 to 5.0 mM. Any disturbances in concentration can cause hypokalemia²² or hyperkalemia^{23,26}. Hence sensing of these ions is of high importance and the indication and evaluation of these ions for medical purpose is necessary.¹⁶⁷

Common methods measuring potassium and sodium include, flame atomic absorption spectroscopy (FAAS)^{168,169} and the ion selective electrode (ISE)^{79,80,170–172}. Both methods, suffer from two main drawbacks. First, these methods require a sample preparation which is tedious and error prone. For example, a delayed separation causes a leakage of potassium from cells. That effect causes the concentration of potassium increases up to 0.4 mM per hour. Such tremendous errors in diagnostics can lead to misinterpretation of data, guiding to the assumption patients suffer from hyperkalemia, but patient do not manifest signs of hyperkalemia. This misdiagnosis is known under the term pseudohyperkalemia.¹⁷³ The second disadvantage of FAAS and ISE is that the analysis is too time-consuming. Intensive care patients often need medication within minutes. Current evaluation of ions in blood takes by far too much time for timely action. Therefore, a less error-prone and faster analysis method and technique is needed, to prevent the above-mentioned disadvantages of current analysis for ions in blood.

In this project we developed an on-line monitoring system for ions in blood. With the use of sodium and potassium fluoroionophores a DLR based sensing system is developed which enables real-time analysis of ions. Since the basic principle of fluoroionophore based optical sensors is already well investigated, the focus was to develop further the sensors, to be someday applicable for whole blood measurements. The main focus of this project was to investigate, the temperature dependency, effects and adjustment of additives (reference, TiO₂), sterilization test, photobleaching tests, shelf life and signal to noise ratios of the sensing layers. Additionally, a novel fluoroionophore was synthesized with enhanced sensing dynamics for potassium in the physiological relevant concentration range.

4.3.1. Dual Lifetime Referencing (DLR)

Various absorption based sensitive ion dyes have been reported in literature.¹⁴¹ These sensors are in general limited on a special format, although they are explained by their simple method. Due to their limitation, such chemo-sensors additionally suffer from one main problem. Light from the excitation source is not only absorbed by the sensing media, but also from the sensor surface, causing interferences. Moreover, optical components, for example connections between fibers and filters may cause difficulties in quantification of the sensor signal. Because of the above-mentioned drawbacks, measurements of ions in tissues and cells, also called scattering media, are virtually impossible.

Fluorescent ion indicators gained more and more attention in recent years, since they show higher sensitivities and less interferences with light. Furthermore, such indicators are compatible with referenced sensing techniques, enabling dual lifetime referencing (DLR)¹⁷⁴ in various formats (planar optodes, nanoparticles, fiber-optic sensors and microsensors).^{104,126,175}

DLR represents a special version of phase shift measurement systems. DLR converts varying fluorophore intensity signals, into phase shift changes. Phase shift changes can be measured with phase fluorimetry systems, which work within the kHz range. In DLR, two signals overlap at the same wavelength range. One signal is acting as a reference (inorganic phosphor), which has a long lifetime, where neither the intensity, nor the phase shift is influenced by any present analyte. The other signal represents the fluorophore signal. The overlap of those signals is measured and represents the indicator dye signal, depending on the present analyte concentration.

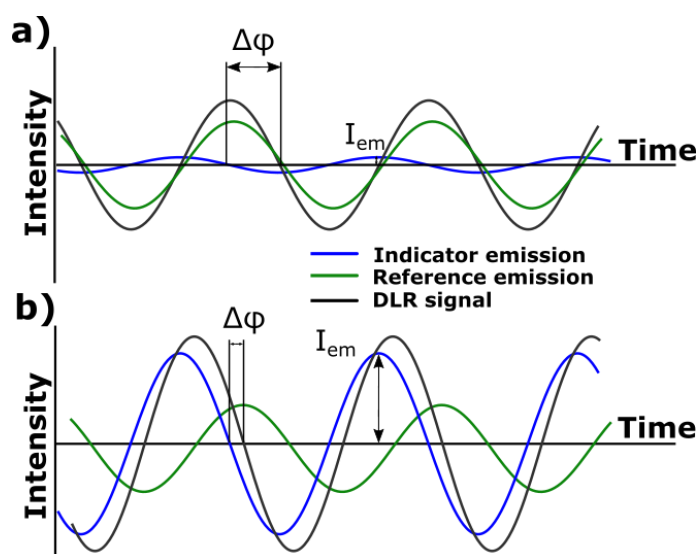


Figure 4-1: DLR signal development at low **a)** and high **b)** indicator fluorescence emission (blue).

In **Figure 4-1**, a low and a high indicator emission signal is shown. Case a) represents a low emission-intensity, derived from the indicator, resulting in a high phase shift. Case b) represents a high ion concentration, resulting in a low phase shift and a high emission intensity from the indicator. Important to note is that the reference signal is not changing and held constant for both scenarios. This crucial characteristic is a key parameter, since changing intensities and phase shifts affect the reproducibility. The overlapping signal is the sum of both emissions, whereas by alternating ion concentrations the phase shift varies, which can be measured. In order to obtain a reliable calibration system a few considerations need to be made:

- Both indicators (reference and fluoroionophore), emit within the same wavelength range
- The reference has to be inert towards changes in analyte concentration
- Composition adjustment to obtain a high phase shift split within the concentration range

Within this thesis, DLR was used for the determination of ions in blood. A measurement system was developed, with either inorganic phosphors Egyptian blue or Cr-GAB. With the used DLR measurement system, reversible and reproducible measurements of potassium and sodium are established. The effects of modulation frequency and the composition of the sensing foils on the sensing properties are investigated. With this research, reliable measurements of potassium and sodium are accomplished, and successfully applied in a sensing device.

4.4. Results and Discussion

This project includes fluoroionophores, which can be used for blood measurements. The reversibility and compatibility of fluoroionophores with commercially available hydrogels is already proven.^{117,118,176} In this project, sensing setups were tested and optimized on the purpose for using fluoroionophores as ion-sensors for whole blood measurements. Therefore, the sensors were tested on different properties and compositions, which are typically not included in traditional sensor development. A classical one-layer sensor consists of hydrogel, indicator and a reference, enabling DLR measurements. All sensors presented in this thesis consist of a composition, indicated in **Figure 4-2**, with either a potassium or sodium fluoroionophore. A fluoroionophore (FI) is immobilized in combination with a reference (Egyptian blue or CrGAB) in a hydrogel, resulting in a cocktail, which is dispersed until a homogeneous distribution is achieved. After knife-coating the resulting foils were placed under the fume hood until the solvent is evaporated. Calibration solutions consist of 20 mM TRIS/HCl buffer (pH 7.4) with different potassium or sodium concentrations. Potassium calibrations for all measurements shown this chapter were performed with 150 mM sodium background, simulating physiological conditions.

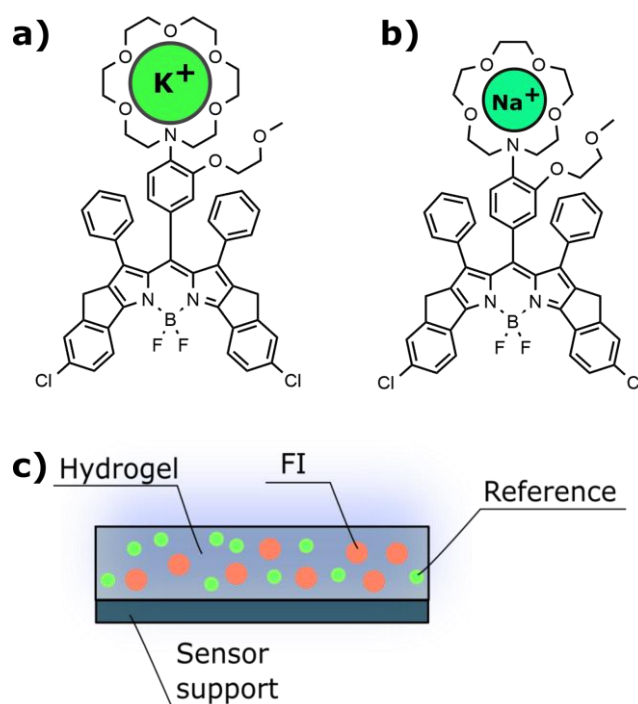


Figure 4-2: a) potassium fluoroionophore b) sodium fluoroionophore c) General sensor composition for the DLR measurements.

The sensing foils were characterized either using the fluorolog (measurement of fluorescence emission and excitation), the lock-in amplifier (measurement of luminescence phase shift and amplitudes) or a special flow through cell, which can be tempered in a climatic chamber (measurement of luminescence phase shift and amplitudes).

4.4.1. Starting point

At the beginning of the project, sensor foils containing 10 w% Egyptian blue and 0.2 w% potassium fluoroionophore were used in respect to hydrogel D4. For simulation of physiological conditions, the sensors were implemented in the climate chamber and calibrated at 23 °C and 37 °C. The reason for this experiment was that crown-ethers show a huge temperature dependency. The binding constants is decreasing with increasing temperature and the sensitivity of the sensor drops. In **Figure 4-3** the temperature effect is shown for a sensor calibrated at different temperatures. One sensor additionally contains a pHEMA protecting layer. This layer is required to ensure that the sensor and the sensing media are not in direct contact. In typical sensor development a protective layer is not necessarily required. For blood measurements and real application to humans, a protective layer is crucial. In order to develop an ion sensor for blood measurements, one of the key parameters is to prevent any leakage from the sensing layer. Although fluoroionophore based sensors hardly show leakage problems a protective layer eliminates last doubts.

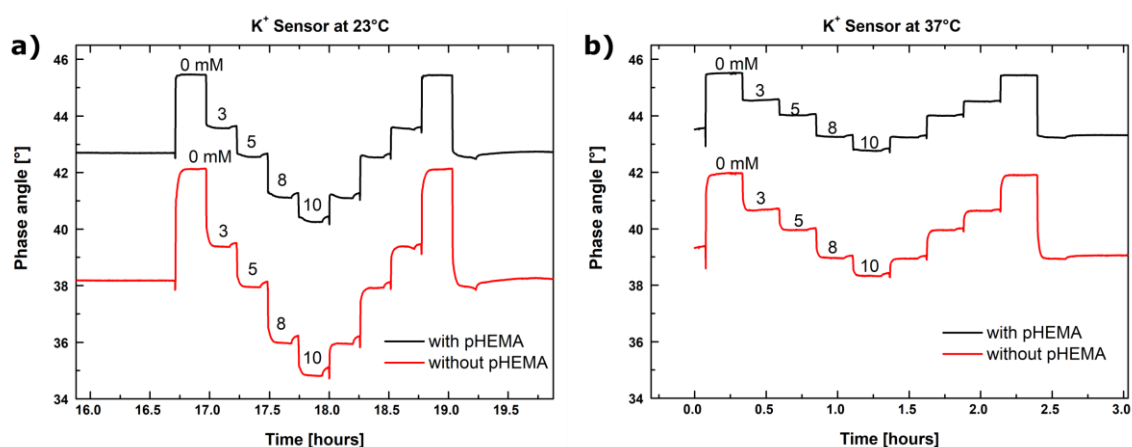


Figure 4-3: Potassium sensor calibrated at 23°C and 37°C. An increase in temperature results in a reduced resolution.

Figure 4-3 shows that the use of a protective layer increases the phase angle for all calibration solutions at 23 °C and 37 °C. In **Table 4-1**, the calculated phase shifts between

0 and 10 mM potassium are given. As expected, the sensitivity drops with increasing temperature. At 37 °C the sensitivity drops almost by half compared to 23 °C. This effect is shown for both, the foil with, and the one without a protecting layer and is related to the reduced complex stability described in **Chapter 2.2**.

Table 4-1: Phase angle differences for a potassium sensor calibrated at 23°C and 37°C.

Temperature	23°C	37°C
$\Delta^\circ(0-10\text{mM})$ with pHEMA	5.20	2.74
$\Delta^\circ(0-10\text{mM})$ without pHEMA	7.29	3.64

Furthermore, the use of pHEMA as a protecting layer makes the absolute intensity values drop, which might be the reason why the phase shift is lowered compared to a foil without a protecting layer. The increased hydrophilicity of the sensing foil increases the ion concentration within the foil, but the absolute sensing intensity dynamic of the chromophore is reduced resulting in a lowered phase shift. This was already shown by investigations in **Chapter 3** where highly hydrophilic foils showed reduced absolute intensities. The following chapters are concerned with one main goal, which was the improvement of the sensitivity of potassium sensors. For comparability all measurements including phase angle measurements were performed at 37 °C.

4.4.2. Composition dependency - Egyptian blue

Via variation of the amount of Egyptian blue, the aim was to increase the phase shift in the physiological potassium concentration. All foils were prepared exact the same way, whereas the amount of reference was varied (10 w%; 7 w%; 5 w%; 2 w%) in respect to the amount hydrogel. The calibrations are illustrated in **Figure 4-4**. With increasing amount of reference, the absolute phase angle is increasing. This phenomenon is explainable with the DLR sensing system (the fluoroionophore shows slight fluorescence at 0 mM potassium) and the theory is described in **Chapter 4.3.1**.

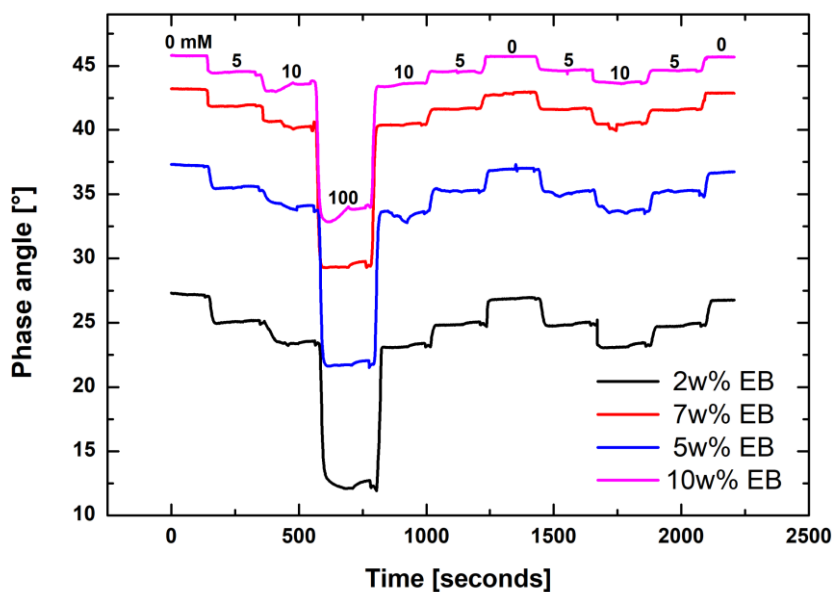


Figure 4-4: Calibration of a potassium sensor foil with different amounts of reference, Egyptian blue.

Some things need to be considered, using fluoroionophores for potassium measurements. Since the dynamic potassium concentration in blood is between 3 and 7 mM and the sensing dynamic of the indicator is far beyond such low potassium concentrations, it makes sense to adapt the amount of reference in the sensing foil. In **Table 4-2** it can be seen that with increasing amount of Egyptian blue, the phase shift is decreasing. This experiment indicated that the ratio and the overlap of the two signals derived from indicator and reference is at best at 2 w% Egyptian blue (3.80°), whereas at 10w% the phase separation is low (2.10°).

Table 4-2: Phase angle differences between 0 and 10 mM potassium at different amounts of reference used.

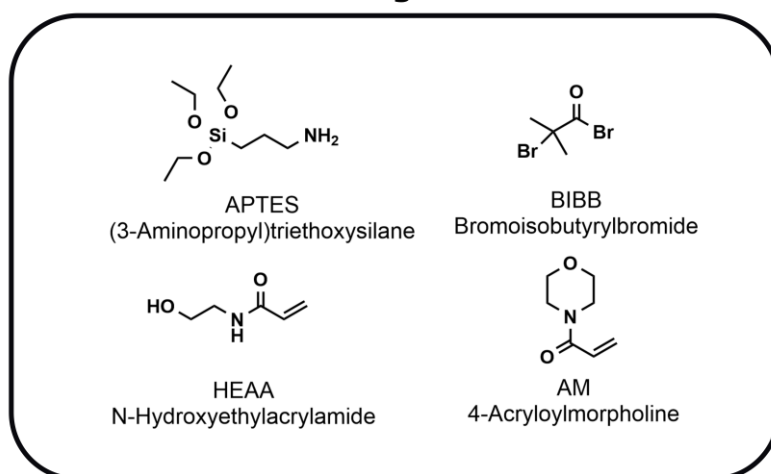
w% EB	10%	7%	5%	2%
$\Delta^\circ(0-10\text{mM})$	2.10	2.54	3.35	3.80

4.4.3. Usage of Hydrophilic Phosphorescent pigments

For further improvement of the sensitivity, the reference was modified in a three-step synthesis to obtain an Egyptian blue with a hydrophilic character. The modification is visualized in **Figure 4-5**. Via a simple polymerization technique, called activators regenerated by electron transfer atom transfer radical polymerization (ARGET ATRP)^{177,178}, the reference is modified to obtain Egyptian blue particles with a higher hydrophilicity. The surface of Egyptian blue was activated in the first step with an amino

silane (APTES; (3-Aminopropyl) triethoxysilane). In this case, N-Hydroxyethyl acrylamide (HEAA) and 4-Acryloylmorpholine (AM) are used for end group capping.

Reagents



Synthesis

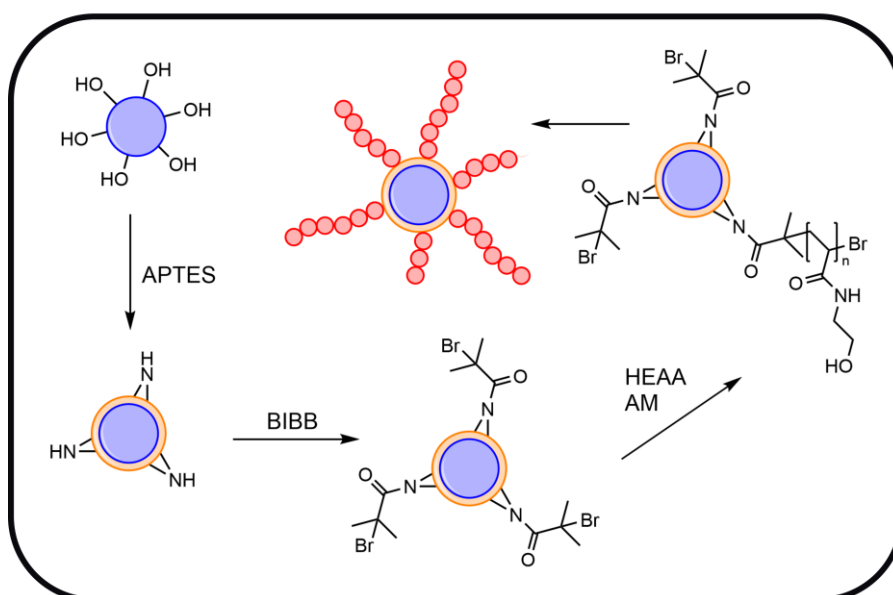


Figure 4-5: Top: Used reagents for the hydrophilization. Bottom: Illustration of the hydrophilization of Egyptian blue.

The reason for the hydrophilization was, that the hydrophobic reference (unmodified) possibly is switching on fluorescence of the fluoroionophore and hence reducing the sensing dynamic of the indicator. This means, that the indicator is more fluorescent at 0 mM potassium reducing the overall sensing dynamic. To verify this theory, a foil with hydrophilic Egyptian blue was calibrated and compared with the unmodified reference (**Figure 4-6**).

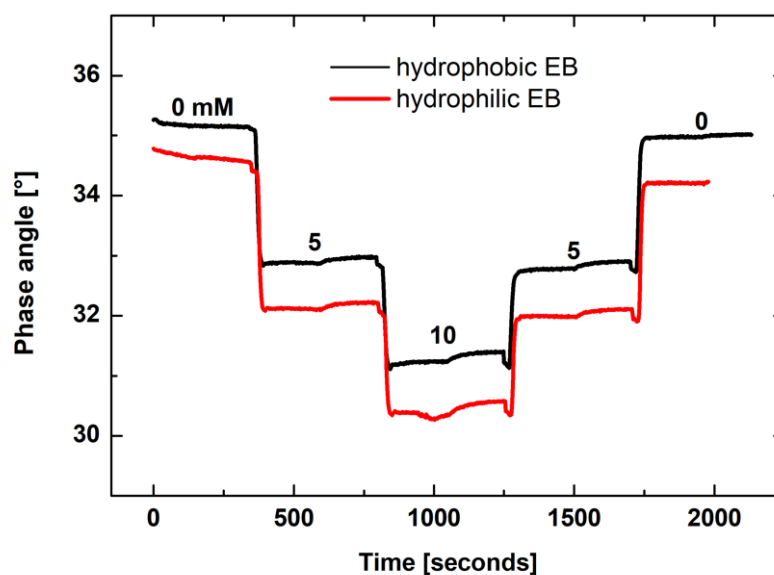


Figure 4-6: Comparison of an unmodified and a hydrophilized reference, Egyptian blue.

Table 4-3: Phase angle differences of a hydrophilic and hydrophobic reference.

2 w% EB	hydrophilic	hydrophobic
$\Delta^{\circ}(0-10\text{mM})$	4.30	3.94

As can be seen from **Figure 4-6** and **Table 4-3**, the modification has a slight positive effect, the phase shift increased from 3.94° to 4.30° . Fluorescence calibrations showed similar dynamics of the sensor foils, revealing that the hydrophobic Egyptian blue does not switch on fluorescence of the fluoroionophore. Investigations of a modified hydrophilic phosphorescent pigment yield in slightly better phase shift within the physiological range for potassium. It was not achieved to gather an enormous improvement, which was normally expected.

Nevertheless, a positive effect was indeed achieved. Since the prepared cocktails contain a mixture of ethanol and water, the cocktails are quite polar. During the suspension with the use of a magnetic stirrer, cocktails with a better homogeneity are achieved. Furthermore, after removing the stirring bar, the suspensions were more stable, resulting in a more reproducible and user-friendly preparation procedure.

4.4.4. Novel potassium fluoroionophore with enhanced hydrophilicity

Previous experiments showed that fluoroionophores display different sensitivities in various hydrogels, polymers and polymer blends. (**Chapter 3**) For example, pHEMA and pHPMA represent promising polymer matrices for ion measurements. Nevertheless, using water swellable polymers can cause some problems. Since the fluoroionophore used in previous studies has a quite hydrophilic character (crown-ether receptor) and a quite hydrophobic character (dye moiety), the possibility of aggregation of the indicator is given. As a consequence, unstable sensing foil are obtained. Therefore, the idea was to synthesize a fluoroionophore with an improved hydrophilicity (**Figure 4-7**) on the dye moiety in order to overcome any aggregation in the corresponding matrix.

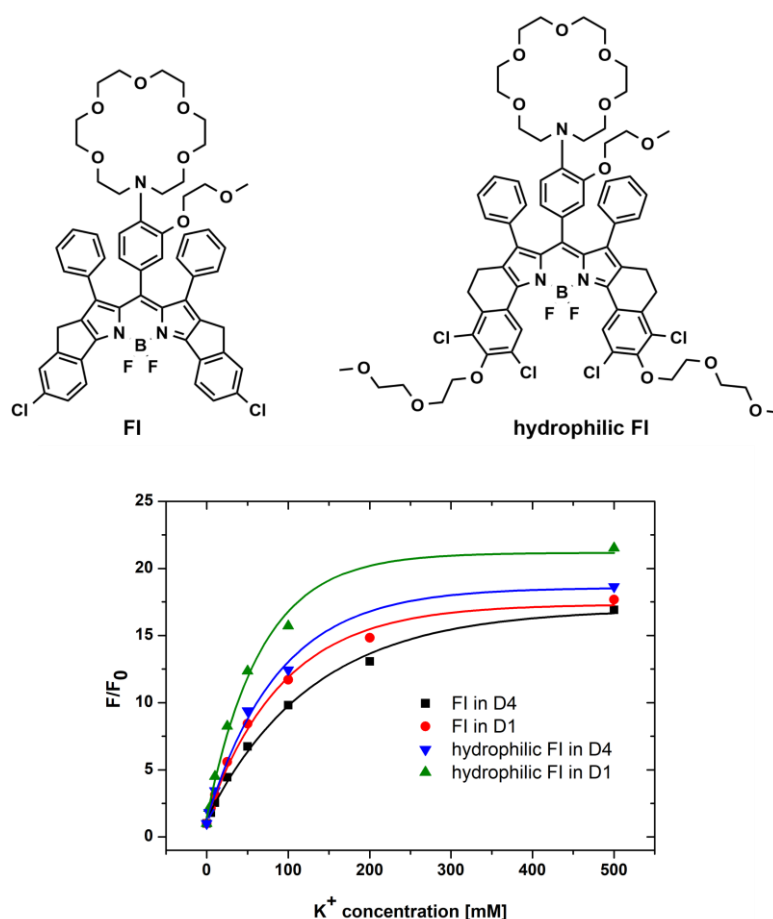


Figure 4-7: Structures of fluoroionophores used for calibrations in different matrices, hydrogel D4 and D1.

Figure 4-7 shows calibrations of two indicators in different hydrogels. Indeed, even though the same ion complexing moiety is used, the more hydrophilic fluoroionophore shows a higher sensitivity, in both hydrogel D1 and D4. Because the hydrophobic indicator showed higher sensitivities in pHEMA, the hydrophilic indicator was immobilized in different concentrations (0.2; 0.4; 0.6 and 0.8 w%) in pHEMA. As expected, the

hydrophilic indicator indeed showed an improvement in the sensitivity, and the most important measurements are shown in **Figure 4-8**. A 0.4 w% hydrophilic fluoroionophore was immobilized in pHEMA and stored in a 0 mM TRIS buffer (pH 7.4). Over time, absorption spectra were recorded to reveal any change in the spectrum. As can be seen the absorption spectra drastically changes over six days, uncovering that pHEMA does not represent a promising matrix. In **Figure 4-8**, graphs **a)** and **b)** instead show that measurements in a commercial hydrogel show full reversibility and promising results. Fluorescence measurements in 0.1 M HCl represent the maximum fluorescence potential of the indicator in this polymer matrix.

Additionally, phase angle measurements were performed in hydrogel D1 at 25 °C, showing similar sensitivity compared to the hydrophobic indicator. An increase in temperature to 37 °C resulted again in a drop of the phase angle shift. Due to the difficult synthesis of the precursor as well as the unknown and unsure stability of the indicator in various matrices the investigations of the hydrophilic fluoroionophore for blood sensing purposes was no longer followed.

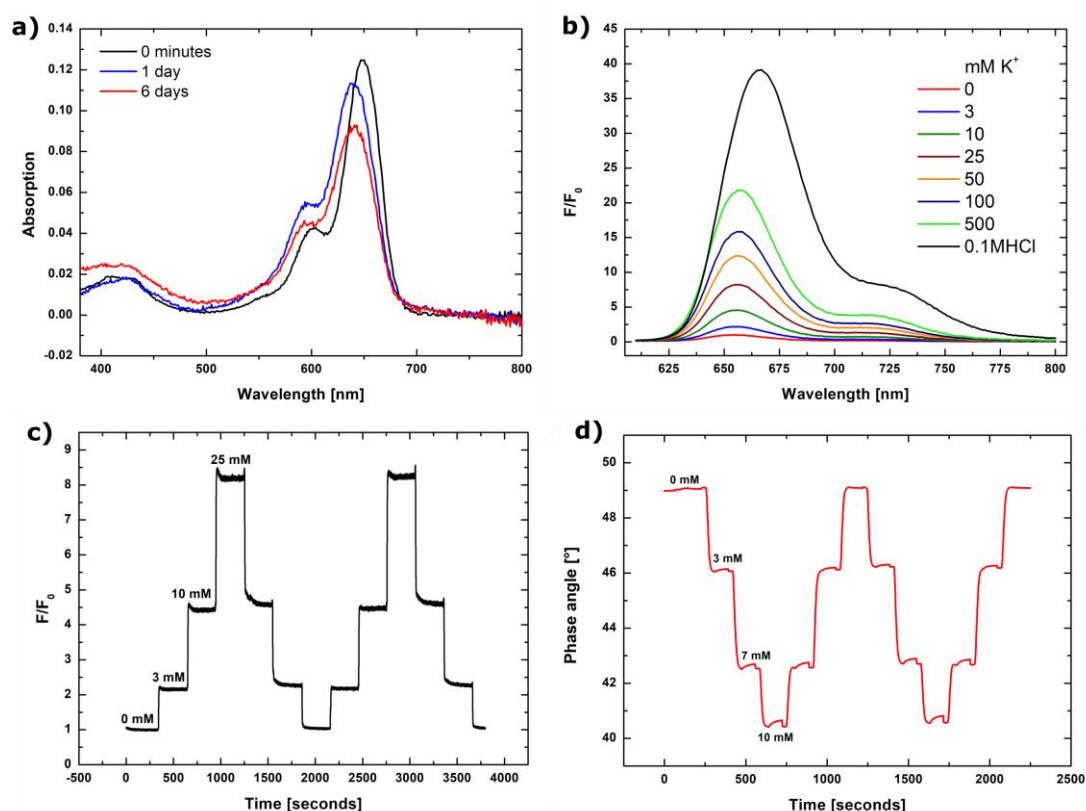


Figure 4-8: **a)** Aggregation of the hydrophilic fluoroionophore in pHEMA in buffer solution over 6 days. The measurements show that pHEMA represents an unstable matrix for this indicator. **b)** Calibration of the hydrophilic FI in hydrogel D1 with 250 mM sodium background. The 0.1 M HCl represents the fluorionophore's full potential within this matrix. **c)** Kinetic measurements in D1. The synthesized indicator showed full reversibility. **d)** Phase angle measurements of the FI in hydrogel D1 at 25 °C.

4.4.5. Implementation of Cr-GAB with enhanced spectral properties

The previously used system with Egyptian blue as a reference for DLR measurements has some drawbacks. In **Figure 4-9** the excitation and emission spectrum of both, the reference and the fluoroionophore is shown. The excitation maximum of the reference is at 618 nm, whereas the one from the fluoroionophore at 638 nm. Egyptian blue reveals a large stokes shift of about 288 nm. The fluoroionophore a small one, 17 nm. The previously shown measurements require a large spectral window. Because of that, a system like that is error prone due to interferences derived from blood.

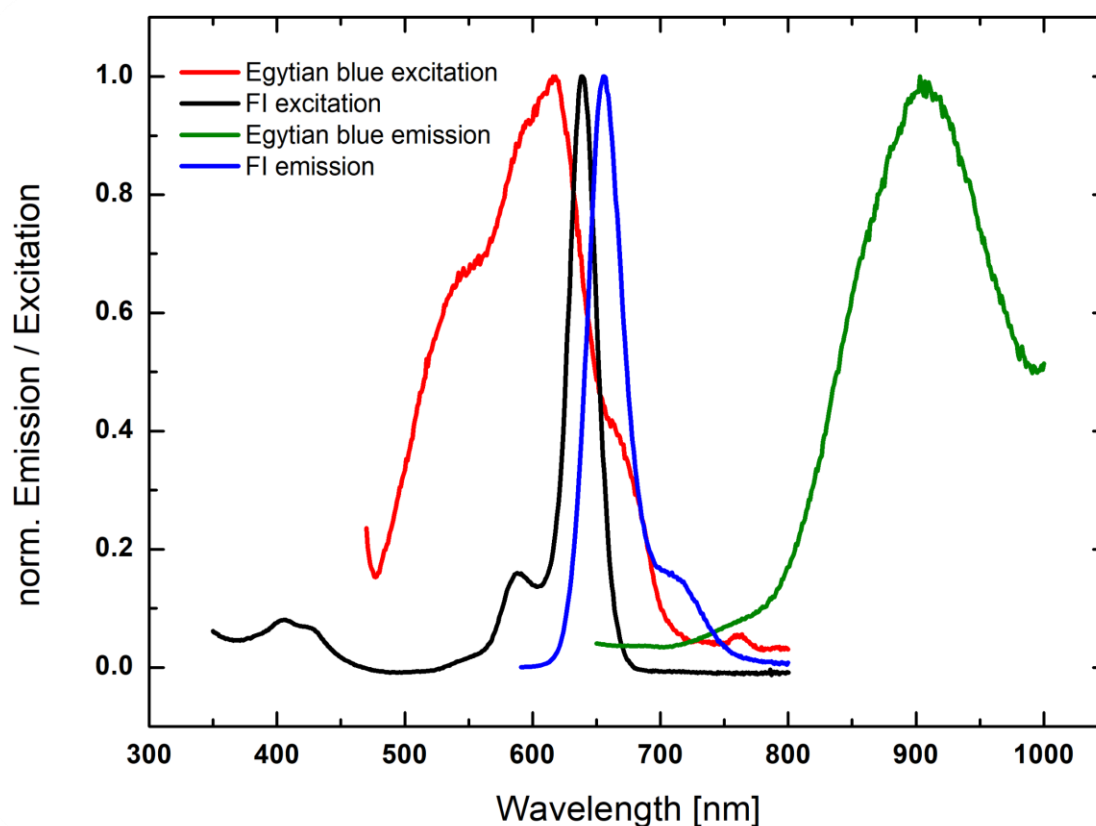


Figure 4-9: Excitation and emission spectrum of Egyptian Blue and the used fluoroionophore.

An ideal reference for BODIPY dyes preferably needs a smaller stokes shift and a second excitation band in the blue region, since BODIPY fluoroionophores can also be excited in the range from 400 to 450 nm. CrGAB has two excitation bands, one at 423 nm and the other at 590 nm, shown in **Figure 4-10**. The emission maximum of CrGAB is at 749 nm and therefore closer to the emission maximum of the fluoroionophore. The implementation of such reference in a final sensor setup would result in reduced interferences. Because of the reduced spectral window, an advanced optical setup could be

used, which reduces interferences derived from blood and wavelength dependent phenomena can be minimized.

A second advantage of CrGAB over Egyptian blue is the second excitation band at 423 nm. A change to an excitation in the blue range of the visible spectrum is possible because BODIPY-dyes also have an excitation region ranging from 390 to 450 nm. The main advantage of an excitation in this region is that the whole emission spectrum can be detected since no overlap of the excitation light with the fluorescence emission takes place. This would result in higher amplitudes during measurements and in the best case, in a higher resolution of the whole sensing system.

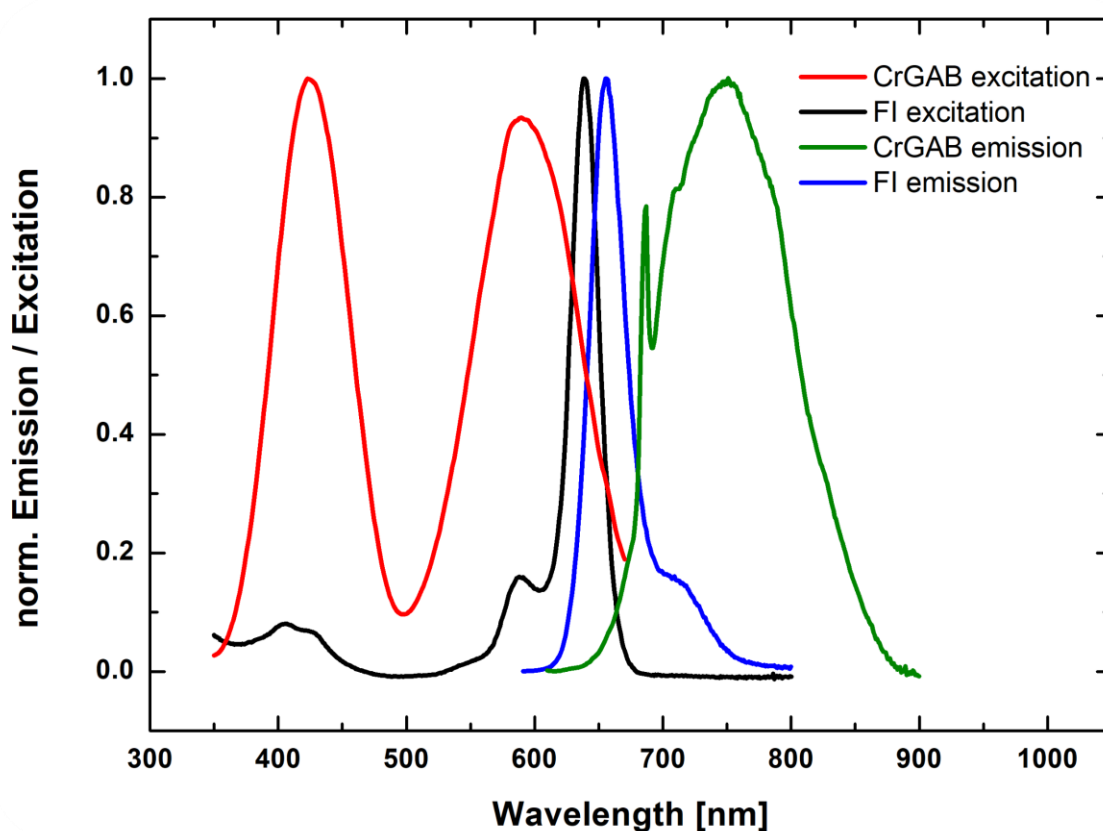


Figure 4-10: Excitation and emission spectrum of CrGAB and the used fluoroionophore.

Compatibility measurements with Cr-GAB

Since developing a new sensing setup with an excitation in the blue region is quite time consuming, the new sensing foils with CrGAB as reference were tested using the red excitation source, at the beginning. In **Figure 4-11** calibrations of two sensing foils are shown. These foils contain 0.2 w% fluoroionophore, 40w % CrGAB in hydrogel D4; and a

one to one blend of D4 and pHPMA. The pure hydrogel D4 achieved a phase shift of 3.95° between 0 and 10 mM potassium and achieved similar results compared to Egyptian blue. Blending D4 with pHEMA in a one to one ratio resulted in a total phase shift of 6.69° and confirm the results displayed in **Chapter 3**. In summary, CrGAB revealed as a possible reference for measurements in blood analysis. Additionally, to the above-mentioned advantages this system, enables the excitation in the red and in the blue region of the visible spectrum.

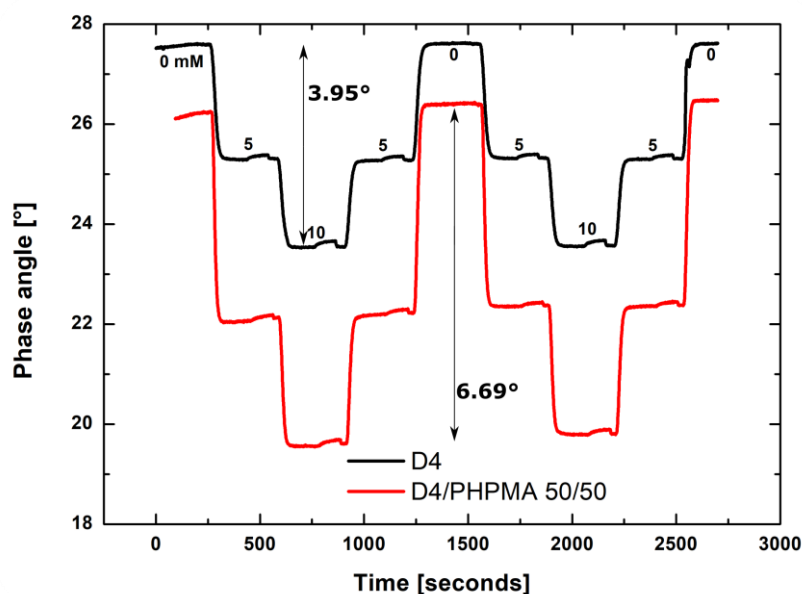


Figure 4-11: Two DLR sensor foils with the containing 0.2 w% FI, 40w% CrGAB in hydrogel D4 and a blend of D4/pHPMA 50/50 were calibrated at 37°C . The blended foil reveals a higher phase angle difference, due to higher water uptake of the sensing foil.

Sensor composition and the effect of the modulation frequency

In this part two different sensing foils containing 0.2 and 0.4 w% fluoroionophore in pHPMA/D1 50/50 with 100 w% CrGAB were calibrated with a modulation frequency of 1917 Hz and 4000 Hz. In **Figure 4-12** and **Table 4-4** the measurements are summarized. Calibration using 0.2 w% fluoroionophore and 100 w% CrGAB yield in a phase shift of 4.32° (1917 Hz; 0-10 mM K^+). An increase of the modulation frequency to 4000 Hz results in phase shift to 7.87° . The demodulation of the reference causes an increase of the phase shift, which also amplifies that current ratio between indicator and reference is not at its optimum.

Comparing 0.2 w% and 0.4 w% fluoroionophore at 1917 Hz, the measurement and the summary in **Table 4-4** shows, that an increase in the amount of fluoroionophore,

increases the phase shift and hence resolution. Although an increase of the modulation frequency results in a decrease of the amplitude for both 0.2 and 0.4 w% fluoroionophore, the overall increase in the phase shift for blood measurements is predominant.

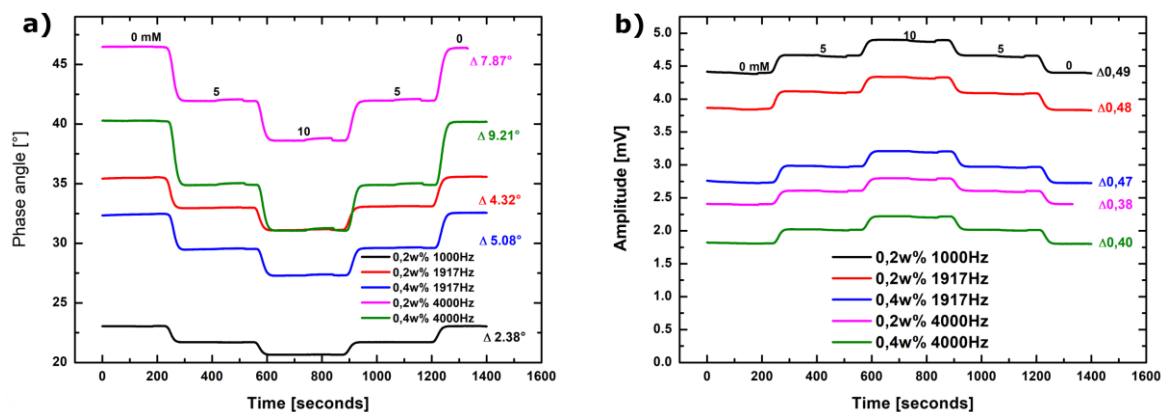


Figure 4-12: Calibration using different amounts of fluoroionophore at 1917 and 4000 Hz. **a)** Phase angle vs. Time. **b)** Amplitude vs. Time.

Table 4-4: Summary of the calibrations with varying amounts of fluoroionophore and different modulation frequencies.

amount FI [w%]	0.2	0.2	0.4	0.4
Frequency [Hz]	1917	4000	1917	4000
Δ phase shift ^o [0-10 mM]	4.23	7.87	5.08	9.21
Δ amplitude [0-10 mM]	0.48	0.38	0.47	0.40

Immobilization of scattering particles - final sensor composition

In this section the aim was to adjust the amount of CrGAB in hydrogel D4 foils and introduce TiO_2 particles to achieve the best sensing setup for measurements within the physiological blood range for potassium. **Figure 4-13 a** shows with decreasing amount of reference the phase angle is decreasing, whereas the phase shifts are increasing from 0.64° (100 w% CrGAB) to 1.23° (40 w% CrGAB) between 3 and 6 mM potassium.

The effect of TiO_2 as scattering additive is shown in **Figure 4-13 b**. TiO_2 acts as an amplifier of all signals derived from the sensing foils, resulting in an improvement of the overall sensing signal, for all sensing components. Sensing foils containing

100 w% CrGAB, mostly the emission of the reference material is amplified. Similar results are achieved in foils without TiO_2 . Adjusting the ratio between reference and indicator results in a positive effect when scattering particles are used. Higher phase shifts between 3 and 6 mM potassium are achieved compared to foils without TiO_2 .

This experiment intensifies, that for a composition of 0.2 w% fluoroionophore and 40 w% CrGAB the enhancement factor for the fluoroionophore is more pronounced, then for the reference. In summary, this results to a better sensing setup for blood analysis.

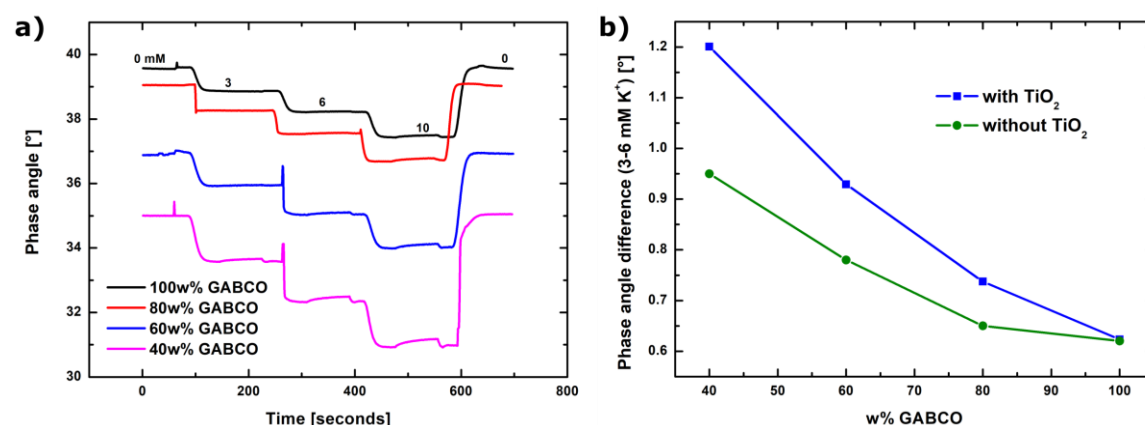


Figure 4-13: a) Variation of amount reference used within the sensing foils at a modulation frequency of 1917 Hz. b) Effect of TiO_2 to the Phase angle difference between 3 and 6 mM K^+ .

A stable and reproducible sensor signal was achieved with 40 w% reference within the sensor foil, all future experiments were made using this sensor composition. To achieve the best resolution of the sensing system the modulation frequencies in the next graph were varied to obtain a better sensitivity of the DLR system.

Figure 4-14 shows that, with increasing modulation frequency the phase angle continuously increases and the phase shift is increasing as well, whereas best measurements were performed at a modulation frequency of 4000 Hz. With this experiment the total phase shift was nearly doubled from 1.20 to 2.14°, between 3 and 6 mM potassium.

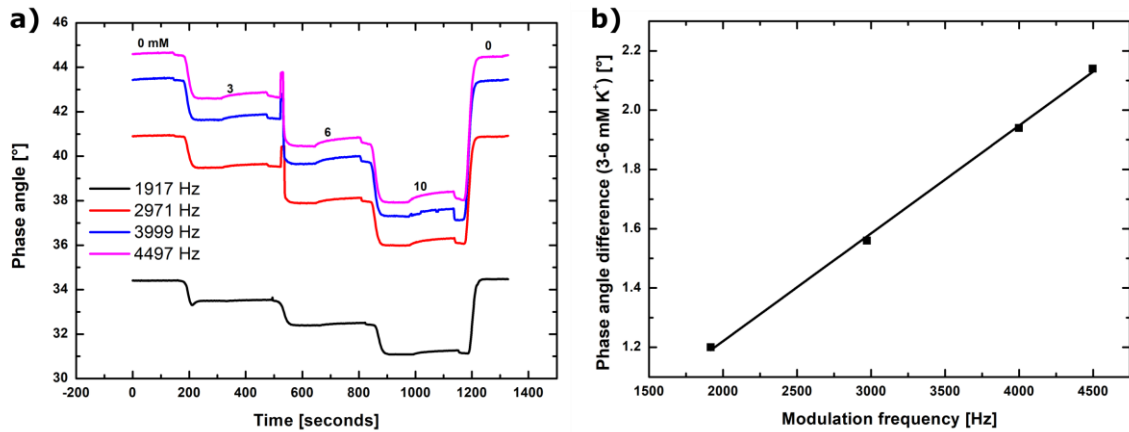


Figure 4-14: a) Sensing foil containing 0.2 w% FI, 40 w% CrGAB and 100 w% TiO₂ at different modulation frequencies. b) Phase angle difference between 3 and 6 mM K⁺. The modulation frequency behaves linear with the sensing dynamic.

At the beginning of this project the maximum phase shift achieved at 37°C was 0.27° per mM potassium. The final sensing composition and sensing setup achieved a maximum of 0.71° per mM potassium. The sensing setup during this project was improved by a factor of 2.6, which is quite remarkable, thinking about all components playing a pivotal role for ion sensing.

4.4.6. Sterilization tests for blood applications

Implementing ion sensors for blood measurements requires additional steps for a real-life application. Sterilization is part of those steps, to ensure a non-poisoning contact surface between blood and the sensing layer. During this step, the DNA of all existing microorganisms is destroyed or inactivated. Radiation sterilization is a process enabling products (in this case sensing foils) to be sterilized without an increase in temperature and without the use of chemicals. Therefore, radiation sterilization is a perfect method to sterilize products, which are in direct contact with body fluids. Furthermore, radiation sterilization is an effective, simple and environmentally friendly alternative to other conventional methods.

Former research has shown that BODIPY-fluoroionophores are partly destroyed during sterilization processes. The use of ascorbic acid inhibits this effect and is therefore mandatory. Ascorbic acid is one of the most powerful reductant and radical scavenger. It is able to reduce stable oxygen, thiyl and nitrogen radicals. Additionally, it is naturally occurring in our blood and it is used as a defense against any kind of formed radicals in our body.^{179,180}

For evaluating the optimum amount of ascorbic acid needed within the foils, different concentrations of the additive are added, sterilized and calibrated with the use of a lock-in amplifier. By comparing the amplitudes and phase angles with an unsterilized foil, it is possible to evaluate the amount of ascorbic acid needed for an effective sterilization process. The foils contained 0.2w% fluoroionophore, 100 w% TiO₂, and 40 w% CrGAB in a Hydrogel D4. The concentration of ascorbic acid varied from 0 to 10%.

Unsterilized foils were packed identical as the foils for sterilization and stored at 7 °C. After receiving the sterilized foils, all sensors were unpacked and calibrated identically, using the lock-in amplifier.

Calibrations using the lock-in amplifier

Calibrations were performed at room temperature with a modulation frequency of 1917 Hz. In **Figure 4-15**, a foil with 5 % ascorbic acid is shown. By comparing the amplitude difference of the sterilized ($\Delta = 12.2$ mV) and the unsterilized ($\Delta = 11.4$ mV) between 3 and 6 mM potassium, it can be seen that both indicators increase their fluorescence emission. In contrast, the total amplitude values already dropped from

180 mV to about 120 mV at 10 mM potassium. This indicated that still quite a huge percentage gets destroyed during sterilization. The phase separation drops from 3.58° (unsterilized) to 1.52° (sterilized). A similar effect can be observed by comparing the absolute change of the phase angle at 0 mM potassium. The unsterilized foil shows a phase angle of 32° and the sterilized a phase angle under 22° , which corresponds to an absolute change of 37%. This effect is usually not expected. The amplitude sinks and the phase angle rises, which might be due to the reason that indicator molecules are attacked during sterilization and cause permanent fluorescence upon excitation.

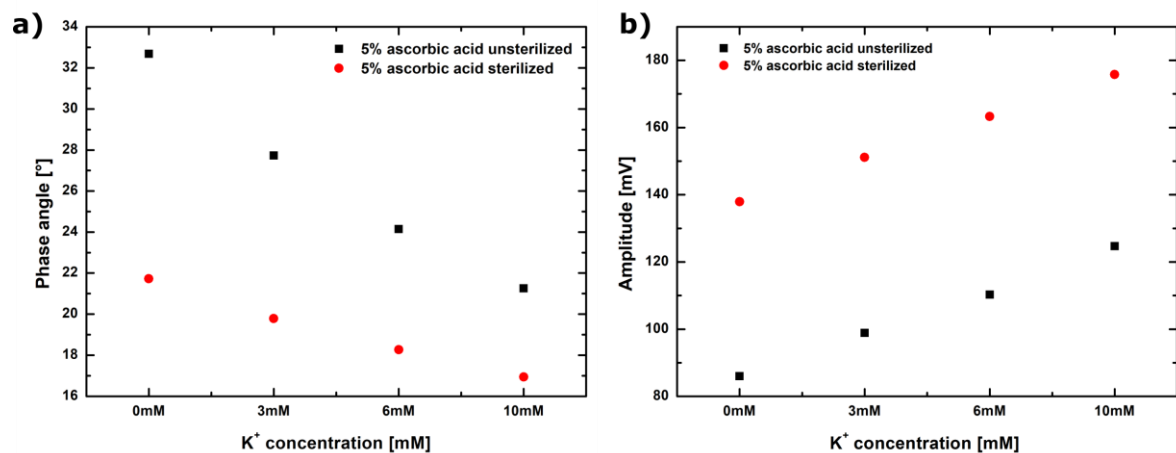


Figure 4-15: Calibration of a potassium sensitive foil containing 5% ascorbic acids, sterilized (red) and unsterilized (black). Concentration vs. **a)** phase angle and **b)** amplitude.

If 10% ascorbic acid (**Figure 4-16**) is used, amplitudes behave similar then foils with 5% ascorbic acid, with a minor total amplitude loss of the sterilized foil. Using this ascorbic acid concentration results only in a minor phase angle splitting loss. In the physiological range a difference of 3.23° was determined for the sterilized foil, whereas 3.72° was determined for the unsterilized version.

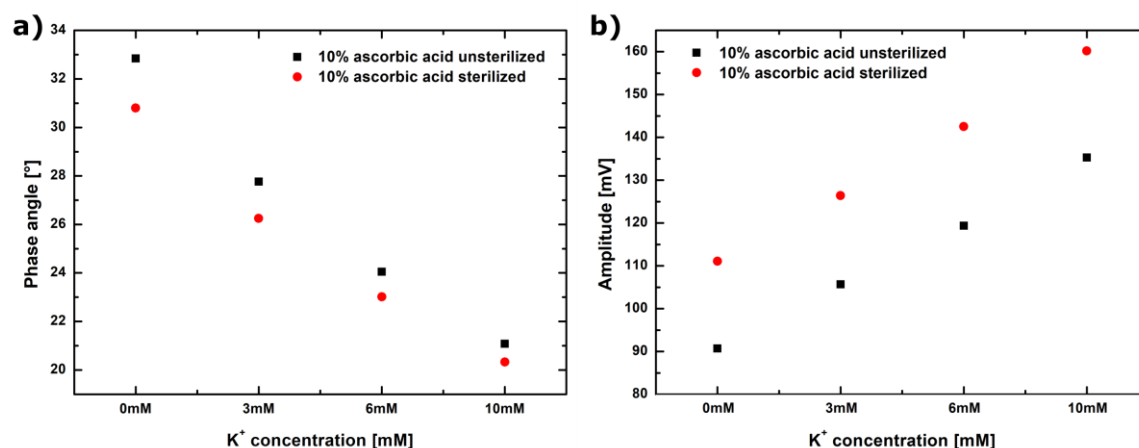


Figure 4-16: Calibration of a potassium sensitive foil containing 10% ascorbic acids, sterilized (red) and unsterilized (black). Concentration vs. **a)** phase angle and **b)** amplitude.

Summing up, lock-in measurements using 10% ascorbic acid within the sensor foils is recommended for radiation sterilization. Although a small portion of fluoroionophore still is destroyed, the phase angle only differs 5% in the absolute values and similar differences between the physiological potassium concentration were measured.

DLR measurements at 37°C of sterilized foils

DLR measurement of sterilized foils were performed at 37°C and physiological conditions with the final sensor foil composition. The foils contained 0.2 w% fluoroionophore, 40 w% CrGAB and 100 w% TiO₂ in respect to the used hydrogel D4. The evaluated and best modulation frequency was determined previously to be 3967 Hz.

In **Figure 4-17** an example of a sensor foil is given to demonstrate the effect what occurs if no ascorbic acid is used for sterilization. The sterilized foil without ascorbic acid shows nearly no phase separation between 3 and 6 mM potassium (0.1°). This effect was expected, since BODIPY-fluoroionophores are destroyed during radiation sterilization, if no radical scavenger is used. The calibrated unsterilized foil works fine. A phase splitting in the range of 2.43° is in the range which was determined previously by optimization experiments.

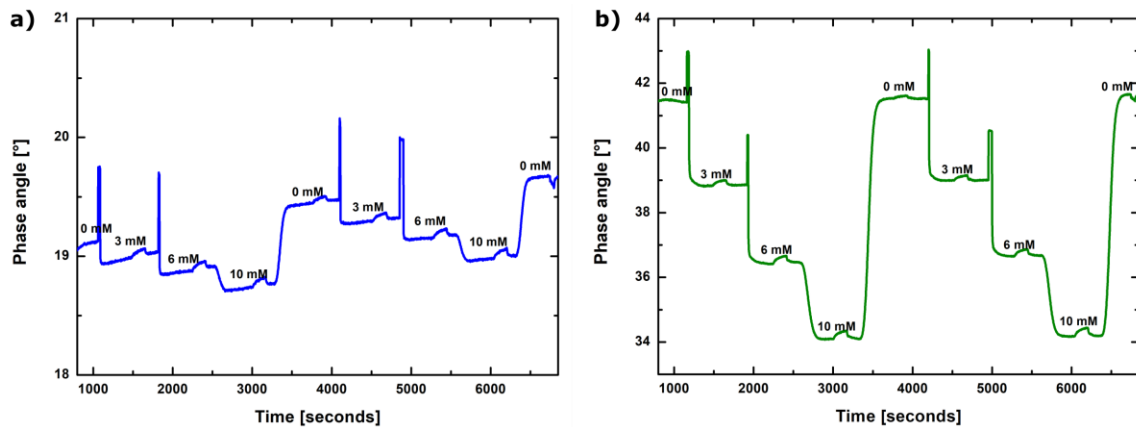


Figure 4-17: DLR measurements of a sensing foil without ascorbic acid. **a)** sterilized. **b)** unsterilized.

Similar to the lock-in measurements, a foil with 10% ascorbic acid (**Figure 4-18**) show best results. Since the unsterilized foil shows a deviation of 2.26° , the sterilized foil shows a deviation of 1.91° between 3 and 6 mM potassium.

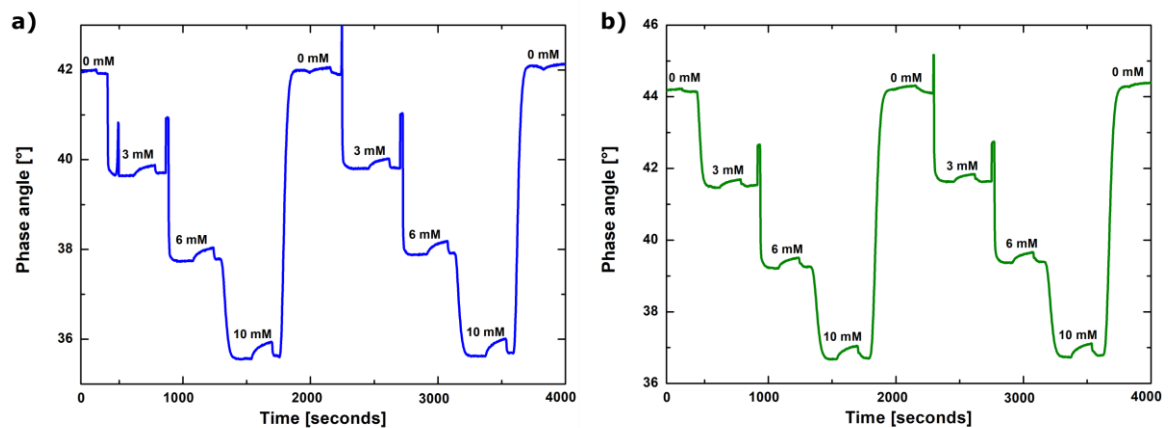


Figure 4-18: DLR measurements of a sensing foil with 10% ascorbic acid. **a)** sterilized. **b)** unsterilized.

The difference between the phase separation of the lock-in measurements (23°C) and the measurements at physiological conditions (37°C) is explained in the next section, which is concerned with temperature effects and the evaluation of the temperature coefficients.

4.4.7. Temperature influence and compensation

The stability of the complex is represented by the stability constant (K_s), which describes the equilibrium between the receptor (host, H) and the analyte (guest, G) to form a

complex (HG) described in **Chapter 2.2**. Complexation of analytes is always connected to energy and therefore the temperature affects the effectivity of the binding event. Therefore, crown-ethers display a high temperature dependency. The binding constant is decreasing with increasing temperature and therefore the sensitivity of the ion indicator is changed. Hence, the temperature also affects the phase angle and the phase change upon concentration changes. Because of that, temperature compensation is not only of high interest but also mandatory in a practical application of an ion sensor for blood analysis.

In **Figure 4-19** a temperature calibration is shown. A sensor was calibrated from 30 to 38 °C. During temperature changes the sensor was stored under a 3 mM potassium buffer solution. At each stage a 6 mM potassium solution was screened for visualization of the temperature effect. It can be seen that the binding constants decrease with increasing temperature.

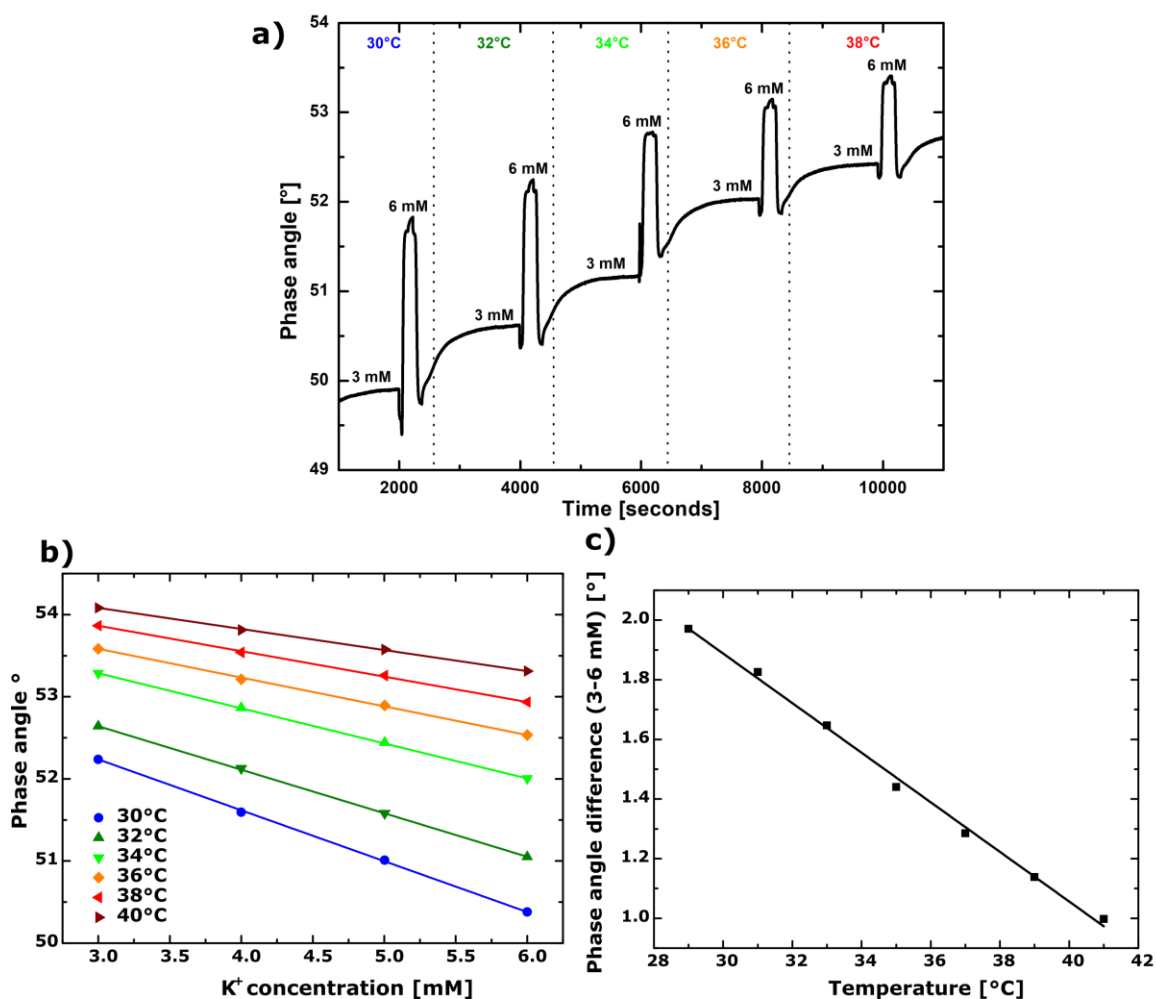


Figure 4-19: a) Phase angle measurements for evaluation of the temperature dependency of a potassium sensor from 30 to 38°C. b) Plot potassium concentration vs. phase angle. The sensor shows a linear behavior for all temperatures. c) Phase angle differences in the physiological relevant region against the temperature.

By plotting of the phase angle versus the concentration of the current temperature a linear behavior was determined. Additionally, by plotting the phase angle differences versus the temperature shows a linear behavior (**Figure 4-19**).

From both linear equations a connection is derived:

$$c = \frac{dPhi - (d + d_T * (T - 37))}{k + k_T * (T - 37)} \quad \text{Equation 4-1}$$

c	ion concentration [mM]
$dPhi$	phase angle [°]
d	intercept at 37°C
k	slope at 37°C
d_t	correction factor for intercept
k_t	correction factor for slope
T	temperature [°C]

The formula (**Equation 4-1**) describes the slope k and the intercept d of the calibration at 37°C. k_T and d_T are the correction factors per °C. Depending on the deviation of the current blood temperature, the temperature effect can be compensated, and the actual ion concentration is calculated.

Table 4-5: Calculated temperature coefficients for a potassium and sodium sensor.

coefficient	sodium	potassium
d_T	0.3341	0.3296
k_T	0.0009	0.0210
k (37°C)	-0.0463	-0.6715
d (37°C)	47.6838	46.6875

An example of a temperature calibration is given in **Figure 4-20**. In this case the hydrophilic fluoroionophore described in **Section 4.4.4** was calibrated from 33 to 39 °C and from 0 to 10 mM potassium. The coefficients for the compensation of the temperature effect can be determined, using the temperature, concentration and the phase angle.

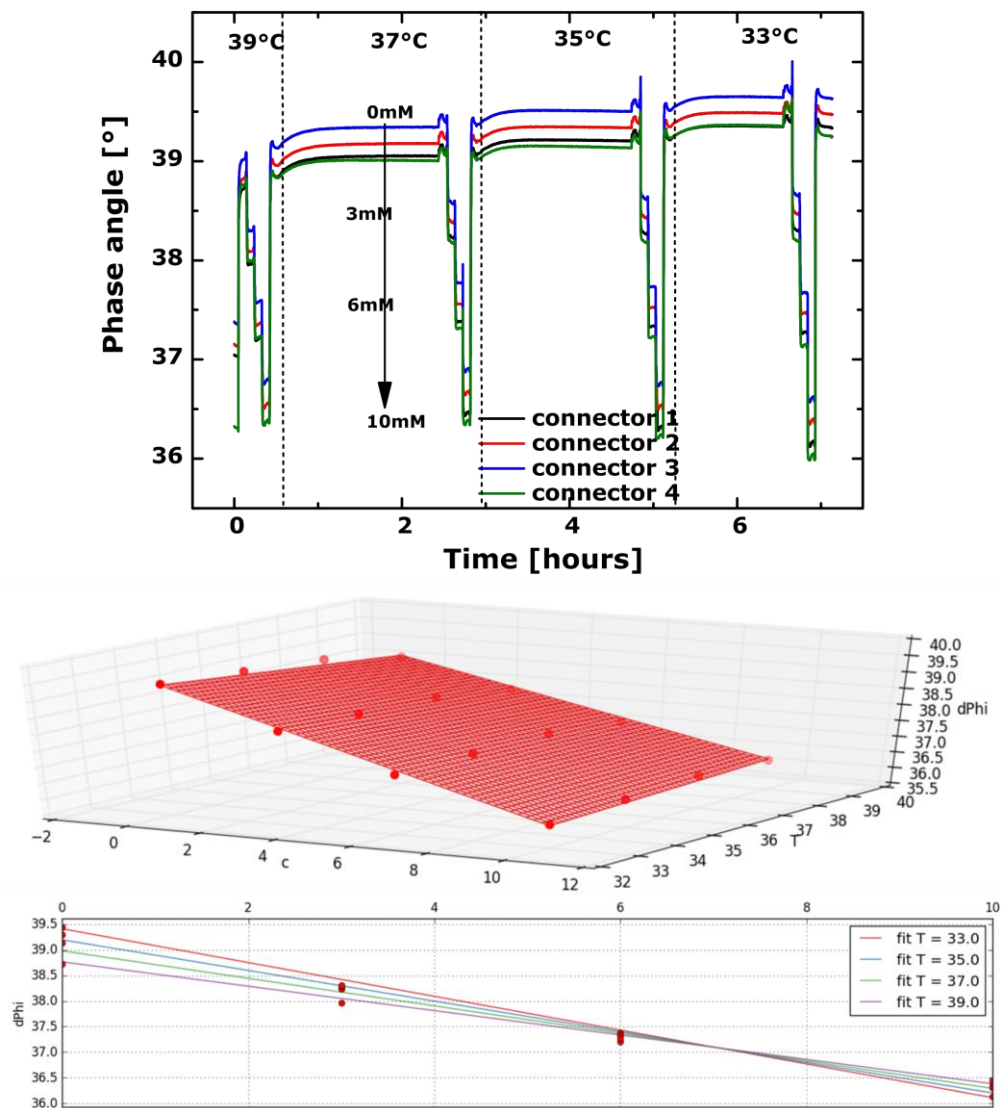


Figure 4-20: Example of a temperature calibration (0.4 w% hydrophilic FI, 40 w% CrGAB, 100 w% TiO₂ in hydrogel D1) and an extract of the data evaluation for the determination of the temperature coefficients.

4.4.8. Additional investigations for whole blood ion sensors

Signal to noise measurements

The change of the phosphorescent pigment from Egyptian blue to CrGAB offered the possibility to excite the reference and the fluoroionophore with a red or blue excitation light. In order to check what kind of excitation wavelength shows the best effort, signal to noise measurements were performed. With the use of the lock-in amplifier, a 0.2 w% fluoroionophore, 40 w% CrGAB and 100 w% D4 foil was investigated with a 430 nm and a 590 nm LED. After the excitation by the LED, a BG39 filter (2 mm), and after the foil, an RG 640 filter (2 mm) with a primary red foil was adjusted. In **Figure 4-21**, the lock-in measurement setup is shown.

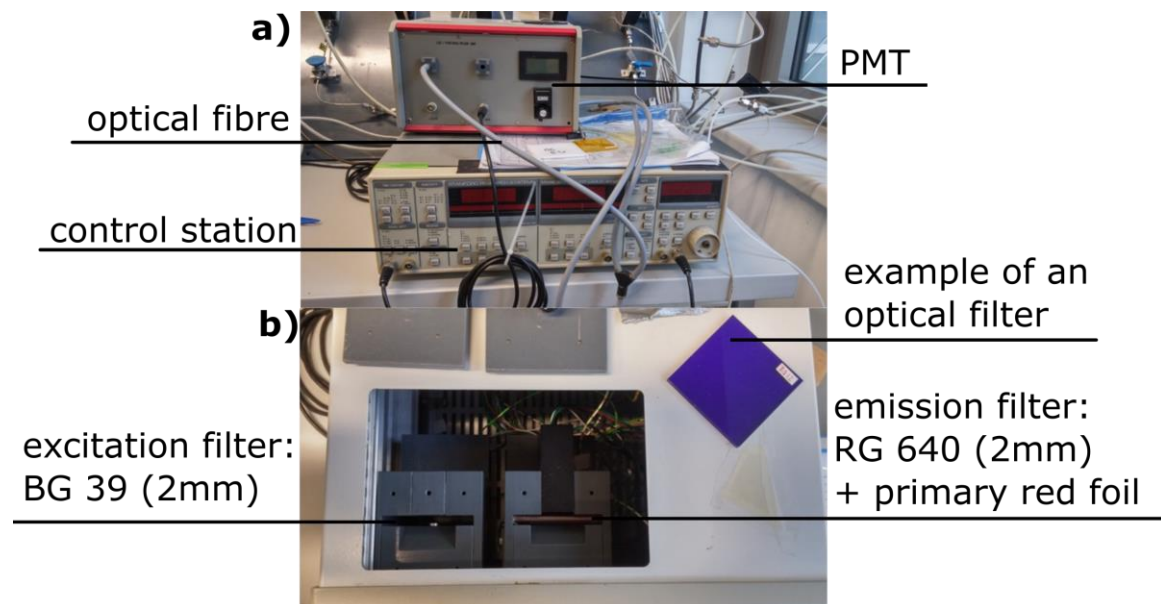


Figure 4-21: a) lock-in amplifier (SR830 DSP, Stanford Research) connected with an optical fiber and PMT. b) Visualization of the inlets for optical filters and an example of an optical filter.

From **Table 4-6** the results of the different excitation sources are shown. A foil without reference and fluoroionophore was used to measure the background of the setup. Values derived from different excitation measurements were used to calculate the signal to noise ratio. The use of an excitation source in the blue range of the visible spectrum is favored since the signal to noise ratio more than double compared to the excitation at 590 nm. Furthermore, the overall signals derived from the sensing foil signals are nearly three times higher.

Table 4-6: Signals from a TiO₂ foil and a sensor foil for evaluation of the noise to signal ratio.

Excitation LED [nm]	TiO ₂ -foil (noise)	Sensor foil (signal)	Ratio noise/signal
430	0.6	60.0	1:100
590	0.5	21.1	1:42

For evaluation of the optimum excitation wavelength additionally measurements using the fluorolog were performed. (**Figure 4-22**) Therefore, a special mount was 3D printed to adjust a commercially available LED with different excitation wavelengths. Similar to the experiment at the lock-in, filters similar to the final blood sensor measurement setup were used. Transmission filters were used to prevent the PMT to overload.

In **Table 4-7** the results are listed. An excitation with a 422 nm LED seems to be the best solution, whereas with increasing red-shift in the spectrum, noise to signal ratios drop.

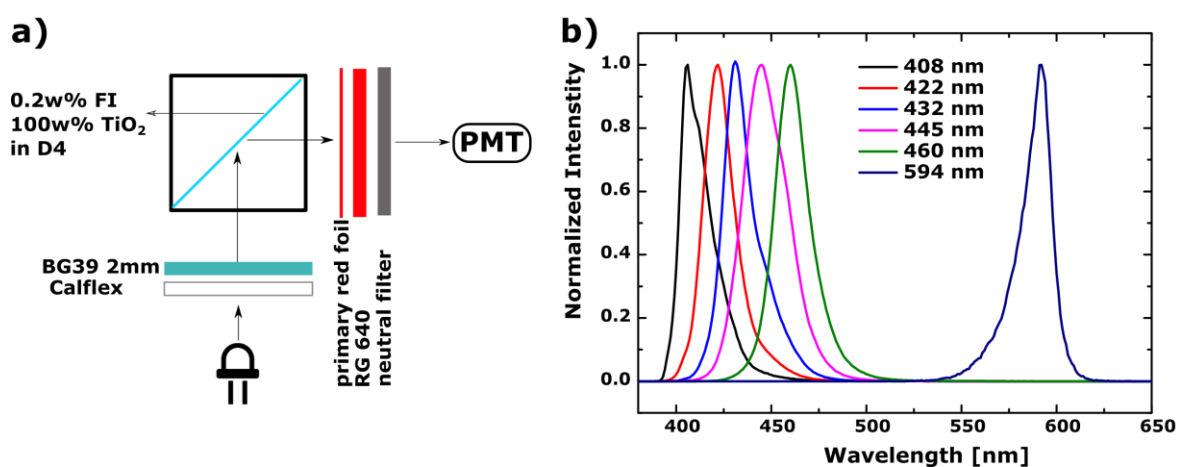


Figure 4-22: **a)** Simplification of the sensing setup used at the fluorolog for determination of background to noise ratios for different excitation wavelength's. **b)** Measured spectrums from the LED excitation sources used for the measurements.

Table 4-7: Results of the performed background to noise measurements. Excitation of the indicator with a 422 nm Led results in best ratios, for this setup.

Excitation LED [nm]	Ratio noise/signal
408	1:28
422	1:93
432	1:87
445	1:80
460	1:61
594	1:60

Photobleaching tests

Since a change in the excitation wavelength to the blue range of the visible spectrum comes in hand with higher energies, a sensor foil was tested regarding its photostability using the lock-in amplifier. Therefore, a sensor foil was adjusted the same way like previously shown in the signal to noise experiments, in the amplifier and calibrated at different potassium concentrations. The foil was permanently exposed to the excitation source for 5.5 hours. A pulsing time from 100 ms would correspond to 200,000 measurement points. The calibration is displayed in **Figure 4-23** and stable signal differences for all buffer concentrations are obtained. Photobleaching of the sensor via illumination with a blue excitation source can be excluded.

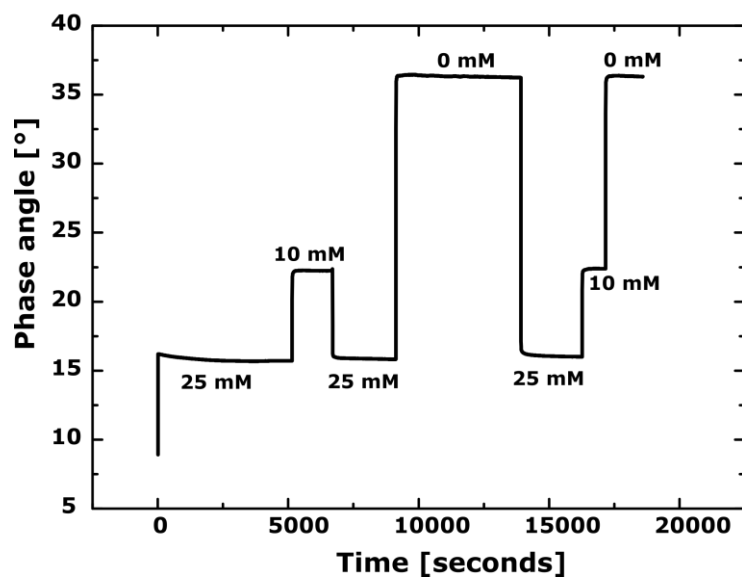


Figure 4-23: Photobleaching experiment performed at the lock-in amplifier for determination of the photostability of the fluoroionophore at an excitation with blue light.

Shelf life of ion sensors

In this project the storage stability of sensor foils was investigated. This subfield of sensor development is especially important for sensors applied in human diagnostics since errors can cause a tremendous impact in medication of patients. Therefore, this part was extensively studied to prevent any misconducts due to sensor failure. The sensor foils were tested with fluorescence-based calibrations and phase angle measurements at 37°C. After 2, 25, 66 and 188 days, measurements of the stored foils were performed.

Overview of performed tests:

- Investigation of influences derived from additives in a fluoroionophore foil (TiO₂/CrGAB/TiO₂+CrGAB)
- Storage behavior under dry conditions at 7 °C

Foils with different compositions were prepared:

- 0.2 w% FI in D4
- 0.2 w% FI in D4 + 40 w% CrGAB
- 0.2 w% FI in D4 + 100 w% TiO₂
- 0.2 w% FI in D4 + 100 w% TiO₂ + 40 w% CrGAB

Following tables and figures contain calibration curves and data of the proceeded measurements. During all experiments the same buffer composition was used and the foils

were always calibrated with the same procedure. Measurements performed using the fluorolog may suffer from slight temperature deviations ($\pm 3^\circ\text{C}$) since they were calibrated at room temperature. The fluoroionophores complex stability is temperature dependent and already discussed in **Section 4.4.7**. Slight deviations of the calibration curves might be due to this effect. Throughout all the measurements, there was no sensor failure. After 188 days storage, the response of the fluoroionophore is similar for all combinations of additives and show reproducible results.

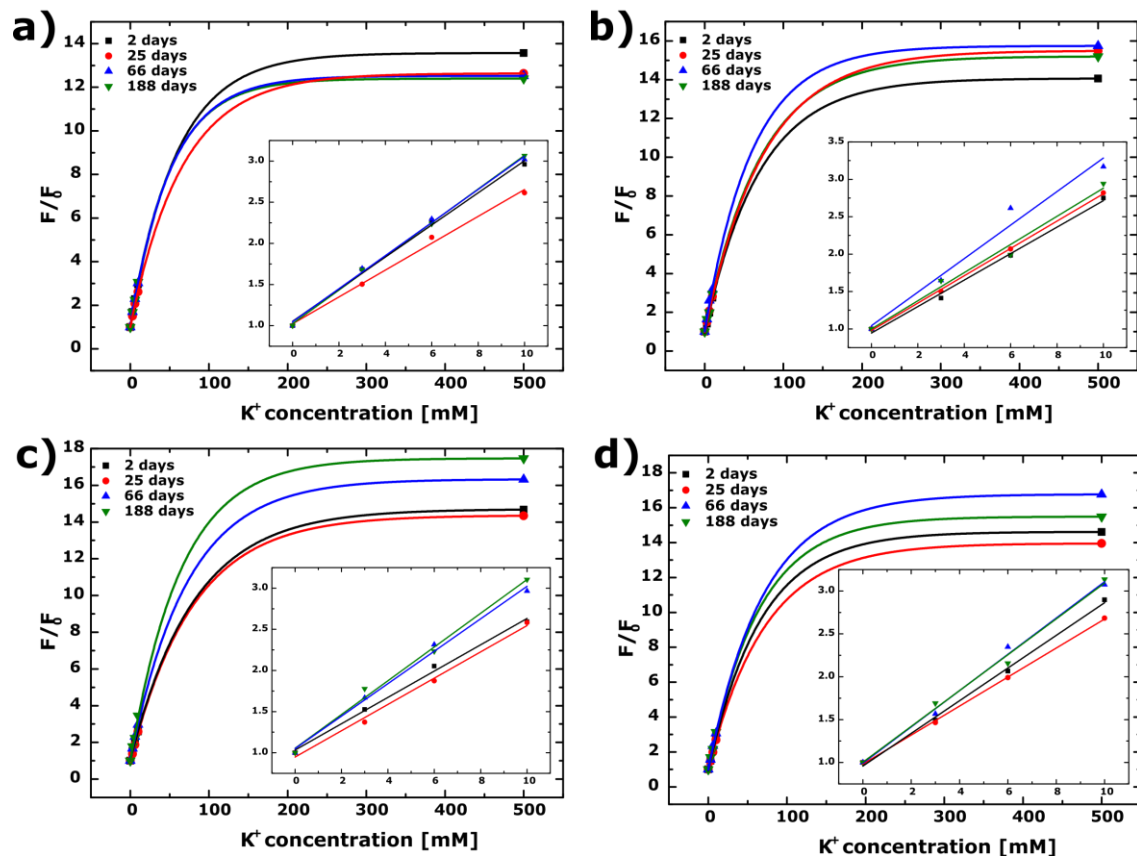


Figure 4-24: **a)** calibrations of a foil containing 0.2 w% FI in D4 after 2, 25, 66 and 188 days. **b)** calibrations of a foil containing 0.2 w% FI and 100 w% TiO_2 in D4 after 2, 25, 66 and 188 days. **c)** calibrations of a foil containing 0.2 w% FI and 40 w% CrGAB in D4 after 2, 25, 66 and 188 days. **d)** calibrations of a foil containing 0.2 w% FI, 40 w% CrGAB and 100 w% TiO_2 in D4 after 2, 25, 66 and 188 days.

Table 4-8: F/F_0 -values from the calibration containing 0.2 w% FI in D4 after 2, 25, 66 and 188 days.

Potassium concentration [mM]	2 days	25 days	66 days	188 days
0	1.00	1.00	1.00	1.00
3	1.68	1.50	1.69	1.68
6	2.28	2.07	2.30	2.24
10	2.96	2.61	3.02	3.07
500	13.57	12.63	12.52	12.39

Table 4-9: F/F_0 -values from the calibration containing 0.2 w% FI in D4 and 100w% TiO_2 after 2, 25, 66 and 188 days.

Potassium concentration [mM]	2 days	25 days	66 days	188 days
0	1.00	1.00	1.00	1.00
3	1.41	1.50	1.65	1.64
6	1.98	2.07	2.61	1.99
10	2.75	2.82	3.17	2.94
500	14.06	15.48	15.74	15.19

Table 4-10: F/F_0 -values from the calibration containing 0.2 w% FI in D4 and 40 w% CrGAB after 2, 25, 66 and 188 days.

Potassium concentration [mM]	2 days	25 days	66 days	188 days
0	1.00	1.00	1.00	1.00
3	1.53	1.37	1.67	1.78
6	2.05	1.87	2.32	2.23
10	2.59	2.58	2.97	3.45
500	14.68	14.34	16.32	17.46

Table 4-11: F/F_0 -values from the calibration containing 0.2 w% FI in D4, 40 w% CrGAB and 100 w% TiO_2 after 2, 25, 66 and 188 days.

Potassium concentration [mM]	2 days	25 days	66 days	188 days
0	1.00	1.00	1.00	1.00
3	1.49	1.47	1.57	1.69
6	2.07	1.99	2.35	2.16
10	2.90	2.68	3.07	3.14
500	14.61	13.95	16.76	15.49

Phase angle measurements were performed at 37°C. Foils were compared after 2 days and 188 days if any kind of alteration was recognized. **Figure 4-25** shows an example of a calibration performed after storage. In all cases the sensors were fully reversible, and no significant differences or trends are observed. Also, reversibility shown in **Figure 4-25** was given for all sensor foils.

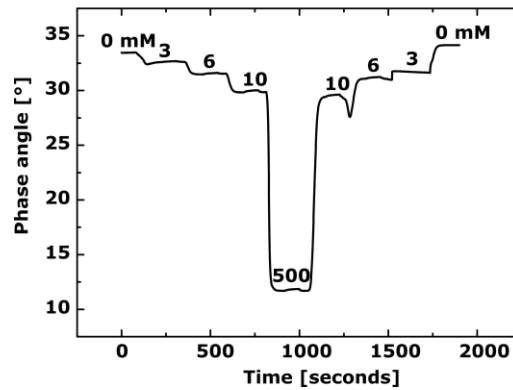


Figure 4-25: Calibration of a foil containing 0.2 w% FI, 40 w% CrGAB and 100 w% TiO₂ in D4.

In the following tables (**Table 4-12** and

Table 4-13) the raw data from the screened foils is shown. It is worth mentioning that sensors without CrGAB do not show a phase angle, which is not surprising, since they do not contain a long lifetime reference and no phase angle can be detected. (see theory DLR **Chapter 4.3.1**) For both cases, CrGAB and TiO₂ containing sensors similar phase splitting and amplitude differences in the physiological blood range is observed after 188 days. Also, DLR-tests were successful without any signs of any kind of alteration, bleaching, leaching or damage.

Table 4-12: Measured phase angles of different sensor compositions for different potassium concentrations after 2 days storage.

Potassium concentration [mM]	FI	FI + TiO ₂	FI + Cr-GAB	FI + TiO ₂ + Cr-GAB
0	-0.33	0.05	32.10	34.03
3	-0.34	0.03	31.60	33.05
6	-0.33	0.00	30.72	31.70
10	-0.33	-0.03	29.64	30.49
500	-0.23	-0.15	12.47	12.05
Phase splitting [3 to 6 mM]	0.00	0.03	0.88	1.35
Amplitude splitting [3 to 6 mM]	0.02	0.10	0.04	0.05

Table 4-13: Measured phase angles of different sensor compositions for different potassium concentrations after 188 days storage.

Potassium concentration [mM]	FI	FI + TiO ₂	FI + Cr-GAB	FI + TiO ₂ + Cr-GAB
0	-0.33	0.18	31.84	33.43
3	-0.33	0.13	31.52	32.64
6	-0.32	0.09	30.60	31.51
10	-0.32	0.05	29.19	29.87
500	-0.25	-0.11	12.24	11.95
Phase splitting [3 to 6 mM]	0.00	0.04	0.92	1.12

Amplitude splitting [3 to 6 mM]	0.02	0.10	0.05	0.07
---------------------------------	------	------	------	------

In summary, storage tests were successfully finished without any influences detected if sensors are stored under dry conditions, without light and at 7°C. The use of additives, TiO₂ and CrGAB for ion sensors is recommended.

4.4.9. Sodium fluoroionophores for blood measurements

Most of the gathered experience from the measurements shown in the previous sections for potassium can be transferred directly for sodium measurements. The same BODIPY dye is used for potassium and sodium measurements. Hence, the compatibility of CrGAB as a reference is ensured. Also, sterilization tests result in similar conclusions, since the composition of the sensor is similar and radiative sterilization works straight forward and consistent. The coefficients needed for the temperature effect compensation are already given in the section for potassium and are evaluated similar. The results for photobleaching, signal to noise experiments and the storability of the sensor can be transferred for sodium measurements since the only difference is in the size of the crown-ether.

Synthesis

Previous research used the sodium indicator of the first generation as a fluoroionophore for sodium, **Figure 4-26**. This indicator showed a low phase angle splitting in the physiological relevant concentration, 110 to 170 mM sodium. Ast et. al.¹¹⁵ showed that an elongated sidearm (methoxy-ethoxy-group) can help in the complexation of ions. Therefore, a fluoroionophore similar to the potassium fluoroionophore was synthesized. The only difference is in the size of the crown-ether, which is one ethylene glycol unit shorter, for the formation of the sodium selective crown-ether. The synthesized fluoroionophore should be more sensitive for sodium ions than the previous one and is investigated in the next subsection.

A big advantage of this new synthesized fluoroionophore is that until the fourth step the synthesis is completely similar to the synthesis of the potassium fluoroionophore. With this strategy, a lot of time can be saved by just increasing batch sizes for these steps.

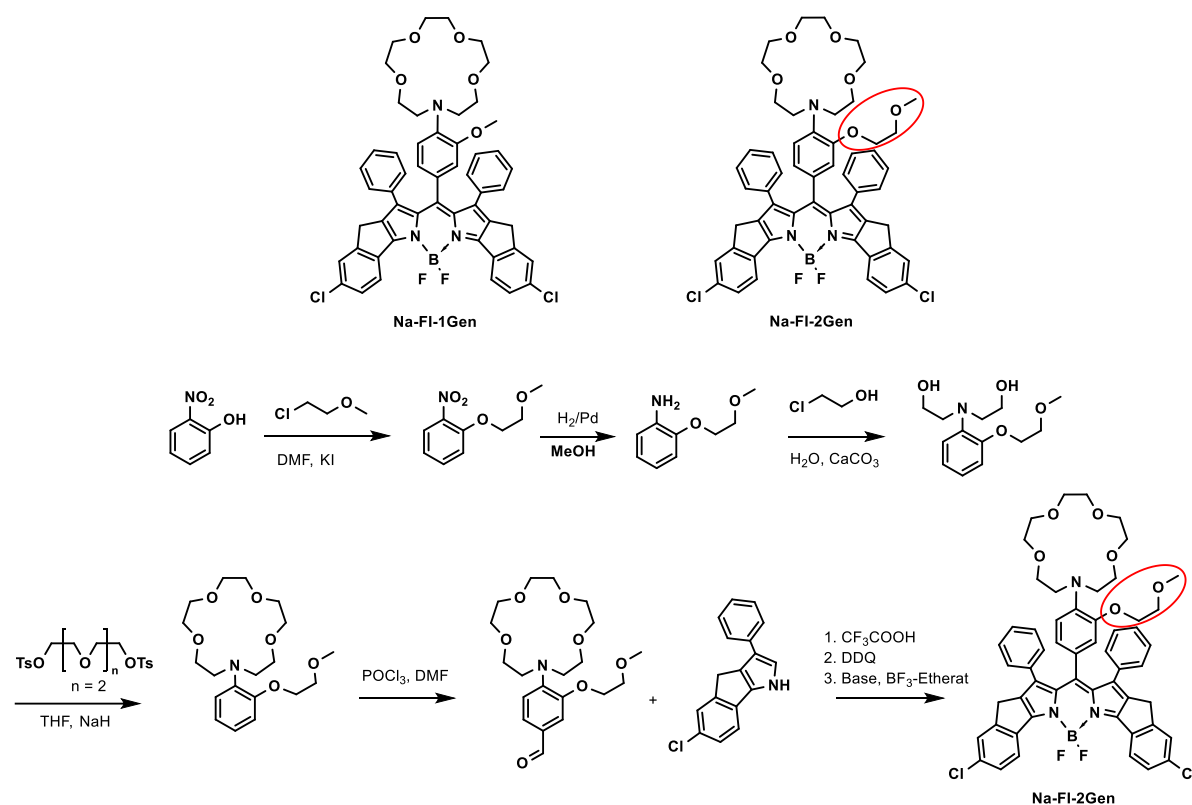


Figure 4-26: Synthesis route for the sodium fluoroionophore, Na-FI2gen. The indicator has an elongated sidearm for better sodium complexation.

Comparison of sodium fluoroionophores first and second generation

In **Figure 4-27** the new synthesized fluoroionophore is compared to the methoxy-sidearm fluoroionophore in different hydrogels. The sensitivity in the physiological relevant region (110 to 170 mM Na⁺) is 19% higher in the hydrogel D4. The introduction of the methoxy-ethoxy sidearm reveals indeed a better complexation of sodium ions within the crown-ether. Furthermore, if D1 (higher water uptake than D4) is chosen as a matrix for the fluoroionophore, the sensitivity is again 30% higher. The use of a fluoroionophore with a methoxy-ethoxy sidearm is therefore favored since the change of the indicator and to another matrix has a huge effect of overall 55% sensitivity enhancement.

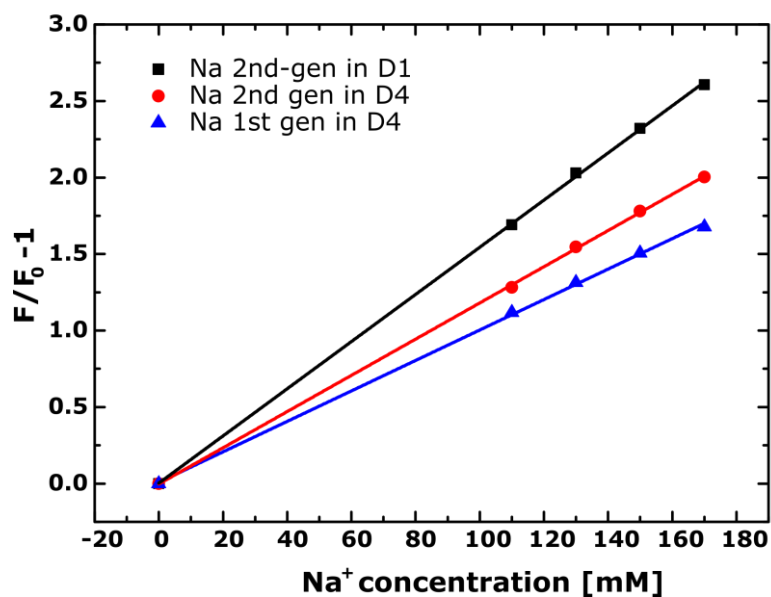


Figure 4-27: Comparison of the new indicator with the previously used fluoroionophore in D4 and D1.

Cross sensitivity to other ions

The new indicator was tested against cross sensitivity to K^+ , Ca^{2+} , Mg^{2+} and NH_4^+ in the hydrogels D4 and D1. Similar to the indicator of first generation, the fluoroionophore shows a cross sensitivity to potassium and ammonium. At a concentration of 500 mM K^+ F/F_0 values of 2.18 (D1) and 1.90 (D4) are evaluated. However, physiological standard blood concentrations for potassium are ranging from 4 to 5 mM, and within this range the fluorescence enhancement factor is 1.03-1.04 and therefore can be neglected. Ca^{2+} and Mg^{2+} did not show a cross sensitivity.

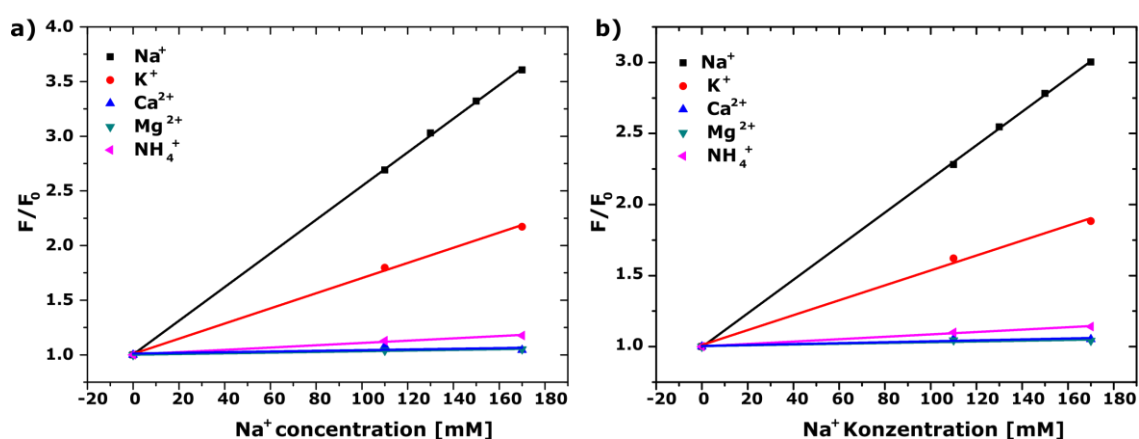


Figure 4-28: Cross sensitivity of the indicator towards competing ions in hydrogel D4 and D1.

Matrix effects (pHEMA)

The indicator was immobilized in pHEMA and calibrated identically to the investigations for potassium fluoroionophores. Remarkable results were obtained with one main drawback. The calibration of the immobilized fluoroionophore in pHEMA delivered a sensitivity enhancement of 530% compared to D4. (**Figure 4-29**) However, after storage in 0 mM buffer solution for 24 hours the sensitivity dropped tremendously, indicating this matrix serves not as a stable matrix. Investigations via absorption measurements revealed the formation of J-aggregates, visible at 780 nm. These experiments provide the evidence that pHEMA is not a suitable matrix for this fluoroionophore, forcing the indicator to aggregate and unable for complexation of ions.

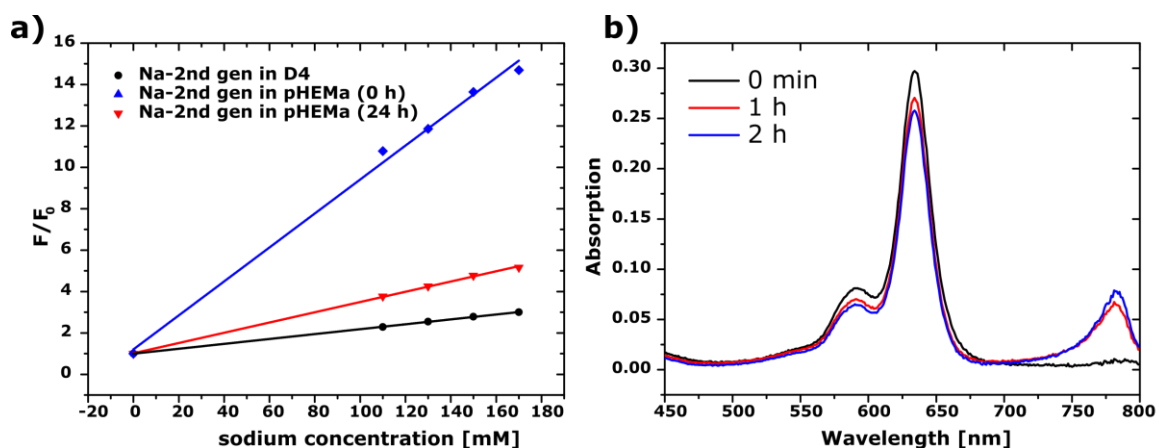
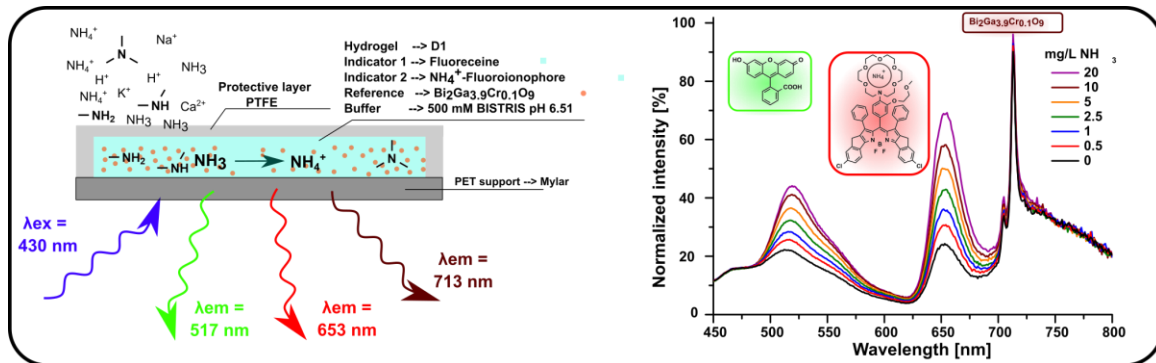


Figure 4-29: a) Loss of sensitivity in pHEMA within 24h. b) aggregation of the indicator in pHEMA within 2 hours.

5. Simultaneous sensing of ammonia and volatile amines with combination of a NH_4^+ fluoroionophore and a fluorescent pH indicator



5.1. Preface for the Manuscript

This chapter describes a new sensing strategy for amines using a NH_4^+ selective BODIPY fluoroionophore (**Chapter 2.8**), fluorescein and a phosphor-reference is presented. The combination of both indicators enables quantification of NH_3 and determination of substituted amines. This concept offers several new pathways for future amine sensing systems and might be a valuable tool for environmental applications and biotechnology.

A new concept for sensing volatile amines and ammonia simultaneously with a single sensor is shown in this chapter of the thesis. It combines a pH-sensitive indicator with a NH_4^+ selective fluoroionophore immobilized in a buffered hydrogel layer. With the usage of an internal buffer NH_4^+ is formed within the sensor membrane, which can be complexed by the fluoroionophore, emitting at 653 nm. The fluoroionophore reveals insensitivity to substituted amines, attributable to the high selectivity of the fluoroionophore towards NH_4^+ . Theoretical background can be found in **Chapter 2.6**.

The detection of substituted amines is enabled via the usage of pH-sensitive fluorescein, emitting at 417 nm. The combination of both indicators enables the quantification of NH_3 and the determination of MA, DMA and TMA. The use of a Cr^{3+} doped $\text{Bi}_2\text{Ga}_4\text{O}_9$ phosphor enables compensation of sensor for inhomogeneities in the thickness of the sensing layer, intensity of the excitation light and sensitivity of the photodetector, resulting in a robust sensing concept. Basic principles for the development of optical sensors is given in **Chapter 2.7**.

This concept offers several new pathways for future amine sensing applications, whereas the sensitivity towards NH_3 can be controlled via the usage of crown-ether based indicators and with the use of pH-indicators, substituted amine detection is arranged. The new approach may be valuable for environmental and biotechnological applications.

5.2. Abstract

An optical sensor for simultaneous measurement of ammonia and volatile amines is presented. The sensor relies on the combination of an ammonia BODIPY-fluoroionophore and fluorescein. Both indicators are embedded into a hydrogel D1 layer soaked with 500 mM BIS-TRIS (pH 6.5) buffer that is covered by gas-permeable hydrophobic porous polytetrafluoroethylene membrane. The fluoroionophore responds with increase of fluorescence intensity upon complexation of ammonium ion that is generated by protonation of ammonia after its diffusion through the hydrophobic membrane into the hydrogel layer. In contrast, fluorescence changes of the pH indicator are caused by dissolution of all species including ammonia, trimethylamine, dimethylamine and methylamine. Such approach allows simultaneous detection and quantification of ammonia and volatile amines. In order to enable ratiometric read-out, Cr(III)-doped $\text{Bi}_2\text{Ga}_4\text{O}_9$ phosphor that emits in the far-red part of the spectrum (emission maximum 713 nm) is immobilized into the sensing layer along with the indicator dyes that emit green light (pH indicator, emission maximum 517 nm) and red light (fluoroionophore, emission maximum 653 nm).

5.3. Introduction

Sensing of ammonia either in the gas phase or in solution has a great relevance for process optimization in biotechnology, agriculture, chemical industry, sewage plants and aquaculture. Ammonia also is an important analyte in clinical diagnostics, environmental monitoring and life sciences. One of the reasons is the fact, that ammonia is toxic to humans and animals^{181–183}. Since ammonia is a key product in many metabolic pathways, it is of fundamental interest to create robust and reliable low-cost sensors for continuous monitoring of this parameter. Very often free ammonia is accompanied by volatile amines¹⁸⁴. On the one hand volatile amines are notorious interferents for ammonia sensors, on the other hand they are also parameters of interest. Among numerous analytical methods to monitor ammonia and amines, optical sensors represent an attractive low cost solution for this task. The classical way to sense ammonia and amines is to utilize their basic properties. Such optical ammonia sensors rely on absorptiometric or fluorescent pH

indicators which are immobilized in hydrophilic or hydrophobic polymers. Ammonia and volatile amines either increase the internal pH of a buffer, or deprotonate an indicator directly. Frequently used indicators includes fluorescein^{185,186} and other xanthene dyes¹⁸⁷⁻¹⁸⁹, aza-BODIPYs^{190,191}, triphenylmethane based dyes¹⁹²⁻¹⁹⁴ and coumarin dyes^{186,195,196}. The absorptiometric indicators are used both directly to induce a visible color change and as FRET acceptors (typically in the deprotonated form) to induce a fluorescence response of other dyes^{188,197,198}. Determination of dissolved ammonia in water requires either utilization of hydrophobic polymers as hosts for the pH indicator or application of additional hydrophobic gas-permeable membrane that covers the sensing layer in order to avoid cross sensitivity of sample pH. Such hydrophobic ion barriers utilize silicone rubbers^{198,199}, sol-gels^{188,200}, plasticized PVC^{188,201}, microporous hydrophobic membranes^{57,190,191} and other materials^{197,201-204}. Unfortunately, such hydrophobic barriers also significantly reduce the diffusion of the analyte that slows down the sensor's response. A more serious drawback of the ammonia sensors that rely on pH transducers is cross-talk of the sensor to volatile amines such as methylamine (MA), dimethylamine (DMA) and trimethylamine (TMA). Similar to ammonia, these volatile bases also diffuse into the sensing layer causing deprotonation of the indicator dye. The presence of such amines is a special problem in ammonia sensing in aquaculture.

Müller et al.¹¹⁶ recently reported a novel approach for selective optical NH_3 sensing. A buffer-soaked hydrogel was used to generate ammonium ions from ammonia passing through a gas-permeable hydrophobic membrane and the formed NH_4^+ were quantified with help of a crown-ether fluoroionophore. Although the fluoroionophore is primarily designed to sense potassium ions, it also shows considerable sensitivity to the ammonium ions due to their similar size^{57,74}. However, the cage of the receptor is too small to complex the protonated forms of volatile amines.

Going a step further, in this contribution we introduce the first double transducer sensing concept to monitor ammonia and volatile amines simultaneously. The new transducer combines the two transducers mentioned above in a single sensing layer: a pH indicator which detects free ammonia and amines simultaneously, and an additional NH_4^+ fluoroionophore that responds to ammonia only. In order to enable ratiometric read-out the selected indicators show different spectral properties (emission in the green and red part of the spectrum) and the sensing material additionally incorporated a Cr(III)-doped $\text{Bi}_2\text{Ga}_4\text{O}_9$ phosphor²⁰⁵ as a far-red emitting luminescent reference. The proof of concept of

the new multiparameter sensing scheme is presented here as a basis for the development such sensors for special analytical tasks in the future.

5.4. Material and Methods

5.4.1. Materials

CAPS, TRIS, BIS-TRIS, Cr_2O_3 and potassium chloride (KCl) were bought from Carl Roth GmbH (www.carlroth.com). Polyurethane hydrogel, Hydromed D1, was purchased from AdvanSource biomaterials (www.advbiomaterials.com). Poly(ethyleneterephthalate) support Melinex 505 was obtained from Pütz (www.puetz-folien.com). Fluoropore™ membrane PTFE (0.45 μm pore) was obtained from Merck Millipore Ltd. (www.merckmillipore.com). Methylamine-, dimethylamine- and trimethylamine-hydrochlorides (MA, DMA and TMA, respectively) were bought from Acros (www.acros.com). Bi_2O_3 , Ga_2O_3 , Ammonium chloride and fluorescein were purchased from Sigma Aldrich (www.sigmaaldrich.at). Ammonium-sensitive BODIPY fluoroionophore was synthesized as described previously¹¹⁷.

5.4.2. pH calibration solutions

pH calibration solutions contained 20 mM universal buffer (CAPS, citrate, BIS-TRIS and TRIS). The pH was adjusted with HCl. A digital pH meter (Seven Easy, Mettler Toledo, www.mt.com) was calibrated at 21 °C with standard buffers of pH 10.0, 7.0 and 4.0 (WTW, www.wtw.com).

5.4.3. Ammonia and amine solutions

The solutions were prepared by dissolving appropriate amounts of the respective chloride salts in a 150 mM phosphate buffer (pH 7.0). The free amine concentrations were calculated with the Henderson-Hasselbach equation using the respective pK_a values of the amines at a temperature of 21 °C.

5.4.4. Fluorescence measurements

Calibrations were performed with the sensing foil fixed in a home-made flow through cell. A peristaltic pump (Gilson miniplus 3, www.gilson.com) was used for pumping buffers through the cell. The temperature of the calibration solution and the flow through cell was held constant at 21 °C using a thermostat (Julabo F12, www.julabo.com). Fluorescence spectra were recorded in the front-face mode on a Fluorolog3 spectrofluorometer (Horiba

Jobin Yvon, www.horiba.com) equipped with a NIR-sensitive photomultiplier R2658 from Hamamatsu (300 – 1050 nm).

5.4.5. Synthesis of $\text{Bi}_2\text{Ga}_{3.9}\text{Cr}_{0.1}\text{O}_9$

Bi_2O_3 , Ga_2O_3 and Cr_2O_3 were homogenously mixed in a stoichiometric ratio using a porcelain mortar and acetone as a dispersant. After evaporation of the solvent the greenish residue was transferred into a porcelain crucible and sintered 6 hours at 750 °C in air. Subsequently, the light brown solid was pulverized and sintered again at 800 °C for 6 hours. The green product is finally grounded again utilizing a mortar and a ball mill to obtain a microcrystalline powder.

5.4.6. Sensor preparation

Hydromed D1 was dissolved in a mixture of ethanol and 500 mM BIS-TRIS buffer (9:1, v/v) to yield a stock solution of 5 w%. Appropriate amount of the indicators were dissolved in the hydrogel stock solution resulting in a indicator concentration of 0.66 w% fluoroionophore and 0.0033 w% fluorescein in respect to the total amount of hydrogel used in the cocktail. The microcrystalline powder of the reference phosphor (6 w% in respect to hydrogel) was dispersed in the “cocktail”. This “cocktail” was knife coated onto the poly(ethyleneterephthalate) foil (12.5 μm wet film thickness). Immediately after the knife-coating, a PTFE membrane was laid onto the still wet film to obtain the composite sensor material after solvent evaporation.

5.5. Results and Discussion

5.5.1. Sensor composition and response mechanism

Figure 5-1 schematically shows the composition of the sensing material. NH_3 and amines but not ionic species present in the analyzed media are able to diffuse through the protective PTFE membrane. The sensing layer made of hydrogel is soaked with internal buffer (pH 6.5) that generates the protonated (alkyl)ammonium species. The generated NH_4^+ ions are selectively complexed by the fluoroionophore, which leads to an increase in fluorescence emission due to reduction in the photoinduced electron transfer based quenching¹¹⁶. In contrast to the fluoroionophore, a pH indicator (fluorescein) that is also immobilized in the sensing foil responds to both ammonia and amines. The concentration

of BIS-TRIS buffer (500 mM) is high enough to enable significant degree of ammonia/amines conversion into the corresponding cations but low enough to show some pH change upon this process and consequently induce the fluorescent response of the pH indicator. Importantly, the pH of the buffer is very close to the pK_a value of fluorescein (6.4)²⁰⁶ that insures the strongest fluorescence response even at considerably low changes in pH of the internal buffer. It should be noted however, that hydrogel media is not purely aqueous (70% water in the swollen state according to the manufacture)²⁰⁷ so that the apparent pK_a value may be slightly different.

As expected, the fluorescence of both indicators responds to ammonia (**Figure S 5-1**). Both for the fluorophore (λ_{max} 653 nm) and the pH indicator (λ_{max} 517 nm) the fluorescence intensity increases with increasing ammonia concentration. As mentioned above, coordination of ammonium ion by the fluoroionophore results in the inhibition of the PET effect. In case of the pH indicator, ammonia promotes conversion of the mono-anionic form of fluorescein to much stronger absorbing and emitting dianionic form.²⁰⁸ The selected excitation wavelength (430 nm) enables excitation of both dyes. Although the most intense absorption band of the fluoroionophore is located at 630 nm, excitation also is possible in the UV-blue part of the spectrum up to about 450 nm so that selected excitation wavelength matches fairly well the secondary absorption maximum of the dye. Due to the fact that absorption of fluorescein at 430 nm is significantly stronger than that of the fluoroionophore and that the fluorescence of the fluoroionophore is mostly “switched off” in the absence of ammonia, much smaller concentration of the fluorescein (0.0033 and 0.66 w% in respect to hydrogel D1 for fluorescein and fluoroionophore, respectively) was used to achieve comparable fluorescence intensities from both dyes.

In order to enable referenced ratiometric read-out we added a microcrystalline powder of chromium(III) doped bismuth gallate²⁰⁵ into the hydrogel layer. This phosphor shows narrow luminescence in the far-red part of the electromagnetic spectrum (λ_{max} 713 nm, **Figure S 5-2**) accompanied by less intense broad emission in the far-red and NIR parts of the spectrum. Broad excitation band (λ_{max} 446 nm) almost ideally matches the excitation wavelength selected for the indicators. The emission spectra of the two probes and the reference are clearly separated (**Figure 5-1**). It should be mentioned that the emission of the phosphor and the shoulder in the emission spectrum of the fluoroionophore are observed at the same wavelengths (**Figure S 5-2**) that explains that explains a minor increase in the overall emission at this wavelength in presence of the analyte (**Figure 5-1**).

5. Simultaneous sensing of ammonia and volatile amines with combination of a NH_4^+ fluoroionophore and a fluorescent pH indicator

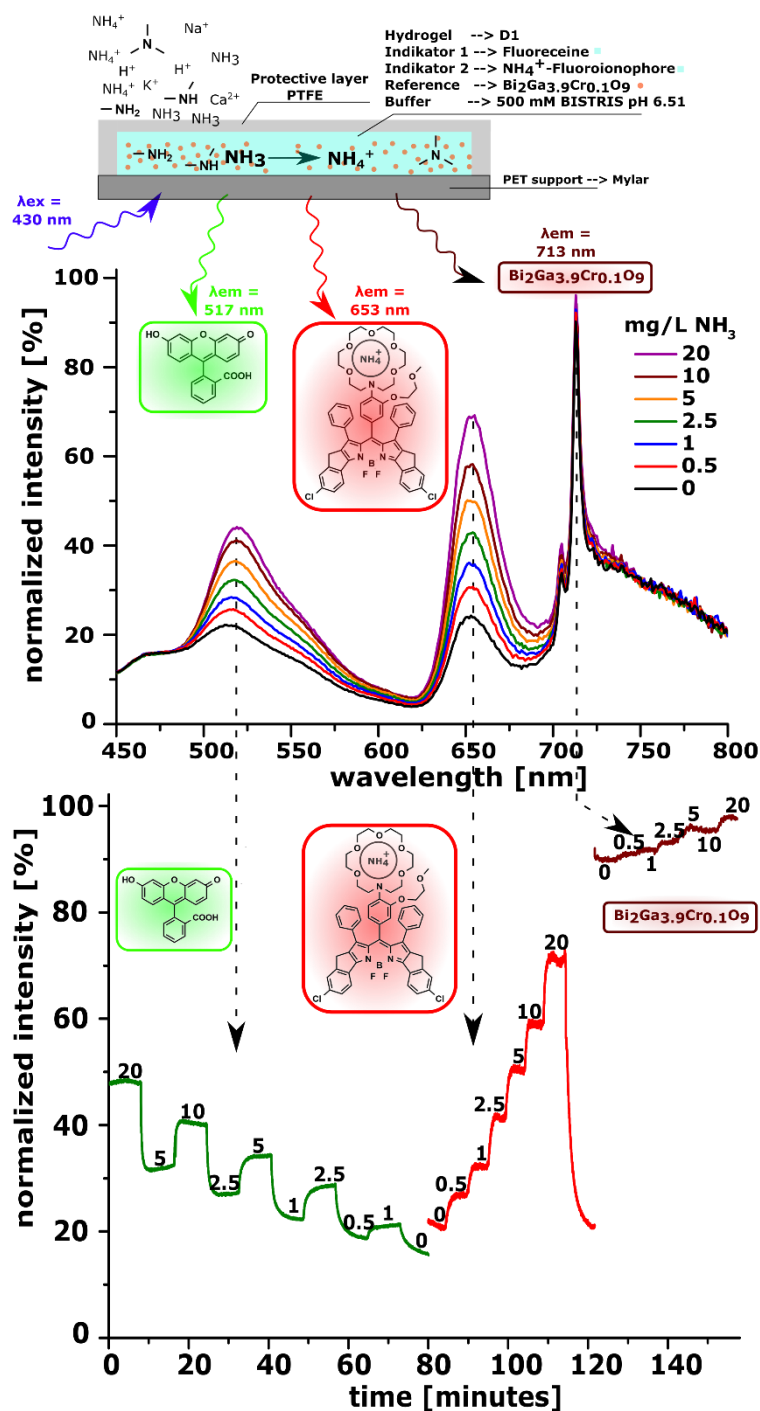


Figure 5-1: Schematic illustration of the sensor composition (A), spectral properties of the emitters (B) and sensor response to ammonia in the steady state (B) and kinetic (C) modes.

5.5.2. Sensor response to ammonia and amines

Figure 5-2 a and c, calibrations for both indicators from 0 to 20 mg/L free amine concentration against the calculated $(F-F_0)/F_{\text{ref}}$ value are shown. The free amine concentration represents a plot typically used in fish farming, showing the toxic aspect of the amines. Since the pK_a of NH_3 is 9.26, in normal seawater both, the ionized and the

unionized forms exist. Therefore, this plot represents the toxic fraction of the amines in water. **Figure 5-2 b** and **d** represent total ammonia concentrations (TAC) and combines the unionized and ionized fractions of amines in water. Since methylamine (MA), dimethylamine (DMA), Trimethylamine (TMA) and ammonia differ in their pK_a value and their molecular weight, the plots for free amine concentration and TAC differ significantly. Typically, the amine equilibrium is highly dependent on pH, ionic concentration and the temperature. For this sensor, a PTFE membrane is used which is impermeable for charged species, therefore the effects derived from fluctuating pH and ion strength can be excluded and sensor response always correlates to the current amine concentration, without any cross-sensitivity, usually persistent for electrode measurements.

Figure 5-2 a shows some cross-sensitivity towards MA in the range from 0 up to 20 mg/L. This effect can be explained by the size of the corresponding analyte. Since ammonium can be perfectly complexed by the crown ether, also methyl ammonium ions are complexed, because they reveal similar cation diameters and the methyl group can be oriented vertically out of plane, it fits in the crown as well. By plotting the TAC this effect relativizes, because the amount of free MA at 21°C is 19.16 times lower compared to NH_3 . Nevertheless, MA still is complexed by the crown ether, revealing a cross-sensitivity. The response towards DMA and TMA is marginally rising with increasing TAC and can be neglected. The precise detection of NH_3 via the fluoroionophore can be used for the compensation of the pH effect towards fluorescein, enabling the determination of the amine concentrations, MA, DMA, TMA.

Fluorescein responds both to ammonia and amines, since the pH is changing within the sensor matrix. Interestingly, TMA shows the highest response whereas MA the lowest. This effect was not expected because the basicity of the amines in water follows pK_b : $DMA > MA > TMA > NH_3$ ($3.25 > 3.40 > 4.19 > 4.74$).²⁰⁹ Two effects are most useful to describe this tendency. (i) The inductive effect, favours tertiary amines to be more basic due to the +I effect of the three alkyl groups which are directly attached to nitrogen. (ii) The solvation effect favours primary amines and ammonia to be more basic due to greater solvation of its cation. Since the hydrogel contains hydrophilic and hydrophobic domains the order is changed. The +I effect increases for higher substituted alkyl-terminated amines, since the hydrophobic domains of the polymer enhance inductive effects. Additionally, the solvation effect increases the basicity for ammonia and lower substituted amines. These effects cause that the response curves follow the $TMA > NH_3 > DMA > MA$ tendency.

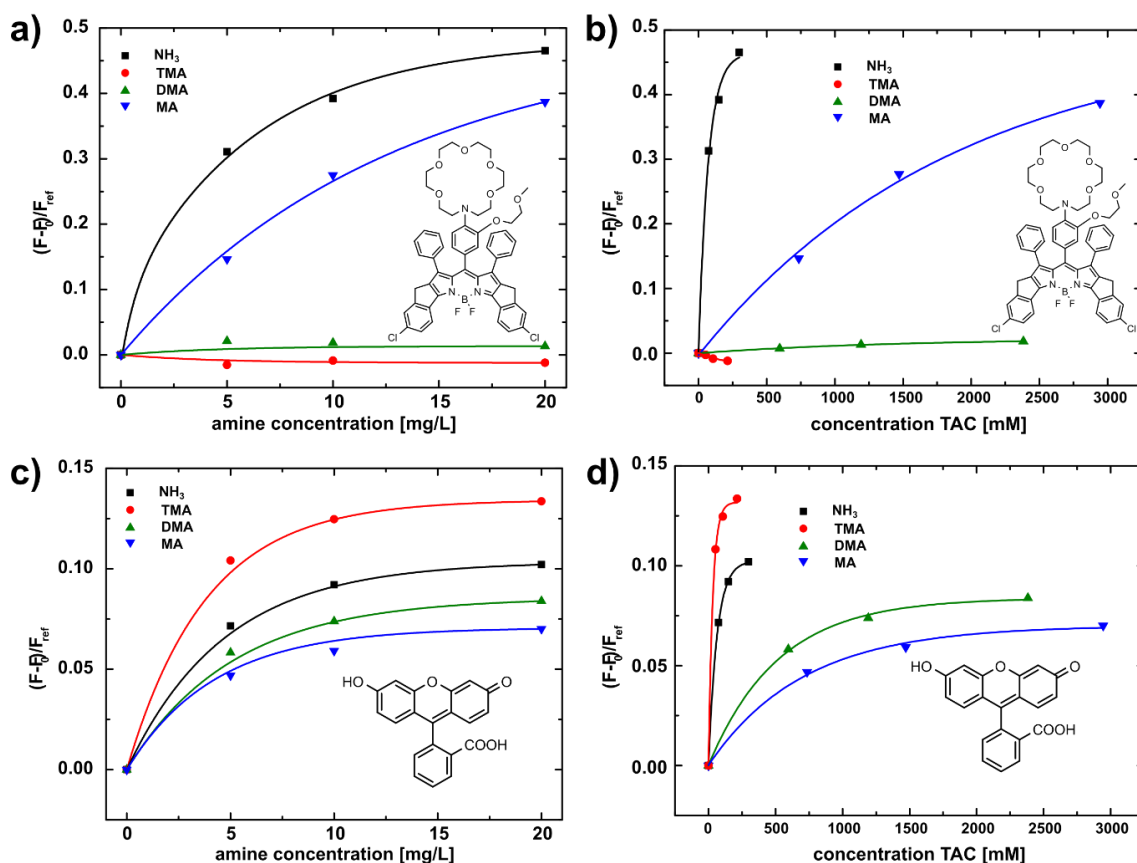


Figure 5-2: Calibrations for fluoroionophore and fluorescein from 0 to 20 mg/L free amine concentration (a,c) and converted plot in total amine concentration (b,d). With the use of the reference the y-axis ($(F-F_0)/F_{ref}$) represents comparable and reproducible values.

5.5.3. Mixtures of ammonia with substituted amines

In order to check the reliability of the sensing system, substituted amines were added to a solution with fixed NH_3 concentration, which was held constant at 150 mM (TAC). **Figure 5-3** shows F/F_0 values for both the fluoroionophore and fluorescein.

The response of the fluoroionophore to 150 mM NH_3 was as expected quite high, revealing a F/F_0 value of 3.00 (**Figure 5-3**). The enhancement factors after addition of amines, TMA (107 mM) and DMA (150 mM), 3.06 and 3.09 were low again, indicating that the fluoroionophore is not complexing dimethylammonium or trimethylammonium ions. Like previously shown, the fluoroionophore reveals a slight cross sensitivity towards MA. At 150 mM NH_3 and 150 mM MA an F/F_0 value of 3.27 was calculated. Additionally, a spectrum at 300 mM NH_3 is shown, revealing a value of 3.43, indicating that the fluorescence has not yet reached its maximum emission intensity. The other way around, fluorescein, shows at 150 mM an enhancement factor of 1.35, whereas additional TMA (107 mM), DMA (150 mM) and MA (150 mM) reveal an enormous increase of 2.02, 1.68

and 1.48. At a TAC of 300 mM NH_3 a F/F_0 value of 1.72 was measured, which is lower than 150 mM NH_3 + 150 mM TMA ($F/F_0 = 2.02$) confirming the theory previously mentioned that TMA causes stronger response within this matrix.

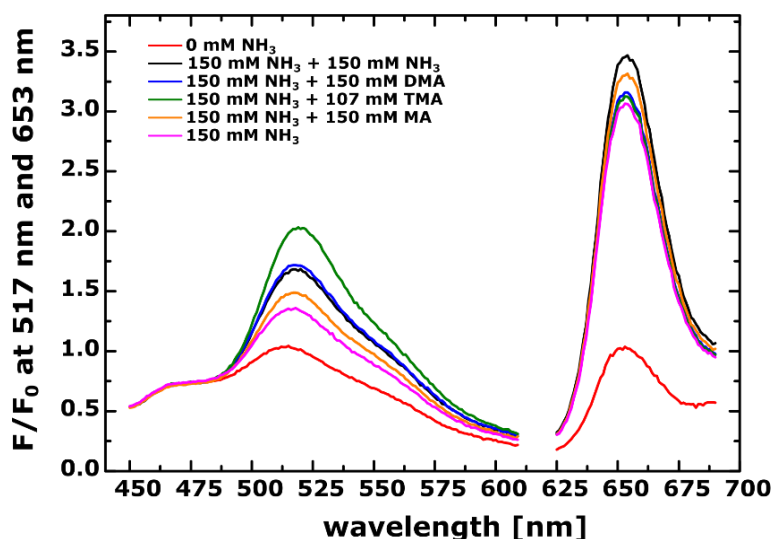


Figure 5-3: F/F_0 values for a calibration with 150 mM NH_3 + different amounts of substituted amines. Both fluorescence emissions were normalized to their 0 mM TAC value. Fluoroionophore does not reveal a significant cross-talk to amines, whereas fluorescein responds to both ammonia and amines.

Kinetic measurements shown in **Figure 5-4 a** and **b** reinforce these data. Since the fluoroionophore showed nearly no dependency on interfering amines, the fluorescein does. That enables a versatile strategy for the detection of substituted amines. With the fluoroionophore the amount of NH_3 can be measured precisely, since all other amines do not show a cross-sensitivity. The concentration of the other amines can be measured with the emission intensity of fluorescein. Since the NH_3 concentration can be determined, the concentration of NH_3 can be compensated and the substituted amine concentration evaluated. Additionally, in **Figure 5-4 a** and **b** the influence of pH and ion strength was investigated, confirming that a PTFE membrane, is only permeable for gases. To verify this property, pH buffer at a pH of 5 and 8 were pumped through the measurement cell and both indicators did not show a response. Also, at 100 mM K^+ no response was measured. Since the NH_4^+ indicator is usually used for K^+ detection this is an important feature, ensuring a stable sensor. Additionally, the indicators show full reversibility, enabling reliable amine detection over time.

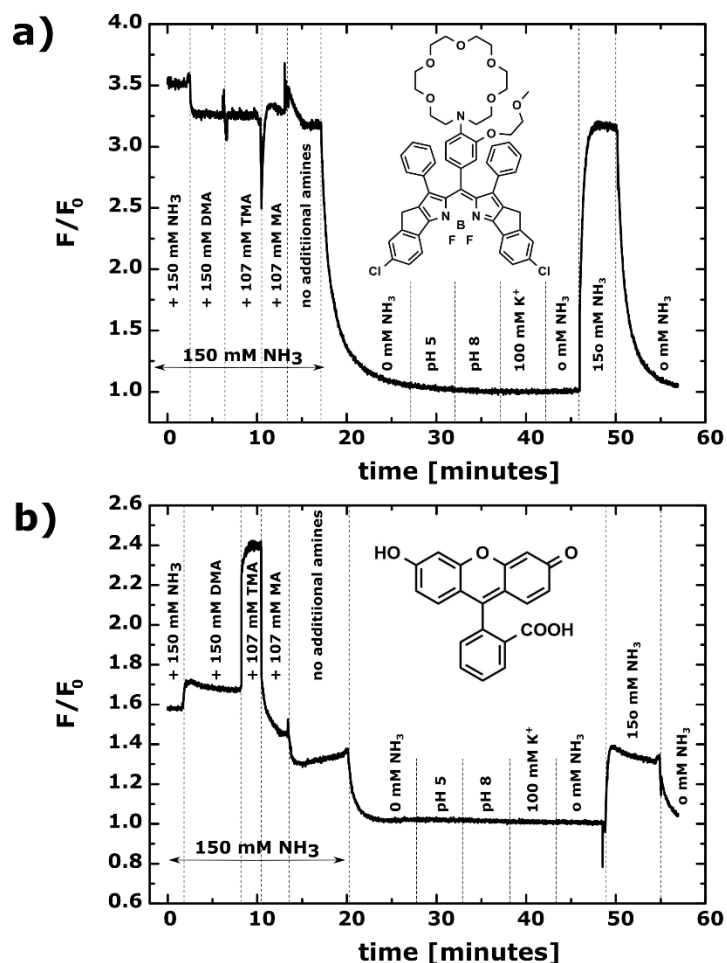


Figure 5-4: Measurements over time at fixed wavelengths and alternating amine concentrations. Plot a) shows the calibrations for the fluoroionophore, plot b) for fluorescein. The fluoroionophore does not reveal cross sensitivity towards substituted amines. The fluorescence intensity of fluorescein shows strong dependency on the concentration of substituted amines. The material was additionally were screened for potential pH dependency between pH 5-8 and interference by 100 mM K^+ , showing a robust and reversible sensing system.

Table 5-1: Calculated F/F_0 values for both indicators for the calibrations using emission spectrums and kinetic measurements. From the deviations at the corresponding amine concentration the overall accuracy was calculated.

buffer composition [mM]	Fluorescein F/F_0		Fluoroionophore F/F_0	
	spectrum	kinetic	spectrum	kinetic
0 NH_3	1.00	1.00	1.00	1.00
150 NH_3	1.35	1.33	3.01	3.12
150 NH_3 + 150 NH_3	1.68	1.58	3.43	3.46
150 NH_3 + 150 MA	1.48	1.44	3.32	3.30
150 NH_3 + 150 DMA	1.72	1.67	3.17	3.23
150 NH_3 + 107 TMA	2.02	2.37	3.14	3.21
overall accuracy [%]	94.3 ± 5.4		98.1 ± 1.2	

For future applications some criteria must be fulfilled. (i) The sensors require a pre-calibration adjusted on the amine concentration measured (depending on the application). (ii) Combinatorial analysis is indispensable for the determination of TMA, DMA and MA, since all amines respond to fluorescein but in a certain strength. (iii) Depending on the application, temperature effects must be considered, since the complexation of ions in crown ethers is temperature dependent.

5.6. Conclusion

A new concept for sensing volatile amines and ammonia simultaneously with a single sensor is presented. It combines a pH-sensitive indicator with a NH_4^+ selective fluoroionophore immobilised in a buffered hydrogel layer. With the usage of an internal buffer NH_4^+ is formed within the sensor membrane, which can be complexed by the fluoroionophore, emitting at 653 nm. The fluoroionophore reveals insensitivity to substituted amines, attributable to the high selectivity of the fluoroionophore towards NH_4^+ . The detection of substituted amines is enabled via the usage of pH-sensitive fluorescein, emitting at 417 nm. The combination of both indicators enables the quantification of NH_3 and the determination of MA, DMA and TMA. The presented sensing system shows fast response times, full reversibility and no cross talk to ionic strength and pH of the external solution. With this novel concept, NH_3 can be measured and compensated for substituted amine detection. The use of a Cr^{3+} doped $\text{Bi}_2\text{Ga}_4\text{O}_9$ phosphor enables compensation of sensor for inhomogeneities in the thickness of the sensing layer, intensity of the excitation light and sensitivity of the photodetector, resulting in a robust sensing concept. This concept offers several new pathways for future amine sensing applications, whereas the sensitivity towards NH_3 can be controlled via the usage of crown-ether based indicators and with the use of pH-indicators, substituted amine detection is arranged. The new approach may be valuable for environmental and biotechnological applications.

5.7. Supporting Information

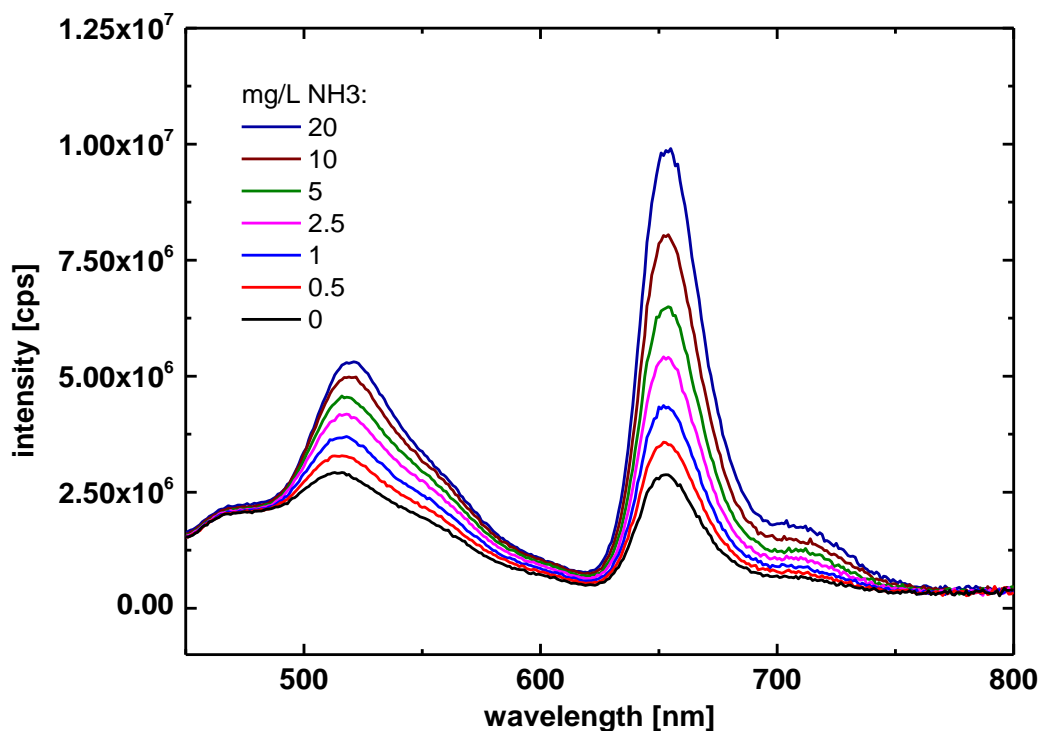


Figure S 5-1: Sensor foil containing 0.66w% fluoroionophore; 0.0033w% fluorescein in hydrogel D1. Buffer contained 500mM BISTRIS with a pH of 6.5.

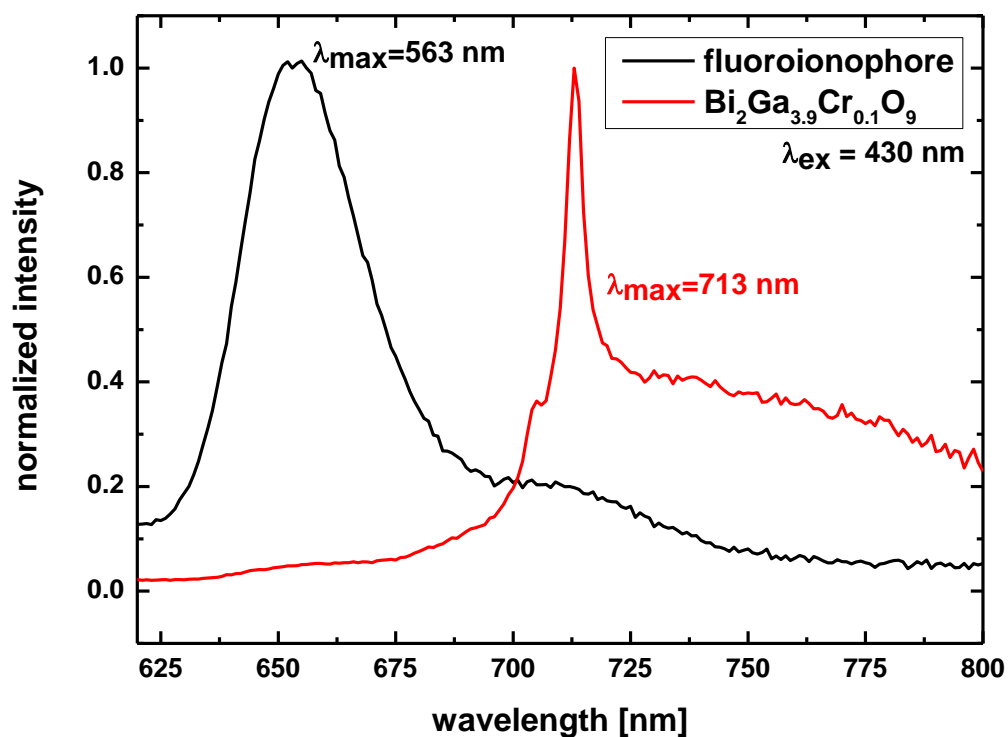


Figure S 5-2: Emission spectra of the NH_4^+ selective BODIPY fluoroionophore and the phosphor $\text{Bi}_2\text{Ga}_4\text{O}_9$. Excitation wavelength was chosen to be 430 nm.

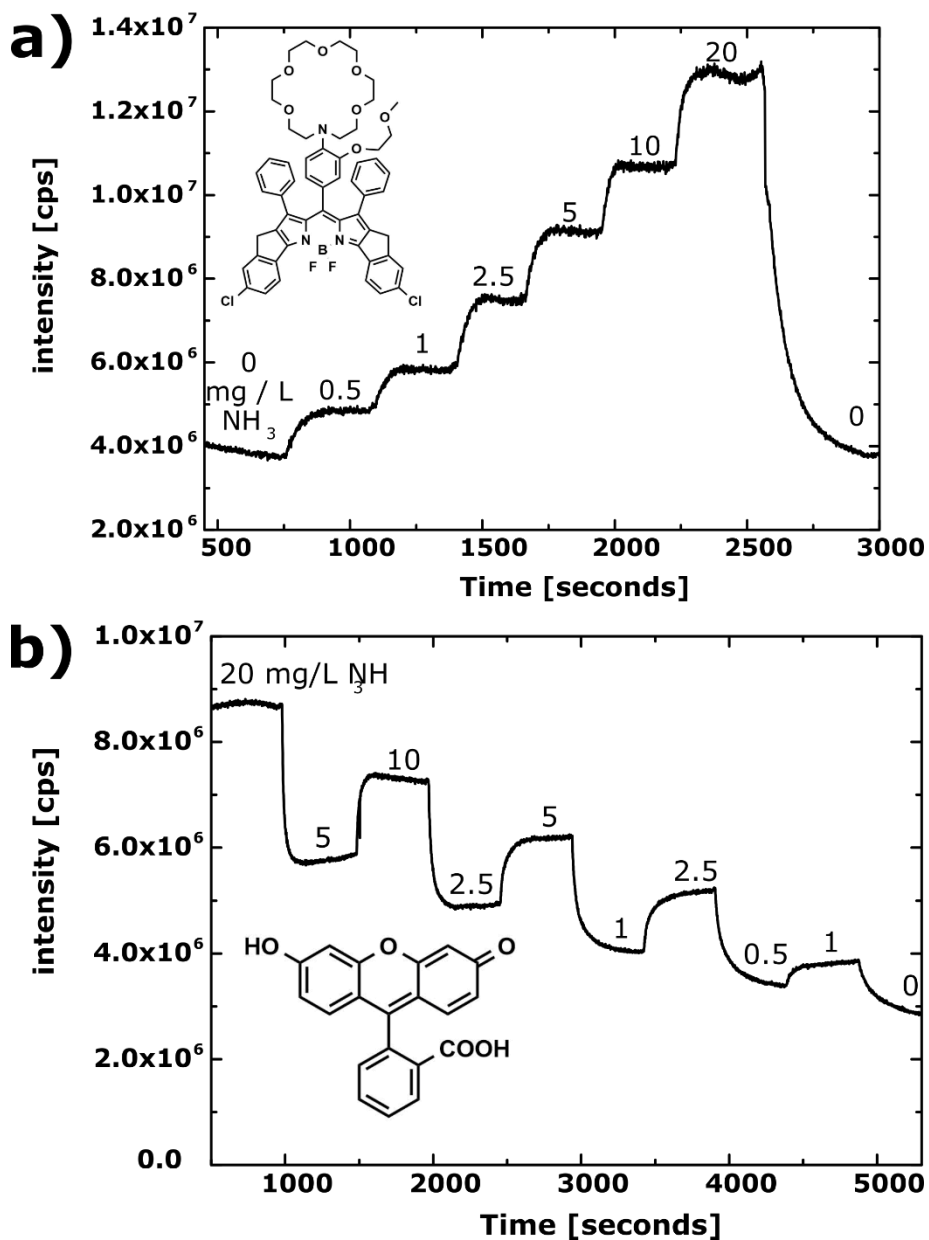
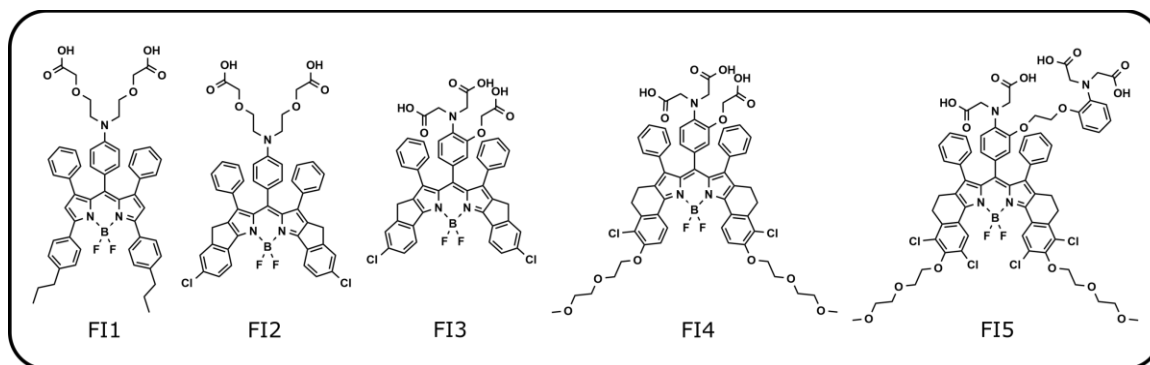


Figure S 5-3: Sensor response to ammonia for fluorescein and the fluorionophore, measured in kinetic mode.

6. Calcium Fluoroionophores



6.1. Preface for the Manuscript

This manuscript focuses on the synthesis of new calcium indicators using BODIPY fluorophores. The aim of this chapter was tackling the challenges of the behavior of charged fluoroionophores in solvents for calcium sensing.

Three different calcium receptors *o*-aminophenol-*N,N,O*-triacetic acid (APTRA), *N*-phenyliminodiethoxyacetic acid (PIDA) and 1,2-bis(*o*-aminophenoxy)ethane-*N,N,N',N'*-tetraacetic acid (BAPTA) with different sensitivities for calcium are used for the synthesis of fluoroionophores (**Chapter 2.2** and **2.7**). Therefore, ester-protected receptors are attached to BODIPY dyes, resulting in a fluoroionophore-intermediates, which are investigated with regard to their photophysical properties. The main properties of BODIPY dyes is described in **Chapter 2.8**.

Saponification of the protected fluoroionophores resulted in the corresponding sodium salts, capable to complex the divalent calcium ion. The resulting fluoroionophores are based on PET, described in **Chapter 2.5**. The FIs properties in ethanolic solutions are investigated, and the behavior in respect to shelf life and pH changes was screened. Additional experiments, using aqueous THF solutions and EDTA resulted in a sensing setup capable of calcium detection in solution. The final immobilization of an indicator in a hydrogel (principle described in **Section 2.7.3**) show first pretests, for a sensing-setup detecting calcium.

6.2. Abstract

Here, five novel calcium fluoroionophores are synthesized, using boron-dipyrromethene (BODIPY) dyes as chromophores. Depending on the extension of the π -system, four indicators possess high molar absorption coefficients (ϵ up to 120 000 M⁻¹cm⁻¹; THF) and emit in the red region (up to 682 nm, DCM; **FI4**) of the electromagnetic spectrum. Additionally, two novel BODIPY dyes, which contain polyethylene glycol groups, were prepared. These side chains increase the hydrophilicity of the fluoroionophores, with the intention of preventing aggregation phenomena in solution and hydrogels. The use of *o*-aminophenol-*N,N,O*-triacetic acid (APTRA) as a receptor, instead of *N*-phenyliminodiethoxyacetic acid (PIDA), not only increases the sensitivity of the corresponding fluoroionophore but also results in the hypsochromic shift of the emission maximum (662 to 667 nm) if the same BODIPY core was used (**FI2** and **FI3**). Saponification of the protected FI-esters, yields in the corresponding fluoroionophore salt of the indicators, which were investigated in several experiments. The indicators behavior in different ethanolic compositions was investigated in terms of their PET-efficiency, shelf life and the dependency on pH changes. Calibrations in THF, resulted in a promising calibration-setup in solution. Indicators **FI3**, **FI4** and **FI5** reveal a high sensitivity (μ M-range): the emission of fluoroionophores was fully switched off in presence of EDTA that ensures calcium-free 0 mM fluorescence emission value. The usage of THF and EDTA for calibrations presents a promising approach for evaluating the sensitivity of the fluoroionophores for the future. Pretests in hydrogels also resulted in a reversible sensing system and represents the basis for future divalent ion sensing.

6.3. Introduction

Calcium is the fifth most common element on the earth`s crust. It plays a key role in processes that include biology and environmental processes.²¹⁰ Ocean acidification is a key parameter, changing the free Ca^{2+} concentration in the food chain and the biodiversity of the ecosystem, effecting shells and skeletons grow thinner or even stop growing.²¹¹ Therefore, calcium levels in local seawater are of great importance.

Calcium exists around two percent of the human body mass.²¹² Calcium boosts bone density and acts as a buffer for the rest of the tissue. A bit more than 50 percent of the calcium in our blood is bound to proteins, while the remainder occurs in its ionized form. Calcium function in our body varies from muscle relaxation, blood coagulation and enzyme activity. Another significant feature is that calcium stabilizes cell membranes²¹³ and releases hormones from the neuron glands and neurotransmitters.^{214,215} Providing an adequate supply of calcium during pregnancy and child development is important. Adequate nutrition prevents osteoporosis in older people.²¹⁶ Since calcium is absorbed by the intestine with the aid of vitamin D, a depletion of vitamin D leads to a reduction of calcium stores and blood levels.²¹⁷ Low calcium concentrations in the human body are called hypocalcemia, whereas high calcium levels are referred as hypercalcemia.^{212,214}

On the basis of the above-mentioned examples, it is crucial to sense calcium in both the environment and the human body^{218,219}. Optical ion sensors and probes represent a powerful tool to measure calcium ions, since fluoroionophores show a versatile sensitivity depending on the receptor used and they reveal a good selectivity towards competing ions. Therefore, the application of optical calcium sensors for clinical diagnostics and environmental monitoring is of great interest.

6.3.1. Indicators for Calcium

The development of hosts for polyvalent cations, such as calcium, is by far more difficult than for monovalent ions because charged moieties for ion complexation are required. Electronic densities of uncharged hosts do not supply sufficient attraction force. Therefore, apart from some exceptions^{220,221}, almost all receptors for doubly charged cations have an open chain like structure and incorporate charged moieties.

The first reported receptor for calcium was published by Tsien et al.⁶³ The working group synthesized an EGTA (Ethylene glycol-bis(2-aminoethylether)-N,N,N,N-tetraacetic acid) derivative, which is known for selective complexation of calcium ions. The synthesized derivatives are shown in **Figure 6-1** and reveal a sensitivity in the μM range with a good selectivity over other divalent ions. Tsien set the starting point for the development of new receptors for calcium complexation events, and since then, various indicators have been developed.⁶⁴⁻⁷⁰

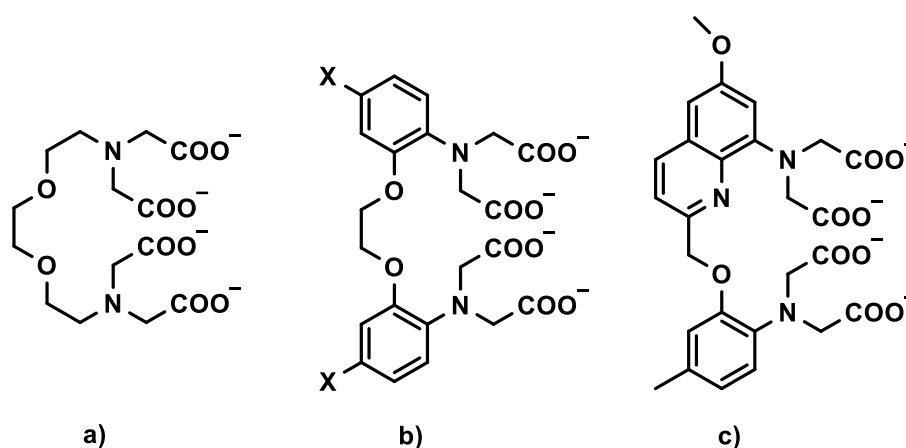


Figure 6-1: Structure of Ethylene glycol-bis(2-aminoethylether)-N,N,N,N-tetraacetic acid, EGTA (**a**) and the developed 1,2-bis(*o*-aminophenoxy)ethane-*N,N,N,N*-tetraacetic acid, BAPTA derivatives (**b + c**) by Tsien and coworkers.⁶³

For the determination of calcium in blood the sensitivity of BAPTA is too high, since the receptor responds in the μM range and the typical Ca^{2+} concentrations in blood are 2.15-2.55 mM/day¹⁵, *N*-phenyliminodiethoxyacetic acid (PIDA), (**Figure 6-2**), , on the other hand, shows sensitivities in the mM range, and therefore better suitable for measurements in whole blood. He et al.⁶⁴ synthesized a derivative of the receptor, mentioned above. In an aqueous solution, this receptor showed a dissociation constant K_d in the range of 0.3 to 2.2 mM, i.e. in the range of calcium concentration characteristic for blood measurements. The receptor (**Figure 6-2**) is very attractive for integration into fluoroionophores and optical ion sensors since it fulfills certain criteria. It contains a tertiary nitrogen, which

performs as electron donating group during interaction with calcium (**Section 2.6.1**). Furthermore, the receptor and the corresponding indicator (such as depicted in **Figure 6-2 b**) are insensitive to any pH changes in the physiological relevant range. This feature, minimizes any undesired pH interferences, and the receptor shows nearly no cross-sensitivity to other cations.

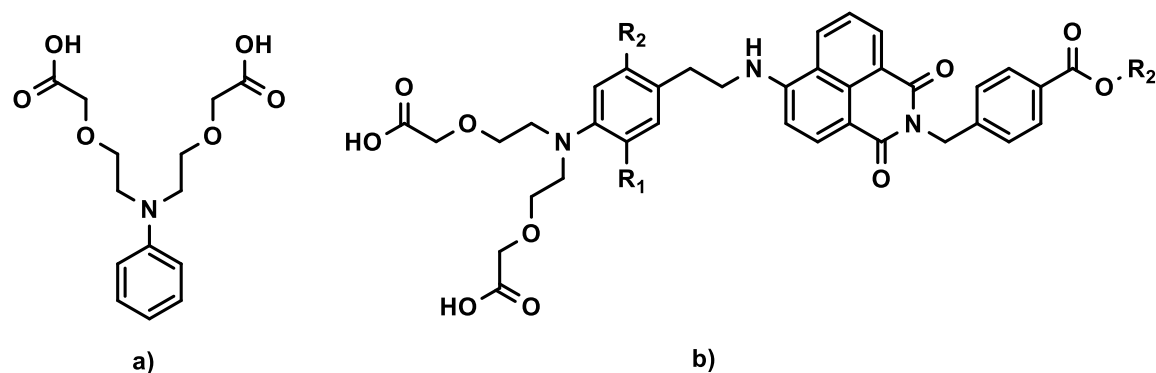


Figure 6-2: **a)** N-phenyliminodiethoxyacetic acid (PIDA) receptor for selective calcium complexation. **b)** fluoroionophore derivative of **a)**, synthesized by He⁶⁴.

In 1988, Levy et. al.²²² synthesized o-aminophenol-N,N,O-triacetic acid (APTRA) (**Figure 6-3**), a receptor for measurements of cytosolic free magnesium via NMR. Although this receptor shows a K_d for magnesium in the mM-range, the sensitivity for calcium ions is much higher; with K_d in the μM -range. By connecting a dye moiety on the receptor (**Figure 6-3 a and b**) a fluorescent optical indicator is generated.^{223–225}

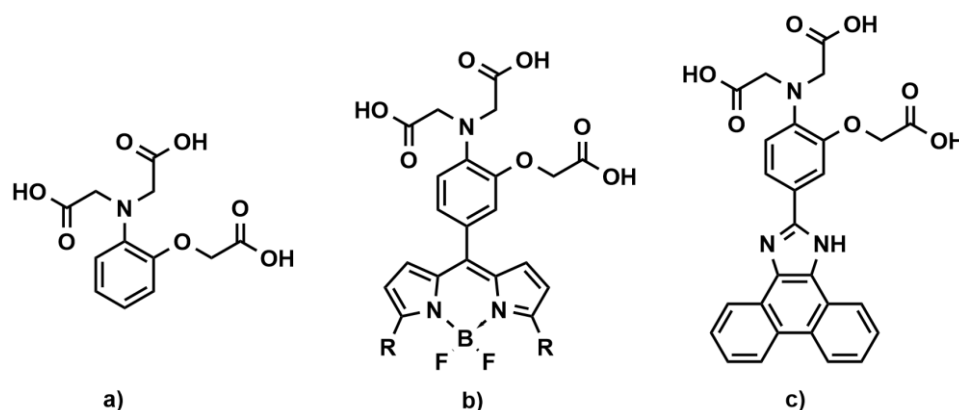


Figure 6-3: **a)** Structure of o-aminophenol-N,N,O-triacetic acid (APTRA)²²² **b)** BODIPY fluoroionophore using APTRA as a recognition unit for calcium ions²²⁵ **c)** APTRA receptor connected to a phenanthrenequinone dye.²²⁴

Since most of the indicators are used as probes^{67,70,123,221,225–227}, immobilization of such indicators in a hydrogel suitable for reversible Ca^{2+} sensing.^{64,65,228}

In this contribution, the concept of calcium ion sensing based on fluorescence quenching is presented. The fluorescent indicator dye consists of a BODIPY fluorophore linked to a

recognition unit (receptor), leading to a fluoroionophore (**FI**). The sensing mechanism is based on intramolecular quenching due to photo-induced electron transfer (PET). Typically, the receptor bears a tertiary amine group, which is responsible for emission enhancement in the presence of calcium ions, due to the reduction of PET.

The synthesis and characterization of new optical ion probes is investigated. Five different calcium fluoroionophores are presented. The indicators either have PIDA, APTRA or BAPTA as a receptor, connected to different BODIPY dyes. The indicators are characterized with respect to their photophysical properties and their suitability as sensor materials. Calibrations of the FIs was performed in solution and via immobilization in a hydrophilic polymer matrix, reversible sensing was proven.

6.4. Materials and Methods

6.4.1. Chemicals

DCM, CHCl_3 , DMF, THF, ethanol, cyclohexane, tert-butanol, TRIS, BIS-TRIS, CAPS, NaCl, KCl, Na_2SO_4 , NaOH, HNO_3 , H_2SO_4 , KI, K_2CO_3 and EDTA were bought from Carl Roth GmbH (www.carlroth.com). Hydrogel (Hydromed, D7) was obtained from AdvanSource biomaterials (www.advbmaterials.com). 2-(2-Chloroethoxy)ethanol, N,N-diisopropylethylamine (DIPEA), N-methyl-2-pyrrolidone (NMP), trifluoroacetic acid (TFA), $\text{NaOCl} \cdot 5\text{H}_2\text{O}$, chloroacetic acid, 2-chloroethoxyacetic acid and 2-aminophenole were from TCI (www.tcichemicals.com). POCl_3 , 1-bromo-2-(2-methoxyethoxy)ethane, BF_3OEt_2 , aniline and DDQ were purchased from Sigma Aldrich (www.sigmaaldrich.at). BAPTA-tetramethylester was purchased from ABCR (www.abcr.de). 6-Hydroxy-1-tetralone and BIS-TRIS was bought from Fluorochem (www.fluorochem.co.uk).

6.4.2. Calibration solutions

Solutions with different pH values contained 20 mM universal buffer (CAPS, citrate, BIS-TRIS and TRIS). The pH was adjusted with HCl. A digital pH meter (Seven Easy, Mettler Toledo, www.mt.com) was used at 21°C with standard buffers of pH 10.0, 7.0 and 4.0 (WTW, www.wtw.com). Buffer solutions containing TRIS, BIS-TRIS or CAPS were prepared with ultra pure water and pH was adjusted with HCl.

6.4.3. Fluorescence measurements

Fluorescence spectra were recorded in front-face mode (sensor foil) or right-angle mode (cuvette) on a Fluorolog3 spectrofluorometer (Horiba Jobin Yvon, www.horiba.com) equipped with a NIR-sensitive photomultiplier R2658 from Hamamatsu (300 – 1050 nm).

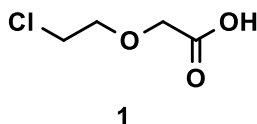
6.4.4. Settings for sensor foil calibration

Calibrations were performed by adjusting the sensing foil in a home-made flow through cell. A peristaltic pump (Gilson miniplus 3, www.gilson.com) was used for pumping different buffers through. The temperature of the calibration solution and the flow through cell was held constant at 21°C using a thermostat (Julabo F12, www.julabo.com).

6.4.5. Experimental

Measurements of listed NMR shifts, HR-MS and LR-MS of the synthesized compounds can be found in the supporting information of this chapter.

2-Chloroethoxyacetic acid (1)

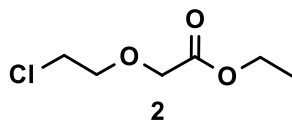


4 mL (37.9 mmol) 2-(2-Chloroethoxy)ethanol was added slowly into conc. HNO₃ (65%) at 50 °C for 8 hours. The solution was stirred at RT overnight and then heated up again for 3 hours. The reaction was controlled via TLC (CH+EE 1+5). The solution was slowly poured into ice water (50 mL) and extracted with (CHCl₃) (4x50 mL). The fractions were combined and dried over Na₂SO₄. The solvent was evaporated to afford 2.2 g (42%) of a yellowish oil. The oil was directly used for the esterification without further purification.

Yield: 2.2 g, 42%

¹H NMR (300 MHz, Chloroform-*d*) δ 11.07 (s, 1H), 4.22 (s, 2H), 3.83 (t, *J* = 5.6 Hz, 2H), 3.65 (t, *J* = 5.6 Hz, 2H).

¹³C NMR (76 MHz, CDCl₃) δ 175.65, 77.16, 71.81, 68.07, 42.58.

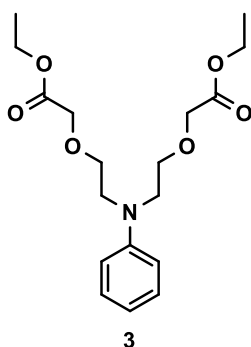
Ethyl 2-chloroethoxyacetate (2)

5.7 g (41.14 mmol) of 2-chloroethoxyacetic acid **1** were dissolved in 50 mL absolute ethanol. The solution was heated to 90 °C and 2 drops of conc. H₂SO₄ were added. After 7 hours, the reaction was neutralized with 1 M NaOH and the solution was evaporated to afford 6.5 g (94%) of a yellow oil.

Yield: 6.5 g, 94%

¹H NMR (300 MHz, Chloroform-*d*) δ 4.22 (q, *J* = 7.1 Hz, 2H), 4.15 (s, 2H), 3.83 (t, *J* = 5.7 Hz, 2H), 3.67 (t, *J* = 5.7 Hz, 2H), 1.29 (t, *J* = 7.1 Hz, 3H).

¹³C NMR (76 MHz, CDCl₃) δ 170.20, 77.16, 71.79, 68.77, 61.13, 42.71, 14.32.

N-Phenylimino-diethoxyethylacetate (PIDA-Diethylester) (3)

2.93 g (31.51 mmol, 1.0 eq) of aniline, 21.00 g (126 mmol, 4.0 eq) 2-chloroethoxyacetate **2**, 16.29 g (126 mmol, 4.0 eq) DIPEA and 20.92 g (126 mmol, 4.0 eq) KI were dissolved in app. 100 mL NMP and stirred for 3 days at 100 °C. The reaction was controlled via TLC (CH+EE = 4+1). A flash column chromatography (CH+EE = 4+0 to 4+1) was performed to remove NMP. A second column chromatography was performed to separate the mono-substituted intermediate from the product.

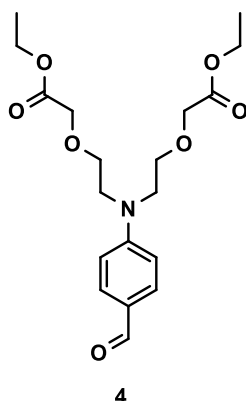
Yield: 9.4 g, 80%

R_f: CH+EA = 2+1: 0.62; R_f: CH+EA = 1+1: 0.80

¹H NMR (300 MHz, Chloroform-*d*) δ 7.21 (t, *J* = 7.7 Hz, 2H), 6.77 – 6.65 (m, 3H), 4.20 (q, *J* = 7.1 Hz, 4H), 4.08 (s, 4H), 3.76 – 3.59 (m, 8H), 1.27 (t, *J* = 7.1 Hz, 6H).

¹³C NMR (76 MHz, DMSO) δ 170.11, 147.56, 129.08, 115.51, 111.47, 68.18, 67.79, 60.13, 50.04, 39.52, 14.04.

LR-MS (APCI): *m/z* calc. for C₁₈H₂₇NO₆: 353.2 [M⁺]; found: 352.3 [MH⁻].

N-(4-Formyl)-Phenylimino-diethoxyethylacetate (PIDA-Diethylester aldehyde)**(4)**

A 100 mL Schlenk-tube was heated out three times under vacuum. 969 mg (2.74 mmol) of N-phenylimino-diethoxyethylacetate **3** were dissolved in 25 mL dry DMF. The solution was cooled to $-70\text{ }^{\circ}\text{C}$ and stirred for 20 minutes. 2.10 g (13.71 mmol, 5 eq.) POCl_3 were added dropwise over 5 minutes. A color change from yellow to greenish was observed. The solution was stirred for another 30 minutes at $-70\text{ }^{\circ}\text{C}$ and was then allowed to warm up to room temperature. The reaction was stirred overnight and the next day 20 mL ice water was added to the solution. The solution was extracted with DCM (3x 50 mL), the organic phase dried with Na_2SO_4 and evaporated. Purification by column chromatography (CH+EE 1+1) afforded 812 mg (77%) of a yellow oil.

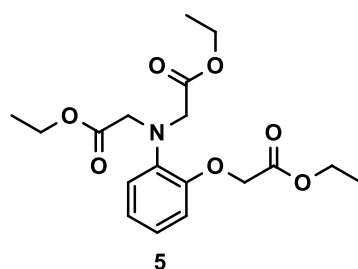
Yield: 812 mg, 77%

R_f: CH+EA = 1+1: 0.33

^1H NMR (300 MHz, Methylene Chloride- d_2) δ 9.70 (s, 1H), 7.69 (d, $J = 8.9$ Hz, 2H), 6.80 (d, $J = 8.8$ Hz, 2H), 4.16 (q, $J = 7.1$ Hz, 4H), 4.06 (s, 4H), 3.80 – 3.70 (m, 8H), 1.24 (t, $J = 7.1$ Hz, 6H).

^{13}C NMR (76 MHz, CD_2Cl_2) δ 190.26, 170.63, 153.23, 132.34, 126.11, 111.77, 69.30, 69.14, 61.32, 54.72, 54.36, 54.00, 54.00, 53.64, 53.28, 51.58, 14.53.

LR-MS (APCI): m/z calc. for $\text{C}_{19}\text{H}_{27}\text{NO}_7$: 381.2 [M^+]; found: 382.4 [MH^+].

Triethyl-o-Aminophenol-N,N,O-triacetate (APTRA-triethylester) (5)

In a 250 mL round bottom flask 3.76 g 2-aminophenol (34.48 mmol, 1 eq.) and 16.29 g chloroacetic acid (172.39 mmol, 5 eq.) were dissolved in 50 mL H₂O. The solution was stirred for 10 minutes and 9.65 g NaOH (241.35 g, 7 eq.) were added slowly over 30 minutes. The resulting solution was heated to 100 °C and stirred for 15 hours. Afterwards the solution was cooled down to room temperature and the water was evaporated under reduced pressure. The suspension was dissolved in 100 mL EtOH and conc. H₂SO₄ was added until pH 2 was reached. The reaction was refluxed for 2 days. After cooling to room temperature, salts were filtered off and the solvent evaporated. The residue was dissolved in ethyl acetate and washed with 1 M NaOH three times. The organic layer was dried with Na₂SO₄ and the solvent was removed under reduced pressure.

Yield: 4.12 g, 42%

R_f: CH+EA = 3+1: 0.29

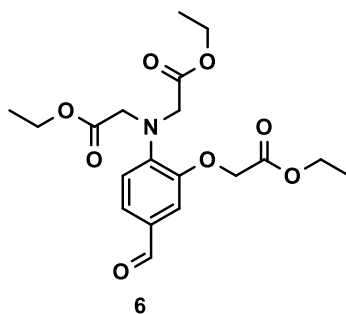
¹H NMR (300 MHz, Chloroform-*d*) δ 7.05 – 7.00 (m, 1H), 6.95 – 6.87 (m, 2H), 6.85 – 6.73 (m, 1H), 4.65 (s, 2H), 4.32 – 4.05 (m, 10H), 1.33 – 1.20 (m, 9H).

¹³C NMR (76 MHz, CDCl₃) δ 171.42, 169.17, 139.75, 124.36, 123.04, 122.75, 122.62, 120.18, 117.31, 115.15, 114.53, 77.16, 67.61, 66.46, 61.28, 60.79, 53.88, 43.08, 14.33.

LR-MS (APCI): *m/z* calc. for C₁₈H₂₅NO₇: 367.2 [M⁺]; found: 368.4 [MH⁺] and 735.7 [2MH⁺].

N-(4-Formyl)-triethyl-o-aminophenol-N,N,O-triacetate

(APTRA-triethylester aldehyde) (6)



A 100 mL Schlenk tube was heated out three times under vacuum and 1 g N-phenylimino-diethoxyethylacetate (PIDA-diethylester) **3** (2.72 mmol, 1 eq.) was dissolved in 40 mL dry DMF. The solution was cooled to – 70 °C and stirred for 10 minutes. 2.09 g POCl₃ (13.61 mmol, 5 eq.) was added slowly and stirred for 20 minutes. The solution was warmed up to room temperature and stirred overnight. The solution was heated to 70 °C for 3 hours. The hot solution was poured on ice and stirred for one hour. The solution was

extracted in DCM (3x 25 mL), dried with Na₂SO₄ and evaporated. Purification by column chromatography (CH+EE 4+1) afforded 760 mg (76%) of a yellow oil.

Yield: 760 mg, 76%

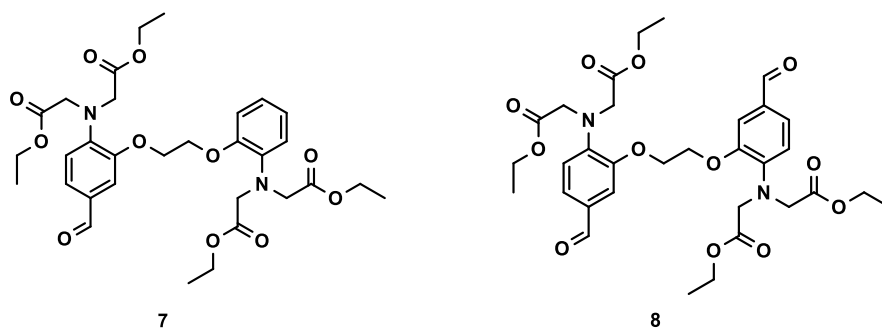
R_f: CH+EA = 1+1: 0.39

¹H NMR (300 MHz, Chloroform-*d*) δ 9.76 (s, 1H), 7.39 (dd, 1H), 7.26 (s, 1H), 6.80 (d, *J* = 8.2 Hz, 1H), 4.65 (s, 2H), 4.31 – 4.17 (m, 10H), 1.33 – 1.23 (m, 9H).

¹³C NMR (76 MHz, CDCl₃) δ 190.34, 170.69, 168.05, 148.70, 145.31, 129.84, 127.29, 117.21, 111.72, 65.65, 61.44, 61.07, 54.09, 14.24.

LR-MS (APCI): *m/z* calc. for C₁₉H₂₅NO₈: 395.2 [M⁺]; found: 396.4 [MH⁺] and 791.7 [2MH⁺].

BAPTA-tetramethylester-aldehyde (7)



A 50 mL Schlenk tube was heated out three times. 305 mg (0.518 mmol 1 eq.) of BAPTA-tetramethylester were dissolved in approximately 10 mL dry DMF. The solution was cooled to – 20 °C and 240 μL POCl₃ (2.59 mmol, 5 eq) were added dropwise. The solution was stirred overnight at room temperature and then heated for 1 hour at 70 °C. The hot solution was poured on approximately 100 mL ice. The solution turned pale yellow and the pH was adjusted to pH 8 with 1 M NaOH. The solution was passed through a filter filtered and extracted in DCM three times. After evaporation of the solvent column chromatography was performed (CH 100% -> CH+EA 1+1). Two products were obtained, the aimed monoaldehyde (**7**) and the disubstituted by-product (**8**).

Yield (**7**): 190 mg (60%)

R_f: CH+EA = 4+1: 0.36

¹H NMR (300 MHz, Chloroform-*d*) δ 9.76 (s, 1H), 7.39 (dd, 2H), 7.26 (s, 2H), 6.80 (d, *J* = 8.2 Hz, 2H), 4.65 (s, 2H), 4.31 – 4.17 (m, 20H), 1.33 – 1.23 (m, 12H).

¹³C NMR (76 MHz, CDCl₃) δ 190.34, 170.69, 168.05, 148.70, 145.31, 129.84, 127.29, 117.21, 111.72, 65.65, 61.44, 61.07, 54.09, 14.24.

LR-MS (APCI): *m/z* calc. for C₃₁H₄₀N₂O₁₁: 616.3 [M⁺]; found: 617.6 [MH⁺].

Yield (**8**): 78 mg (24%)

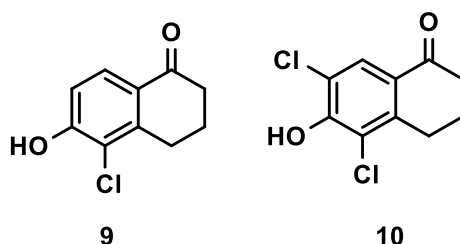
R_f: CH+EA = 4+1: 0.22

¹H NMR (300 MHz, Chloroform-*d*) δ 9.80 (s, 2H), 7.38 – 7.36 (m, 2H), 7.26 (s, 2H), 6.76 (d, *J* = 8.0 Hz, 2H), 4.31 (s, 4H), 4.22 (s, 8H), 4.06 (q, *J* = 7.1 Hz, 8H), 1.14 (t, *J* = 7.1 Hz, 12H).

¹³C NMR (76 MHz, CDCl₃) δ 190.40, 170.73, 149.55, 145.24, 126.91, 116.71, 110.83, 77.46, 77.03, 76.61, 67.11, 61.25, 53.75, 29.74, 14.01.

LR-MS (APCI): *m/z* calc. for C₃₂H₄₀N₂O₁₂: 644.3 [M⁺]; found: 645.7 [MH⁺].

5-Chloro-6-hydroxy-1-tetralone (**9**) and 5,7-dichloro-6-hydroxy-1-tetralone (**10**)



25.3 mL tert-butanol and 21 mL acetic acid were vigorously stirred in a 1 L round bottom flask. 75 g NaOCl*5H₂O in 450 mL H₂O were added within 10 minutes at 0 °C. After addition, the flask was sealed with aluminium foil and flushed with nitrogen, since the formed tert-butyl hypochlorite is sensitive to light and air. After 10 minutes, the magnetic stirrer was turned off and the yellow upper layer was filled in a light protected glass vial. The intermediate reagent (tert-butyl hypochlorite) was stored in the fridge under argon atmosphere.

1.62 g of 6-Hydroxy-1-tetralone (9.99 mmol, 1 eq.) was dissolved in 100 mL chloroform. 2.82 mL tert-butyl hypochlorite (24.97 mmol, 2.5 eq.) were added dropwise within 2 minutes. The flask was sealed with aluminum foil and the solution stirred under nitrogen for 4 hours. The solution was extracted with water and brine, dried over Na₂SO₄ and evaporated. Column chromatography (CH 100% → CH+EE=3+1) yielded in mono and di-substituted products (**9** and **10**, respectively).

Yield (**9**): 504 mg (22%)

R_f: CH+EA = 1+1: 0.48

¹H NMR (300 MHz, DMSO-*d*₆) δ 7.74 (d, *J* = 8.6 Hz, 1H), 6.95 (d, *J* = 8.6 Hz, 1H), 2.92 (t, *J* = 5.8 Hz, 2H), 2.50 (t, 2H), 2.01 (p, 2H).

¹³C NMR (76 MHz, DMSO) δ 195.54, 157.75, 143.92, 126.76, 125.61, 118.69, 114.37, 39.52, 37.40, 26.84, 21.98.

LR-MS (APCI): *m/z* calc. for C₁₀H₉ClO₂: 196.0 [M⁺]; found: 196.9 [MH⁺].

Yield (**10**): 900 mg (38%)

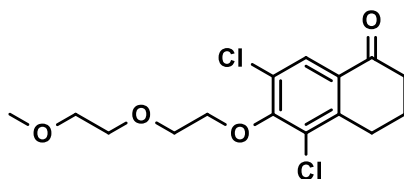
R_f: CH+EA = 1+1: 0.77

¹H NMR (300 MHz, DMSO-*d*₆) δ 7.80 (s, 1H), 2.91 (t, *J* = 5.7 Hz, 2H), 2.55 (t, *J* = 6.9 Hz, 2H), 2.05 (p, 2H).

¹³C NMR (76 MHz, DMSO) δ 194.81, 153.37, 142.55, 126.24, 125.83, 121.16, 120.33, 39.52, 37.19, 26.77, 21.72.

LR-MS (APCI): *m/z* calc. for C₁₀H₈Cl₂O₂: 230.0 [M⁺]; found: 230.9 [MH⁺].

5,7-Dichloro-6-[2-(2-methoxyethoxy)ethoxy]-1-tetralone (12)



12

155 mg 5,7-Dichloro-6-hydroxy-1-tetralone (**10**) (0.670 mmol, 1 eq.), 307 mg 1-bromo-2-(2-methoxyethoxy)ethane (1.68 mmol, 2.5 eq.), 92 mg K₂CO₃ (0.670 mmol, 1 eq.) and 111 mg KI (0.670 mmol, 1 eq.) were stirred in 10 mL dry DMF at 60 °C for 6 h. The solvent was removed under reduced pressure, the product dissolved in DCM and the impurities extracted with water. The organic phase was dried with Na₂SO₄ and evaporated. Column chromatography (CH 100% → CH+EE=1+1) gave the desired product.

Yield: 75 mg (34%)

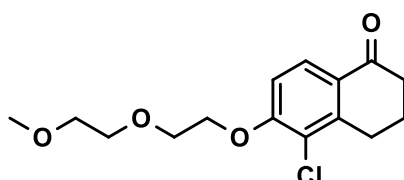
R_f: CH+EA = 4+1: 0.23; R_f: CH+EA = 1+1: 0.74

¹H NMR (300 MHz, Methylene Chloride-*d*₂) δ 7.97 (s, 1H), 4.23 (t, 2H), 3.85 (t, 2H), 3.66 (t, 2H), 3.51 (t, 2H), 3.33 (s, 3H), 2.98 (t, *J* = 6.1 Hz, 2H), 2.59 (t, 2H), 2.12 (p, 2H).

¹³C NMR (76 MHz, CD₂Cl₂) δ 195.90, 155.93, 143.14, 130.74, 129.63, 128.09, 127.76, 73.51, 72.48, 71.14, 70.73, 59.23, 54.00, 38.47, 27.76, 22.74.

LR-MS (APCI): *m/z* calc. for C₁₅H₁₈Cl₂O₄: 332.1 [M⁺]; found: 333.1 [MH⁺].

5-Chloro-6-[2-(2-methoxyethoxy)ethoxy]-1-tetralone (11)



11

Compound **11** was synthesized analogously to compound **12** but using compound **9** (201 mg) instead of compound **10**.

Yield: 287 mg (49%)

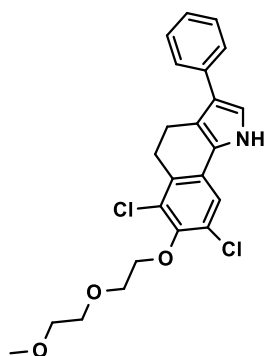
R_f: CH+EA = 4+1: 0.10; R_f: CH+EA = 1+1: 0.55

¹H NMR (300 MHz, Chloroform-*d*) δ 7.98 (d, *J* = 8.7 Hz, 1H), 6.90 (d, *J* = 8.8 Hz, 1H), 4.27 (t, 2H), 3.93 (t, 2H), 3.77 (t, 2H), 3.57 (t, 2H), 3.39 (s, 3H), 3.02 (t, *J* = 6.1 Hz, 2H), 2.60 (t, 2H), 2.13 (p, *J* = 6.3 Hz, 2H).

¹³C NMR (76 MHz, CD₂Cl₂) δ 129.10, 127.61, 111.96, 111.29, 72.53, 71.47, 69.85, 69.80, 69.64, 59.86, 59.23, 54.00, 38.66, 25.06, 23.00.

LR-MS (APCI): *m/z* calc. for C₁₅H₁₉ClO₄: 298.1 [M⁺]; found: 299.4 [MH⁺].

6,8-dichloro-7-(2-(2-methoxyethoxy)ethoxy)-3-phenyl-4,5-dihydro-1H-benzo[g]indole (14)



14

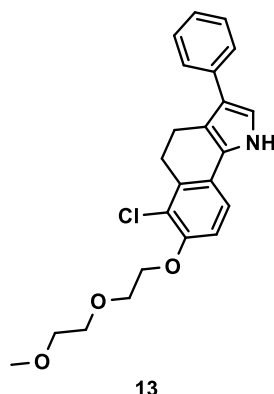
The synthesis of pyrrole **14** was similar to the literature procedure. (Müller et al.)¹¹⁷ 135 mg 5,7-dichloro-6-{2-(2-methoxyethoxy)ethoxy}-1-tetralone (**12**, 1 eq.) and 59 mL phenylazirine (1.10 eq) and 212 mL of a 2M lithium diisopropylamide solution (in THF, 1.05 eq.) was used for the synthesis of compound **14**. The product was additionally purified via column chromatography (CH 100% → CH+EE=1+2). The product was obtained as a yellow oil and turned brownish under air conditions. The product was not stable during NMR measurements. LR-MS measurements were performed and the pyrrole was directly used for BODIPY synthesis without further purification.

Yield: 114 mg (64%)

R_f: CH+EA = 4+1: 0.54

LR-MS (APCI): *m/z* calc. for C₂₃H₂₃Cl₂NO₃: 431.1 [M⁺]; found: 432.3 [MH⁺].

6-chloro-7-(2-(2-methoxyethoxy)ethoxy)-3-phenyl-4,5-dihydro-1H-benzo[g]indole (13)



The synthesis of pyrrole **13** was similar to Müller et al.¹¹⁷ 433 mg 5-chloro-6-[2-(2-methoxyethoxy)ethoxy]-1-tetralone (**11**, 1 eq.) and 172 mL phenylazirine (1.10 eq) and 770 mL of a 2M lithium diisopropylamide solution (in THF, 1.05 eq.) was used for the synthesis of compound **13**. The product was additionally purified via column chromatography (CH 100% → CH+EE=1+2). The product was obtained as a yellow oil and turned greenish under air conditions. The product was not stable for NMR measurements. LR-MS measurements were performed and the pyrrole was directly used for BODIPY synthesis.

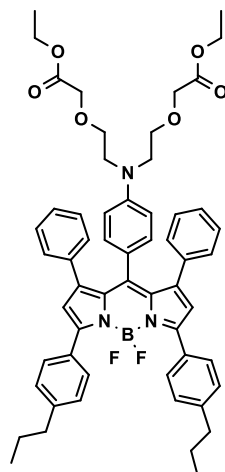
Yield: 187 mg (52%)

R_f: CH+EA = 4+1: 0.42

LR-MS (APCI): *m/z* calc. for C₂₃H₂₄ClNO₃: 397.18 [M⁺]; found: 396.2 [MH⁻].

General synthesis of BODIPY fluorophores

A Schlenk tube was heated out three times. 1 eq. of aldehyde and 2.05 eq. of pyrrole were dissolved in dry DCM. The vessel was sealed from light and 1 drop TFA was added under argon atmosphere. The reaction was controlled via TLC and after consumption of the aldehyde, 1.05 eq. DDQ was added and stirred for one hour. Then 10 eq. DIPEA was added and stirred again for 5 minutes. 15 eq. BF₃OEt₂ was added and stirred for 30 minutes. Typical work up is done via extraction of impurities with water, evaporation of the organic solvent and column chromatography. (DCM 100% → DCM + EtOH 95 + 5)

F11-ester

70 mg of N-(4-Formyl)-Phenylimino-diethoxyethylacetate (**4**, 1 eq.), 101 mg 2-(4-Propylphenyl)-4-Phenylpyrrol (2 eq.), 43 mg 2,3-dichloro-5,6-dicyano-1,4-benzoquinone (DDQ, 1 eq.), 330 mL N,N-diisopropylethylamine (DIPEA, 10 eq.) and 350 mL BF_3OEt_2 (15 eq.) was used for **F11-ester**.

Yield: 12 mg (11%)

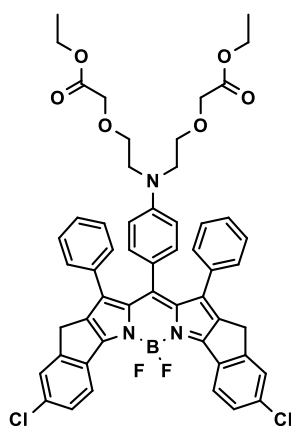
R_f : CH+EA = 4+1: 0.23; R_f : CH+EA = 3+2: 0.57

^1H NMR (300 MHz, Methylene Chloride- d_2) δ 7.74 (d, $J = 7.9$ Hz, 4H), 7.27 (d, $J = 7.9$ Hz, 4H), 6.88 (dd, $J = 20.4, 4.0$ Hz, 10H), 6.68 (d, $J = 8.5$ Hz, 2H), 6.57 (s, 2H), 5.77 (d, $J = 8.7$ Hz, 2H), 4.23 (q, $J = 7.1$ Hz, 4H), 4.09 (s, 4H), 3.42 (dd, $J = 19.3, 5.3$ Hz, 8H), 2.65 (t, 4H), 1.69 (q, 4H), 1.26 (t, 6H), 0.99 (t, $J = 7.3$ Hz, 6H).

^{13}C NMR (76 MHz, CD_2Cl_2) δ 156.55, 149.03, 144.92, 136.98, 134.61, 130.93, 129.96, 129.54, 128.73, 127.75, 126.16, 123.34, 110.32, 69.63, 69.29, 61.38, 54.00, 51.27, 38.51, 30.27, 25.00, 14.63, 14.34.

LR-MS (APCI): m/z calc. for $\text{C}_{57}\text{H}_{60}\text{BF}_2\text{N}_3\text{O}_6$: 931.5 [M^+]; found: 932.6 [MH^+]; 913.6 [$\text{MH}^+ - \text{F}^-$]; 931.6 [MH^-].

HR-MS (MALDI-TOF): m/z calc. for $\text{C}_{57}\text{H}_{60}\text{BF}_2\text{N}_3\text{O}_6$: 931.4543 [M^+]; found: 932.4124 [MH^+].

F12-ester

96 mg of N-(4-Formyl)-Phenylimino-diethoxyethylacetate (**4**, 1 eq.), 134 mg 5-chloro-3-phenyl-1,4-dihydroindeno[1,2-b]pyrrole (2 eq.), 57 mg 2,3-dichloro-5,6-dicyano-1,4-benzoquinone (DDQ, 1 eq.), 450 mL N,N-diisopropylethylamine (DIPEA, 10 eq.) and 465 mL BF_3OEt_2 (15 eq.) was used for **F12-ester**.

Yield: 33 mg (14%)

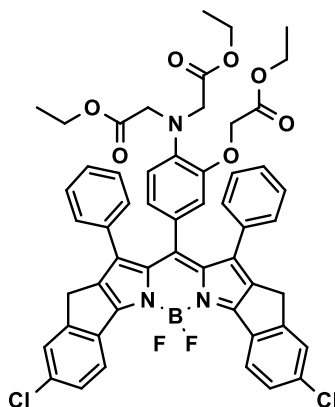
R_f : CH+EA = 4+1: 0.18; R_f : CH+EA = 3+2: 0.52

^1H NMR (300 MHz, Methylene Chloride- d_2) δ 8.29 (d, J = 8.6 Hz, 2H), 7.50 (s, 4H), 6.93 (s, 6H), 6.87 – 6.79 (m, 4H), 6.64 (d, J = 8.5 Hz, 2H), 5.76 (d, J = 8.6 Hz, 2H), 4.23 (q, J = 7.1 Hz, 4H), 4.09 (s, 4H), 3.42 (dd, J = 22.6, 5.1 Hz, 8H), 6.83 – 6.80 (m, 1H), 3.59 (s, 4H), 1.31 (d, J = 7.1 Hz, 6H).

^{13}C NMR (76 MHz, CD_2Cl_2) δ 170.74, 152.87, 148.68, 139.65, 135.80, 135.47, 134.16, 132.10, 129.55, 128.66, 127.89, 126.65, 126.23, 125.27, 110.35, 69.64, 69.29, 61.37, 54.00, 51.25, 30.35, 30.27, 14.64.

LR-MS (APCI): m/z calc. for $\text{C}_{53}\text{H}_{46}\text{BCl}_2\text{F}_2\text{N}_3\text{O}_6$: 939.3 [M^+]; found: 940.5 [MH^+]; 922.5 [$\text{MH}^+ - \text{F}^-$]; 939.6 [MH^-].

HR-MS (MALDI-TOF): m/z calc. for $\text{C}_{53}\text{H}_{46}\text{BCl}_2\text{F}_2\text{N}_3\text{O}_6$: 939.2825 [M^+]; found: 940.2913 [MH^+].

F13-ester

50 mg of N-(4-Formyl)-triethyl-o-aminophenol-N,N,O-triacetate (**6**, 1 eq.), 71 mg 5-chloro-3-phenyl-1,4-dihydroindeno[1,2-b]pyrrole (2 eq.), 53 mg 2,3-dichloro-5,6-dicyano-1,4-benzoquinone (DDQ, 1 eq.), 220 mL N,N-diisopropylethylamine (DIPEA, 10 eq.) and 245 mL BF_3OEt_2 (15 eq.) was used for **FI3-ester**.

Yield: 72 mg (35 %)

R_f : CH+EA = 3+2: 0.24; R_f : CH+EA = 2+3: 0.88

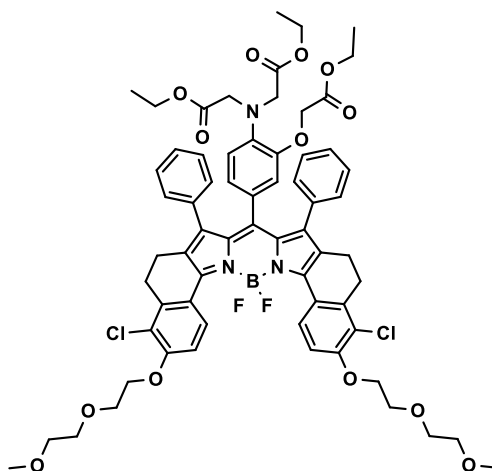
^1H NMR (300 MHz, Methylene Chloride- d_2) δ 8.30 (d, $J = 8.7$ Hz, 2H), 7.56 – 7.47 (m, 4H), 7.04 – 6.93 (m, 6H), 6.90 – 6.79 (m, 4H), 6.50 – 6.41 (m, 1H), 6.33 – 6.22 (m, 1H), 6.03 (d, $J = 8.2$ Hz, 1H), 4.21 (q, $J = 7.1$ Hz, 6H), 4.14 (s, 2H), 3.88 (s, 4H), 3.59 (s, 4H), 1.34 – 1.24 (m, 12H).

^{13}C NMR (76 MHz, CD_2Cl_2) δ 171.48, 169.06, 158.49, 153.10, 148.79, 140.86, 139.66, 138.70, 135.91, 135.52, 131.83, 129.30, 128.76, 128.02, 127.55, 126.96, 126.74, 125.60, 125.51, 119.39, 118.86, 66.17, 61.72, 61.19, 54.00, 53.12, 30.28, 14.68, 14.56.

LR-MS (APCI): m/z calc. for $\text{C}_{53}\text{H}_{44}\text{BCl}_2\text{F}_2\text{N}_3\text{O}_7$: 953.3 [M^+]; found: 954.5 [MH^+]; 934.4 [MH^+-F]; 953.6 [MH^-].

HR-MS (MALDI-TOF): m/z calc. for $\text{C}_{53}\text{H}_{44}\text{BCl}_2\text{F}_2\text{N}_3\text{O}_7$ [M^+]: 953.2617; found: 976.2508 [MNa^+].

FI4-ester



15 mg of N-(4-Formyl)-triethyl-o-aminophenol-N,N,O-triacetate (**6**, 1 eq.), 30 mg 6-chloro-7-(2-(2-methoxyethoxy)ethoxy)-3-phenyl-4,5-dihydro-1H-benzo[g]indole (**13**, 2 eq.), 9 mg 2,3-dichloro-5,6-dicyano-1,4-benzoquinone (DDQ, 1 eq.), 70 mL N,N-diisopropylethylamine (DIPEA, 10 eq.) and 64 mL BF_3OEt_2 (15 eq.) was used for **FI4-ester**.

Yield: 7 mg (8%)

R_f : CH+EA = 3+2: 0.03; R_f : CH+EA = 2+3: 0.52

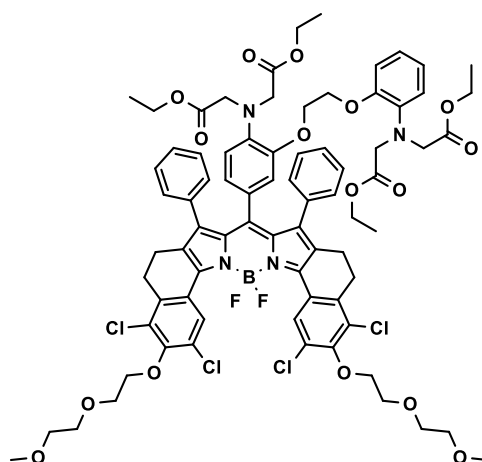
^1H NMR (300 MHz, Methylene Chloride- d_2) δ 8.73 (d, $J = 9.1$ Hz, 2H), 7.07 (d, $J = 9.1$ Hz, 2H), 6.99 – 6.88 (m, 6H), 6.73 (d, $J = 6.4$ Hz, 4H), 6.38 (d, 1H), 6.19 (s, 1H), 5.96 (d, $J =$

8.3 Hz, 1H), 4.31 (t, 4H), 4.24 – 4.17 (m, 8H), 3.93 (t, 4H), 3.85 (s, 4H), 3.75 (t, $J = 5.5, 3.7$ Hz, 4H), 3.56 (t, 4H), 3.36 (s, 6H), 3.04 (t, $J = 6.7$ Hz, 4H), 2.45 (t, $J = 6.8$ Hz, 4H), 1.34 – 1.26 (m, 12H).

^{13}C NMR (76 MHz, CD_2Cl_2) δ 171.58, 141.03, 135.40, 132.54, 129.94, 128.70, 127.77, 126.63, 122.61, 119.47, 119.04, 111.50, 72.57, 71.48, 69.97, 69.62, 61.70, 61.15, 59.27, 54.00, 45.52, 35.00, 27.48, 20.79, 14.68.

HR-MS (MALDI-TOF): m/z calc. for $\text{C}_{65}\text{H}_{68}\text{BCl}_2\text{F}_2\text{N}_3\text{O}_{13}$ [M^+]: 1217.4190; found: 1218.4190 [MH^+].

FI5-ester



50 mg of BAPTA-tetramethylester-aldehyde (**7**, 1 eq.), 70 mg 6-6,8-dichloro-7-(2-(2-methoxyethoxy)ethoxy)-3-phenyl-4,5-dihydro-1H-benzo[g]indole (**14**, 2 eq.), 18 mg 2,3-dichloro-5,6-dicyano-1,4-benzoquinone (DDQ, 1 eq.), 135 mL N,N -diisopropylethylamine (DIPEA, 10 eq.) and 150 mL BF_3OEt_2 (15 eq.) was used for **FI5-ester**.

Yield: 22 mg (17%)

R_f : CH+EA = 1+2: 0.26; R_f : CH+EA = 1+1: 0.41

^1H NMR (300 MHz, Methylene Chloride- d_2) δ 8.88 (s, 2H), 7.00 – 6.90 (m, 10H), 6.81 – 6.69 (m, 4H), 6.36 (d, $J = 6.7$ Hz, 1H), 6.29 (s, 1H), 5.91 (d, $J = 8.1$ Hz, 1H), 4.28 (t, 4H), 4.17 (s, 4H), 4.11 (q, 8H), 3.98 – 3.79 (m, 12H), 3.71 (t, 4H), 3.56 (t, 4H), 3.36 (s, 6H), 3.00 (t, $J = 7.0$ Hz, 4H), 2.47 (t, $J = 6.8$ Hz, 4H), 1.28 – 1.19 (m, 12H).

^{13}C NMR (76 MHz, CD_2Cl_2) δ 171.63, 171.48, 152.93, 139.60, 135.05, 133.03, 129.84, 129.39, 127.94, 126.85, 126.56, 125.68, 122.98, 122.31, 120.82, 118.56, 118.06, 115.18, 100.57, 73.51, 72.55, 71.18, 70.82, 67.82, 67.44, 61.17, 59.27, 54.16, 54.00, 53.13, 27.41, 20.52, 14.63.

HR-MS (MALDI-TOF): m/z calc. for $\text{C}_{77}\text{H}_{81}\text{BCl}_4\text{F}_2\text{N}_4\text{O}_{16}$: 1506.4463 [M^+]; found: 1531.3038 [MNa^+].

6.5. Results and Discussion

The following sections of this chapter include, the synthesis of the fluoroionophores as well as pretests for the development of a suitable sensor materials. The investigations give an impression how charged indicators behave in solutions and matrices. The following sections may be essential for any future development of calcium-based indicator sensors.

6.5.1. Synthesis of fluoroionophore esters

The synthesis of the receptors PIDA, and APTRA was performed according to the literature.^{64,224,225} Two novel BODIPY cores were synthesized starting with the chlorination of 6-hydroxy-1-tetralone, to yield mono- and disubstituted-intermediates (compound **9** and **10** in the supporting information). Both tetralone intermediates were further modified using 1-bromo-2-(2-methoxyethoxy)ethane, to yield tetralones with a improved hydrophilicity (compound **11** and **12**). The synthesis of the corresponding pyrroles was similar to Müller et. al.¹¹⁷ Classical BODIPY synthesis yields in fluoroionophores **FI4-ester** and **FI5-ester**. The synthesized compounds reveal higher hydrophilicity, which should prevent aggregation in hydrogel matrices. Additionally, it should preferably provide better complexation of calcium ions within the polymer matrix. In general, the synthesis of the **FI-esters** was significantly more challenging than crown-ether based fluoroionophores. Deprotection and destruction of the receptor-precursors often occurred during BODIPY synthesis, and purification of the indicators was tricky and time consuming. A lot of documentation and several TLC plates were necessary to obtain purified FI-esters (**Figure 6-4**). A detailed description of the purification as well as all NMR and HR-MS (Maldi-TOF) are given in the supporting information and in the experimental section.

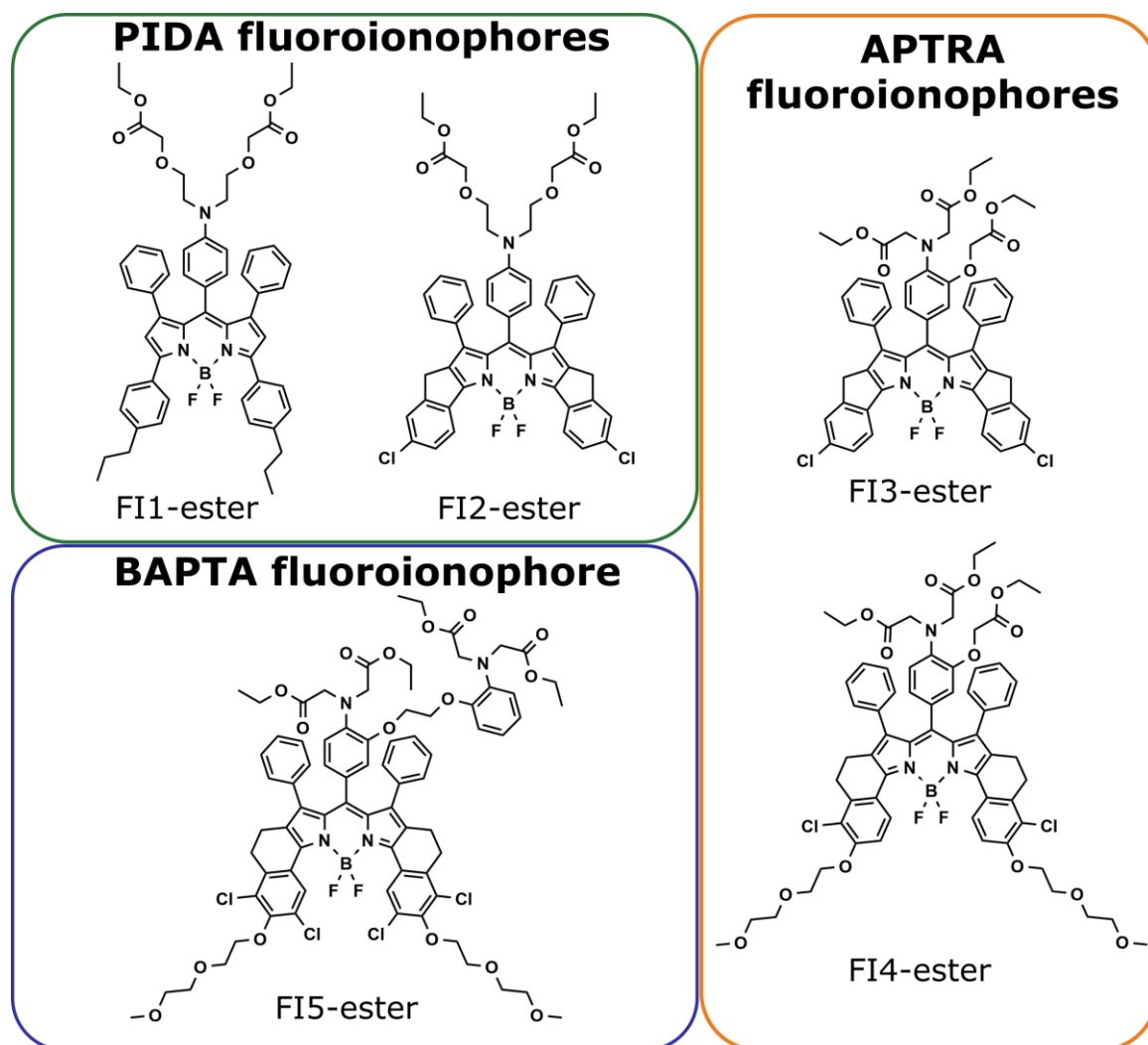


Figure 6-4: Overview of the synthesized fluoroionophores in their protected ethyl ester form (**FI-ester**), before saponification.

Saponification of fluoroionophore esters

Saponification experiments were carried by varying the amount of NaOH and the ratio between ethanol and water. It was found that saponification worked best at an ethanol content higher than 80% and 3 eq. NaOH per ester group, which needs to be deprotected. By heating the solutions to 50 °C, deprotection of all indicators was achieved within 24 hours. It is important to note that the final products get stuck on the TLC plate after deprotection (**Figure 6-5 a**). Therefore, purification via column chromatography is not an option. Because of that reason, purification got way harder. After the completion of the reaction the ethanol was evaporated, and the residue was dissolved in ultra-pure water. The solution was further treated with DCM to extract any protected starting compounds from the aqueous phase. The colored, aqueous solution was neutralized with 1 M HCl to

pH 7 whereas the fluoroionophore precipitated, was filtered and washed with ultra-pure water. With this step, excess of NaOH used for deprotection was eliminated. The aqueous phase was removed via lyophilization. The product was weighted and the amount of NaOH calculated needed to get the sodium salt again. Therefore, the residue was dissolved in equimolar NaOH added and stirred for at least five days. For calibrations the product was again dried via lyophilization. NMR experiments were not successful. The NMR-samples in D₂O visually appeared to be suitable, but no meaningful NMR spectrum was obtained (**Figure 6-5 c**). A possible explanation is aggregation of the fluoroionophores in water at high concentration necessary for the NMR measurements. Since they have a hydrophobic and a highly hydrophilic (charged moieties) character, aggregation phenomena take place, making any pulses in NMR experiments useless. The solubility of the fluoroionophores in deuterated ethanol was too low to obtain proper NMR-spectra. NMR experiments in mixtures of D₂O and deuterated ethanol might be an option for future experiments.

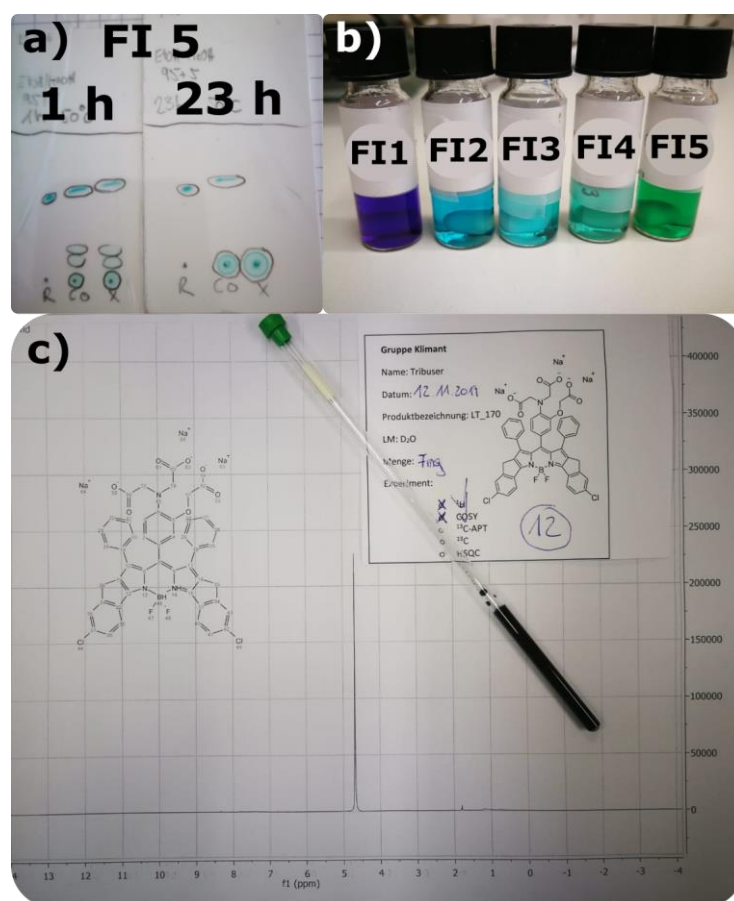


Figure 6-5: a) TLC of the saponification of FI5-ester to FI5. Uncompleted deprotection is seen after 1 h. After 23 h only one spot can be seen via TLC. b) Salt-forms of the FIs, dissolved in water. c) Although the FIs are soluble in D₂O, no peaks were found in ¹H-NMR measurements.

6.5.2. Properties of fluoroionophore esters

In **Table 6-1** a summary of the properties of the **FI-esters** is given. Detailed spectra can be seen in **Figure S 6-1** and **Figure S 6-2** in the supporting information. Absorption spectra were measured in DCM and THF. **FI1-ester** reveals the lowest absorption maximum at 560 nm (DCM), whereas the **FI4-ester** shows the highest absorption maximum at 647 nm in the electromagnetic spectrum. In general, with the increasing extension of the aromatic system and the rigidity of the dye moiety, the larger bathochromic shift in the absorption of the corresponding dye is observed. Furthermore, by comparing **FI2-ester** and **FI3-ester** it can be seen that they have the same dye structure, but the absorption of **FI3-ester** is 6 nm bathochromically shifted. This effect comes from the additional side group, which has an electron-donating character, on the phenyl ring. The side group additionally hinders the phenyl ring in the rotation and vibration, resulting in an even more rigid system. Except for **FI1-ester**, all indicators reveal a high molar absorption coefficient above $120\,000\text{ M}^{-1}\text{cm}^{-1}$. BODIPY dyes are known for their sharp and narrow excitation and emission spectra²²⁹, which can be seen by comparing the Stokes shift listed in Fehler! Ungültiger Eigenverweis auf Textmarke.. **FI1-ester** reveals a shift of 49 nm, which is way higher than the others. The large Stokes shift is attributed to the possible rotation of the phenyl rings. This rotation also causes broadening of the spectrum and significantly smaller molar absorption coefficients in maximum.

FI 2 to 5-ester can be excited using red or blue (albeit less efficiently) light and emit in the red region of the electromagnetic spectrum. **FI4-ester** shows the longest emission maximum of 682 nm, in the spectrum (DCM + drop TFA). Note that upon protonation of the nitrogen in the receptor, a bathochromic shift of the excitation (10-18 nm) is observed (compare absorption spectrum in DCM and excitation in DCM + drop TFA, Fehler! Ungültiger Eigenverweis auf Textmarke.). The introduction of additional chlorine atoms does not necessarily cause a bathochromic shift, whereas PET is in general enhanced with the introduction of chlorine atoms.¹¹⁷ This theory was proven by the synthesis of an indicator shown in **Figure S 6-3**. It is a potassium indicator with a similar BODIPY core. This indicator lacks chlorine groups at the dye moiety, and still emits at 676 nm (hydrogel D1). The enhancement factor (PET efficiency) for this fluoroionophore is relatively low, if compared to others (**Chapter 3**).

Table 6-1: Spectral properties of the fluoroionophore precursors, **FI-esters**.

Property	FI1-ester	FI2-ester	FI3-ester	FI4-ester	FI5-ester
Absorption maximum [nm] (DCM)	560	628	634	647	637
Absorption maximum [nm] (THF)	566	626	629	644	633
Molar decadic absorption coefficient [ϵ] [$M^{-1} \cdot cm^{-1}$] (THF)	54 600	125 900	122 800	151 600	154 400
Excitation maximum [nm] (DCM + drop TFA)	578	643	647	662	645
Emission maximum [nm] (DCM + drop TFA)	627	662	667	682	660
Stokes shift [nm]	49	19	20	20	15

6.5.3. pH calibrations in solution

For the synthesized fluoroionophores, pH calibrations were performed in order to evaluate their pK_a value. Therefore, a 40 mM universal buffer (5 mM Tris, 5 mM BIS-TRIS, 5 mM CAPS and 5 mM citrate) was used and the pH was adjusted using 1 M HCl. The measured solutions contained an ethanol/buffer composition of a 1+1 ratio. Absorptions of the fluoroionophores were adjusted to 0.05. In **Figure 6-6** the emission intensities of the measurements are plotted, whereas the solutions were measured instantly after preparation, and after one day storage.

FI1 and **FI2** showed an intensity increase starting at pH 3 to lower pH values. A plateau for those indicators at pH 1 was not reached, hence no pK_a value was determined. Nevertheless, **FI1** and **FI2** according to the pH calibrations are applicable for the usage in seawater and blood analysis, considering the physiological pH-range. After one day storage, similar results are achieved, hence assuming stable calibration solutions in this

ethanol composition. The other fluoroionophores show some ambiguities for the pH calibrations. For **FI3** and **FI4**, it is unclear why the fluorescence is continuously increasing, starting from pH 8 to 3.5. Typically, receptors having a nitrogen atom as a PET group on the phenyl ring, reveal pK_a value ranging around 3.2.^{116,117} Phenylacetic acid typically has a pK_a of 4.3.²³⁰ Similar literature pK_a values do not explain why the indicators **FI3** and **FI4** are already fluorescent. Nevertheless, the ortho positioned acid on the receptor might describe the strange behavior in the pH range 3-4. The pK_a of methoxy acetic acid is 3.6.²³¹ and for o-anisidine the pK_a value is 4.4, hence some zwitterionic structure may be involved. The o-positioned substituent is flexible to be in proximity of N and form a kind of zwitter-ion. That means at high pH all acids are protonated, whereas at a certain pH value the nitrogen gets protonated, probably from the o-positioned acid, forming a zwitter-ion. Furthermore, below pH 3.6 some solubility problems with the receptor occur, since intensities drop again. Future experiments should include investigations via absorption spectra. **FI5** showed promising results, if measured instantly after preparation, but after 24 hours the indicator shows an increased fluorescence at higher pH values. The measurement solutions were stored overnight in a vial and were transferred back into a cuvette; hence fluorescence increase due to slight impurities of calcium may be possible. Since the indicator's sensitivity (**FI5**) is in the μM range, this theory sounds feasible. What remains a mystery is that the emission intensities seem to decrease from pH 8 to 4.5. If there is a contamination derived from the vials it should be the same for every pH vial, resulting in the similar enhancement factors.

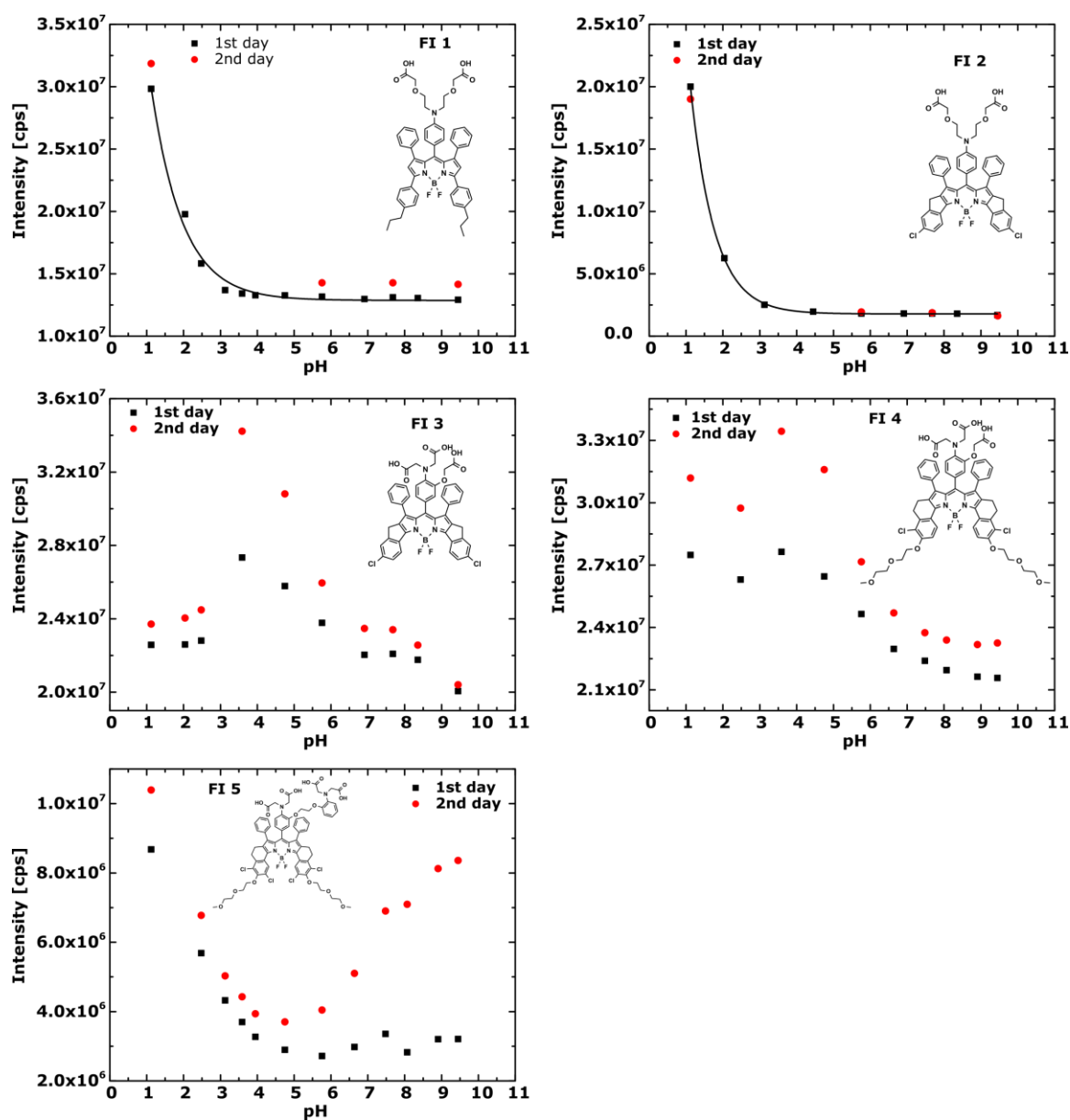


Figure 6-6: pH dependency of the fluorescence intensity in EtOH + universal buffer 1+1 for **FI1-5**. The solutions were measured instantly after preparation and after one day storage. **FI 3** and **4** do not show a clear pH-dependency between pH 1 to 9.5. **FI5** shows an increased fluorescence intensity after one day, more pronounced at higher pH values.

6.5.4. Behavior of fluoroionophores in solution

Since pH calibration did not result in clear tendencies, the behavior of the fluoroionophores in solutions with different ethanol content was investigated. The **FI** was dissolved in ethanol and 100 μL were pipetted in a vial. For obtaining different ratios of ethanol to water, x μL ethanol and y μL buffer (20 mM HEPES) were added resulting in a 1 mL solution. **Figure 6-7** shows the behavior of **FI2** in solution with varying ethanol content. Interestingly, PET works best in 100% ethanol and is lower when water is added (red fluorescence visible without Ca^{2+} , **Figure 6-7**).

These results are quite remarkable because normally the PET is enhanced in aqueous solutions. From a certain water content (about 60%) the emission is very weak even in presence of Ca^{2+} that may indicate aggregation of the dye (featuring a hydrophobic chromophore core) in mostly aqueous solution.

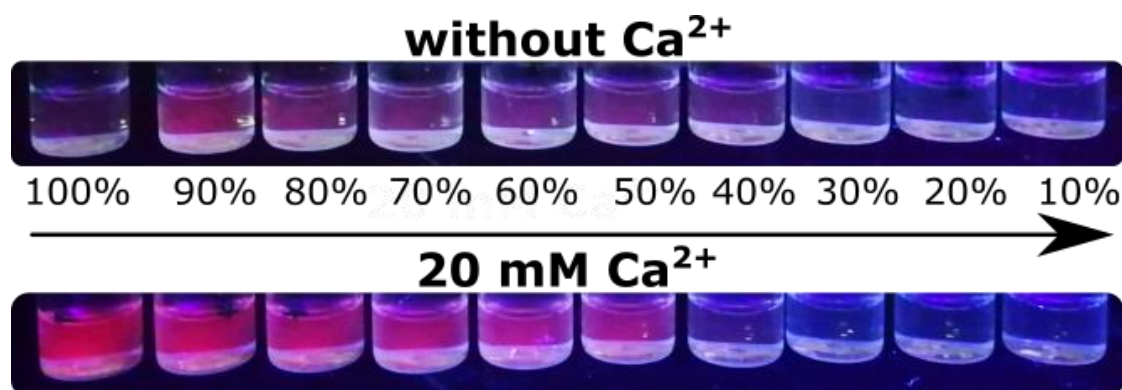


Figure 6-7: Fluorescence intensity for **FI2** upon illumination with UV light for different ethanolic compositions, with and without calcium. With increasing amount of ethanol, the PET is more pronounced. (aqueous buffer: 20 mM HEPES; pH 7.4). At high water content the dye is virtually non-fluorescent even in presence of Ca^{2+} that may be due to aggregation.

The same experiment was performed by recording the fluorescence emission of all indicators. Therefore, the absorption of the solution was adjusted to 0.05 for all solutions to reduce the probability of aggregation formation in the solutions. In **Figure 6-8** the plots for the **FI**s are shown. By plotting the intensity versus the amount of ethanol percentage it can be easily seen how the indicator behaves in the different solutions. Again, none of them really worked at low ethanolic compositions, that may be caused by aggregation of the dyes, and only **FI2** and **FI5** showed promising results at higher ethanol content.

Since the most irritating result was that the PET is not working in more aqueous media, different buffers were tested. In **Figure 6-9**, 20 mM TRIS, HEPES and MOPS in 20%

ethanol was tested in order to figure out if any buffer substance has an influence on the ON-OFF system, disturbing the PET. As can be seen from the figures, the 20% ethanolic solution shows for all buffer systems unexpected results under the UV-illumination. **FI1**, **FI3** and **FI4** showed highest fluorescence in all the buffers in the absence of Ca^{2+} and no visible red fluorescence in presence of the ion. This is in contrast to the behavior described in literature where the fluorescence of the fluoroionophores was enhanced upon complexation of calcium.^{64,123,225}

FI2 showed no red fluorescence at all and for **FI5** the reddish fluorescence was extremely weak and again observed only in the absence of Ca^{2+} . As can be seen from the figure, after two days in nearly all of the vials having added Ca^{2+} , the **FI** precipitated, indicating an unstable solution composition. It can be concluded that in solutions containing very little ethanol the complexed form appears to form non-fluorescent aggregates directly after addition of Ca^{2+} and even almost completely precipitates from the solutions during storage. In contrast, the uncomplexed form shows better solubility and is fluorescent in case of several fluoroionophores. The overlap of the effect of dye aggregation with the

fluorescence modulation via PET effect does not allow to observe the expected behavior (fluorescence enhancement in presence of Ca^{2+}) in these conditions.

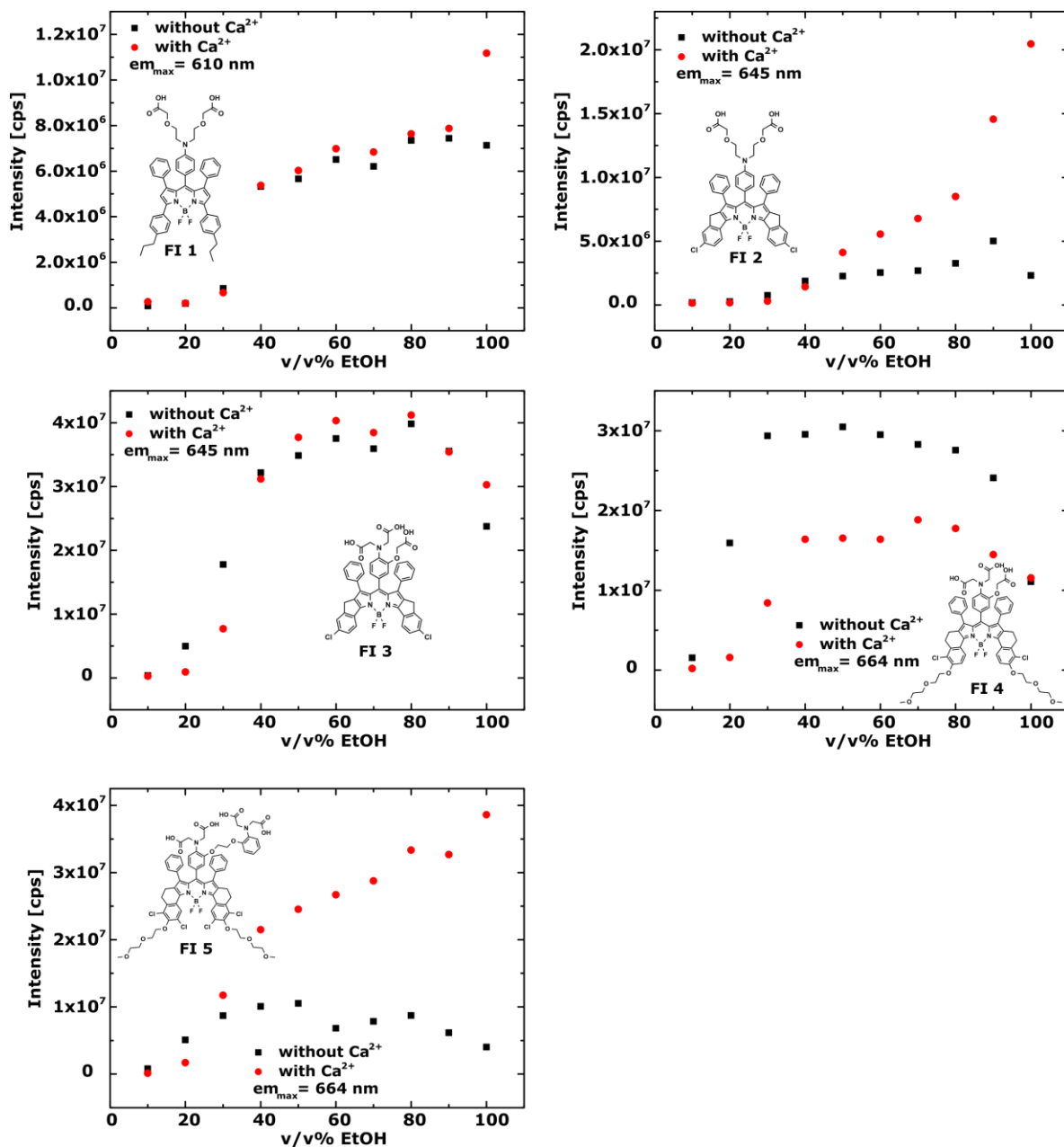


Figure 6-8: Fluorescence intensity for FI 1-5 in different ethanolic compositions, with and without 20 mM calcium. With increased amount of ethanol, the PET is in general more pronounced. Aqueous buffer contained 20 mM HEPES; pH 7.4. Ca^{2+} concentration was adjusted to be 20 mM for each calibration solution.

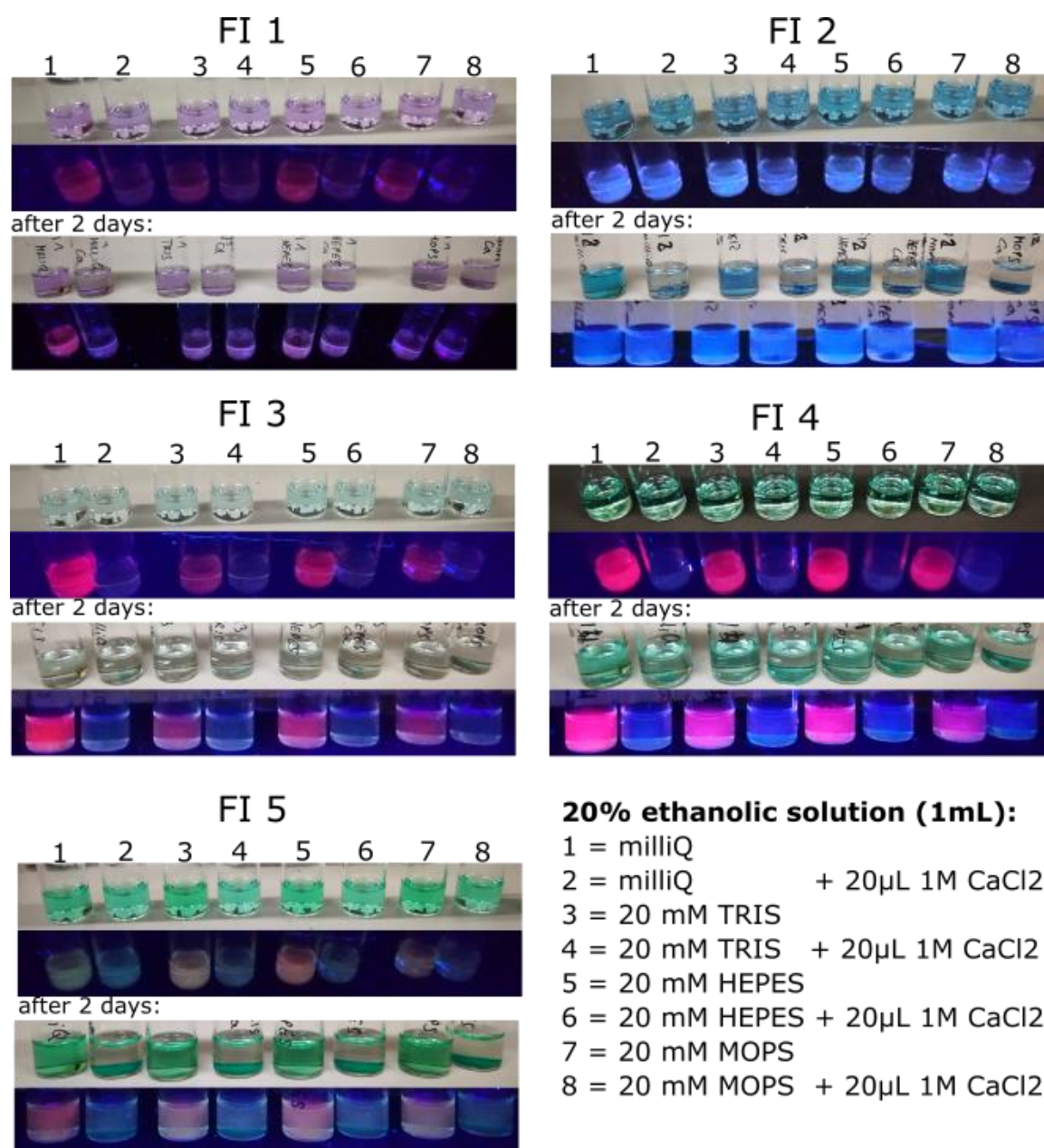


Figure 6-9: Fluorescence pretests for the fluoroionophores via illumination with a UV-lamp. Solutions contained 20% ethanol and different buffers (TRIS, HEPES, MOPS) to investigate any influences of the derived from the sort of buffer used. After 2 days, solutions were screened again. In most cases the **FI** precipitates in the solution, indicating an unstable solution composition.

Since all buffered solutions did not result in clear tendencies, short pretests were performed with **FI2** and **FI5** in ethanol + ultra-pure water; 1+1, without adjusting the pH. From **Figure 6-10** it can be seen that the indicator **FI5** shows a good sensitivity increase at 20 mM calcium on the first day. After 3 days the solution was measured again, and the solution was transferred again in a cuvette. The 0 mM calcium intensity drastically

increased, which might come from some contamination of calcium in the cuvette, although the cuvette was washed beforehand. The BAPTA indicator shows such high sensitivity in the μM range that any contamination at low volumes (1 mL) can have a huge effect. Even small crumps from the ceiling after opening the vials, which are probably not recognized by the human eye may have an effect. Another explanation might be impurities in the glass. Windows and bottles sometimes contain calcium impurities, which might describe the above-mentioned behavior. **FI2** supports the theory of the contamination derived from glass, since the receptor is less sensitive and small extractions of Ca^{2+} do not have any effect. For the 0 mM solution, similar intensities were measured after 3 days, whereas the 20 mM calcium solution drops 30% without showing any signs of aggregation in the emission spectrum. Since the **FIs** previously precipitated there might be the possibility that the indicator also partly present in almost non-fluorescent aggregated form that does not contribute to the emission spectrum.

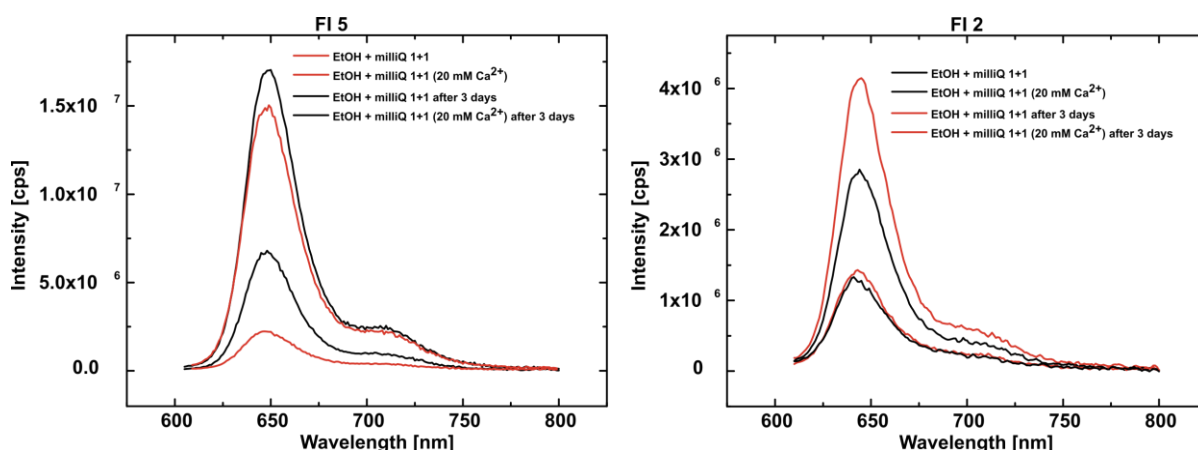


Figure 6-10: Fluorescence spectra of **FI5** and **FI2** in EtOH + ultra-pure water 1+1, with and without 20 mM calcium. The solutions were measured directly after preparation and after 3 days storage. **FI5** shows an increased fluorescence after 3 days storage. **FI2** shows a decreased fluorescence after 3 days for 20 mM Ca^{2+} , without any signs of aggregation visible in the fluorescence spectrum.

Since the indicators revealed a better PET in ethanol (pretest with the UV-lamp), solutions containing 90% ethanol in ultra-pure water were prepared and absorption and emission spectra were recorded. After 1 h both indicators, **FI1** and **FI3** showed aggregation phenomena (**Figure 6-11 a** and **b**). **FI1** shows a broad emission aggregation peak at around 750 nm, whereas **FI3** a sharp aggregation peak at 800 nm. In this case, it is difficult to evaluate which type of aggregation is predominant. Typically, J-aggregates (“head-to-tail” alignment) possess very narrow, bathochromically shifted absorption and emission spectra, with an increased molar absorption coefficient. H-aggregates (“side-by-side” alignment) reveal a larger bathochromic shift in the spectrum.^{232–234} Since **FI1**

reveals a very broad absorption spectrum due to the rotating phenyl groups, it is difficult to evaluate which type of aggregation predominant, whereas the emission of the aggregation peak is not drastically shifted, hence J-aggregation might be favored. The emission peak ($\lambda_{\text{max}} = 744 \text{ nm}$) is narrow that also indicates presence of J-aggregated species. **FI3** seems to be a special case, because absorption in the red part of the spectrum disappears and instead it appears in the NIR part of the spectrum. A new emission peak at about 800 nm appears that is strongly bathochromically shifted compared to the emission from the monomeric species that also can be detected (**Figure 6-11 b**). Such spectral shifts are characteristic for formation of J-aggregates. In order to develop a reversible and stable sensing system for calcium ions, it is highly recommended to further investigate the behavior of calcium fluorophores in solutions. If the characteristics of such indicators in solution is known, the development of calcium sensors might be easier and more effective.

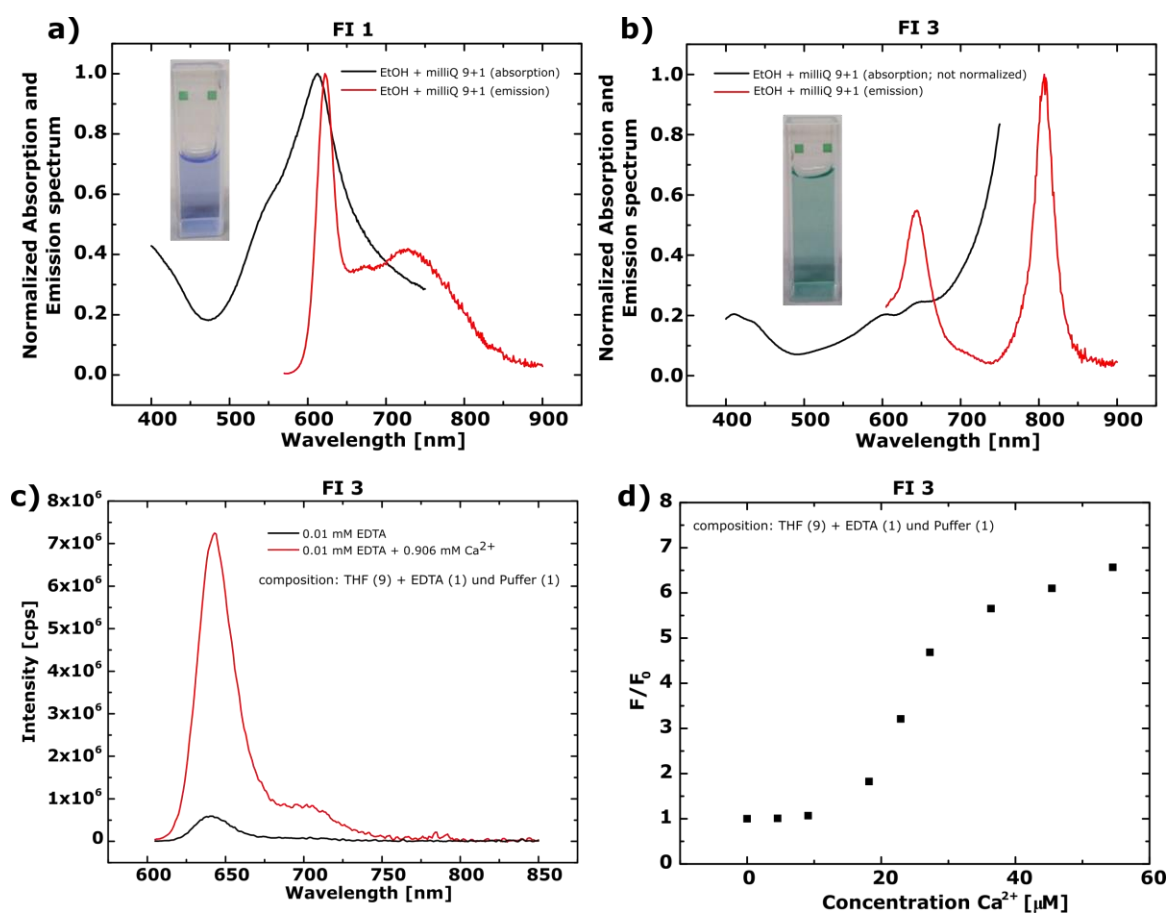


Figure 6-11: **a)** Absorption and emission spectrum of **FI1** in EtOH + ultra-pure water 9+1. The indicator shows aggregation phenomena indicated in both spectra. **b)** Absorption and emission spectrum of **FI3** in EtOH + ultra-pure water 9+1. The indicator shows formation of J-aggregates with a distinct emission band at 808 nm. **c)** Fluorescence emission of **FI3** in a mixture of THF+EDTA (0.01 mM) + buffer (20 mM HEPES; pH 7.4) 9+1+1; without and with 0.906 mM calcium. **d)** calibration of **FI3** from 0 to 60 μM calcium. Fluorescence intensities start to increase at 10 μM calcium.

Since experiments so far did not result in clear tendencies, investigations in THF with the **FI3** were made in solution. Additionally, the solutions contained a total EDTA concentration of 0.01 M to ensure an absolute PET-ON-state. In **Figure 6-11 (c and d)** the emission spectra and the corresponding calibration is shown. The emission spectra did not reveal aggregation formation anymore. Moreover, as expected emission enhancement upon addition of Ca^{2+} was observed. The enhancement factor between 0 and 0.906 mM calcium was around 14, indicating a high sensitivity towards calcium. Calibrations in the μM range revealed sensitivity between 10 and 40 μM calcium. For the first time, we were able to measure calcium in a stable solution composition. Although, because of the presence of EDTA some of the calcium used in the calibration solution gets complexed, it was managed to obtain a stable system. A possible calibration setup might be to adjust the amount of EDTA to a certain point where the emission is not changed anymore, to obtain a solution completely in its off state, ready for calibrations.

6.5.5. Calibrations in hydrogels

Calibrations in hydrogel D7 were also performed. Since the indicators showed unstable behavior with increasing water amount and D7 has a water uptake of 30% this polymer seemed to be the best applicable matrix. In **Figure 6-12**, calibrations are shown using a flow through cell, enabling time resolved intensity measurements. **Figure 6-12** shows a calibration using a very high calcium concentration of 200 mM and a 0.1 M EDTA solution, which was permanently pumped through the cell to achieve stable plateaus. **Figure 6-12 b** shows a calibration of the sensor foil in the μM range. At 3 μM calcium the indicator has not reached a plateau, and at higher concentrations no distinct intensity changes for different calcium concentrations were measured. Nevertheless, via pumping an EDTA solution through the cell the fluoroionophore was decomplexed again, indicating a host-guest interaction within the sensing layer. Further research will be needed to develop a reliable and reversible sensing system. Several influences and factors are yet unknown and need to be investigated in the future. A future prospect about calcium fluoroionophores is given in the outlook of this chapter.

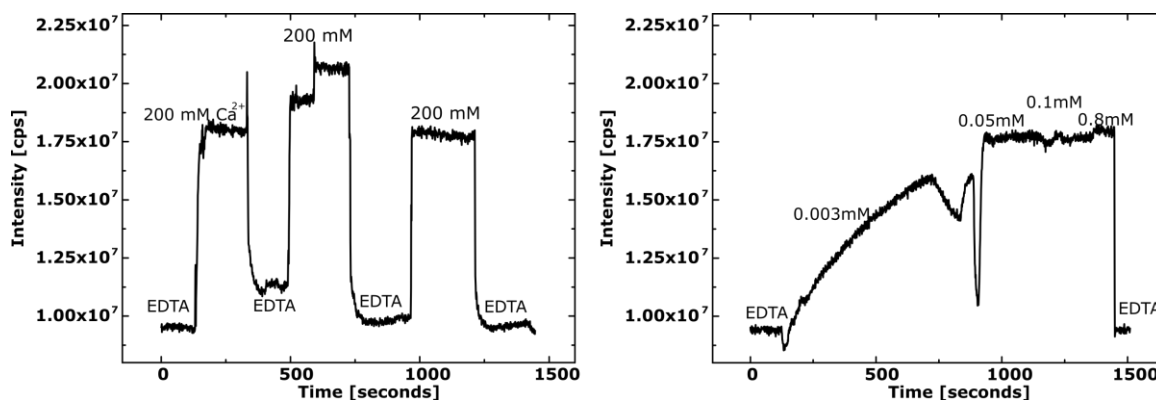


Figure 6-12: Calibration of a sensor foil containing 0.2 w% **FI3** in hydrogel D7. The sensor shows a fluorescence increase with increased calcium concentration. (left) The sensor does not show any difference by variation of the calcium concentration. (right)

6.6. Conclusion

Here, five new calcium fluoroionophores were successfully synthesized in their protected ester forms. The photophysical properties of **FI-esters** were characterized. Two new BODIPY dyes were designed to have an increased hydrophilicity, with molar absorption coefficients above $150\,000\text{ M}^{-1}\cdot\text{cm}^{-1}$. Except **FI1-ester** all dyes emit in the red part of the electromagnetic spectrum. Saponification of the **FI-esters** was carried out in NaOH, resulting in the corresponding sodium salts of the fluoroionophores. The behavior of the fluoroionophores was studied in respect to their dependency of pH and the amount of organic solvent used. In general, the **FI** showed better PET in organic solvent compositions, whereas at 100% H_2O no intensity changes were detected which however may be due to aggregation of the dyes in these conditions. The prepared solutions turned to be unstable and precipitation was observed after two days of storage in 20% ethanolic solution. **FI1** and **FI3** revealed aggregation phenomena in a 90% ethanolic solution showing spectral properties typical for J-aggregates. The usage of THF for the calibrations was successful with no aggregates visible. By additionally using EDTA, the fluoroionophores were fully “switched off”, preventing any contamination of calcium for the 0 mM emission value. The first pretests of **FI3** in hydrogel D7 with the use of EDTA solution were successful. The sensor foil showed good reversibility, representing a promising starting point for future development.

6.7. Outlook

This project gives a starting point for future calcium sensor development. Some of the measurements performed in solution and in hydrogels offer contradictory results and further research is necessary in order to obtain a reliable detection and sensing system. Since the handling of charged fluoroionophores is by far one of the most difficult disciplines, following outlook provides some general thoughts about future considerations for calcium fluoroionophores used as sensors.

The saponification itself seemed to work quite good with NaOH. Nevertheless, workup of fluoroionophores requires enormous effort. A simpler way of deprotection or workup would result in a time-consuming process. Pretests with esterase's for deprotection and/or the usage of ion exchangers for purification might be a good starting point. Although FI-esters were fully characterized via NMR and HR-MS, analysis of deprotected FI-esters was unsuccessful. In general, it would be practicable to characterize the final products to ensure full deprotection as well as any side products formed during saponification, although the possibility for any other reaction is quite low. Therefore, investigations developing a characterization technique is recommended, not just for synthesis control, also with regard to an easier acceptance of a publication.

Calibrations in THF/buffer with EDTA worked for **FI3** and showed promising results. Still those experiments are the starting point of the project and the amount of EDTA used in this calibration was not yet optimal. Because most of the indicators show a sensitivity in the μM range, a sophisticated calibration strategy is needed. A possible calibration technique would be to prepare a stock solution of **FI** and titrate this solution with EDTA until the fluorescence emission remains unchanged. The titrated solution can be used for calibrations without any influence by EDTA, since traces of calcium within the solution are already bound by EDTA.

For calibrations in hydrogels covalent coupling of the indicator onto polymers might be an option. Since charged **FIs** sometimes showed aggregation phenomena, direct coupling technique could prevent any kind of aggregations. He et al.⁶⁴ coupled a PIDA fluoroionophore on aminocellulose via NHS/DDC coupling and reversibly measured calcium on a sensor disk, using a mixture of hydrogel D4 and the synthesized amino-cellulose fibres. Staudinger et al.²³⁵ cross-linked aza-BODIPY dyes on hydrogels based on poly(acryloylmorpholine) polymers and with the use of borontrichloride (BCl_3) they

managed covalent coupling to the boron center of the an aza-BODIPY dye via an B-O linkage. Investigations showed that this technique also works for BODIPY dyes and with any polymer having terminal hydroxy groups. In **Figure 6-13** a K^+ fluoroionophore was coupled on cellulose acetate propionate (CAP) with 4% terminal hydroxy groups. The exchange of the fluorine groups of the boron center was performed under inert conditions with BCl_3 . With the addition of CAP under basic conditions covalent coupling of the dye moiety on the polymer was achieved. The CAP can be hydrolyzed under basic conditions, resulting in a water-insoluble cellulose polymer. **Figure 6-13 b** shows a 24 h-hydrolyzed foil which shows sensor response and a clear difference to an unhydrolyzed foil. Additionally, **Figure 6-13 c** shows that by varying the hydrolyzation times different sensing dynamics are achieved.

This technique seems to be one of the most promising solutions for calcium sensors, not just for minimizing aggregation phenomena, also sensitivities and sensing dynamics can be controlled by adjusting hydrolyzation times.

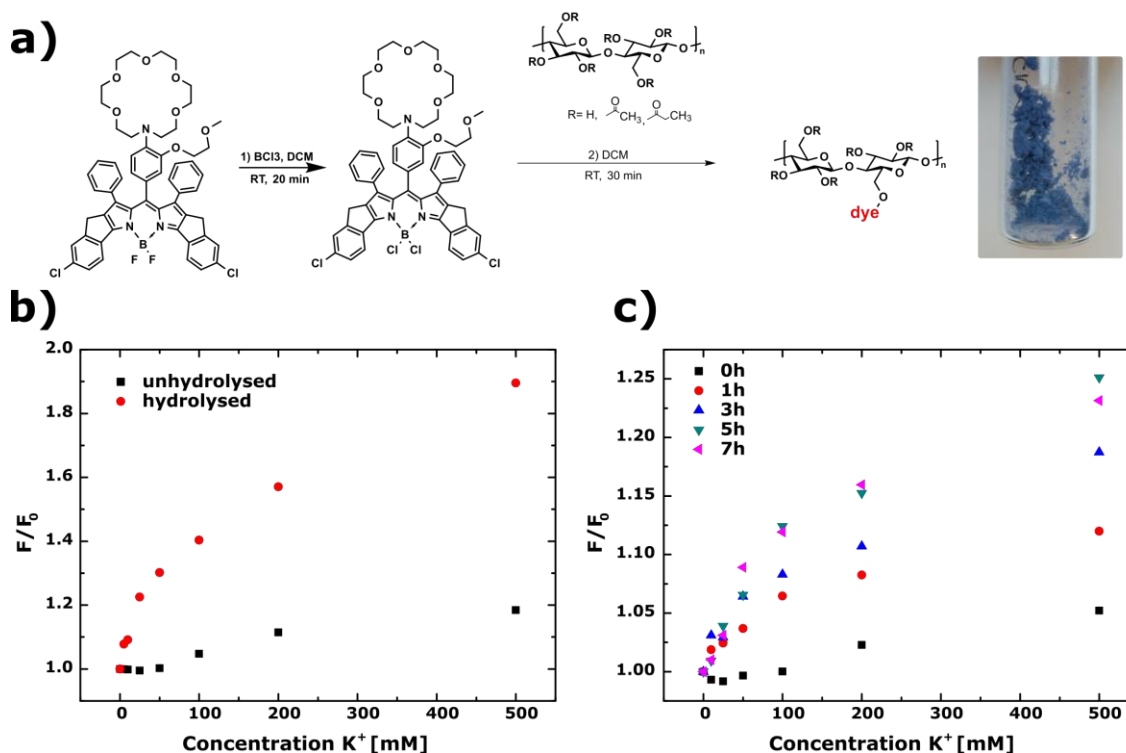


Figure 6-13: **a)** Covalent coupling of a K^+ sensitive BODIPY fluoroionophore on CAP. **b)** Calibration of an 24 h hydrolyzed (pH 13) CAP-indicator foil and a unhydrolyzed sensor foil, for comparison. **c)** Effect of hydrolyzation times. (pH 13)

6.8. Supporting Information

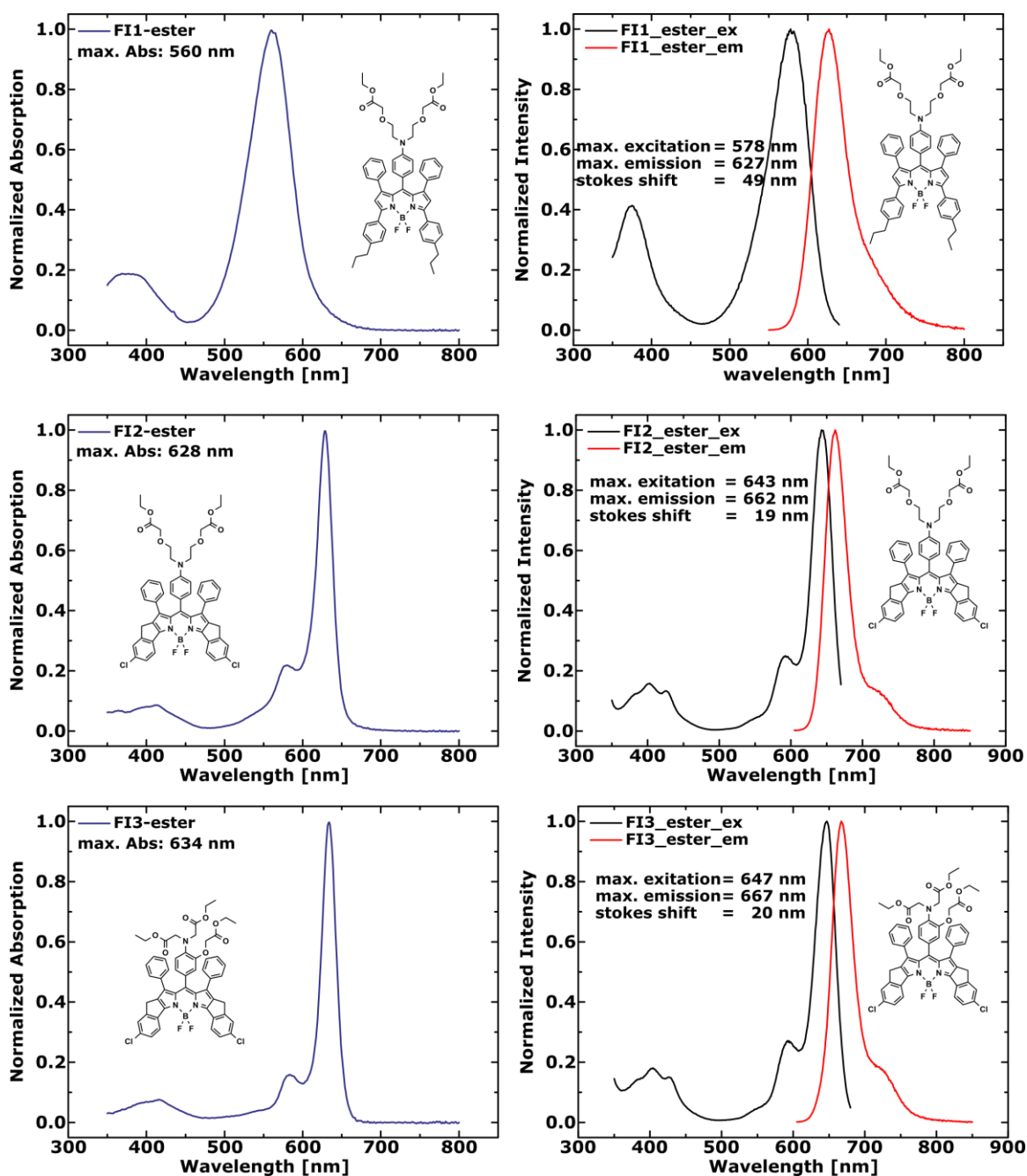


Figure S 6-1: Absorption, Excitation and Emission spectra of FI1-ester, FI2-ester and FI3-ester.

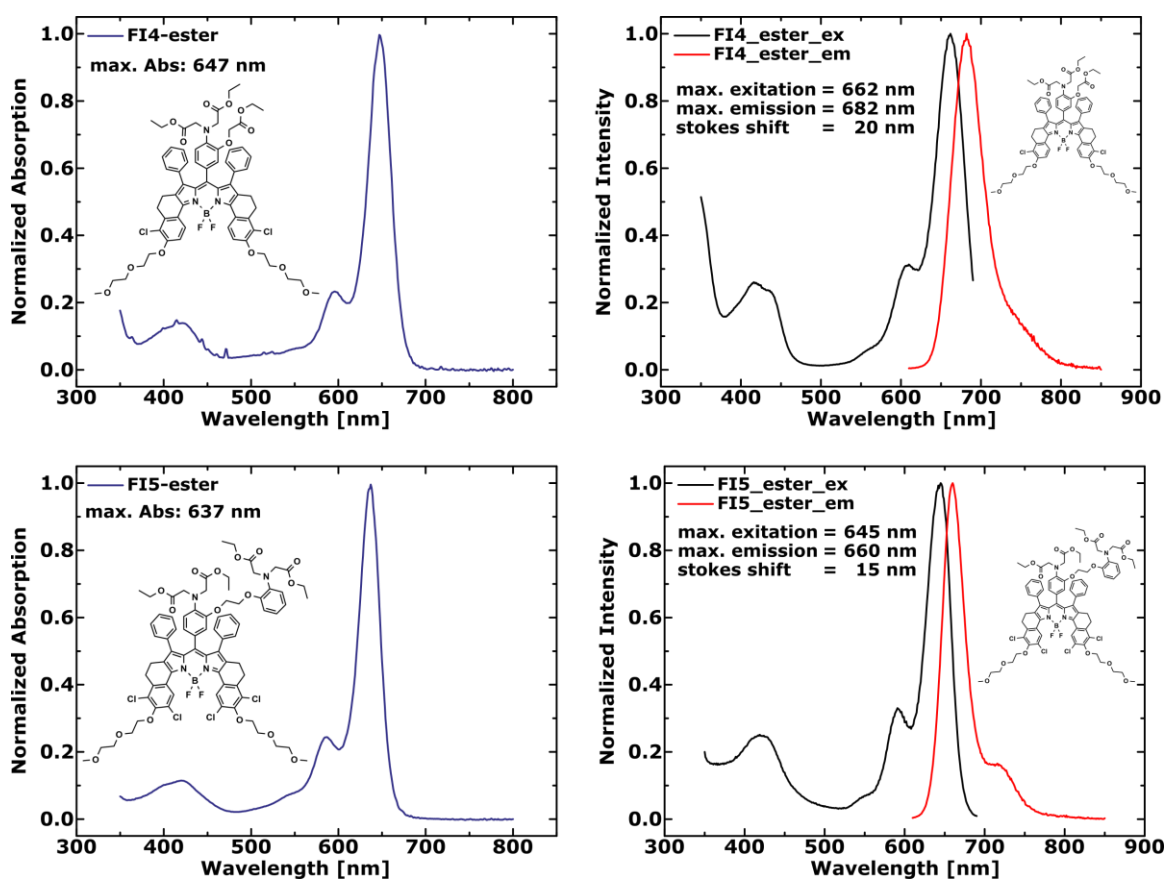


Figure S 6-2: Absorption, Excitation and Emission spectra of FI4-ester and FI5-ester.

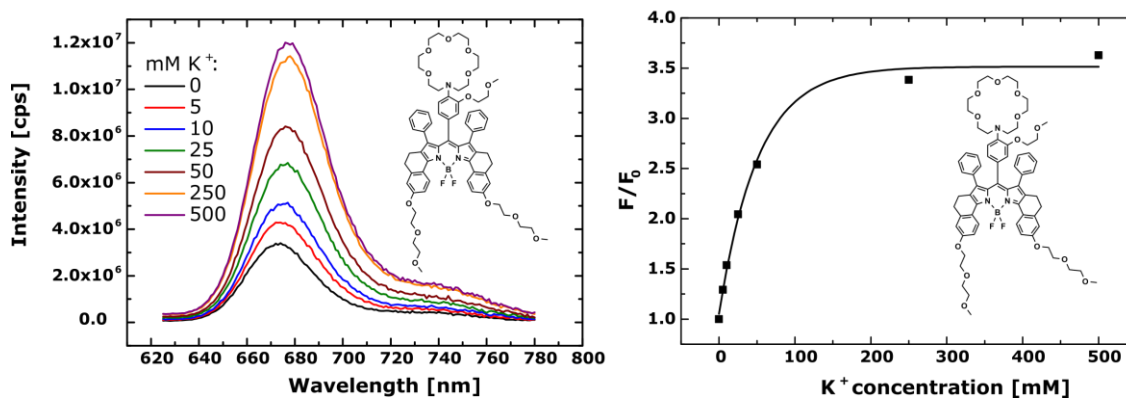


Figure S 6-3: Calibration of a potassium indicator (in hydrogel D1) for comparison of the spectral properties in section 6.5.2.

6.8.1. NMR and MS data

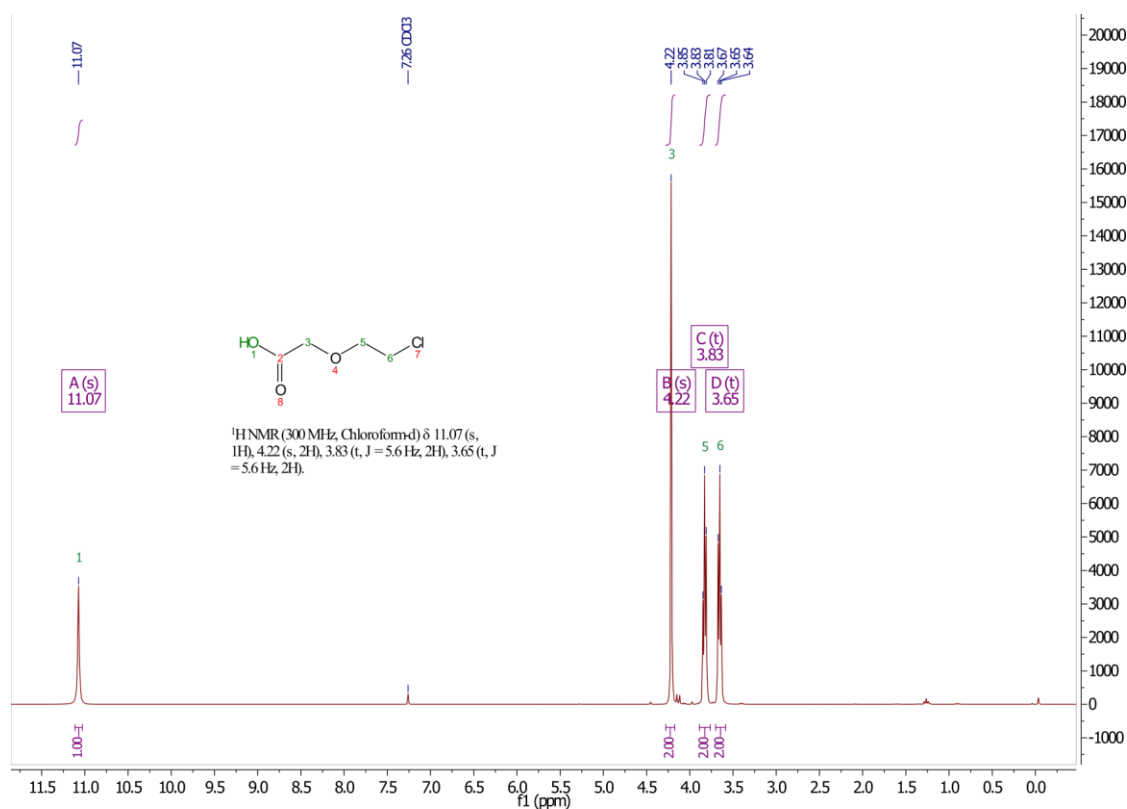


Figure S 6-4: ^1H NMR (300Hz), in CDCl_3 of **1**.

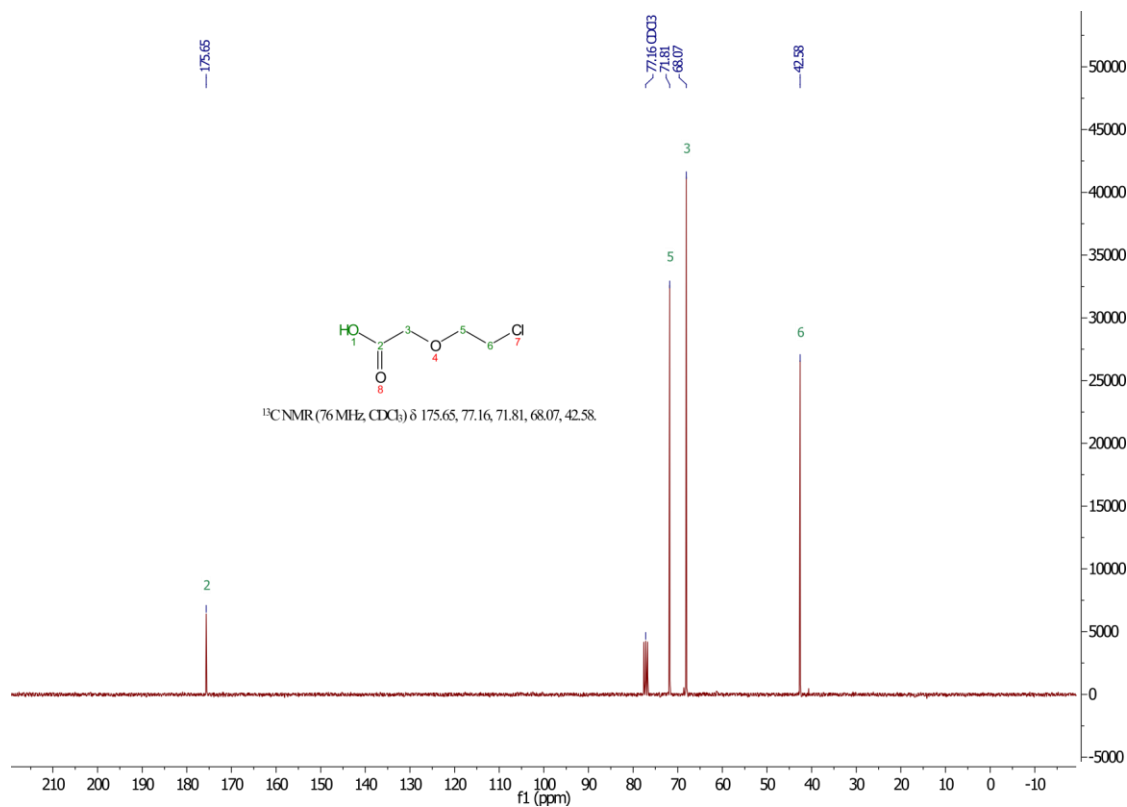
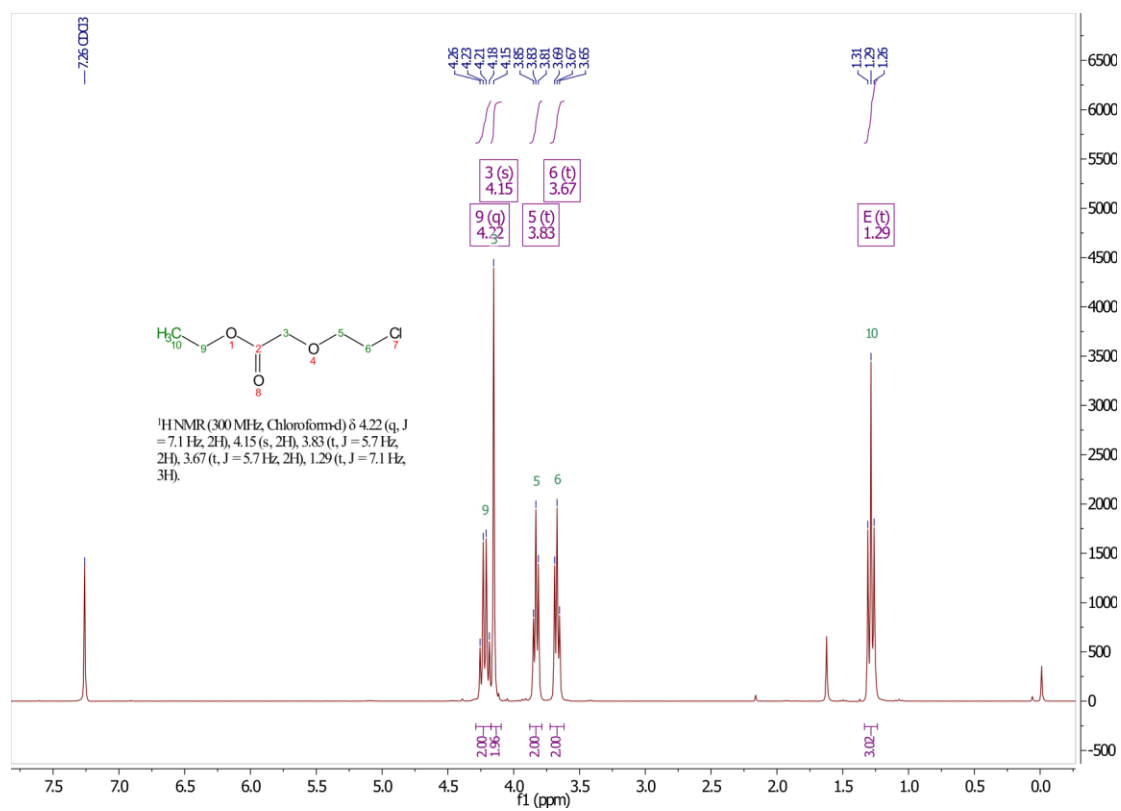
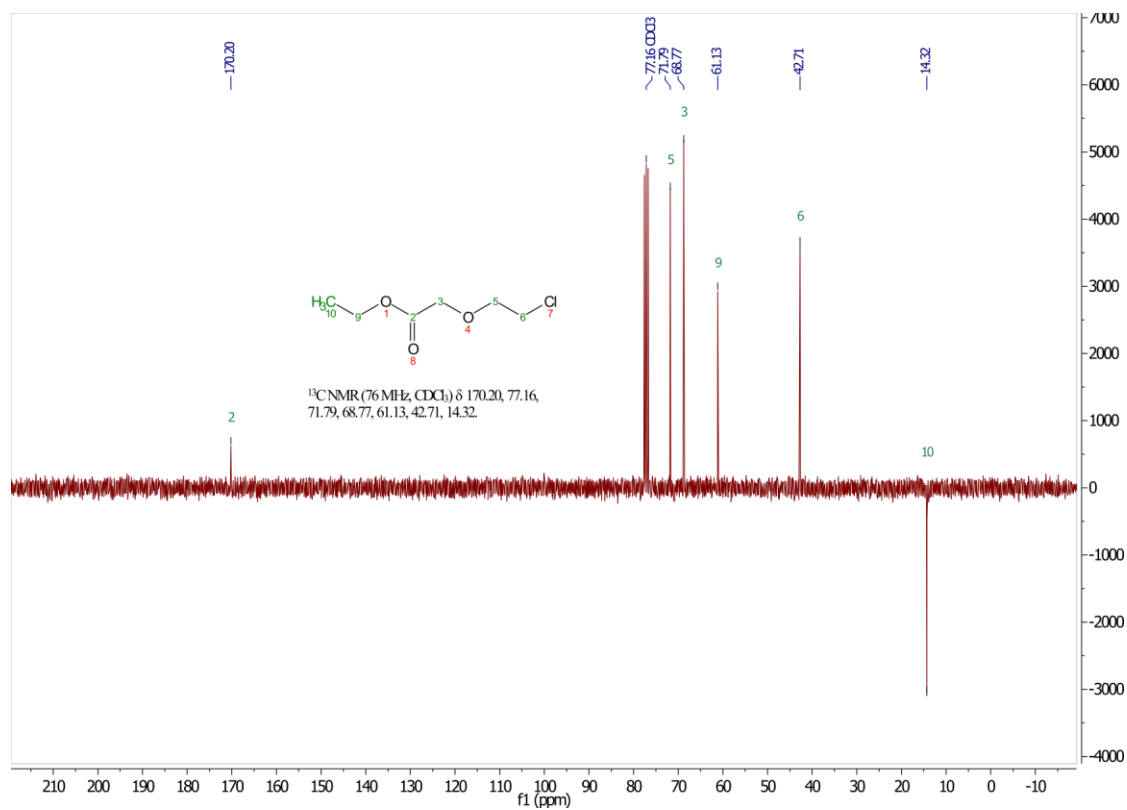
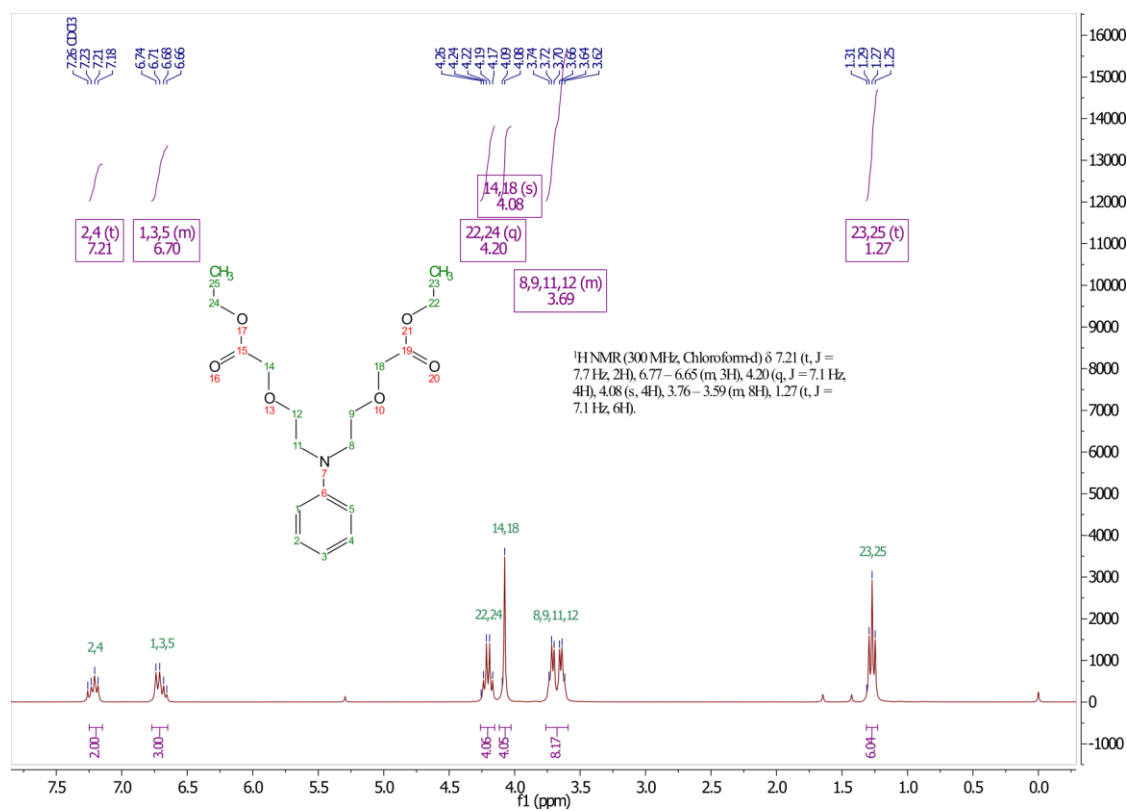
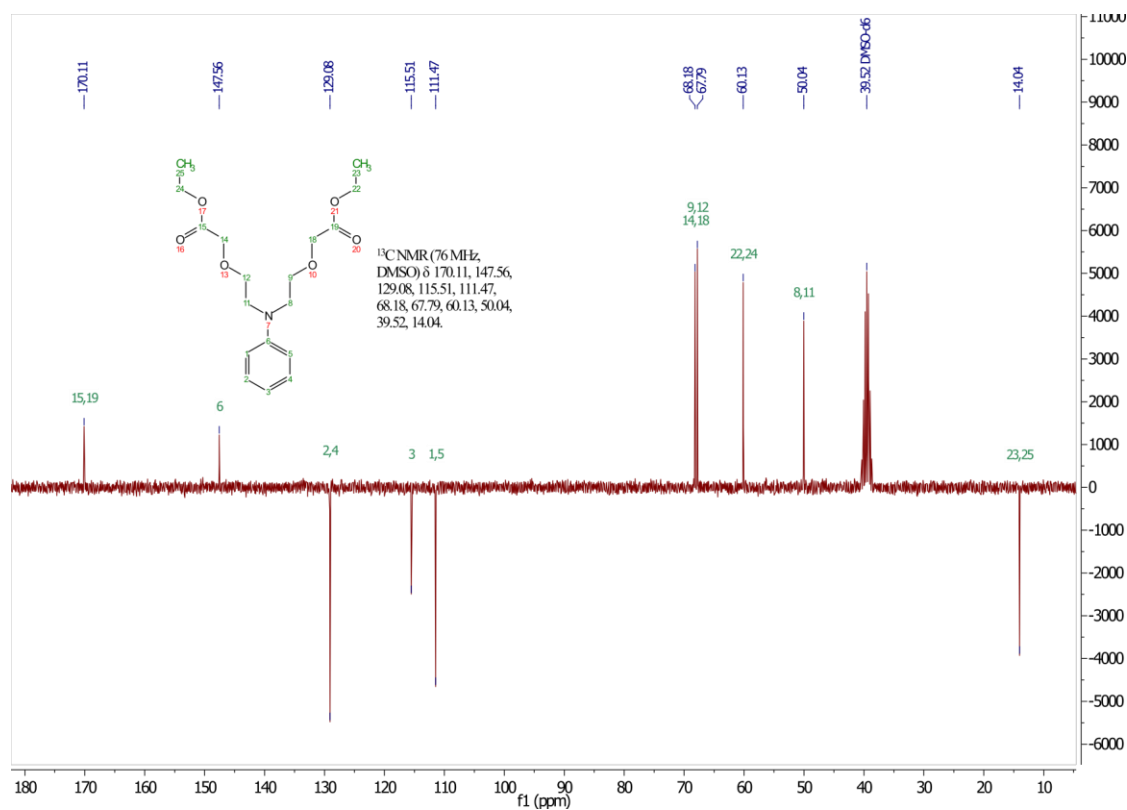


Figure S 6-5: ^{13}C -APT NMR (76Hz, CDCl_3) of **1**.

Figure S 6-6: $^1\text{H NMR}$ (300Hz), in CDCl_3 of **2**.Figure S 6-7: ^{13}C -APT NMR (76Hz, CDCl_3) of **2**.

Figure S 6-8: ¹H NMR (300Hz), in CDCl₃ of **3**.Figure S 6-9: ¹³C-APT NMR (76Hz, DMSO-d₆) of **3**.

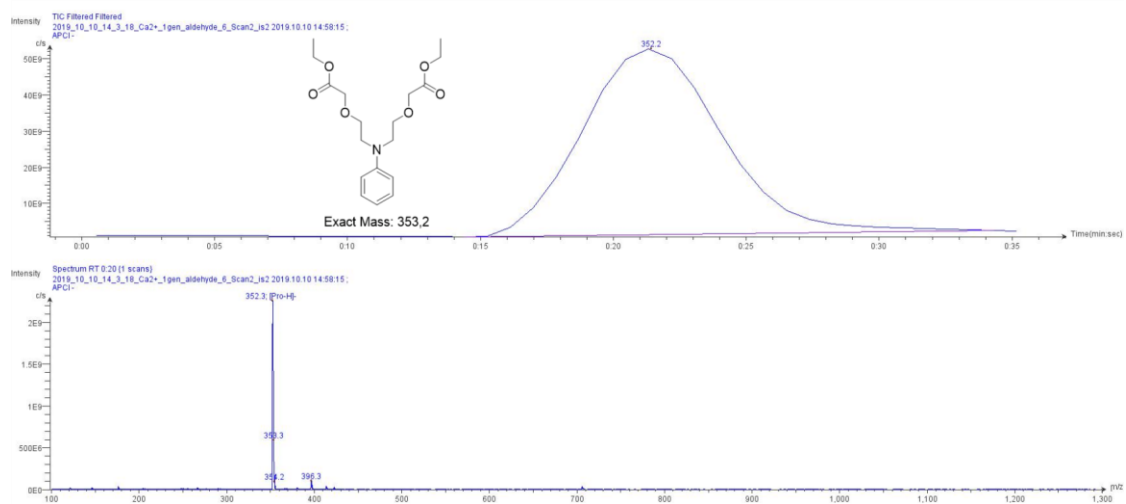


Figure S 6-10: LR-Mass Spectrum of **3** recorded on Advion expression CMS.

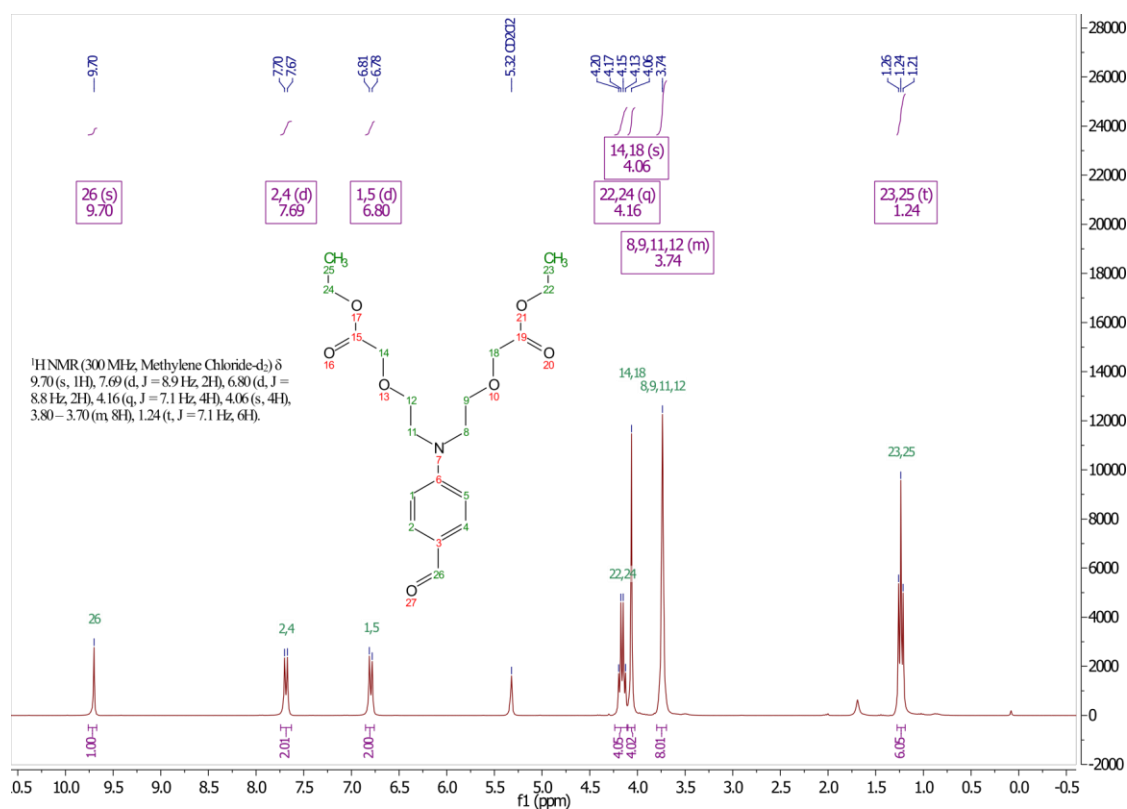
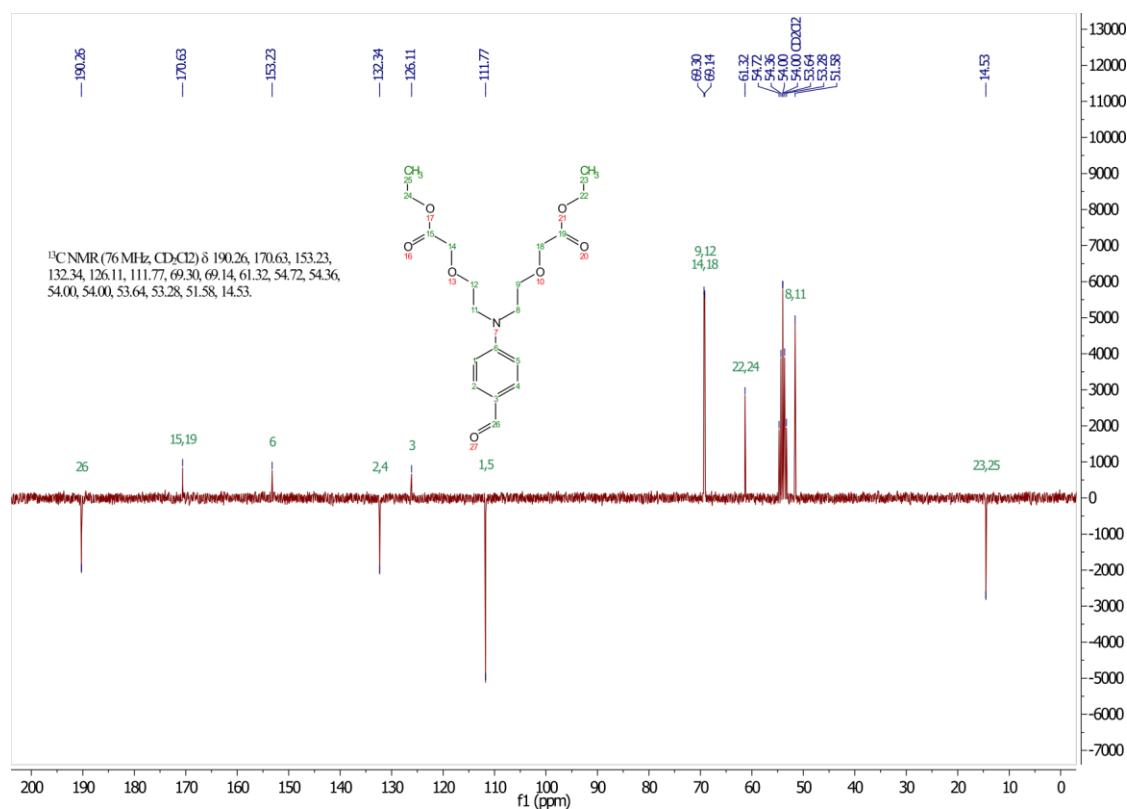
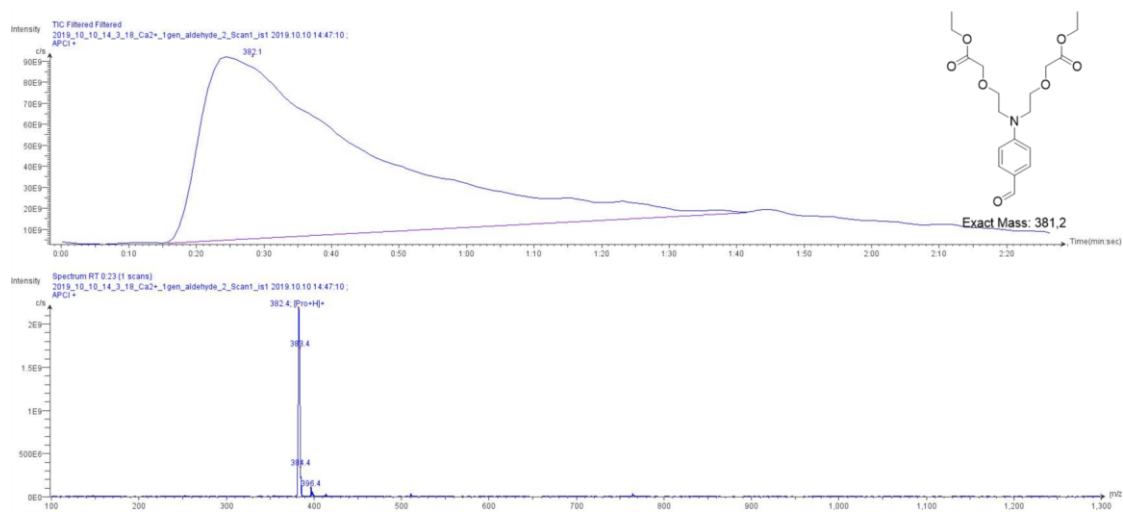


Figure S 6-11: ^1H NMR (300Hz), in CDCl_3 of **4**.

Figure S 6-12: ^{13}C -APT NMR (76Hz, CD_2Cl_2) of **1**.Figure S 6-13: LR-Mass Spectrum of **4** recorded on Advion expression CMS.

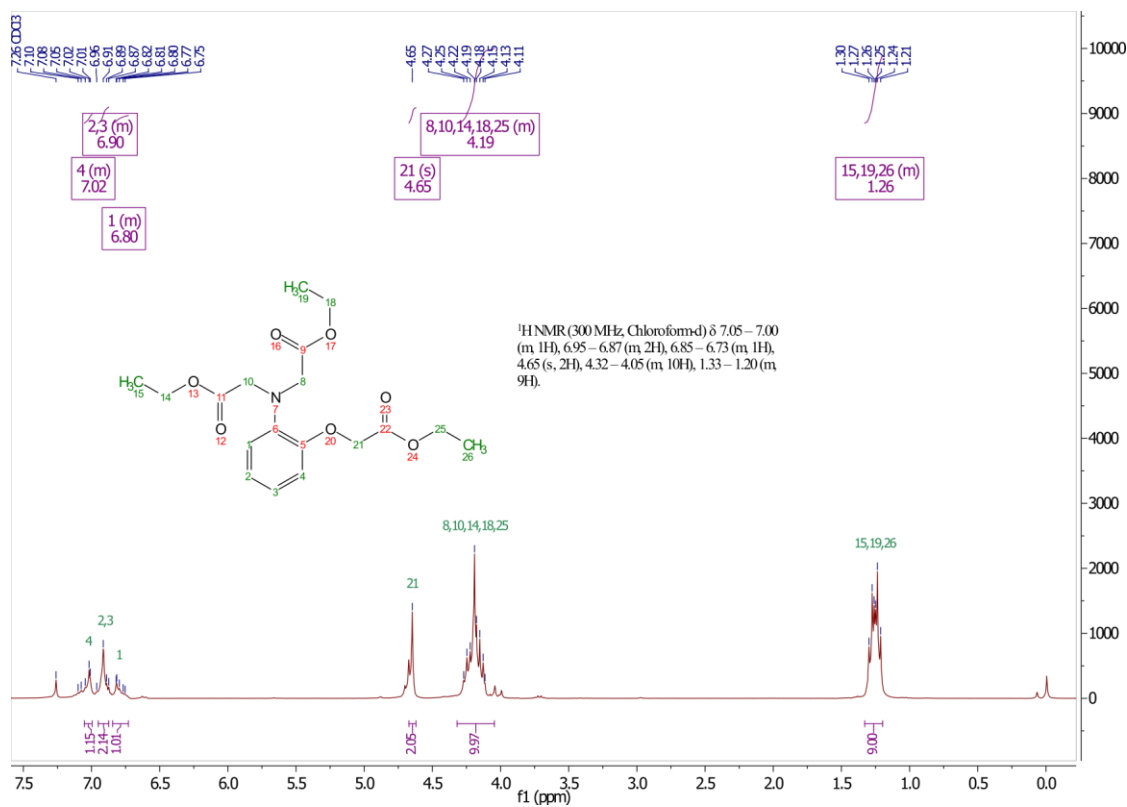


Figure S 6-14: ¹H NMR (300Hz), in CDCl₃ of **5**.

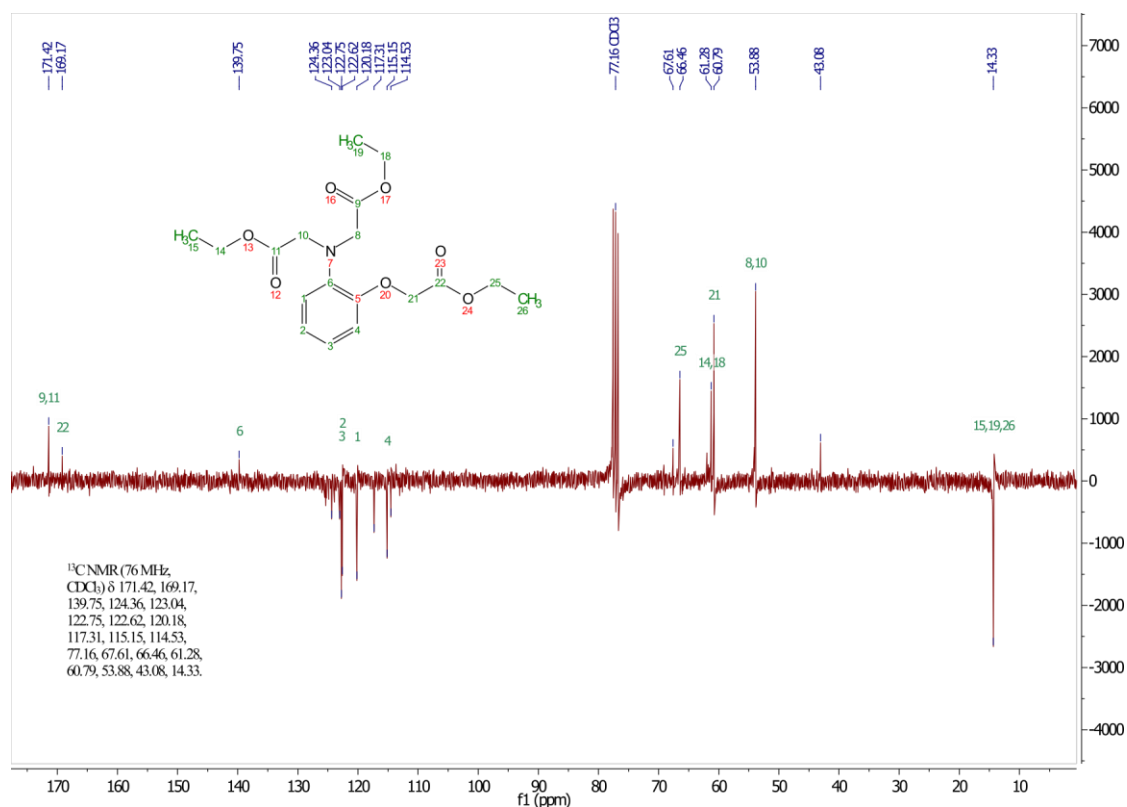


Figure S 6-15: ¹³C-APT NMR (76Hz, CDCl₃) of **5**.

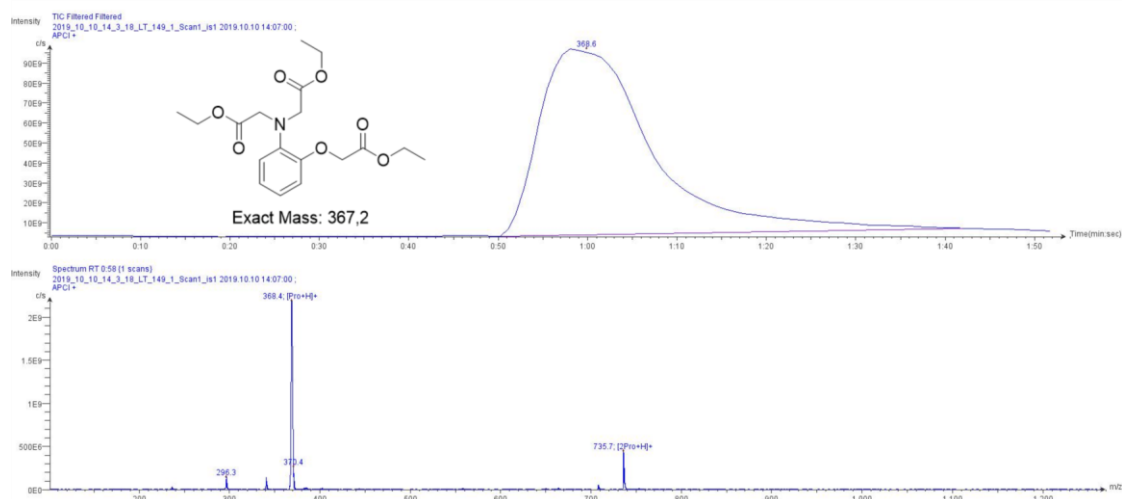


Figure S 6-16: LR-Mass Spectrum of **5** recorded on Advion expression CMS.

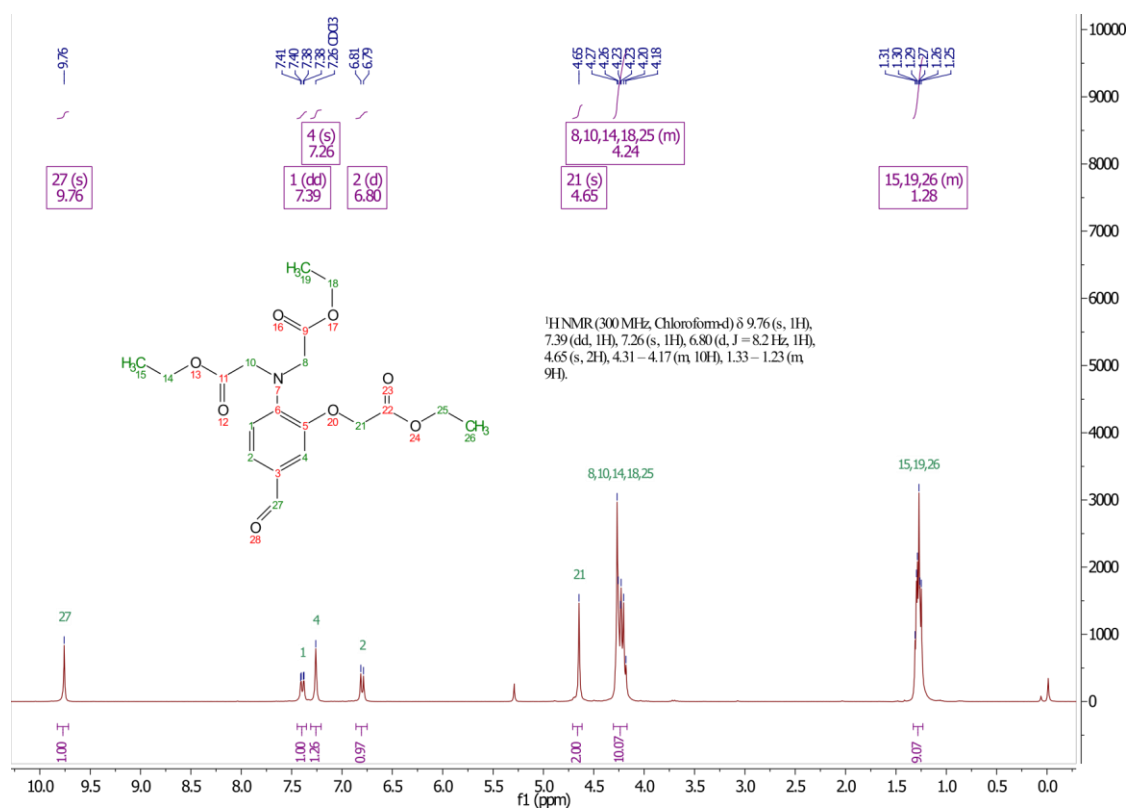


Figure S 6-17: ¹H NMR (300Hz), in CDCl₃ of **6**.

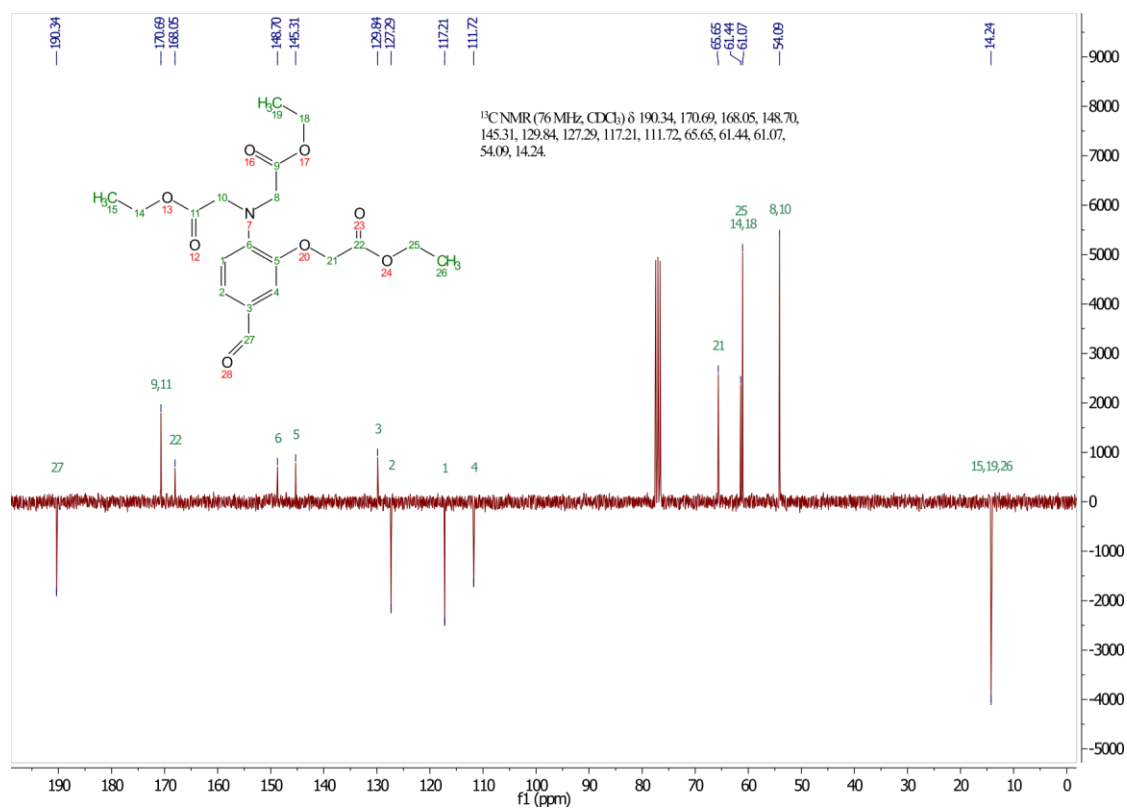


Figure S 6-18: ^{13}C -APT NMR (76Hz, CDCl_3) of **6**.

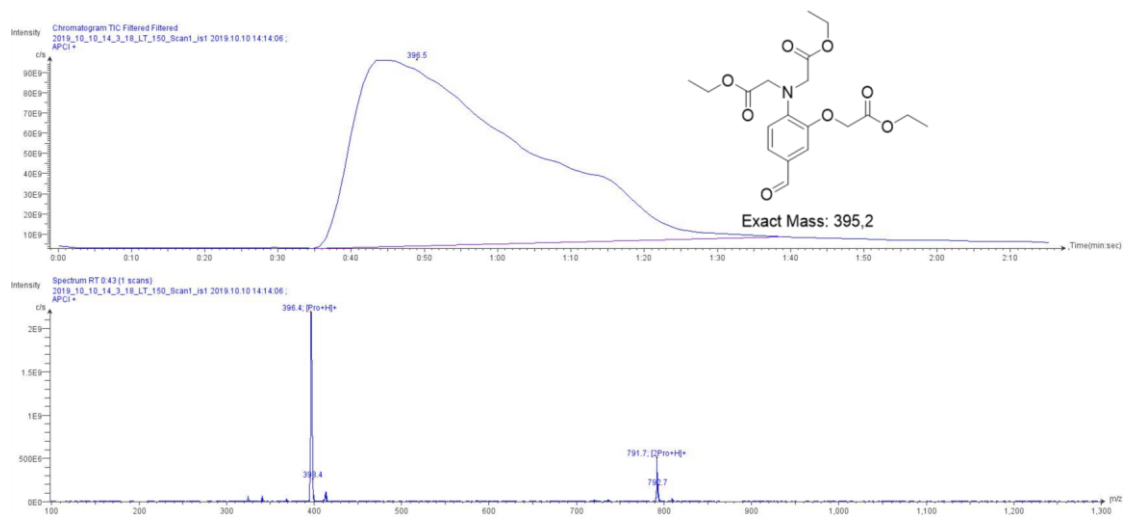


Figure S 6-19: LR-Mass Spectrum of **6** recorded on Advion expression CMS.

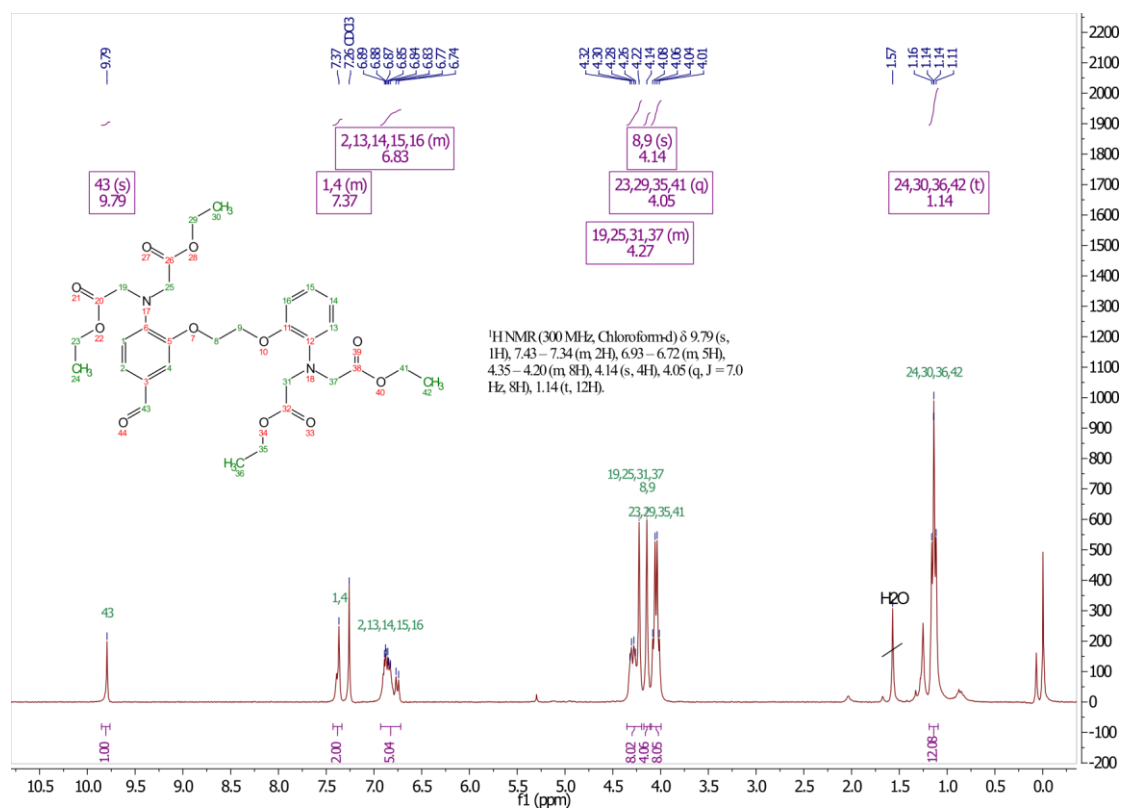


Figure S 6-20: ^1H NMR (300Hz), in CDCl_3 of **7**.

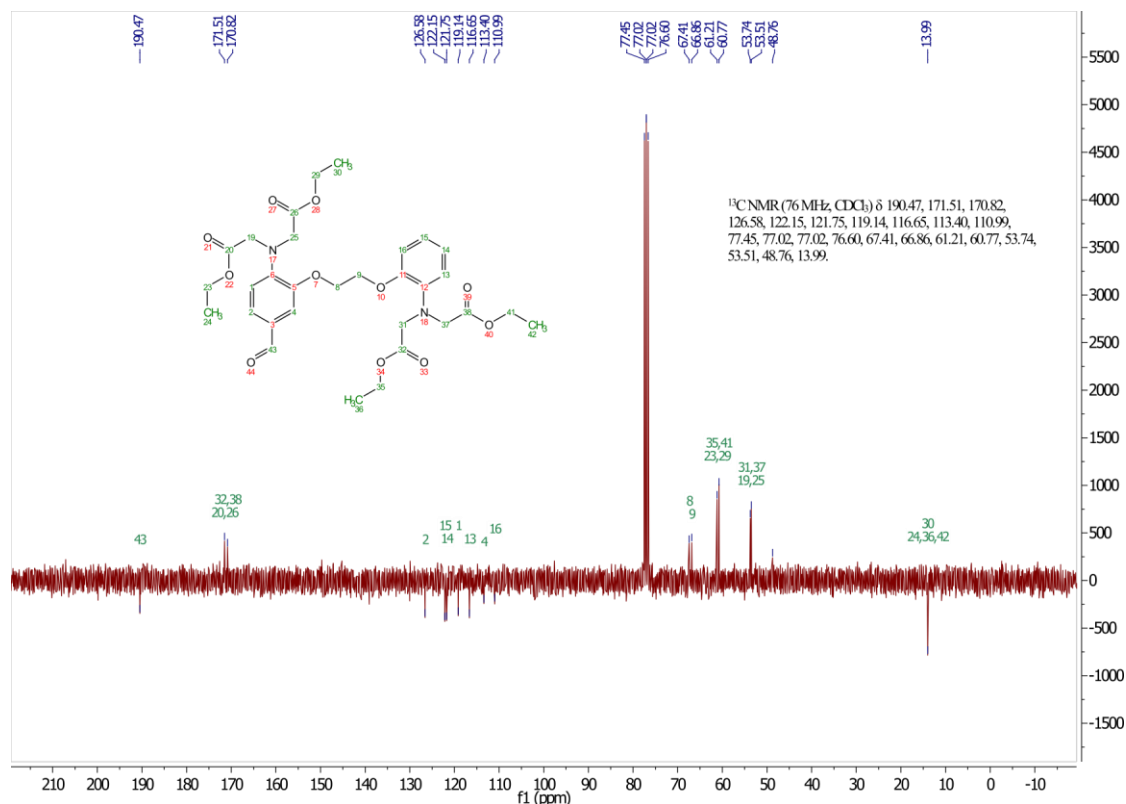


Figure S 6-21: ^{13}C -APT NMR (76Hz, CDCl_3) of **7**.

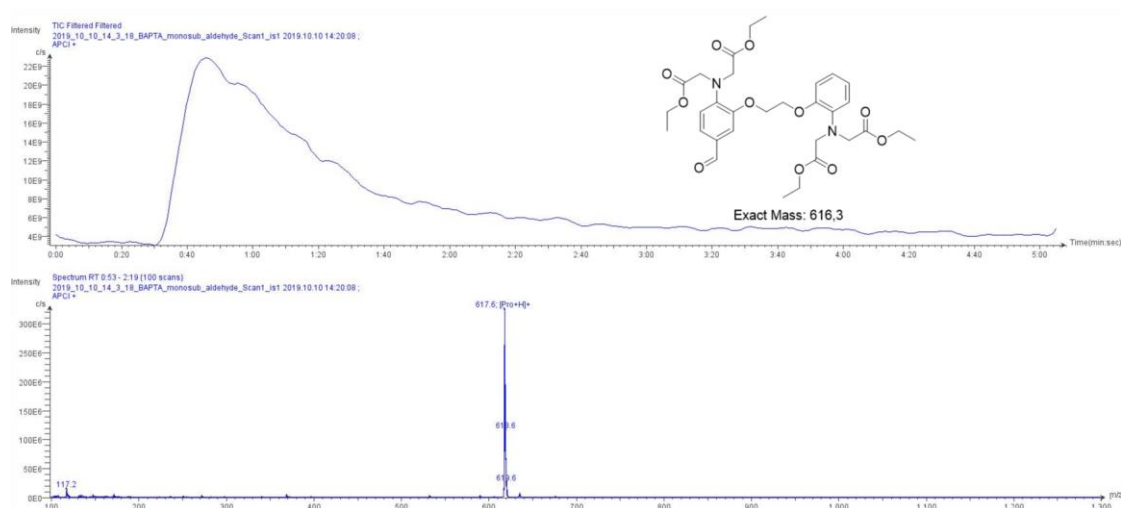


Figure S 6-22: LR-Mass Spectrum of **7** recorded on Advion expression CMS.

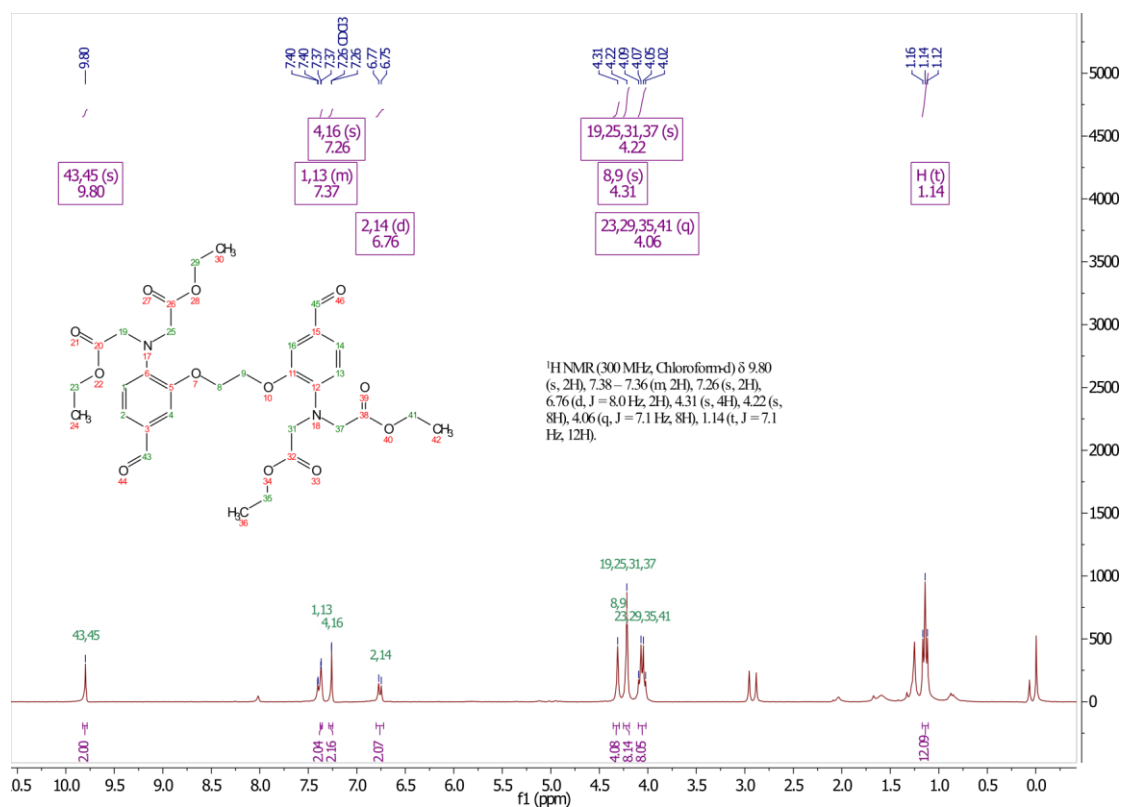


Figure S 6-23: ¹H NMR (300Hz), in CDCl₃ of **8**.

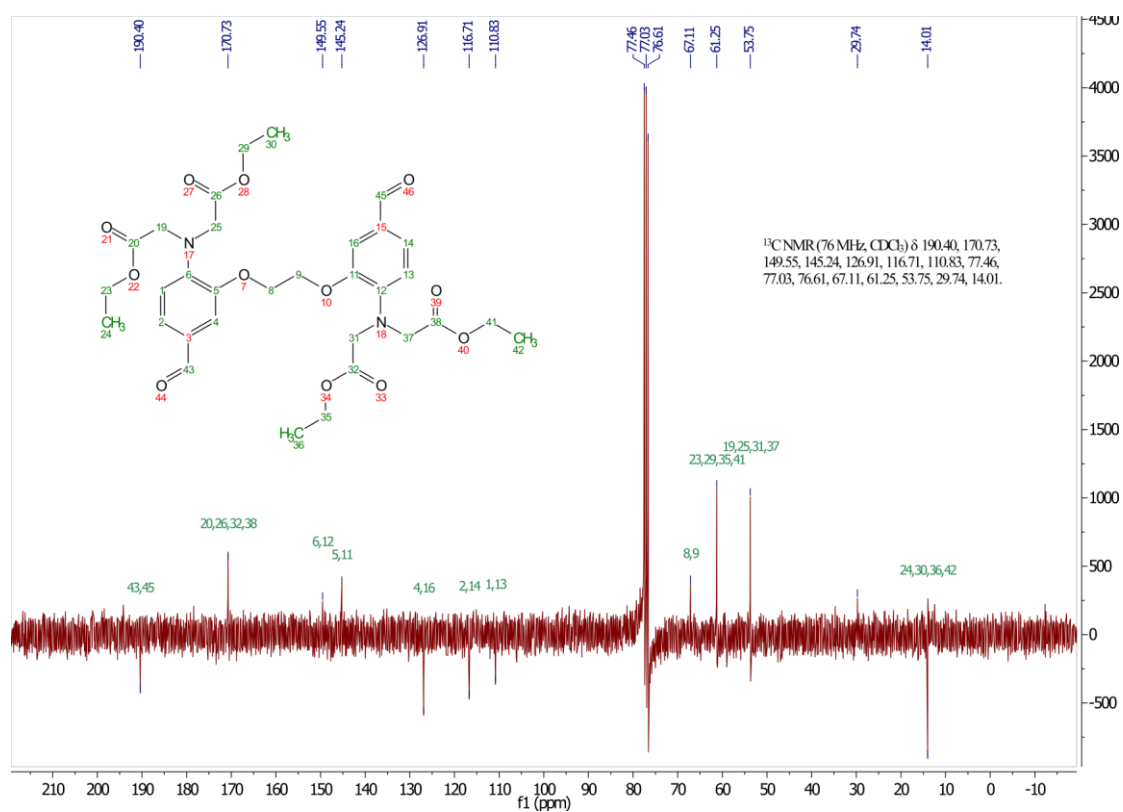


Figure S 6-24: ^{13}C -APT NMR (76Hz, CDCl_3) of **8**.

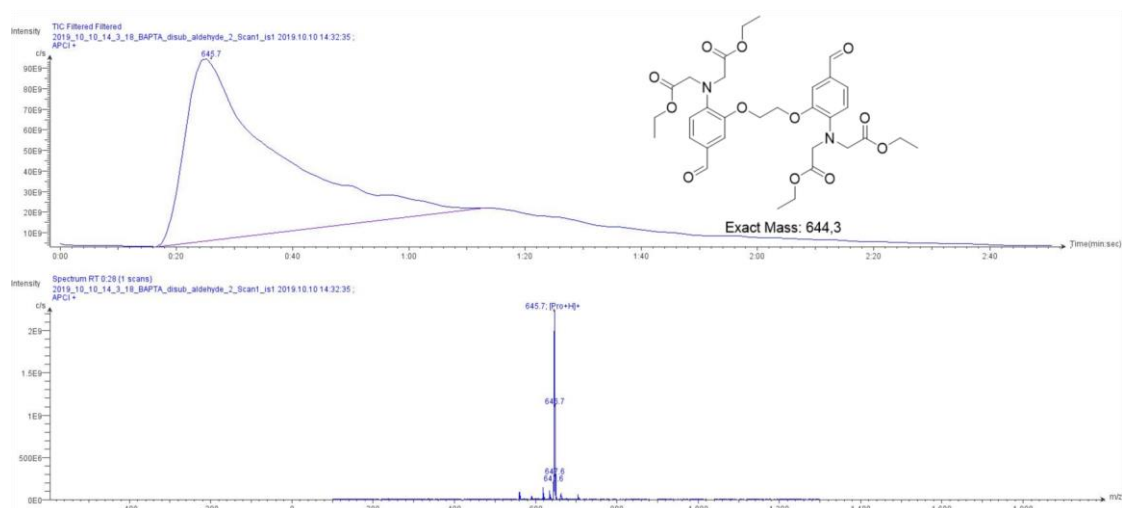


Figure S 6-25: LR-Mass Spectrum of **8** recorded on Advion expression CMS.

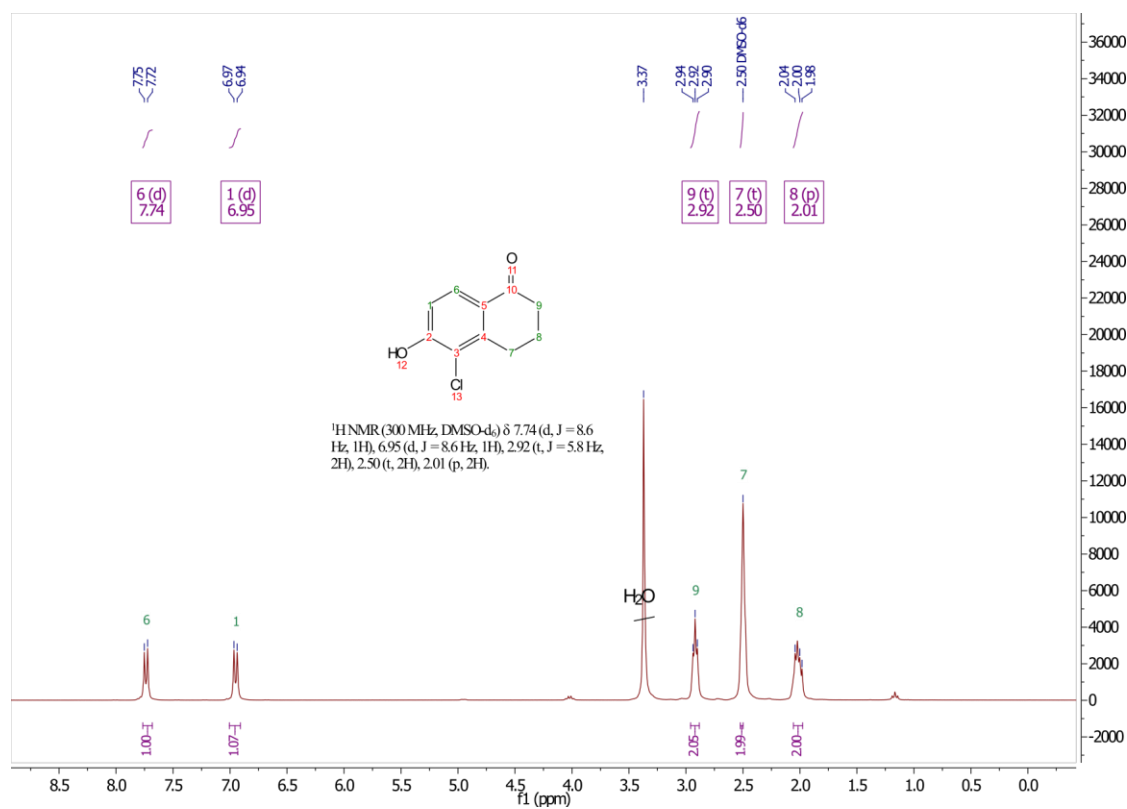


Figure S 6-26: ¹H NMR (300Hz), in DMSO-d₆ of **9**.

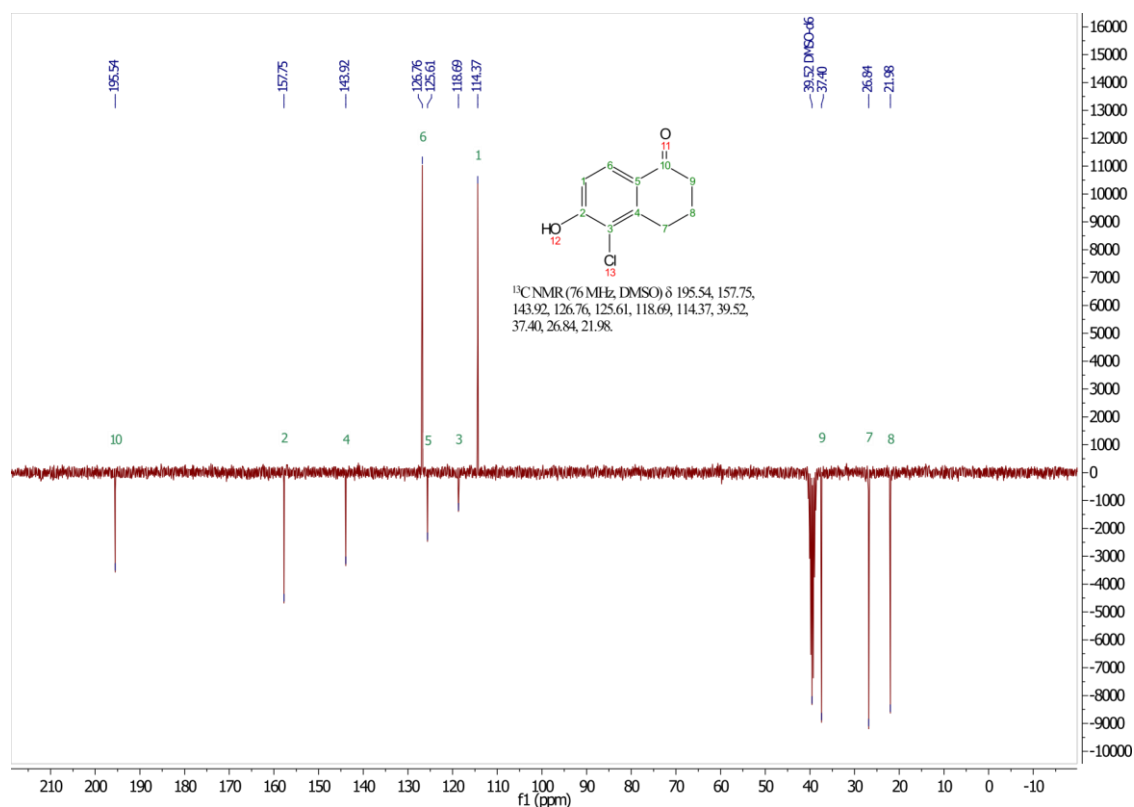


Figure S 6-27: ¹³C-APT NMR (76Hz, DMSO-d₆) of **9**.

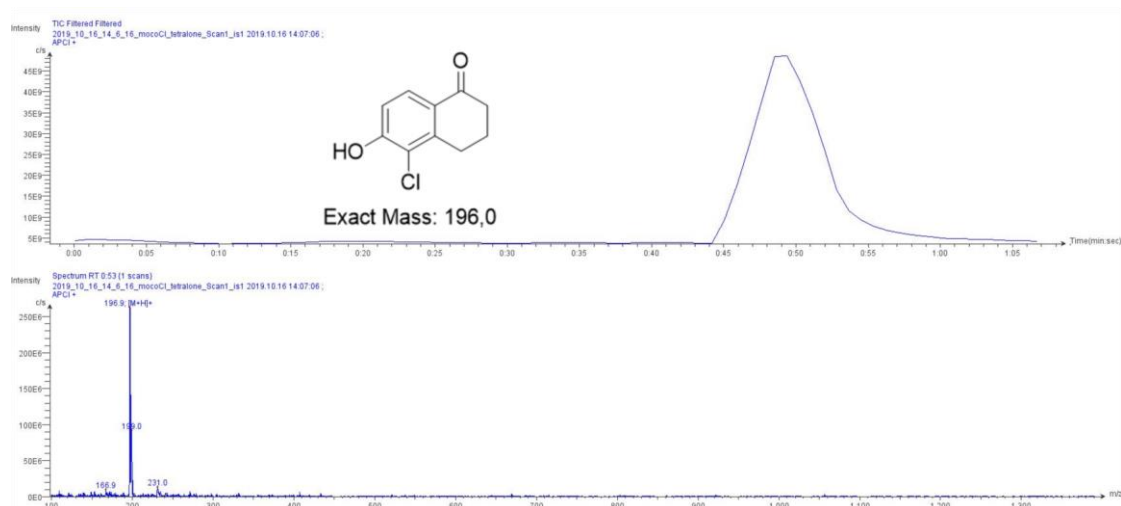


Figure S 6-28: LR-Mass Spectrum of **9** recorded on Advion expression CMS.

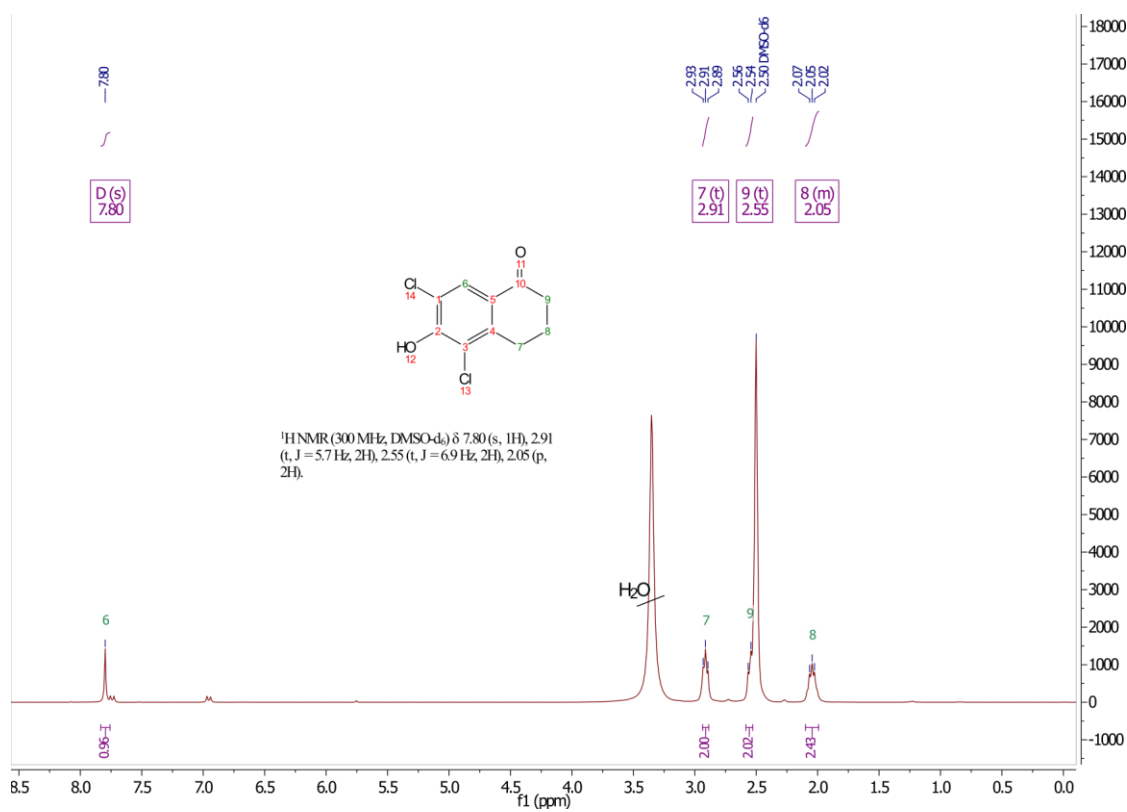


Figure S 6-29: $^1\text{H NMR}$ (300Hz), in DMSO-d_6 of **10**.

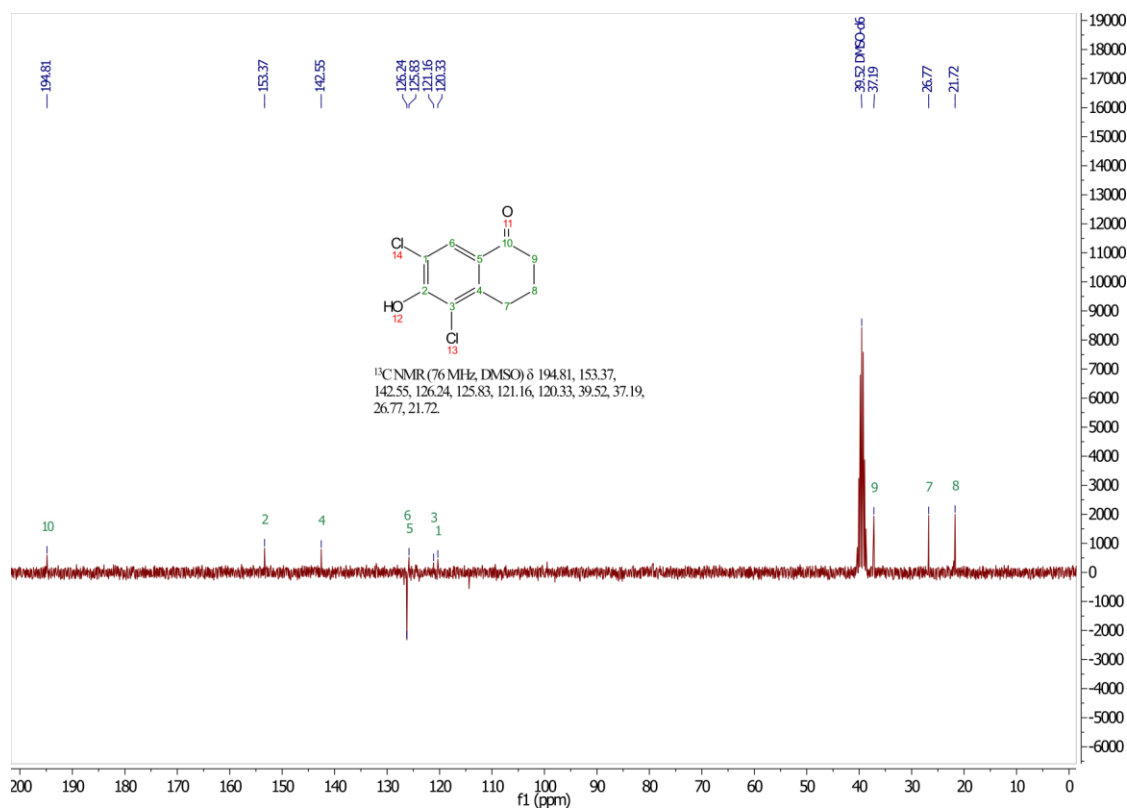


Figure S 6-30: ¹³C-APT NMR (76Hz, DMSO-d₆) of **10**.

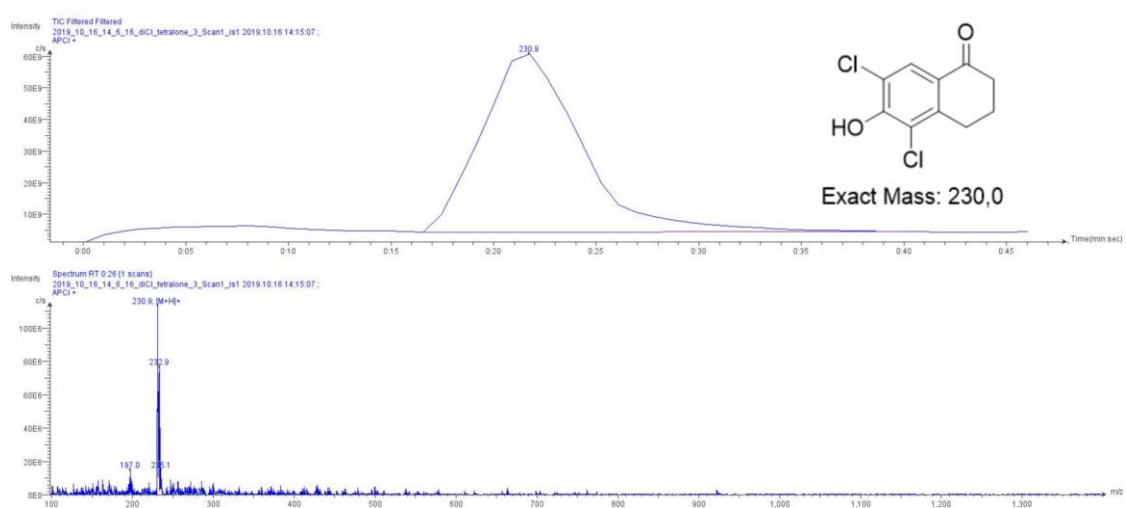
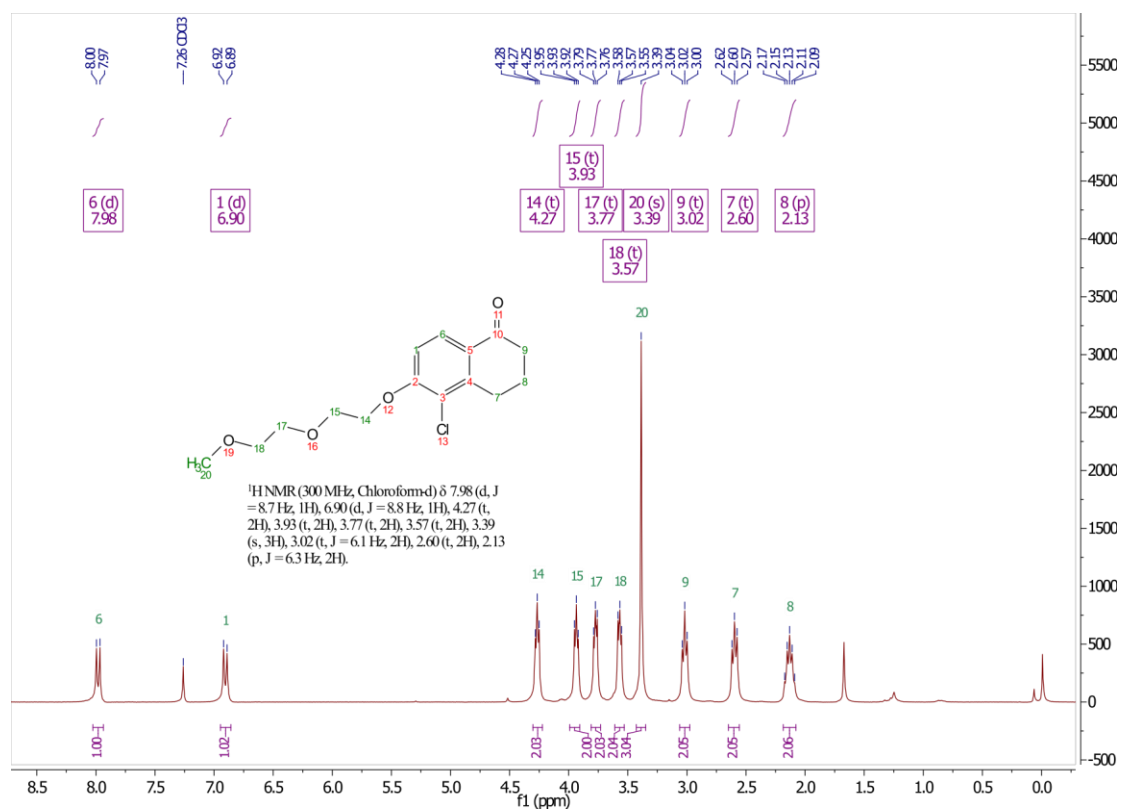
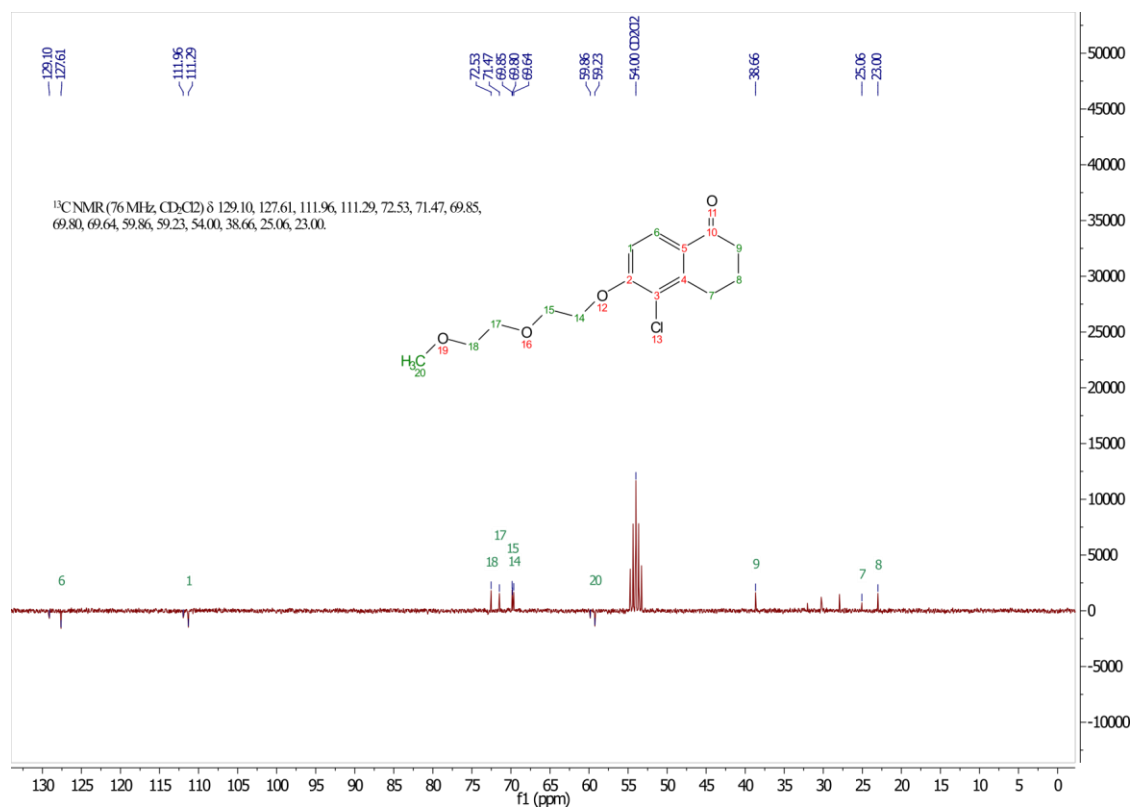


Figure S 6-31: LR-Mass Spectrum of **10** recorded on Advion expression CMS.

Figure S 6-32: ¹H NMR (300Hz), in CDCl₃ of **11**.Figure S 6-33: ¹³C-APT NMR (76Hz, CD₂Cl₂) of **11**.

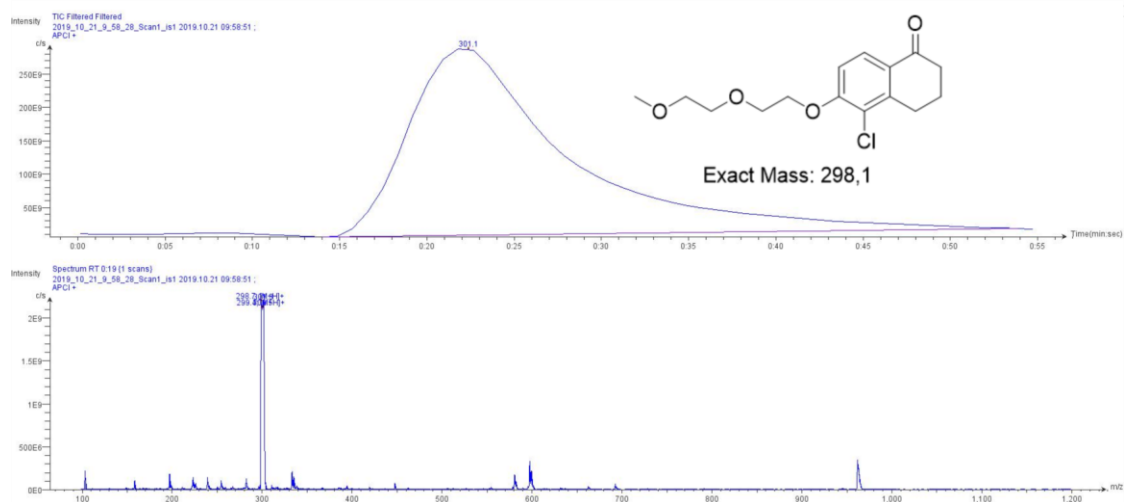


Figure S 6-34: LR-Mass Spectrum of **11** recorded on Advion expression CMS.

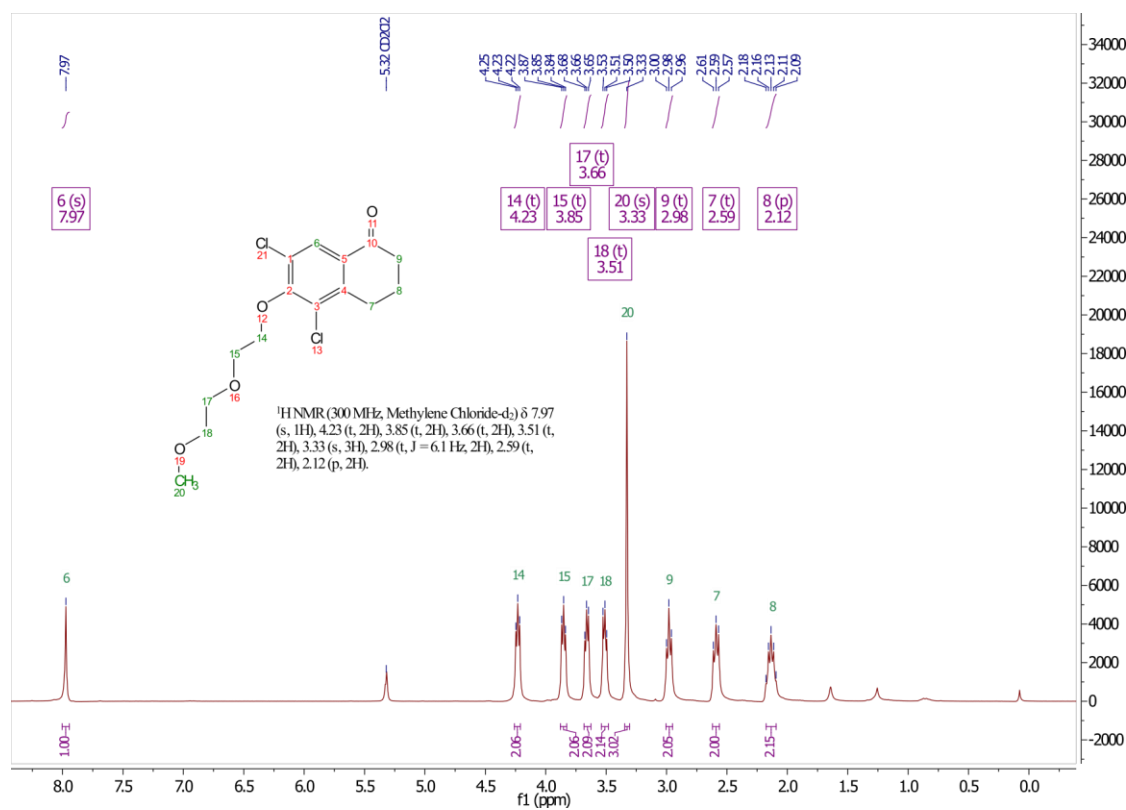


Figure S 6-35: ¹H NMR (300MHz), in CD₂Cl₂ of **12**.

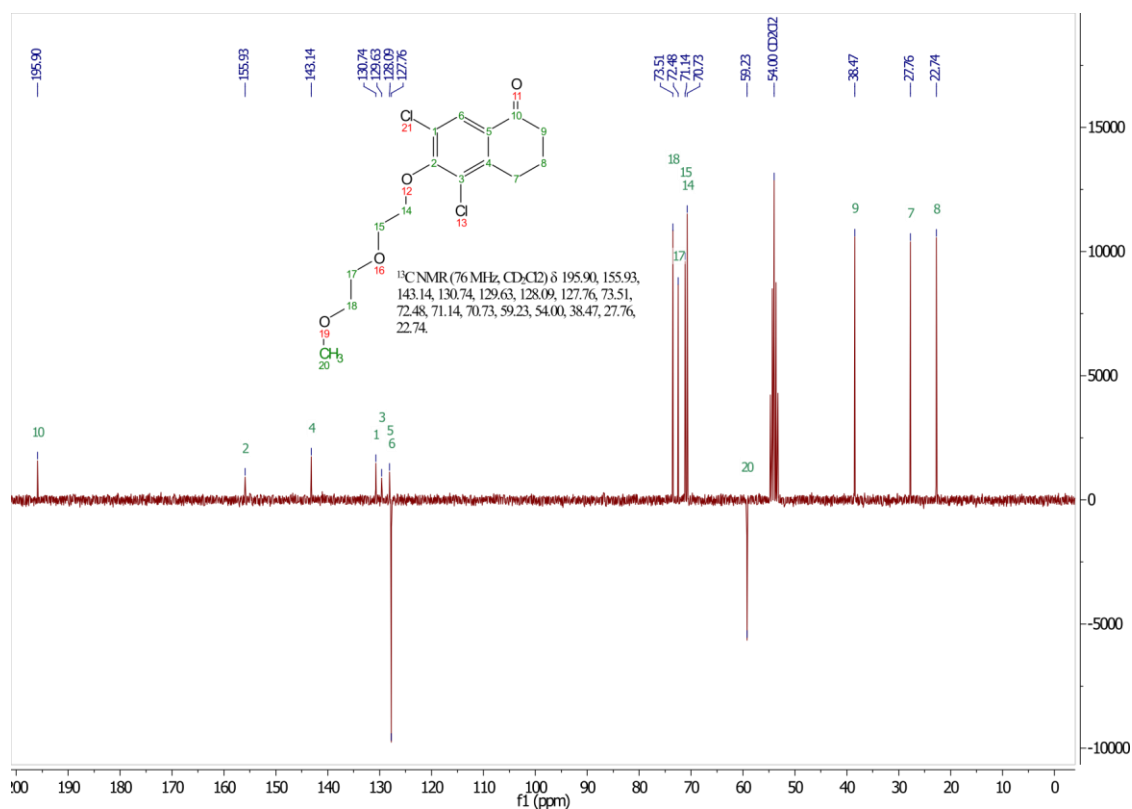


Figure S 6-36: ^{13}C -APT NMR (76Hz, CD_2Cl_2) of **12**.

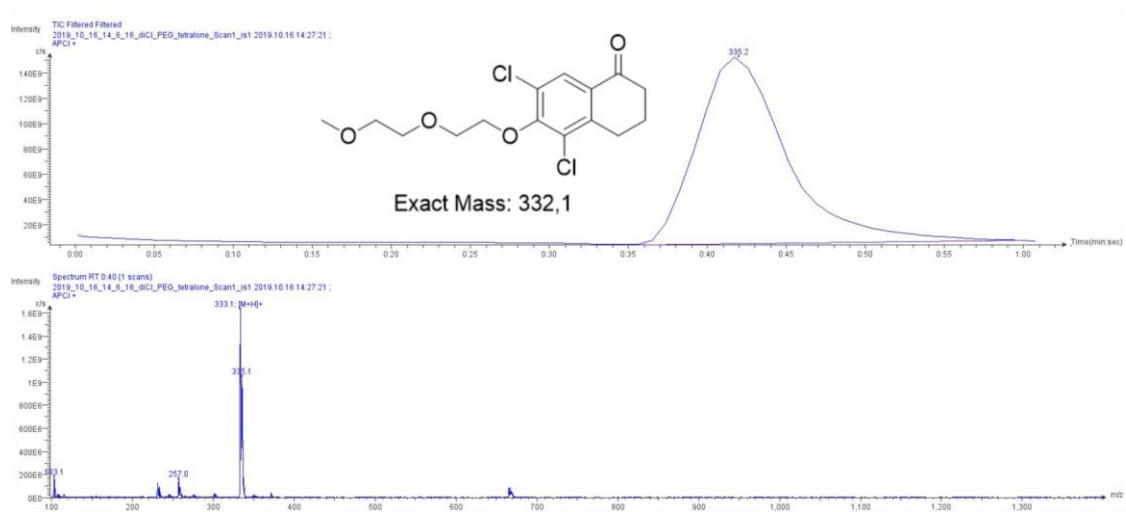


Figure S 6-37: LR-Mass Spectrum of **12** recorded on Advion expression CMS.

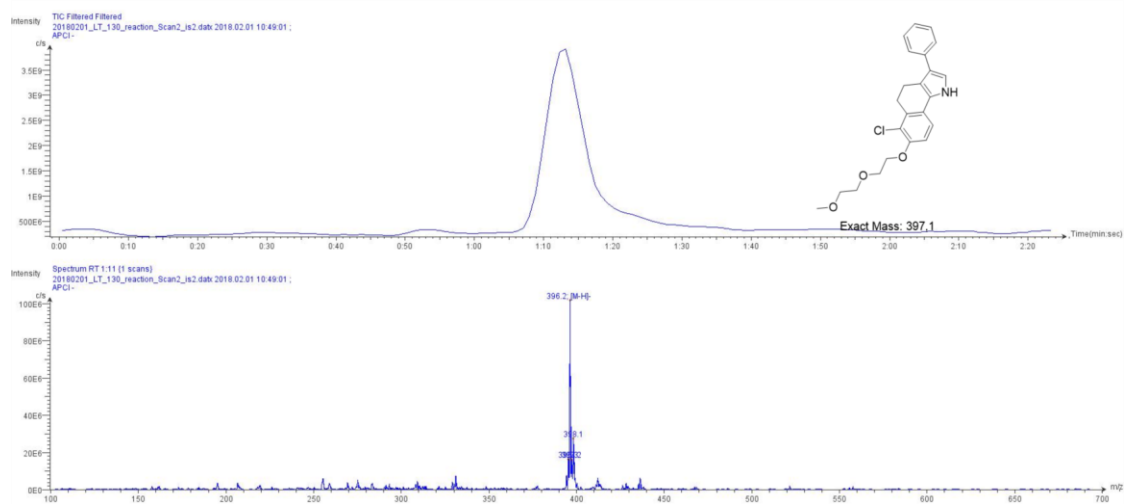


Figure S 6-38: LR-Mass Spectrum of **13** recorded on Advion expression CMS.

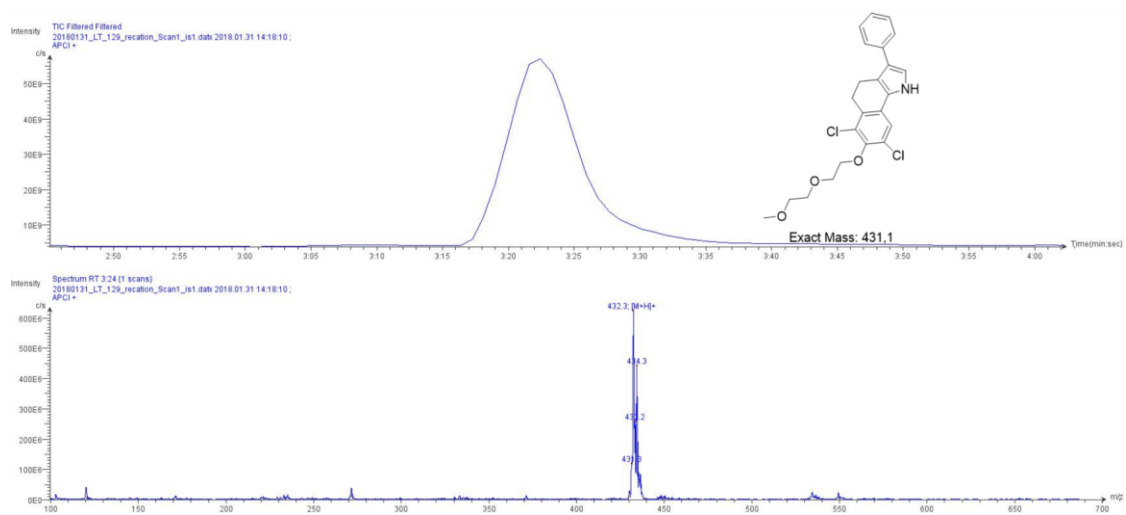
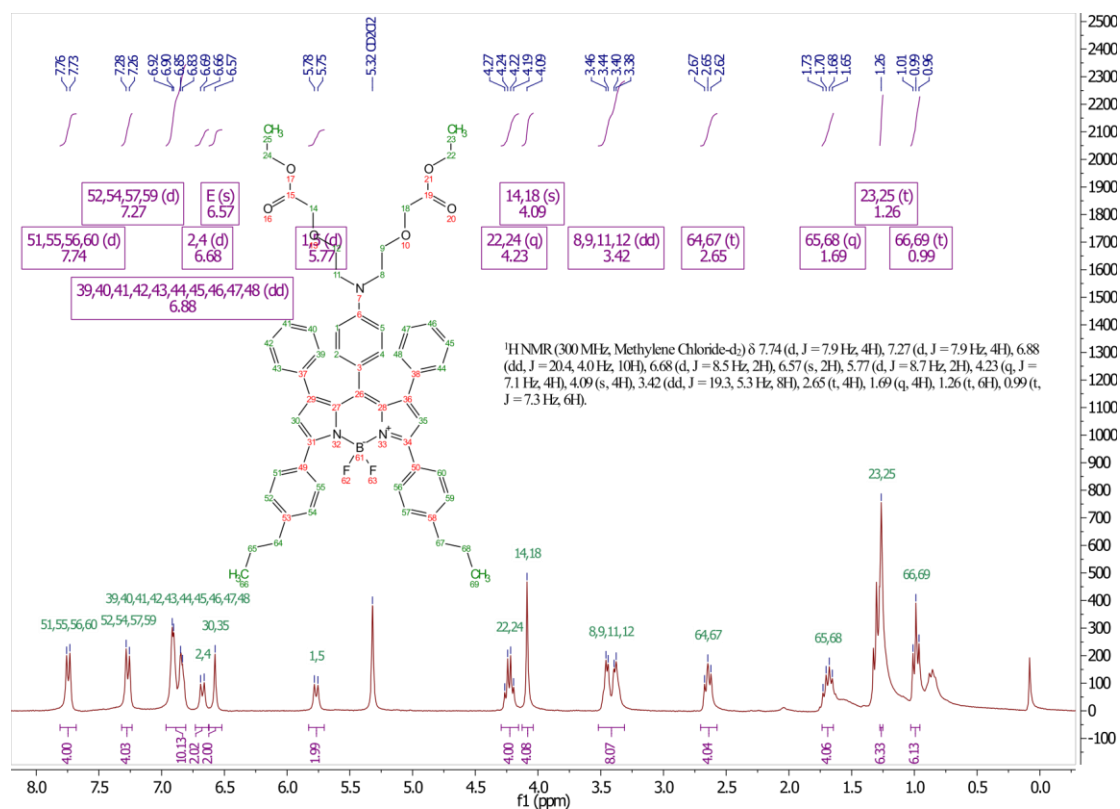
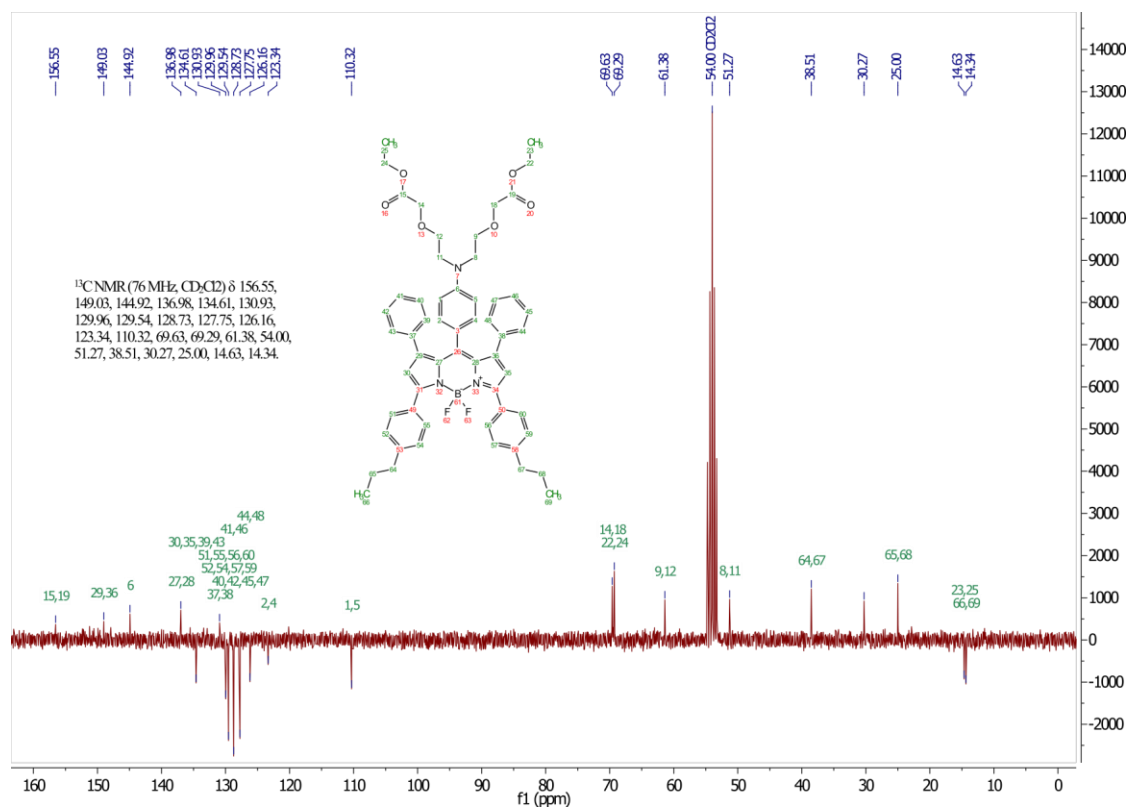


Figure S 6-39: LR-Mass Spectrum of **14** recorded on Advion expression CMS.

Figure S 6-40: ¹H NMR (300Hz), in CD₂Cl₂ of F11-ester.Figure S 6-41: ¹³C-APT NMR (76Hz, CD₂Cl₂) of F11-ester.

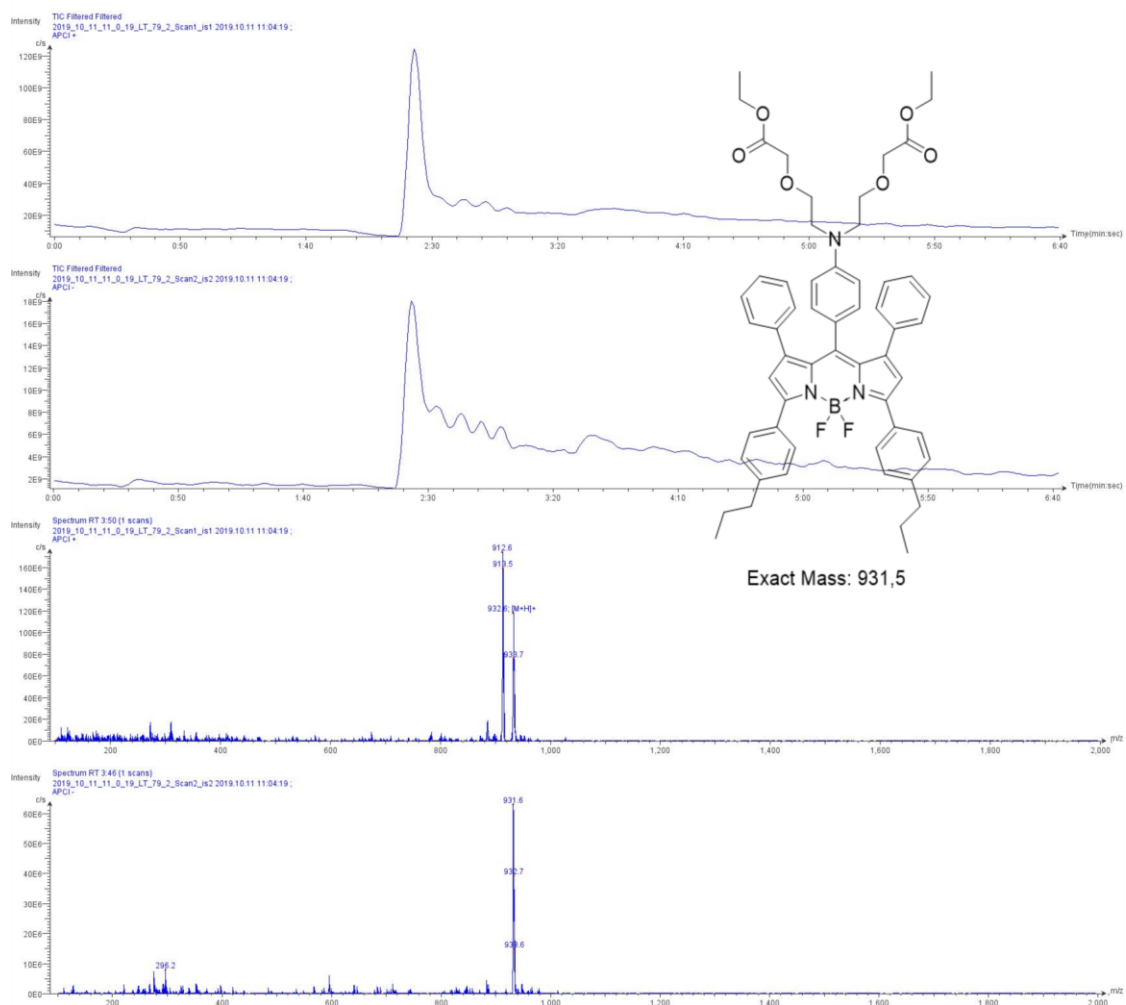


Figure S 6-42: LR-Mass Spectrum of **F11-ester** recorded on Advion expression CMS.

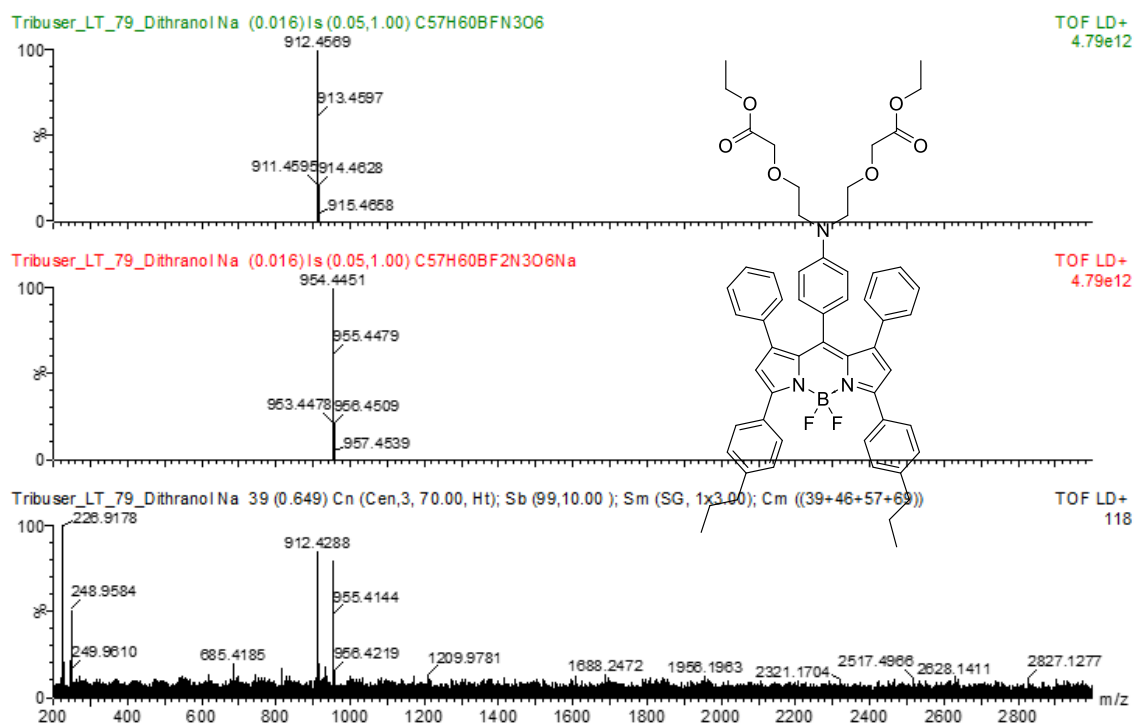


Figure S 6-43: Theoretical isotope pattern (top) of $C_{57}H_{60}BFN_3O_6$ (F11-ester - F); Theoretical isotope pattern (middle) of $C_{57}H_{60}BF_2N_3O_6Na$ (F11-ester + Na); Experimental MALDI-TOF-MS of F11-ester (bottom).

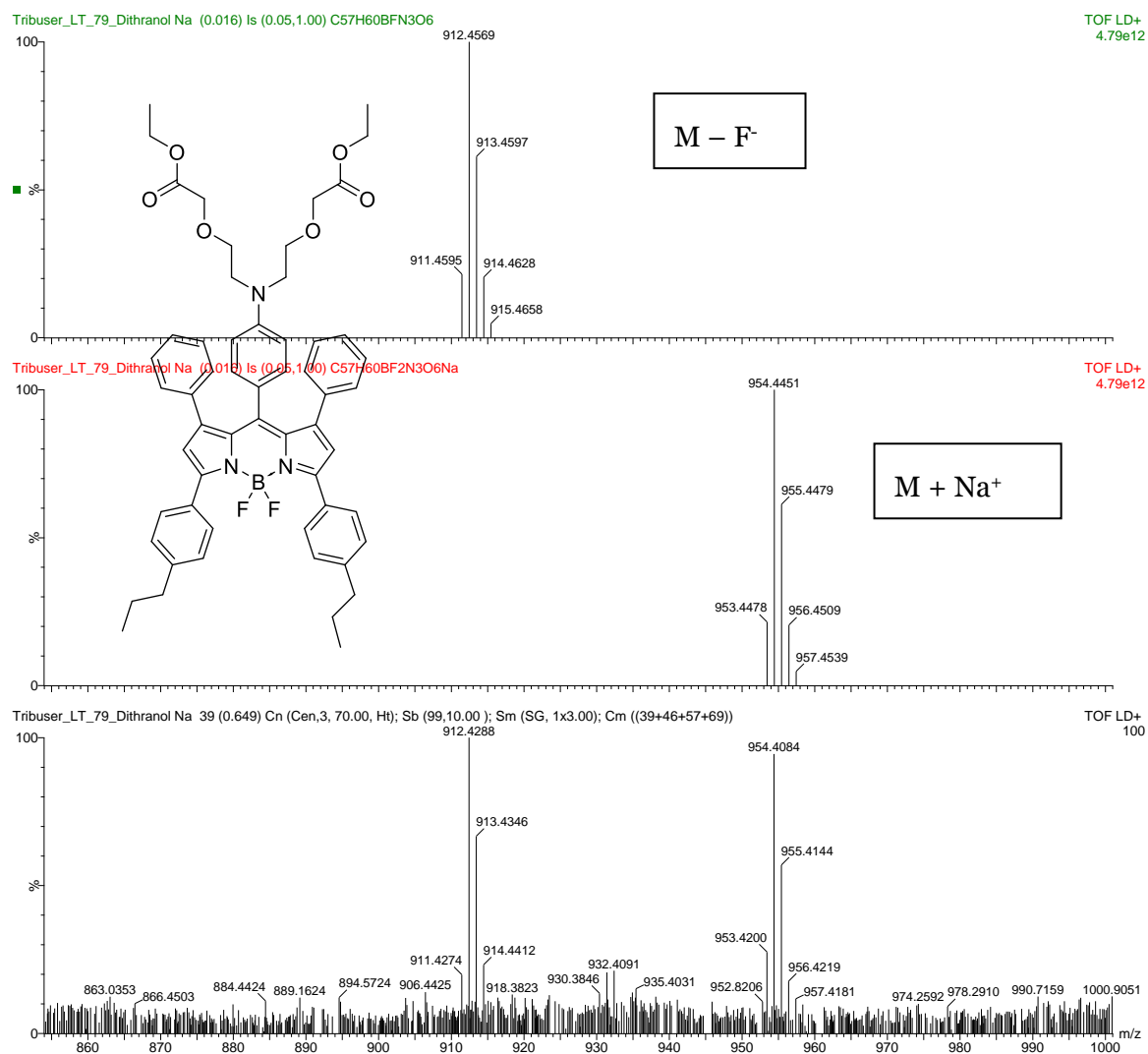
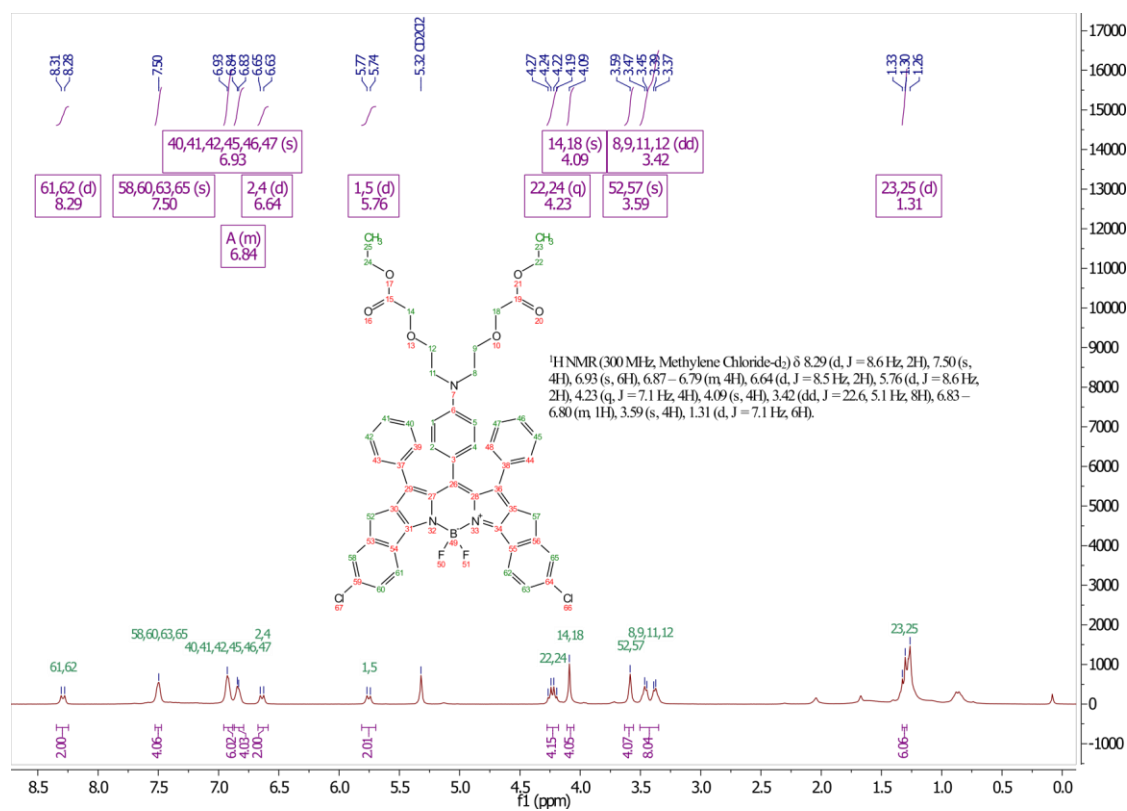
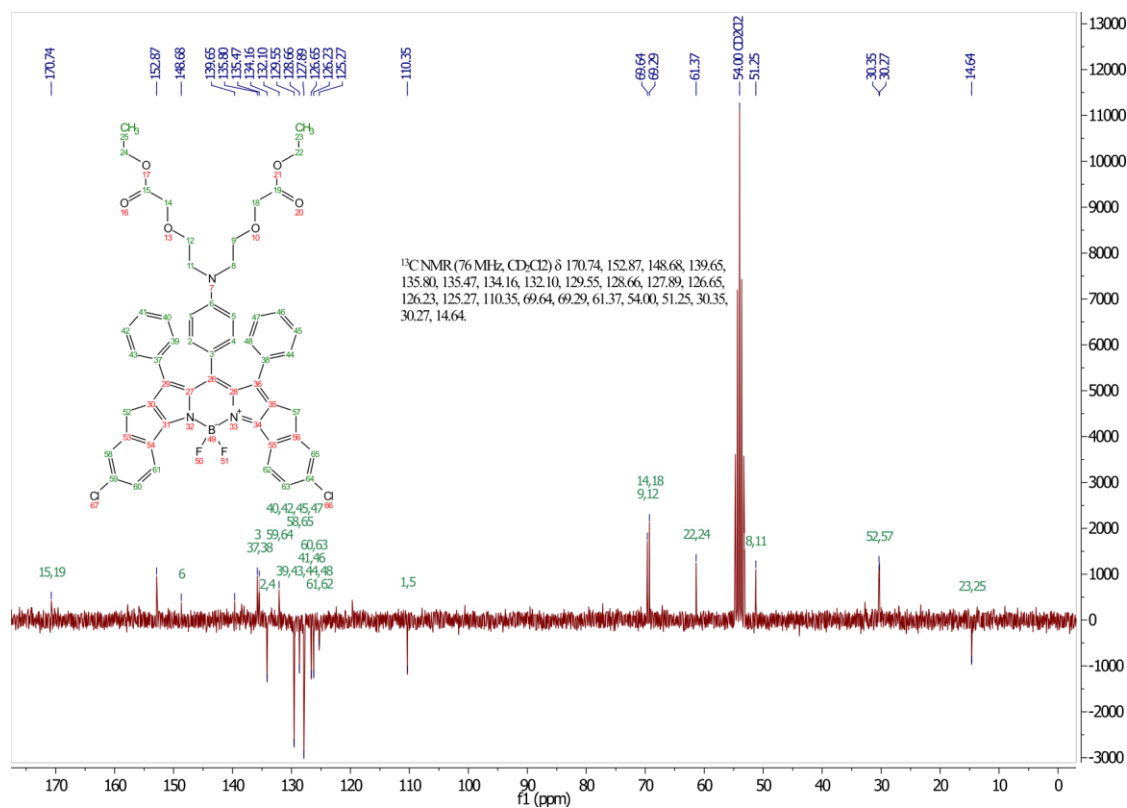


Figure S 6-44: Mass relevant theoretical isotope pattern (top) of C₅₇H₆₀BFN₃O₆ (FI1-ester - F) and theoretical isotope pattern (middle) of C₅₇H₆₀BF₂N₃O₆Na (FI1-ester + Na); Experimental mass relevant range (MALDI-TOF-MS) of FI1-ester (bottom).

Figure S 6-45: ¹H NMR (300Hz), in CD₂Cl₂ of Fl2-ester.Figure S 6-46: ¹³C-APT NMR (76Hz, CD₂Cl₂) of Fl2-ester.

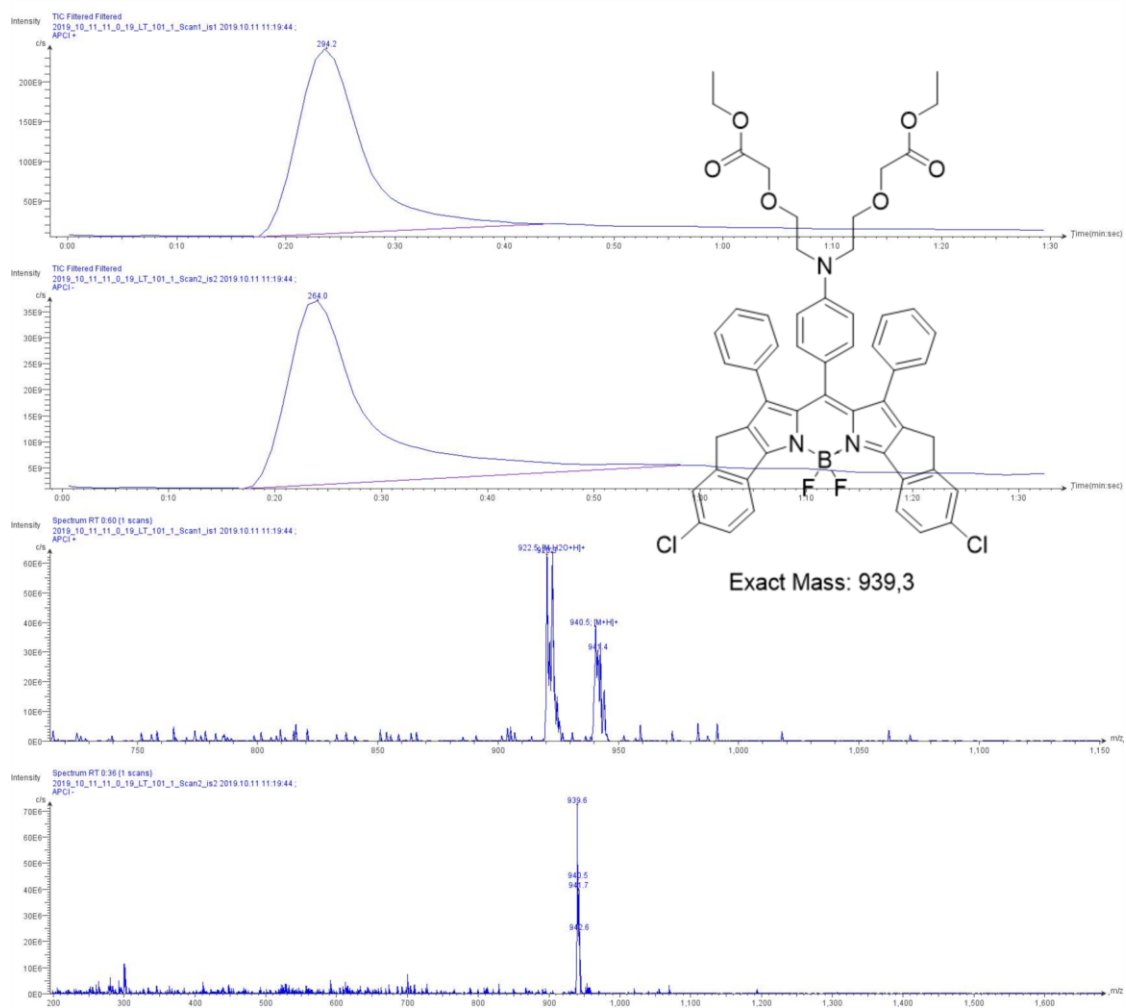


Figure S 6-47: LR-Mass Spectrum of **F12-ester** recorded on Advion expression CMS.

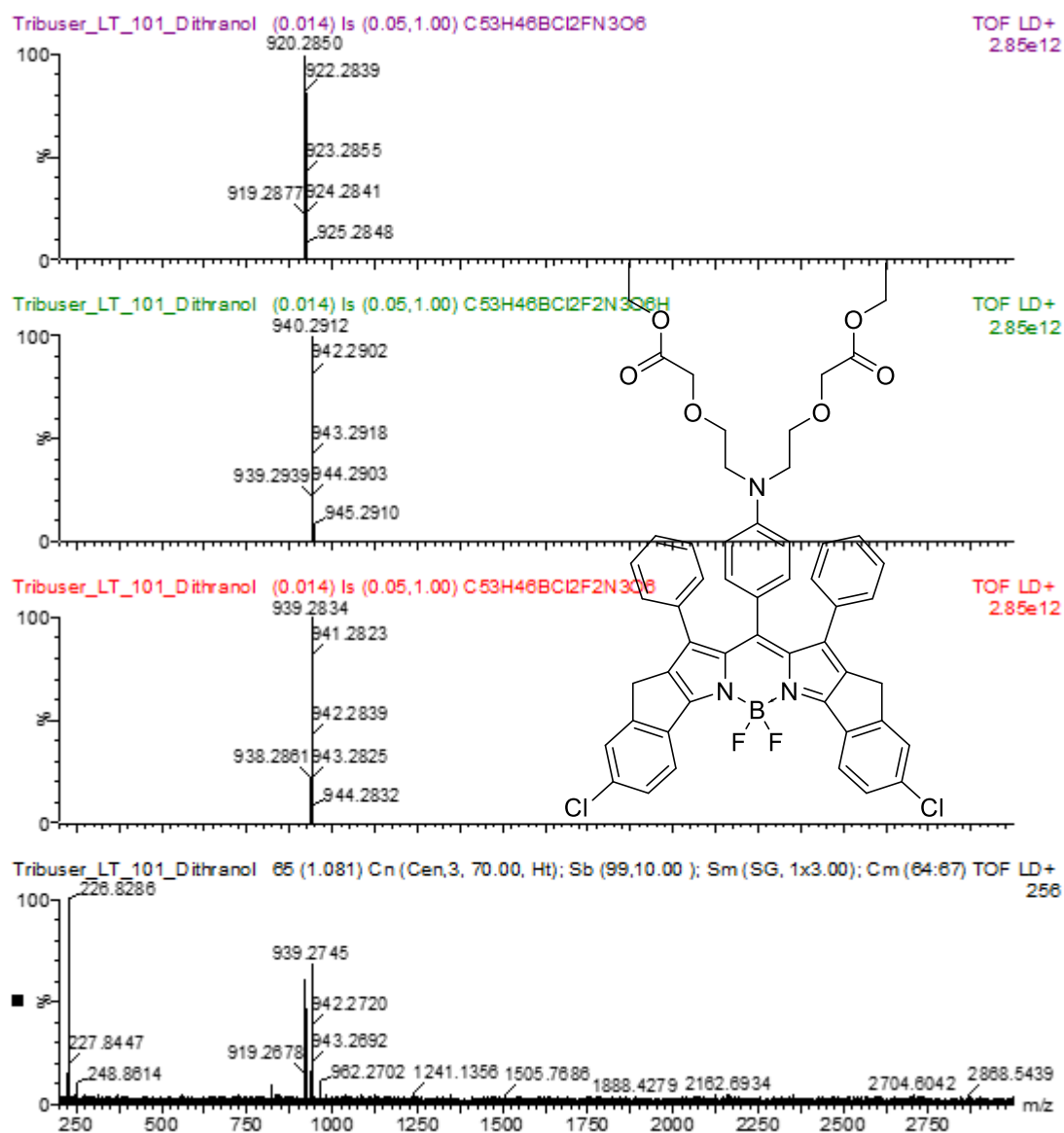


Figure S 6-48: Theoretical isotope pattern (upper part) of C₅₃H₄₆BCl₂FN₃O₆ (Fl2-ester - F), C₅₃H₄₆BCl₂F₂N₃O₆H (Fl2-ester + H), C₅₃H₄₆BCl₂F₂N₃O₆ (Fl2-ester). Experimental MALDI-TOF-MS of Fl2-ester (bottom).

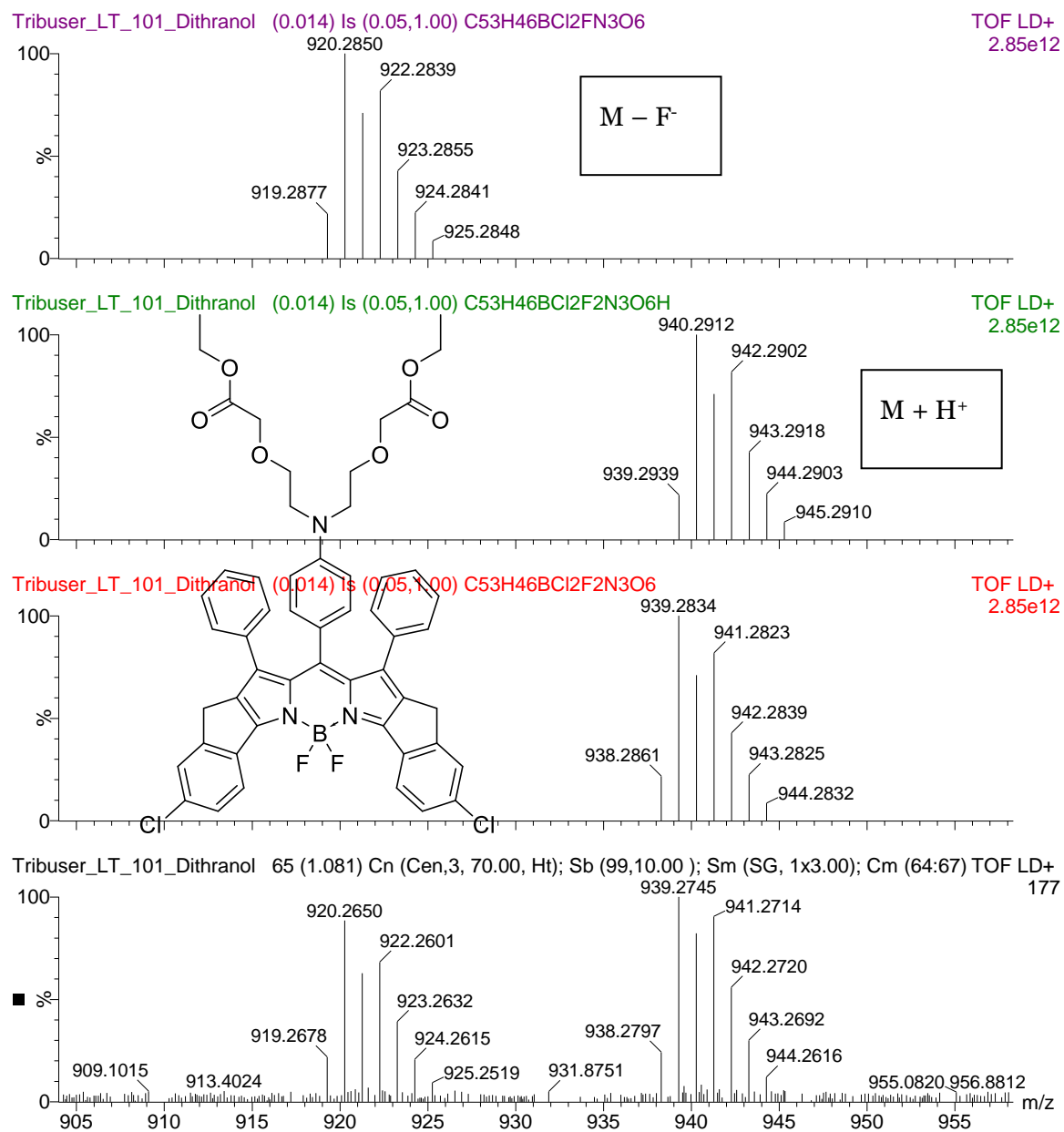
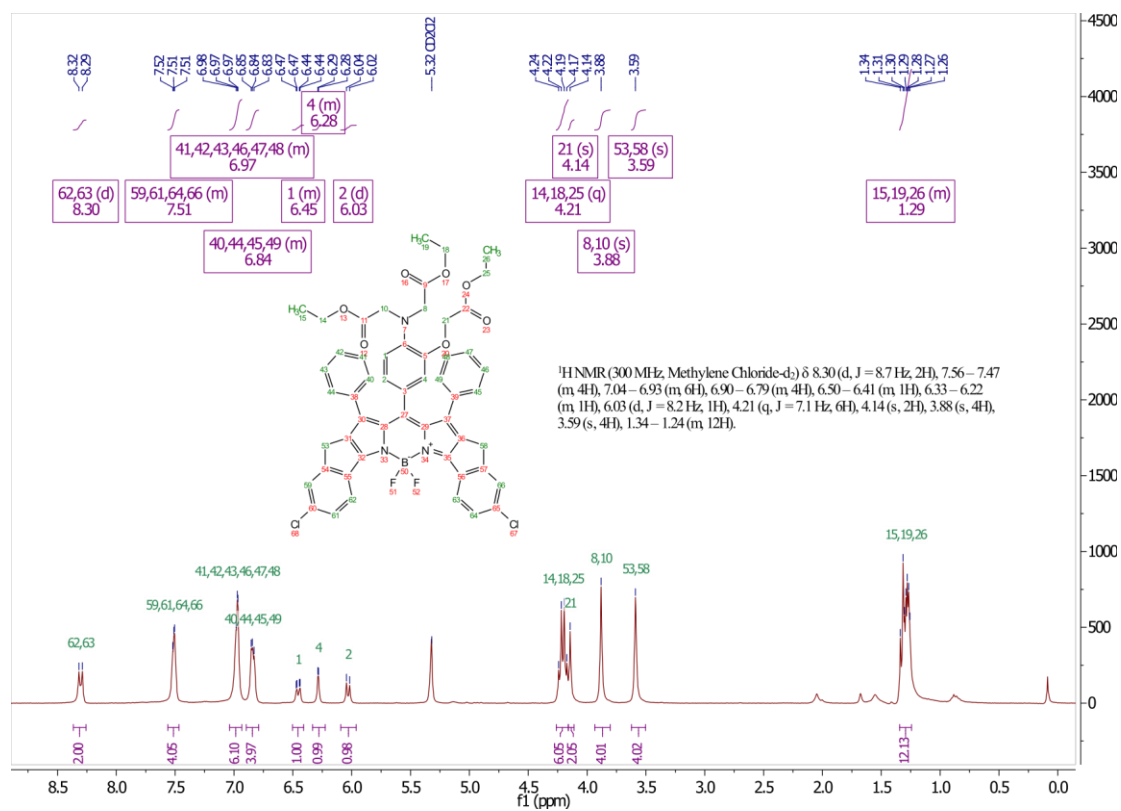
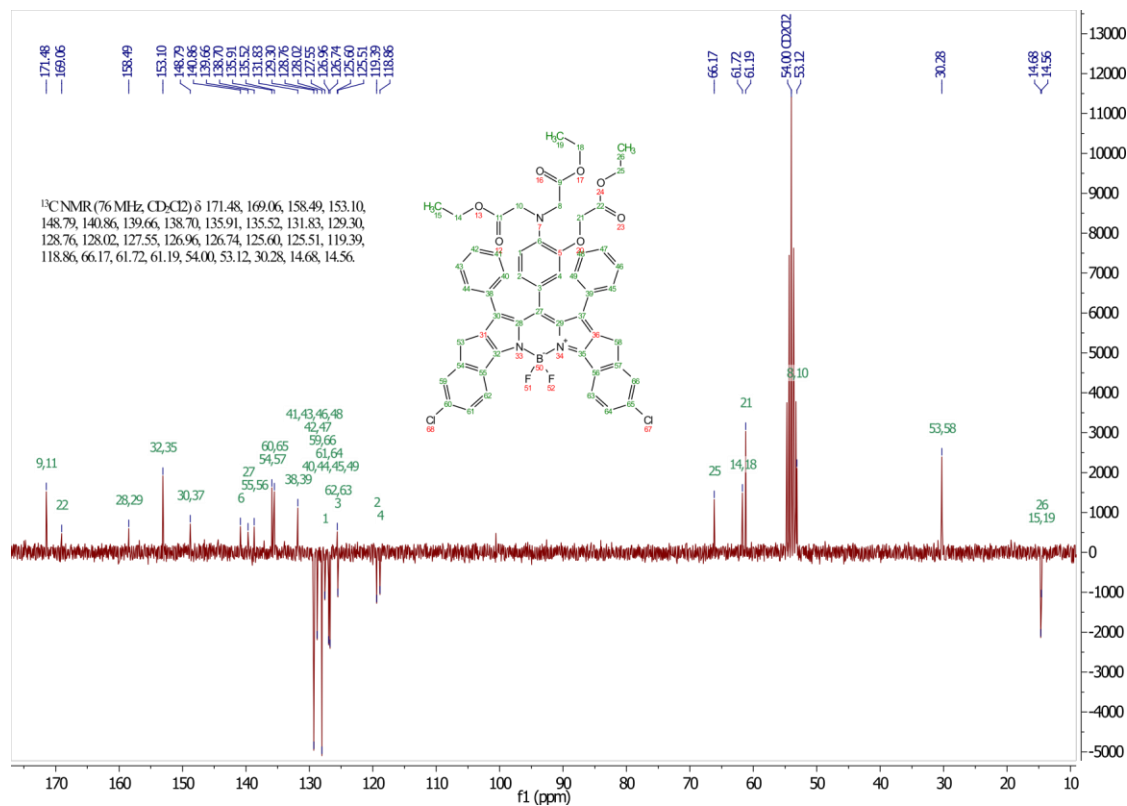


Figure S 6-49: Mass relevant theoretical isotope pattern (upper part) of C₅₃H₄₆BCl₂FN₃O₆ (FI2-ester - F), C₅₃H₄₆BCl₂F₂N₃O₆H (FI2-ester + H), C₅₃H₄₆BCl₂F₂N₃O₆ (FI2-ester). Experimental mass relevant range (MALDI-TOF-MS) of FI2-ester (bottom).

Figure S 6-50: ¹H NMR (300Hz), in CD₂Cl₂ of F13-ester.Figure S 6-51: ¹³C-APT NMR (76Hz, CD₂Cl₂) of F13-ester.

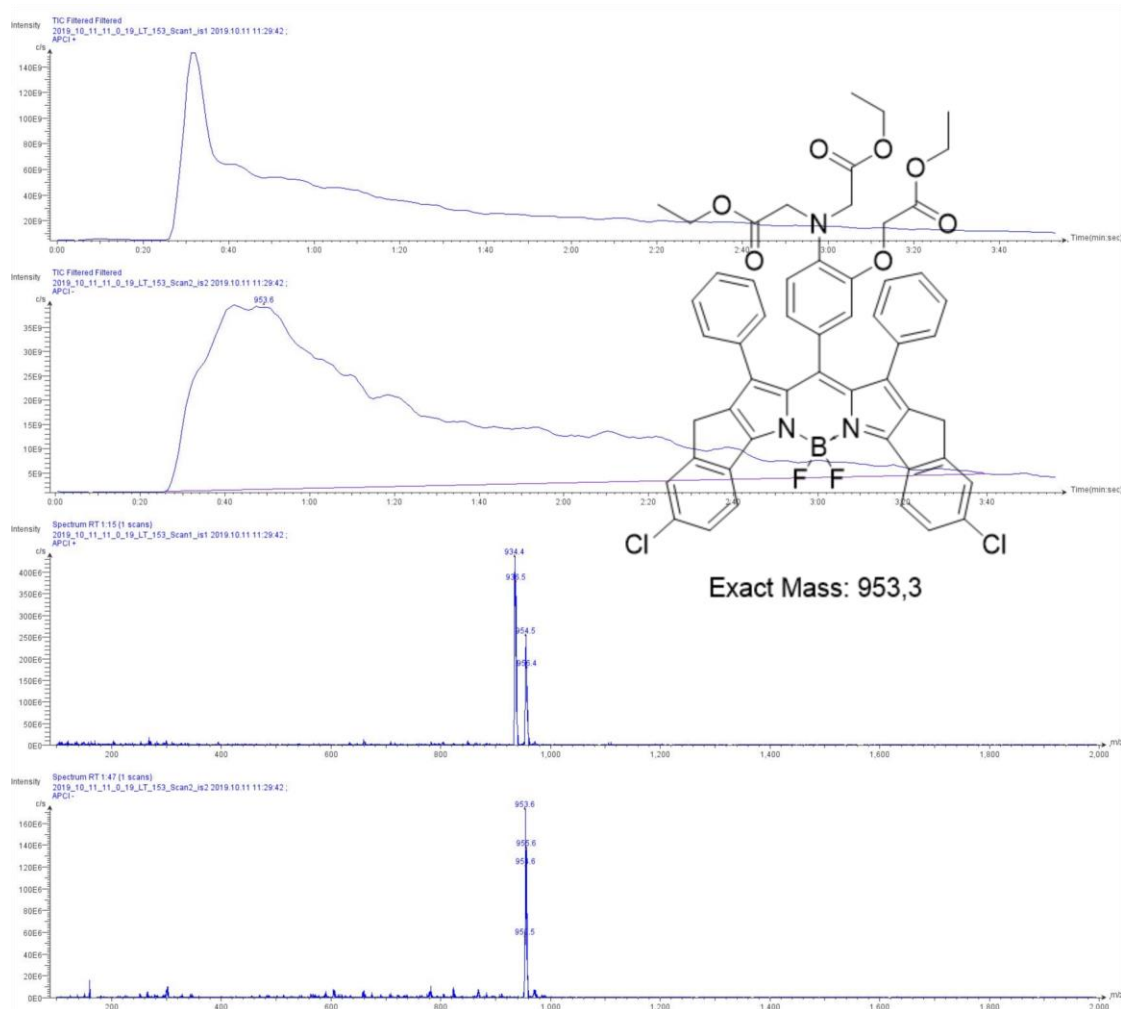


Figure S 6-52: LR-Mass Spectrum of **F13-ester** recorded on Advion expression CMS.

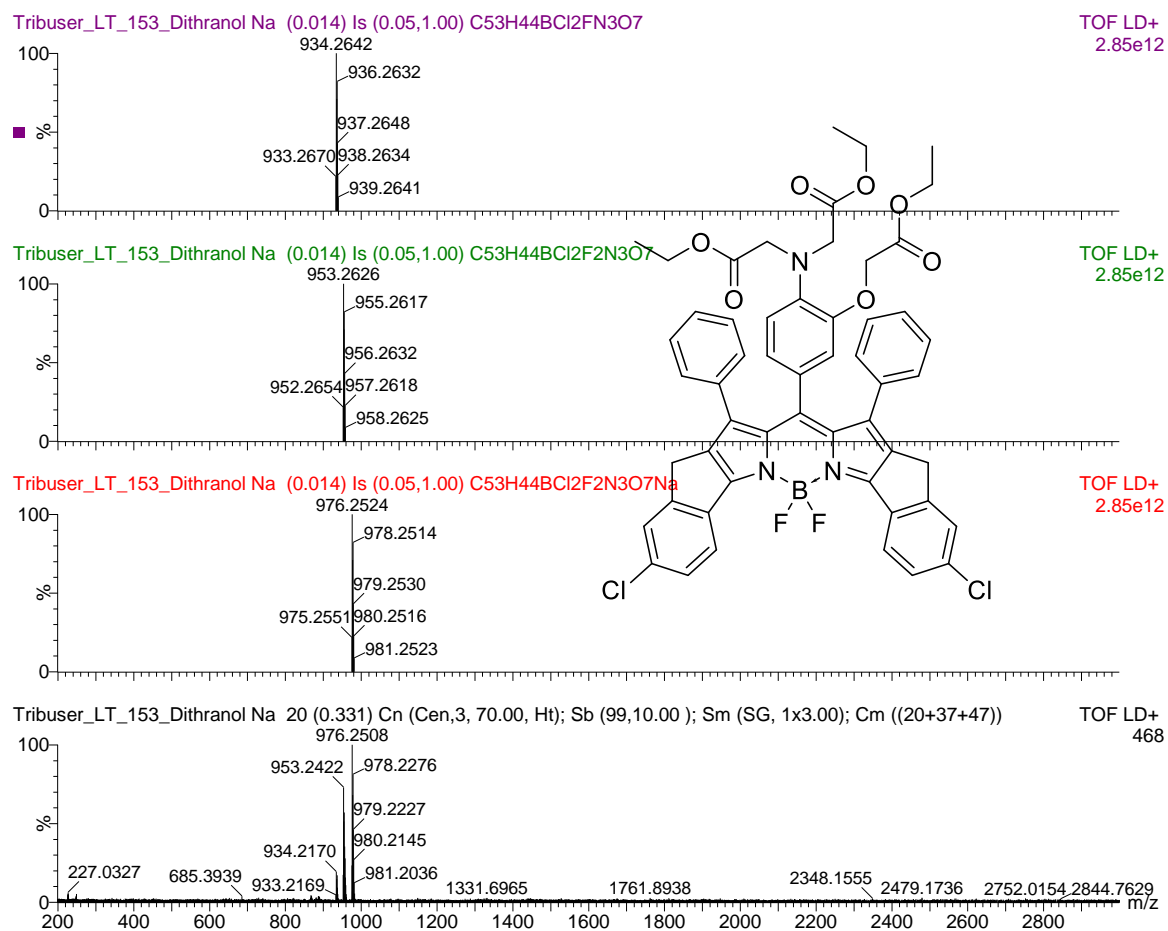


Figure S 6-53: Theoretical isotope pattern (upper part) of C₅₃H₄₄BCl₂FN₃O₇ (FI₃-ester - F), C₅₃H₄₄BCl₂F₂N₃O₇ (FI₃-ester), C₅₃H₄₄BCl₂F₂N₃O₇Na (FI₃-ester + Na). Experimental MALDI-TOF-MS of FI₃-ester (bottom).

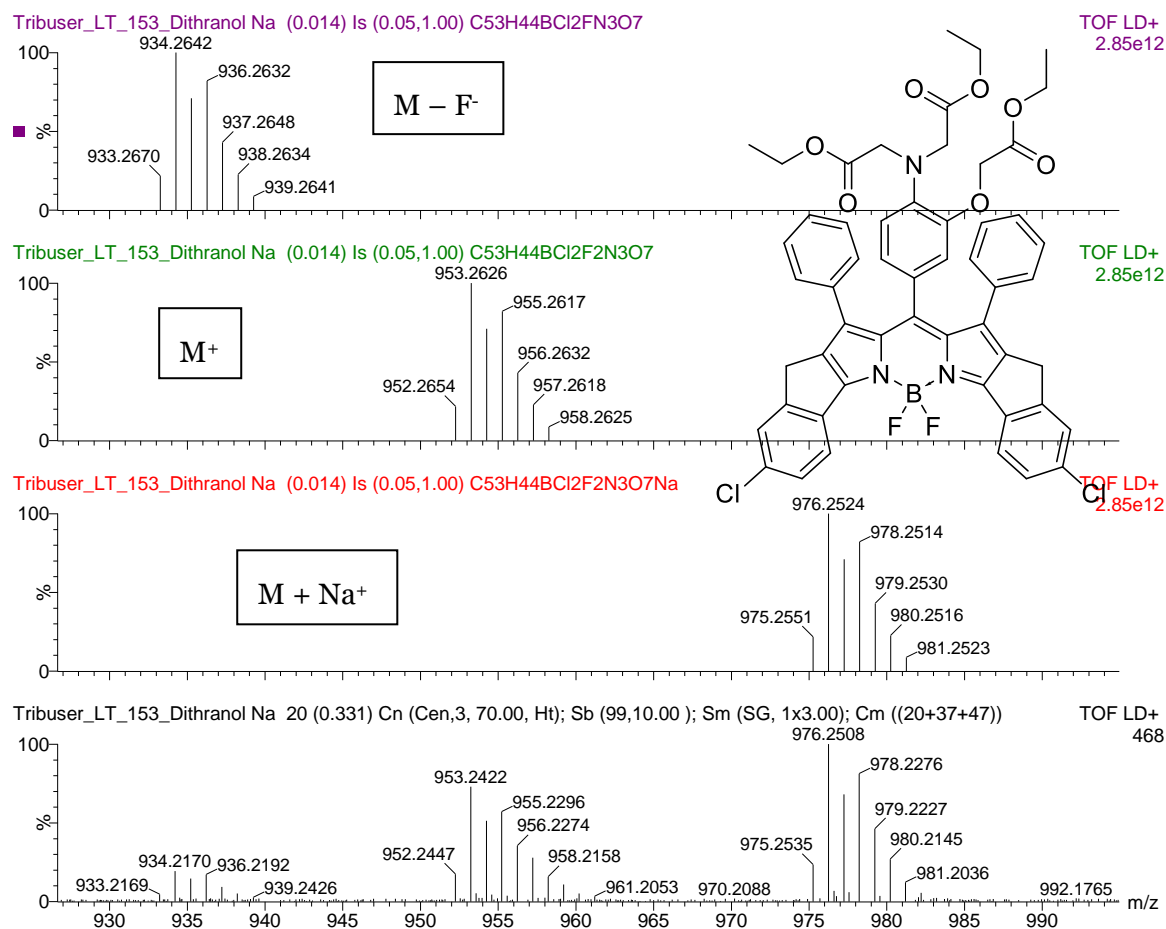
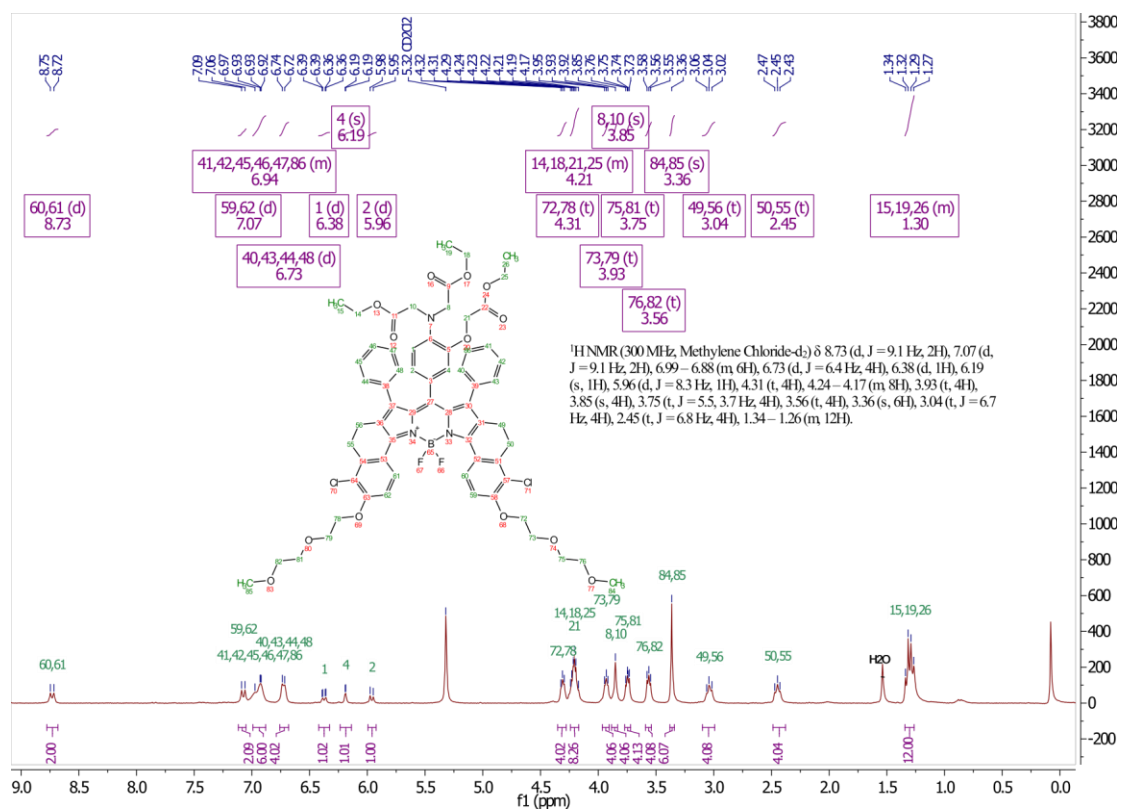
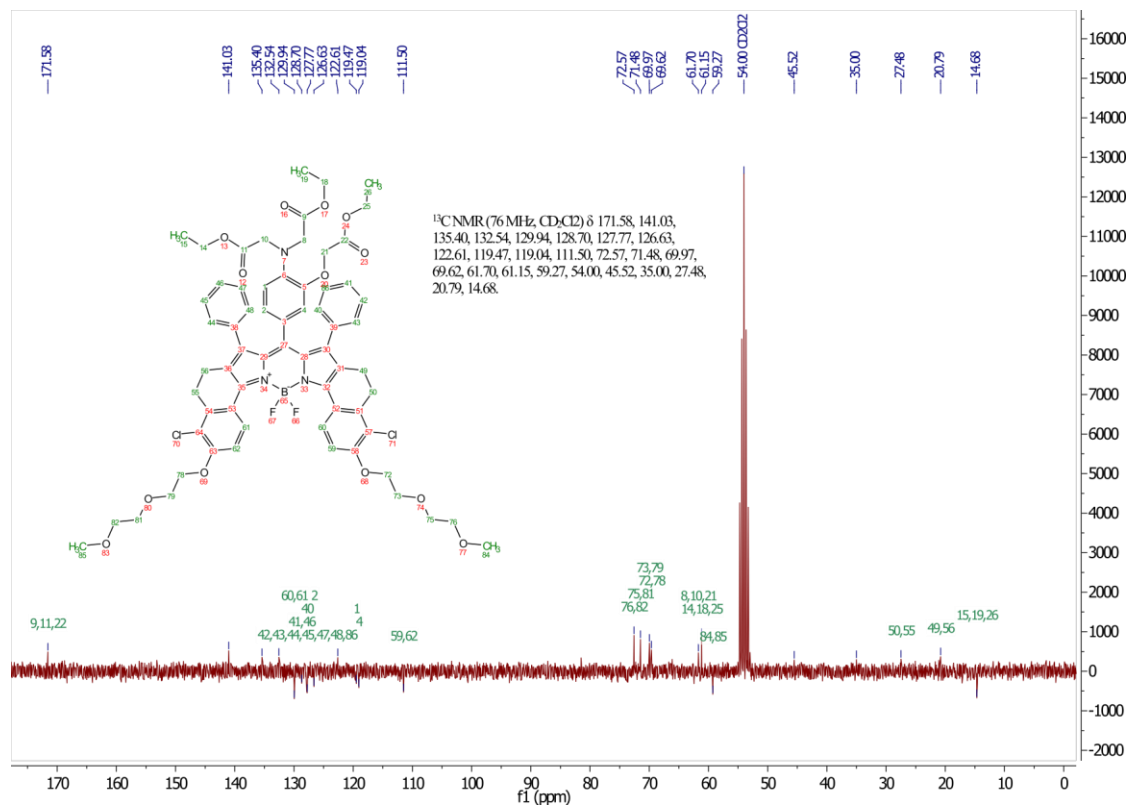


Figure S 6-54: Mass relevant theoretical isotope pattern (upper part) of C₅₃H₄₄BCl₂FN₃O₇ (FI3-ester - F), C₅₃H₄₄BCl₂F₂N₃O₇ (FI3-ester), C₅₃H₄₄BCl₂F₂N₃O₇Na (FI3-ester + Na). Experimental mass relevant range (MALDI-TOF-MS) of FI3-ester (bottom).

Figure S 6-55: ¹H NMR (300Hz), in CD₂Cl₂ of FI4-ester.Figure S 6-56: ¹³C-APT NMR (76Hz, CD₂Cl₂) of FI4-ester.

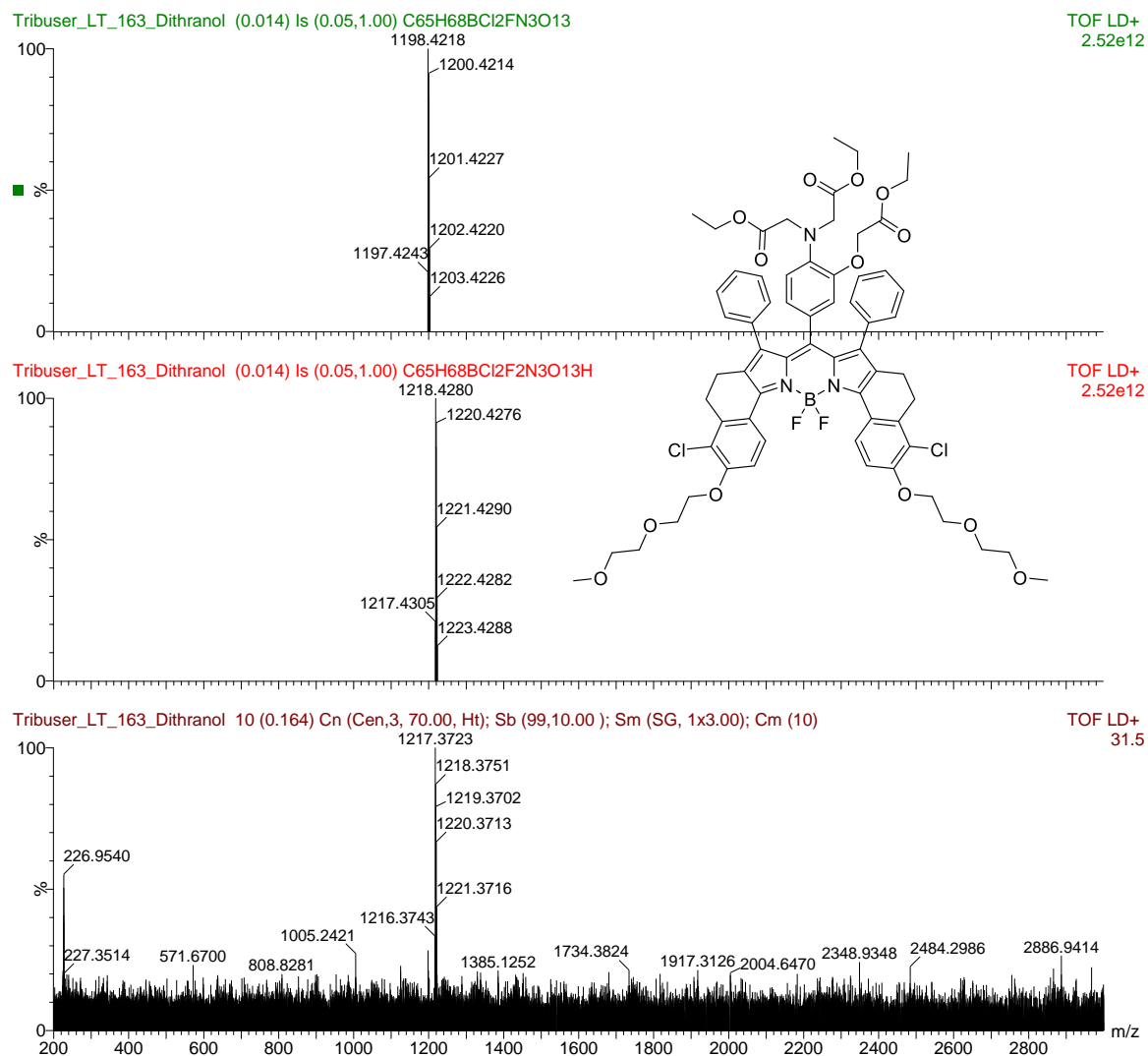


Figure S 6-57: Theoretical isotope pattern (upper part) of C₆₅H₆₈BCl₄FN₃O₁₃ (FI4-ester - F), C₆₅H₆₈BCl₄F₂N₃O₁₃Na (FI4-ester + Na). Experimental MALDI-TOF-MS of FI4-ester (bottom).

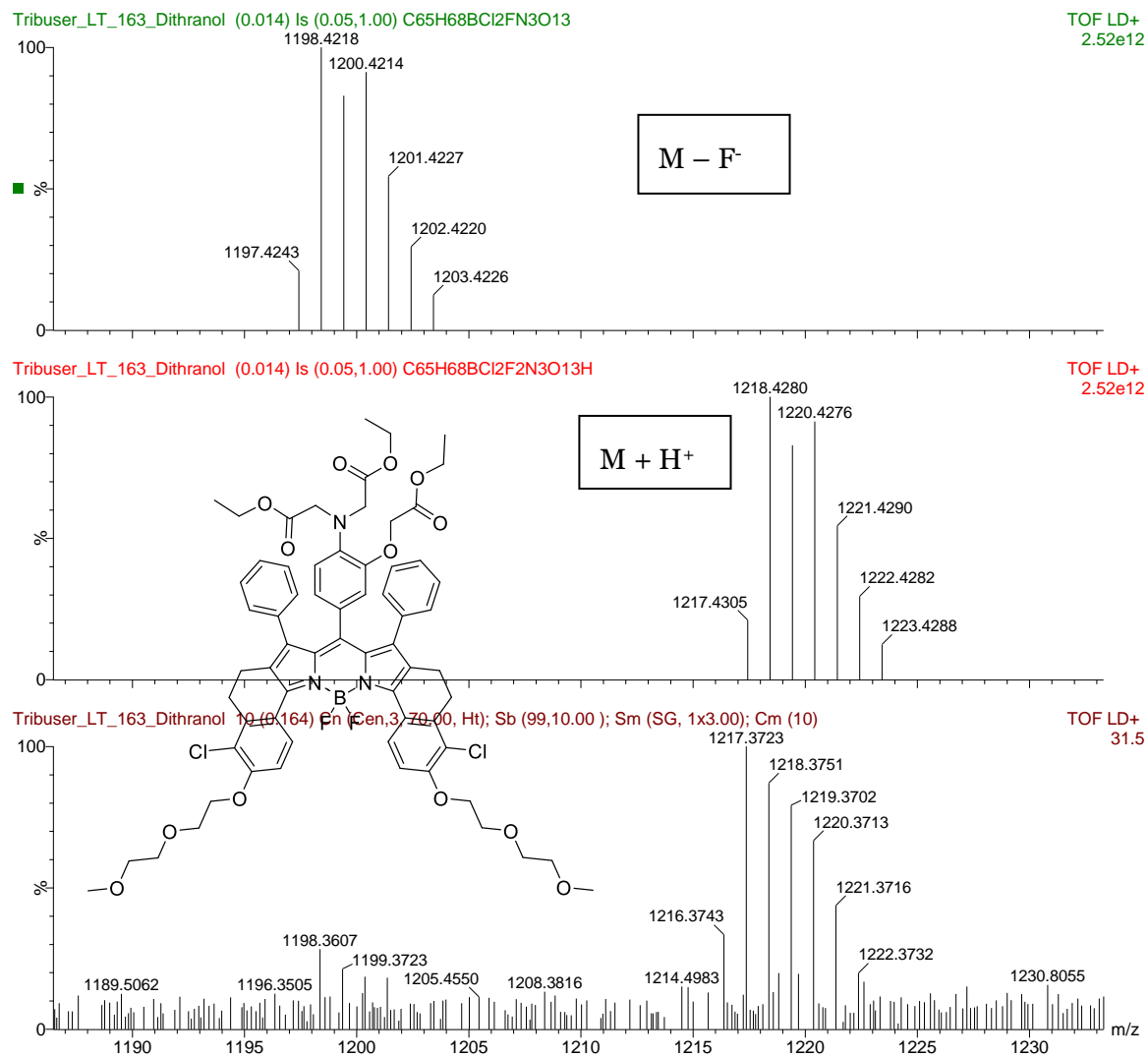
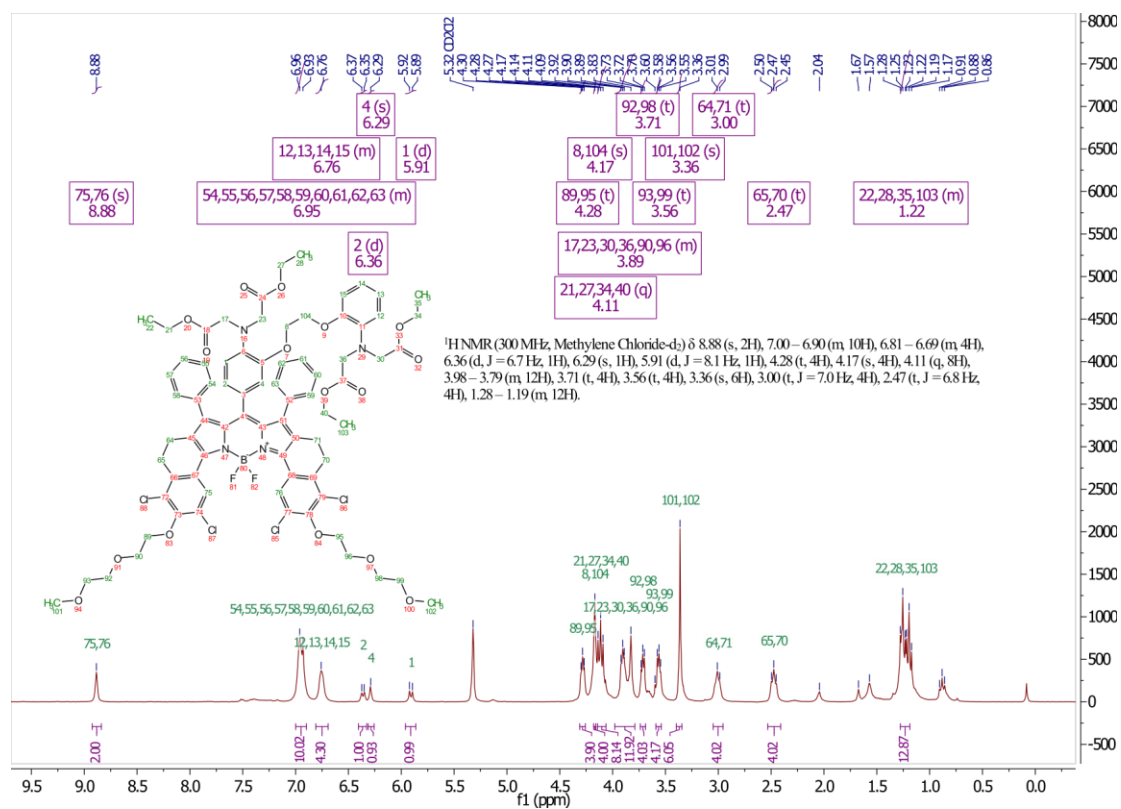
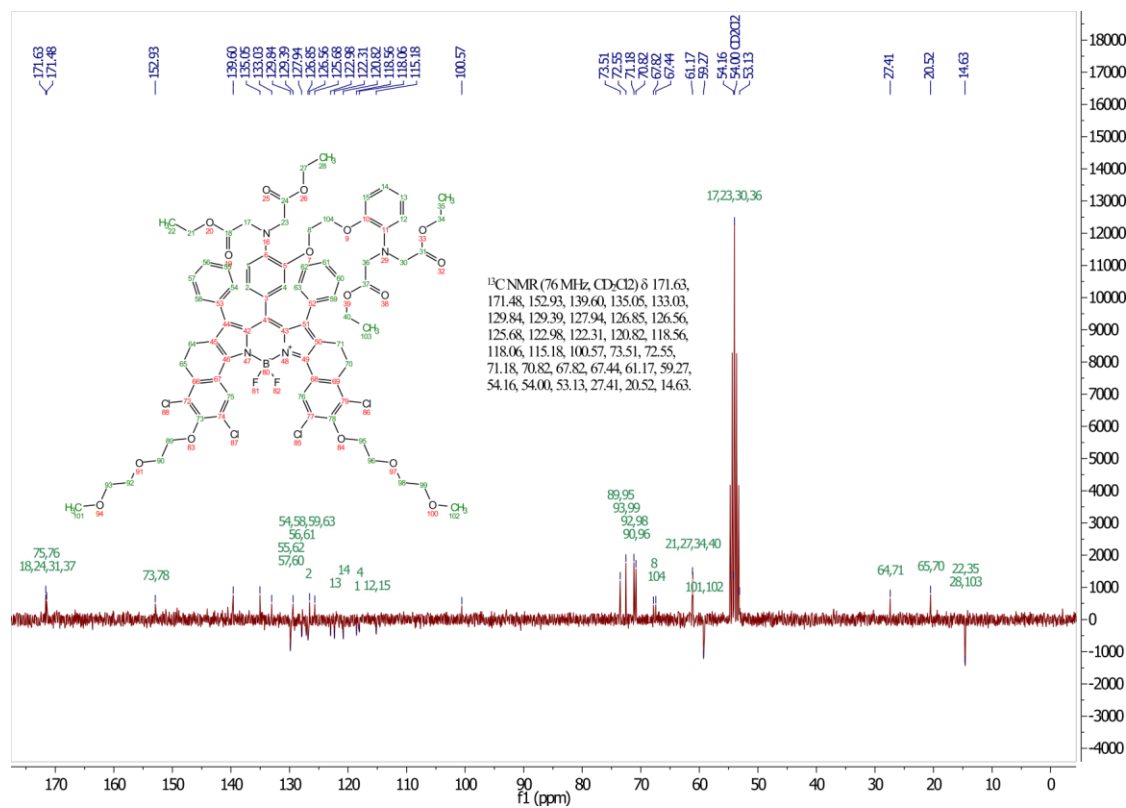


Figure S 6-58: Mass relevant theoretical isotope pattern (upper part) of C₆₅H₆₈BCl₄FN₃O₁₃ (FI4-ester - F), C₆₅H₆₈BCl₄F₂N₃O₁₃Na (FI4-ester + Na). Experimental mass relevant range (MALDI-TOF-MS) of FI4-ester (bottom).

Figure S 6-59: ¹H NMR (300Hz), in CD₂Cl₂ of FI₅-ester.Figure S 6-60: ¹³C-APT NMR (76Hz, CD₂Cl₂) of FI₅-ester.

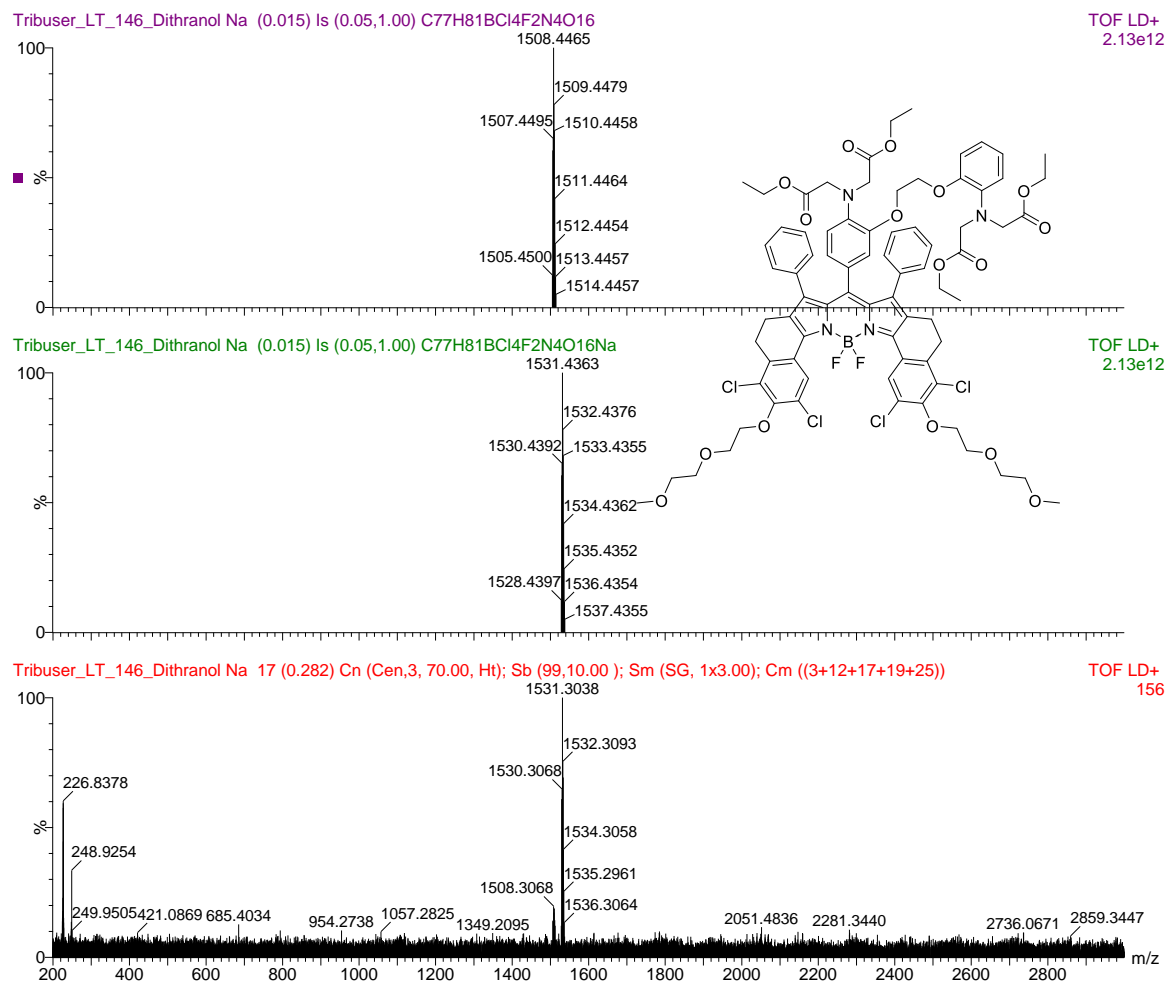


Figure S 6-61: Theoretical isotope pattern (upper part) of C₇₇H₈₁BCl₄F₂N₄O₁₆ (FI5-ester), C₇₇H₈₁BCl₄F₂N₄O₁₆Na (FI5-ester + Na). Experimental MALDI-TOF-MS of FI5-ester (bottom).

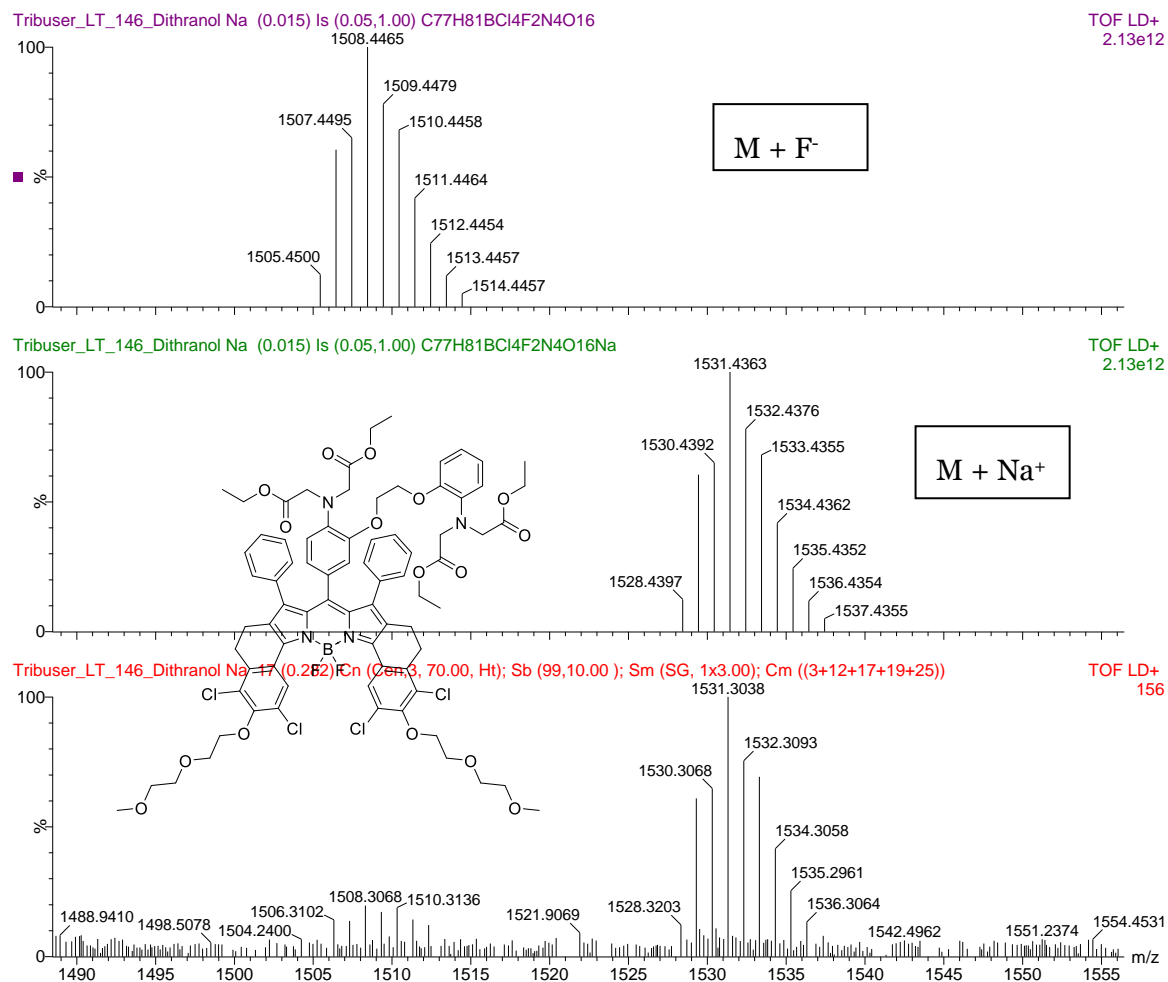


Figure S 6-62: Mass relevant theoretical isotope pattern (upper part) of C₇₇H₈₁BCl₄F₂N₄O₁₆ (FI5-ester), C₇₇H₈₁BCl₄F₂N₄O₁₆Na (FI5-ester + Na). Experimental mass relevant range (MALDI-TOF-MS) of FI5-ester (bottom).

7. Summary and conclusion

This thesis shows the high potential of optical ion sensors and its technology for measurements of cation-based analytes. Several sensing concepts in different sensing materials were developed, which enabled the measurement of Ca^{2+} , K^+ , Na^+ , dissolved NH_3 and substituted amines. The straight forward synthesis of fluoroionophores enabled the development of various fluorescent indicator dyes, whereas the spectral properties can be easily tuned. The indicators consisted of a phenyl-aza-receptor and a highly photostable BODIPY dye. This concept enabled the fabrication of sensors based on fluoroionophores, which change their fluorescence intensity through analyte interactions, due to the photo-induced electron transfer (PET). Immobilization of the indicators in water swellable polymers lead to time-resolved measurements, capable determining ionic species in aqueous solutions.

The effects of polymer nature on the sensing characteristics like stability, sensitivity, fluorescence brightness and response time was investigated. It was shown that the nature of polymers can have a huge impact on the sensing properties. This research builds a foundation for future sensor improvements.

A highly sophisticated novel sensing strategy for amines using a NH_4^+ -selective fluoroionophore, fluorescein and a phosphor-reference is presented. The combination of both indicators enabled the quantification of NH_3 and the determination of substituted amines.

The necessities of measurements and different testings for an application of fluoroionophores for whole blood sensors is presented. The challenges for the implementation of such sensors for a diagnostic application is shown. An improved DLR sensing system using fluoroionophores and phosphorescent pigments was developed. This research differentiates from the rest of the thesis, since it shows all other relevant specifications and testings typically not performed in classical sensor development.

Five novel calcium indicators using BODIPY fluorophores were synthesized and their photophysical properties were characterized. The center of attention of this work was tackling the challenges of the behavior of charged fluoroionophores in solvents for Ca^{2+} sensing.

Appendix

8. References

- (1) Hodgkin, A. L. The Ionic Basis of Electrical Activity in Nerve and Muscle. *Biological Reviews* **1951**, *26* (4), 339–409.
- (2) Clayton, R. The Electrical Human. *Phys. World* **2013**, *26* (05), 47–48.
- (3) Steitz, T. A.; Steitz, J. A. A General Two-Metal-Ion Mechanism for Catalytic RNA. *PNAS* **1993**, *90* (14), 6498–6502.
- (4) Catterall, W. A. Structure and Function of Voltage-Sensitive Ion Channels. *Science* **1988**, *242* (4875), 50–61.
- (5) Hebert, S. C.; Brown, E. M.; Harris, H. W. Role of the Ca(2+)-Sensing Receptor in Divalent Mineral Ion Homeostasis. *Journal of Experimental Biology* **1997**, *200* (2), 295–302.
- (6) Waterman, T. *Metabolism and Growth*; Elsevier, **2012**.
- (7) Silbernagl, S. *Taschenatlas Physiologie*, 8th ed.; Thieme: Stuttgart New York, **2012**.
- (8) Horn, F.; Moc, I.; Schneider, N.; Grillhösl, C.; Berghold, S.; Lindenmeier, G.; Helferich, S.; Hopf, I.; Hunsicker, A. *Biochemie des Menschen: Das Lehrbuch für das Medizinstudium*, 3., vollst. überarb. u. erw.; Thieme: Stuttgart, **2005**.
- (9) Hills, A. G.; Parsons, D. W.; Webster, G. D.; Rosenthal, O.; Conover, H. Influence the renal excretion of sodium chloride upon the renal excretion of magnesium and other ions by human subjects. *J Clin Endocrinol Metab* **1959**, *19* (10), 1192–1211.
- (10) Söremark, R. Excretion of Bromide Ions by Human Urine. *Acta Physiologica Scandinavica* **1960**, *50* (3–4), 306–310.
- (11) Lemann, J. J.; Adams, N. D.; Gray, R. W. Urinary Calcium Excretion in Human Beings
- (12) Moviat, M.; Terpstra, A. M.; van der Hoeven, J. G.; Pickkers, P. Impaired Renal Function Is Associated with Greater Urinary Strong Ion Differences in Critically Ill Patients with Metabolic Acidosis. *Journal of Critical Care* **2012**, *27* (3), 255–260.
- (13) Geleijnse, J. M.; Witteman, J. C. M.; Stijnen, T.; Kloos, M. W.; Hofman, A.; Grobbee, D. E. Sodium and Potassium Intake and Risk of Cardiovascular Events and All-Cause Mortality: The Rotterdam Study. *Eur J Epidemiol* **2007**, *22* (11), 763–770.
- (14) Bek-Jensen, H.; Tiselius, H.-G. Repeated Urine Analysis in Patients with Calcium Stone Disease. *EUR* **1998**, *33* (3), 323–332.
- (15) OpenStax. *Anatomy and Physiology*; OpenStax, **2013**.
- (16) Cordain, L.; Eaton, S. B.; Sebastian, A.; Mann, N.; Lindeberg, S.; Watkins, B. A.; O'Keefe, J. H.; Brand-Miller, J. Origins and Evolution of the Western Diet: Health Implications for the 21st Century. *Am J Clin Nutr* **2005**, *81* (2), 341–354.
- (17) Karppanen, H.; Mervaala, E. Sodium Intake and Hypertension. *Progress in Cardiovascular Diseases* **2006**, *49* (2), 59–75.
- (18) Alberts, B.; Bray, D.; Johnson, A.; Lewis, J.; Raff, M.; Roberts, K.; Walter, P. *Lehrbuch der Molekularen Zellbiologie*, 2., korrigierte Auflage.; Wiley-VCH: Weinheim, **2001**.

- (19) Adrogué, H. J.; Madias, N. E. Hyponatremia. *New England Journal of Medicine* **2000**, *342* (21), 1581–1589.
- (20) Adrogué, H. J.; Madias, N. E. Hyponatremia. *New England Journal of Medicine* **2000**, *342* (20), 1493–1499.
- (21) Rastegar, A. Serum Potassium. In *Clinical Methods: The History, Physical, and Laboratory Examinations*; Walker, H. K., Hall, W. D., Hurst, J. W., Eds.; Butterworths: Boston, **1990**.
- (22) Gennari, F. J. Hypokalemia. *New England Journal of Medicine* **1998**, *339* (7), 451–458.
- (23) Parham, W. A.; Mehdirad, A. A.; Biermann, K. M.; Fredman, C. S. Hyperkalemia Revisited. *Tex Heart Inst J* **2006**, *33* (1), 40–47.
- (24) Giebisch, G.; Windhager, E. E. Renal Tubular Transfer of Sodium, Chloride and Potassium. *The American Journal of Medicine* **1964**, *36* (5), 643–669.
- (25) Madias, N. E.; Homer, S. M.; Johns, C. A.; Cohen, J. J. Hypochloremia as a Consequence of Anion Gap Metabolic Acidosis. *The Journal of Laboratory and Clinical Medicine* **1984**, *104* (1), 15–23.
- (26) Carroll, H. J.; Farber, S. J. Hyperkalemia and Hyperchloremic Acidosis in Chronic Pyelonephritis. *Metabolism* **1964**, *13* (9), 808–817.
- (27) Cordat, E.; Casey, J. R. Bicarbonate Transport in Cell Physiology and Disease. *Biochem J* **2009**, *417* (2), 423–439.
- (28) Vasuvattakul, S.; Warner, L. C.; Halperin, M. L. Quantitative Role of the Intracellular Bicarbonate Buffer System in Response to an Acute Acid Load. *American Journal of Physiology-Regulatory, Integrative and Comparative Physiology* **1992**, *262* (2), 305–309.
- (29) Knochel, J. P. Hypophosphatemia. *West J Med* **1981**, *134* (1), 15–26.
- (30) Hruska, K. A.; Mathew, S.; Lund, R.; Qiu, P.; Pratt, R. Hyperphosphatemia of Chronic Kidney Disease. *Kidney International* **2008**, *74* (2), 148–157.
- (31) Ross, A. C.; Caballero, B. H.; Cousins, R. J.; Tucker, K. L.; Ziegler, T. R. *Modern Nutrition in Health and Disease: Eleventh Edition*; Wolters Kluwer Health Adis (ESP), **2012**.
- (32) Serefko, A.; Szopa, A.; Poleszak, E. Magnesium and Depression. *Magnesium Research* **2016**, *29* (3), 112–119.
- (33) Elin, R. J. Assessment of Magnesium Status for Diagnosis and Therapy. *Magn Res* **2010**, *23* (4), S194-198.
- (34) Magnesium — Health Professional Fact Sheet. 9.
- (35) Gibson, R. S. *Principles of Nutritional Assessment*, Second Edition.; Oxford University Press: Oxford, New York, **2005**.
- (36) Wu, J.; Carter, A. Magnesium: The Forgotten Electrolyte.
- (37) Lameris, A. L.; Monnens, L. A.; Bindels, R. J.; Hoenderop, J. G. J. Drug-Induced Alterations in Mg²⁺ Homeostasis. *Clin Sci (Lond)* **2012**, *123* (1), 1–14.
- (38) Cram, D. J.; Cram, J. M. Host-Guest Chemistry. *Science* **1974**, *183* (4127), 803–809.
- (39) Vögtle, F.; Weber, E. *Host Guest Complex Chemistry Macrocycles: Synthesis, Structures, Applications*; Springer Science & Business Media, **2012**.

- (40) Wagner, B. D. *Host-Guest Chemistry, Supramolecular Inclusion in Solution*; De Gruyter: Berlin, Boston, **2020**.
- (41) Jean-Marie Lehn. *Supramolecular Chemistry: Concepts and Perspectives*.
- (42) Ma, X.; Zhao, Y. Biomedical Applications of Supramolecular Systems Based on Host–Guest Interactions. *Chem. Rev.* **2015**, *115* (15), 7794–7839.
- (43) Tsukanov, A. V.; Dubonosov, A. D.; Bren, V. A.; Minkin, V. I. Organic Chemosensors with Crown-Ether Groups (Review). *Chem Heterocycl Comp* **2008**, *44* (8), 899–923.
- (44) Del Valle, E. M. M. Cyclodextrins and Their Uses: A Review. *Process Biochemistry* **2004**, *39* (9), 1033–1046.
- (45) Ramaiah, D.; Neelakandan, P. P.; Nair, A. K.; Avirah, R. R. Functional Cyclophanes: Promising Hosts for Optical Biomolecular Recognition. *Chem. Soc. Rev.* **2010**, *39* (11), 4158–4168.
- (46) Baldini, L.; Casnati, A.; Sansone, F.; Ungaro, R. Calixarene-Based Multivalent Ligands. *Chem. Soc. Rev.* **2007**, *36* (2), 254–266.
- (47) Diamond, D.; McKervey, M. A. Calixarene-Based Sensing Agents. *Chem. Soc. Rev.* **1996**, *25* (1), 15–24.
- (48) Xue, M.; Yang, Y.; Chi, X.; Zhang, Z.; Huang, F. Pillararenes, A New Class of Macrocycles for Supramolecular Chemistry. *Acc. Chem. Res.* **2012**, *45* (8), 1294–1308.
- (49) Barrow, S. J.; Kasera, S.; Rowland, M. J.; del Barrio, J.; Scherman, O. A. Cucurbituril-Based Molecular Recognition. *Chem. Rev.* **2015**, *115* (22), 12320–12406.
- (50) Schneider, H.-J. Mechanisms of Molecular Recognition : Investigations of Organic Host–Guest Complexes. *Angewandte Chemie International Edition in English* **1991**, *30* (11), 1417–1436.
- (51) Shamsipur, M.; Talebpour, Z.; Alizadeh, N. NMR Study of the Stoichiometry, Stability, and Ligand Interchange of Silver Ion-Hexathia-18-Crown-6 Complex in Binary Dimethyl Sulfoxide Solvent Mixtures at 300 K. *Journal of Solution Chemistry* **2003**, *32* (3), 227–238.
- (52) Hirose, K. A Practical Guide for the Determination of Binding Constants. *Journal of Inclusion Phenomena* **2001**, *39* (3), 193–209.
- (53) Blair, S. M.; Kempen, E. C.; Brodbelt, J. S. Determination of Binding Selectivities in Host-Guest Complexation by Electrospray/Quadrupole Ion Trap Mass Spectrometry. *J Am Soc Mass Spectrom* **1998**, *9* (10), 1049–1059.
- (54) Buschmann, H.-J. A Comparison of Different Experimental Techniques for the Determination of the Stabilities of Polyether, Crown Ether and Cryptand Complexes in Solution. *Inorganica Chimica Acta* **1992**, *195* (1), 51–60.
- (55) Piekarski, H.; Taniewska-Osińska, S.; Biernat, J. F. Calorimetric Research on the Electrolyte-Crown Ether-Methanol System at 298.15 K. *Inorganica Chimica Acta* **1986**, *124* (3), 115–120.
- (56) Vögtle, F.; Weber, E. Multidentate Acyclic Neutral Ligands and Their Complexation. *Angewandte Chemie International Edition in English* **1979**, *18* (10), 753–776.
- (57) Pedersen, C. J. The Discovery of Crown Ethers (Noble Lecture). *Angewandte Chemie International Edition in English* **1988**, *27* (8), 1021–1027.

- (58) Gokel, G. W.; Leevy, W. M.; Weber, M. E. Crown Ethers: Sensors for Ions and Molecular Scaffolds for Materials and Biological Models. *Chem. Rev.* **2004**, *104* (5), 2723–2750.
- (59) Masaki Yoshio; Hideyuki Noguchi. Crown Ethers for Chemical Analysis: A Review. *Anal. Lett.* **1982**, *15* (15), 1197–1276.
- (60) Jonathan W. Steed. First- and Second-Sphere Coordination Chemistry of Alkali Metal Crown Ether Complexes. *Coord. Chem. Rev.* **2001**, *215* (1), 171–221.
- (61) Hiroshi Tsukube. Armed Crown Ether Complexes in Supramolecular Assembly. *Coord. Chem. Rev.* **1996**, *148*, 1–17.
- (62) Hiroshi Tsukube. Double Armed Crown Ethers and Armed Macrocycles as a New Series of Metal-Selective Reagents: A Review. *Talanta* **1993**, *40* (9), 1313–1324.
- (63) Tsien, R. Y. New Calcium Indicators and Buffers with High Selectivity against Magnesium and Protons: Design, Synthesis, and Properties of Prototype Structures. *Biochemistry* **1980**, *19* (11), 2396–2404.
- (64) He, H.; Jenkins, K.; Lin, C. A Fluorescent Chemosensor for Calcium with Excellent Storage Stability in Water. *Anal. Chim. Acta* **2008**, *611* (2), 197–204.
- (65) Liu, D.; Qi, J.; Yu, Z.; Liu, X.; Yang, R.; Yang, H.; Chang, H.; He, H.; Yang, G. A Fluorescent Sensor with High Selectivity for Ca²⁺ against Mg²⁺ in Seawater. *Anal. Methods* **2014**, *6* (11), 3555–3559.
- (66) Gryniewicz, G.; Poenie, M.; Tsien, R. Y. A New Generation of Ca²⁺ Indicators with Greatly Improved Fluorescence Properties. *J. Biol. Chem.* **1985**, *260* (6), 3440–3450.
- (67) Adams, S. R.; Kao, J. P. Y.; Gryniewicz, G.; Minta, A.; Tsien, R. Y. Biologically Useful Chelators That Release Ca²⁺ upon Illumination. *J. Am. Chem. Soc.* **1988**, *110* (10), 3212–3220.
- (68) Minta, A.; Kao, J. P. Y.; Tsien, R. Y. Fluorescent Indicators for Cytosolic Calcium Based on Rhodamine and Fluorescein Chromophores. *J. Biol. Chem.* **1989**, *264* (Copyright (C) 2019 American Chemical Society (ACS). All Rights Reserved.), 8171–8178.
- (69) Shortreed, M.; Kopelman, R.; Kuhn, M.; Hoyland, B. Fluorescent Fiber-Optic Calcium Sensor for Physiological Measurements. *Anal. Chem.* **1996**, *68* (8), 1414–1418.
- (70) Smith, G. A.; Metcalfe, J. C.; Clarke, S. D. The Design and Properties of a Series of Calcium Indicators Which Shift from Rhodamine-like to Fluorescein-like Fluorescence on Binding Calcium. *J. Chem. Soc., Perkin Trans. 2* **1993**, No. 6, 1195–1204.
- (71) Arnaud-Neu, F.; Delgado, R.; Chaves, S. Critical Evaluation of Stability Constants and Thermodynamic Functions of Metal Complexes of Crown Ethers (IUPAC Technical Report). *Pure and Applied Chemistry* **2003**, *75* (1), 71–102.
- (72) Gokel, G. W.; Goli, D. M.; Minganti, C.; Echegoyen, L. Clarification of the Hole-Size Cation-Diameter Relationship in Crown Ethers and a New Method for Determining Calcium Cation Homogeneous Equilibrium Binding Constants. *J. Am. Chem. Soc.* **1983**, *105* (23), 6786–6788.
- (73) Saalfrank, R. W.; Bernt, I. Ligand and Metal Controlled Multicomponent Self-Assembly of Oligonuclear Two- and Three-Dimensional Complex Molecular Architectures. *Current Opinion in Solid State and Materials Science* **1998**, *3* (4), 407–413.

- (74) Pedersen, C. J.; Frensdorff, H. K. Macrocyclic Polyethers and Their Complexes. *Angewandte Chemie International Edition in English* **1972**, *11* (1), 16–25.
- (75) Valeur, B. *Molecular Fluorescence: Principles and Applications*, 1st ed.; Wiley-VCH: Weinheim ; New York, **2001**.
- (76) Lakowicz, J. R. *Principles of Fluorescence Spectroscopy*, 3rd ed.; Springer US, **2006**.
- (77) Quaranta, M.; Borisov, S. M.; Klimant, I. Indicators for Optical Oxygen Sensors. *Bioanal Rev* **2012**, *4* (2–4), 115–157.
- (78) Gründler, P. *Chemische Sensoren: Eine Einführung für Naturwissenschaftler und Ingenieure*; Springer-Verlag: Berlin Heidelberg, **2004**.
- (79) Daniel C. Harris, D. *Quantitative Chemical Analysis 8th Edition*.
- (80) Bobacka, J.; Ivaska, A.; Lewenstam, A. Potentiometric Ion Sensors. *Chem. Rev.* **2008**, *108* (2), 329–351.
- (81) Mark E. Meyerhoff; Yvonne M. Fraticelli. Ion-selective electrodes | Analytical Chemistry
- (82) Bakker, E.; Crespo, G.; Grygoliowicz-Pawlak, E.; Mistlberger, G.; Pawlak, M.; Xie, X. Advancing Membrane Electrodes and Optical Ion Sensors. *Chimia (Aarau)* **2011**, *65* (3), 141–149.
- (83) Bakker, E.; Lerchi, M.; Rosatzin, T.; Rusterholz, B.; Simon, W. Synthesis and Characterization of Neutral Hydrogen Ion-Selective Chromoionophores for Use in Bulk Optodes. *Analytica Chimica Acta* **1993**, *278* (2), 211–225.
- (84) Bakker, E.; Bühlmann, P.; Pretsch, E. Carrier-Based Ion-Selective Electrodes and Bulk Optodes. 1. General Characteristics. *Chem. Rev.* **1997**, *97* (8), 3083–3132.
- (85) Bühlmann, P.; Pretsch, E.; Bakker, E. Carrier-Based Ion-Selective Electrodes and Bulk Optodes. 2. Ionophores for Potentiometric and Optical Sensors. *Chem. Rev.* **1998**, *98* (4), 1593–1688.
- (86) Xie, X.; Bakker, E. Ion Selective Optodes: From the Bulk to the Nanoscale. *Anal Bioanal Chem* **2015**, *407* (14), 3899–3910.
- (87) Huber, C.; Klimant, I.; Krause, C.; Werner, T.; Wolfbeis, O. S. Nitrate-Selective Optical Sensor Applying a Lipophilic Fluorescent Potential-Sensitive Dye. *Analytica Chimica Acta* **2001**, *449* (1), 81–93.
- (88) Mohr, G. J.; Wolfbeis, O. S. Optical Sensing of Anions via Polarity-Sensitive Dyes: A Bulk Sensor Membrane for Nitrate. *Analytica Chimica Acta* **1995**, *316* (2), 239–246.
- (89) Wolfbeis, O. S. Fluorescence-Based Ion Sensing Using Potential-Sensitive Dyes. *Sensors and Actuators B: Chemical* **1995**, *29* (1), 140–147.
- (90) Bissell, R. A.; de Silva, A. P.; Thilak, W.; Fernando, M. L.; Patuwathavithana, S. T.; Shantha, T. K.; Samarasinghe, D. Fluorescent PET (Photoinduced Electron Transfer) Indicators for Solvent Polarity with Quasi-Step Functional Response. *Tetrahedron Letters* **1991**, *32* (3), 425–428.
- (91) Bakker, Eric.; Simon, Wilhelm. Selectivity of Ion-Sensitive Bulk Optodes. *Anal. Chem.* **1992**, *64* (17), 1805–1812.
- (92) Kessler, M. A.; Gailer, J. G.; Wolfbeis, O. S. Optical Sensor for On-Line Determination of Solvent Mixtures Based on a Fluorescent Solvent Polarity Probe. *Sensors and Actuators B: Chemical* **1991**, *3* (4), 267–272.

- (93) Panchenko, P. A.; Fedorov, Y. V.; Fedorova, O. A.; Jonusauskas, G. Comparative Analysis of the PET and ICT Sensor Properties of 1,8-Naphthalimides Containing Aza-15-Crown-5 Ether Moiety. *Dyes and Pigments* **2013**, *98* (3), 347–357.
- (94) Bozdemir, O. A.; Guliyev, R.; Buyukcakil, O.; Selcuk, S.; Kolemen, S.; Gulseren, G.; Nalbantoglu, T.; Boyaci, H.; Akkaya, E. U. Selective Manipulation of ICT and PET Processes in Styryl-Bodipy Derivatives: Applications in Molecular Logic and Fluorescence Sensing of Metal Ions. *J. Am. Chem. Soc.* **2010**, *132* (23), 8029–8036.
- (95) Oliver, N. S.; Toumazou, C.; Cass, A. E. G.; Johnston, D. G. Glucose Sensors: A Review of Current and Emerging Technology. *Diabetic Medicine* **2009**, *26* (3), 197–210.
- (96) Burgess, L. W. Absorption-Based Sensors. *Sensors and Actuators B: Chemical* **1995**, *29* (1), 10–15.
- (97) Razeghi, M.; Nguyen, B.-M. Advances in Mid-Infrared Detection and Imaging: A Key Issues Review. *Rep. Prog. Phys.* **2014**, *77* (8), 082401.
- (98) Borisov, S. M.; Wolfbeis, O. S. Optical Biosensors. *Chem. Rev.* **2008**, *108* (2), 423–461.
- (99) Li, M.; Cushing, S. K.; Wu, N. Plasmon-Enhanced Optical Sensors: A Review. *Analyst* **2014**, *140* (2), 386–406.
- (100) Muehlethaler, C.; Leona, M.; Lombardi, J. R. Review of Surface Enhanced Raman Scattering Applications in Forensic Science. *Anal. Chem.* **2016**, *88* (1), 152–169.
- (101) Homola, J. Surface Plasmon Resonance Sensors for Detection of Chemical and Biological Species. *Chem. Rev.* **2008**, *108* (2), 462–493.
- (102) Lee, B. Review of the Present Status of Optical Fiber Sensors. *Optical Fiber Technology* **2003**, *9* (2), 57–79.
- (103) Schlücker, S. Surface-Enhanced Raman Spectroscopy: Concepts and Chemical Applications. *Angewandte Chemie International Edition* **2014**, *53* (19), 4756–4795.
- (104) McDonagh, C.; Burke, C. S.; MacCraith, B. D. Optical Chemical Sensors. *Chem. Rev.* **2008**, *108* (2), 400–422.
- (105) Ruedas-Rama, M. J.; Walters, J. D.; Orte, A.; Hall, E. A. H. Fluorescent Nanoparticles for Intracellular Sensing: A Review. *Analytica Chimica Acta* **2012**, *751*, 1–23.
- (106) Schäferling, M. The Art of Fluorescence Imaging with Chemical Sensors. *Angewandte Chemie International Edition* **2012**, *51* (15), 3532–3554.
- (107) Silva, A. P. de; Rupasinghe, R. A. D. D. A New Class of Fluorescent PH Indicators Based on Photo-Induced Electron Transfer. *J. Chem. Soc., Chem. Commun.* **1985**, No. 23, 1669–1670.
- (108) Weller, A. Electron-Transfer and Complex Formation in the Excited State. *Pure Appl. Chem.* **1968**, *16* (1), 115–124.
- (109) Silva, A. P. de; Gunnlaugsson, T.; Rice, T. E. Recent Evolution of Luminescent Photoinduced Electron Transfer Sensors. A Review. *Analyst* **1996**, *121* (12), 1759–1762.
- (110) Bissell, R. A.; Silva, A. P. de; Gunaratne, H. Q. N.; Lynch, P. L. M.; Maguire, G. E. M.; Sandanayake, K. R. A. S. Molecular Fluorescent Signalling with ‘Fluor–Spacer–Receptor’ Systems: Approaches to Sensing and Switching Devices via Supramolecular Photophysics. *Chem. Soc. Rev.* **1992**, *21* (3), 187–195.

- (111) Gareis, T.; Huber, C.; Wolfbeis, O. S.; Daub, J. Phenol/Phenolate-Dependent on/off Switching of the Luminescence Of 4,4-Difluoro-4-Bora-3a,4a-Diaza-s-Indacenes. *Chem. Commun.* **1997**, No. 18, 1717–1718.
- (112) Yokoi, H.; Nakano, T.; Fujita, W.; Ishiguro, K.; Sawaki, Y. In-Cage Formation of Carbanions in Photoinduced Electron-Transfer Reaction of Carboxylate Ions. *J. Am. Chem. Soc.* **1998**, *120* (48), 12453–12458.
- (113) Aigner, D.; Freunberger, S. A.; Wilkening, M.; Saf, R.; Borisov, S. M.; Klimant, I. Enhancing Photoinduced Electron Transfer Efficiency of Fluorescent PH-Probes with Halogenated Phenols. *Anal. Chem.* **2014**, *86* (18), 9293–9300.
- (114) Müller, B. J.; Zhdanov, A. V.; Borisov, S. M.; Foley, T.; Okkelman, I. A.; Tsytsarev, V.; Tang, Q.; Erzurumlu, R. S.; Chen, Y.; Zhang, H.; Toncelli, C.; Klimant, I.; Papkovsky, D. B.; Dmitriev, R. I. Nanoparticle-Based Fluoroionophore for Analysis of Potassium Ion Dynamics in 3D Tissue Models and In Vivo. *Advanced Functional Materials* **2018**, *28* (9), 1704598.
- (115) Ast, S.; Schwarze, T.; Müller, H.; Sukhanov, A.; Michaelis, S.; Wegener, J.; Wolfbeis, O. S.; Körzdörfer, T.; Dürkop, A.; Holdt, H.-J. A Highly K⁺-Selective Phenylaza-[18]Crown-6-Lariat-Ether-Based Fluoroionophore and Its Application in the Sensing of K⁺ Ions with an Optical Sensor Film and in Cells. *Chemistry – A European Journal* **2013**, *19* (44), 14911–14917.
- (116) Müller, B. J.; Steinmann, N.; Borisov, S. M.; Klimant, I. Ammonia Sensing with Fluoroionophores – A Promising Way to Minimize Interferences Caused by Volatile Amines. *Sensors and Actuators B: Chemical* **2018**, *255*, 1897–1901.
- (117) Müller, B. J.; Borisov, S. M.; Klimant, I. Red- to NIR-Emitting, BODIPY-Based, K⁺-Selective Fluoroionophores and Sensing Materials. *Adv. Funct. Mater.* **2016**, *26* (42), 7697–7707.
- (118) Müller, B. J.; Rappitsch, T.; Staudinger, C.; Rüschtz, C.; Borisov, S. M.; Klimant, I. Sodium-Selective Fluoroionophore-Based Optodes for Seawater Salinity Measurement. *Anal. Chem.* **2017**, *89* (13), 7195–7202.
- (119) Li, J.; Yim, D.; Jang, W.-D.; Yoon, J. Recent Progress in the Design and Applications of Fluorescence Probes Containing Crown Ethers. *Chem. Soc. Rev.* **2017**, *46* (9), 2437–2458.
- (120) Silva, A. P. de; Moody, T. S.; Wright, G. D. Fluorescent PET (Photoinduced Electron Transfer) Sensors as Potent Analytical Tools. *Analyst* **2009**, *134* (12), 2385–2393.
- (121) Stubing, D. B.; Heng, S.; Abell, A. D. Crowned Spiropyran Fluoroionophores with a Carboxyl Moiety for the Selective Detection of Lithium Ions. *Org. Biomol. Chem.* **2016**, *14* (15), 3752–3757.
- (122) Gunnlaugsson, T.; Leonard, J. P. Synthesis and Evaluation of Colorimetric Chemosensors for Monitoring Sodium and Potassium Ions in the Intracellular Concentration Range. *J. Chem. Soc., Perkin Trans. 2* **2002**, No. 12, 1980–1985.
- (123) Sui, B.; Liu, X.; Wang, M.; Belfield, K. D. A Highly Selective Fluorescence Turn-On Sensor for Extracellular Calcium Ion Detection. *Chem. Eur. J.* **2016**, *22* (30), 10351–10354.
- (124) Wang, Q.; Wang, X.; Li, L. Density Functional Theory Study on a Fluorescent Chemosensor Device of Aza-Crown Ether. *Journal of Physical Organic Chemistry* **2014**, *27* (7), 546–554.
- (125) Kaur, P.; Kaur, N.; Kaur, M.; Dhuna, V.; Singh, J.; Singh, K. ‘Turn-on’ Coordination Based Detection of Pd²⁺ and Bioimaging Applications. *RSC Adv.* **2014**, *4* (31), 16104–16108.

- (126) Wolfbeis, O. S. Materials for Fluorescence-Based Optical Chemical Sensors. *J. Mater. Chem.* **2005**, *15* (27–28), 2657–2669.
- (127) Sulzer, P.; Lebl, R.; Kappe, C. O.; Mayr, T. Oxygen Sensors for Flow Reactors – Measuring Dissolved Oxygen in Organic Solvents. *React. Chem. Eng.* **2019**, *4* (12), 2081–2087.
- (128) Zhou, X.; Su, F.; Gao, W.; Tian, Y.; Youngbull, C.; Johnson, R. H.; Meldrum, D. R. Triazacryptand-Based Fluorescent Sensors for Extracellular and Intracellular K⁺ Sensing. *Biomaterials* **2011**, *32* (33), 8574–8583.
- (129) Zhu, H.; Zhou, X.; Su, F.; Tian, Y.; Ashili, S.; Holl, M. R.; Meldrum, D. R. Micro-Patterning and Characterization of PHEMA-Co-PAM-Based Optical Chemical Sensors for Lab-on-a-Chip Applications. *Sensors and Actuators B: Chemical* **2012**, *173*, 817–823.
- (130) Rüdiger, V.; Schneider, H.-J.; Solov'ev, V. P.; Kazachenko, V. P.; Raevsky, O. A. Crown Ether–Ammonium Complexes: Binding Mechanisms and Solvent Effects. *European Journal of Organic Chemistry* **1999**, *1999* (8), 1847–1856.
- (131) Treibs, A.; Kreuzer, F.-H. Difluorboryl-Komplexe von Di- Und Tripyrrylmethenen. *Justus Liebig's Ann. Chem.* **1968**, *718* (1), 208–223.
- (132) Ulrich, G.; Ziessel, R.; Harriman, A. The Chemistry of Fluorescent Bodipy Dyes: Versatility Unsurpassed. *Angew. Chem. Int. Ed. Engl.* **2008**, *47* (7), 1184–1201.
- (133) Loudet, A.; Burgess, K. BODIPY Dyes and Their Derivatives: Syntheses and Spectroscopic Properties. *Chem. Rev.* **2007**, *107* (11), 4891–4932.
- (134) Sui, B.; Tang, S.; Liu, T.; Kim, B.; Belfield, K. D. Novel BODIPY-Based Fluorescence Turn-on Sensor for Fe³⁺ and Its Bioimaging Application in Living Cells. *ACS Appl. Mater. Interfaces* **2014**, *6* (21), 18408–18412.
- (135) Sui, B.; Yue, X.; Tichy, M. G.; Liu, T.; Belfield, K. D. Improved Synthesis of the Triazacryptand (TAC) and Its Application in the Construction of a Fluorescent TAC-BODIPY Conjugate for K⁺ Sensing in Live Cells. *European Journal of Organic Chemistry* **2015**, *2015* (6), 1189–1192.
- (136) Hirata, T.; Terai, T.; Komatsu, T.; Hanaoka, K.; Nagano, T. Development of a Potassium Ion-Selective Fluorescent Sensor Based on 3-Styrylated BODIPY. *Bioorg. Med. Chem. Lett.* **2011**, *21* (20), 6090–6093.
- (137) Erten-Ela, S.; Yilmaz, M. D.; Icli, B.; Dede, Y.; Icli, S.; Akkaya, E. U. A Panchromatic Boradiazaindacene (BODIPY) Sensitizer for Dye-Sensitized Solar Cells. *Org. Lett.* **2008**, *10* (15), 3299–3302.
- (138) Wolfbeis, O. S. Fiber-Optic Chemical Sensors and Biosensors. *Anal. Chem.* **2006**, *78* (12), 3859–3874.
- (139) Qazi, H. H.; Mohammad, A. B. bin; Akram, M. Recent Progress in Optical Chemical Sensors. *Sensors (Basel)* **2012**, *12* (12), 16522–16556.
- (140) Narayanaswamy, R.; Wolfbeis, O. S. *Optical Sensors: Industrial Environmental and Diagnostic Applications*; Springer Science & Business Media, **2013**.
- (141) Wolfbeis, O. S. Editorial: Probes, Sensors, and Labels: Why Is Real Progress Slow? *Angewandte Chemie International Edition* **2013**, *52* (38), 9864–9865.
- (142) Gibb, I. Evaluation and Assessment of New Disposable Strip for Determination of Plasma Potassium Concentration. *Journal of Clinical Pathology* **1987**, *40* (3), 298–301.

- (143) Harjes, D. I.; Dubach, J. M.; Rosenzweig, A.; Das, S.; Clark, H. A. Ion-Selective Optodes Measure Extracellular Potassium Flux in Excitable Cells. *Macromol Rapid Commun* **2010**, *31* (2), 217–221.
- (144) Bamsey, M.; Berinstain, A.; Dixon, M. Development of a Potassium-Selective Optode for Hydroponic Nutrient Solution Monitoring. *Analytica Chimica Acta* **2012**, *737*, 72–82.
- (145) Hideaki Hisamoto; Nami Miyashita; Kazuhiko Watanabe; Eriko Nakagawa; Noriko Yamamoto; Koji Suzuki. Ion Sensing Film Optodes: Disposable Ion Sensing Probes for the Determination of Na⁺, K⁺, Ca²⁺ and Cl⁻ Concentrations in Serum. *Sensors and Actuators B: Chemical* **1995**, *29* (1), 378–385.
- (146) Johnson, R. D.; Bachas, L. G. Ionophore-Based Ion-Selective Potentiometric and Optical Sensors. *Anal Bioanal Chem* **2003**, *376* (3), 328–341.
- (147) Mistlberger, G.; Crespo, G. A.; Bakker, E. Ionophore-Based Optical Sensors. *Annual Review of Analytical Chemistry* **2014**, *7* (1), 483–512.
- (148) Namkung, W.; Padmawar, P.; Mills, A. D.; Verkman, A. S. Cell-Based Fluorescence Screen for K⁺ Channels and Transporters Using an Extracellular Triazacryptand-Based K⁺ Sensor. *J. Am. Chem. Soc.* **2008**, *130* (25), 7794–7795.
- (149) He, H.; Mortellaro, M. A.; Leiner, M. J. P.; Fraatz, R. J.; Tusa, J. K. A Fluorescent Sensor with High Selectivity and Sensitivity for Potassium in Water. *J. Am. Chem. Soc.* **2003**, *125* (6), 1468–1469.
- (150) Besouw, M. T.; Bockenbauer, D. Chapter 3 - Potassium Metabolism. In *Nephrology and Fluid/electrolyte Physiology (Third Edition)*; Oh, W., Baum, M., Eds.; Philadelphia, **2019**; pp 31–46.
- (151) Malval, J.-P.; Leray, I.; Valeur, B. A Highly Selective Fluorescent Molecular Sensor for Potassium Based on a Calix[4]Bisazacrown Bearing Boron-Dipyromethene Fluorophores. *New J. Chem.* **2005**, *29* (8), 1089–1094.
- (152) Schwarze, T.; Schneider, R.; Riemer, J.; Holdt, H.-J. A Highly K(+) -Selective Fluorescent Probe - Tuning the K(+) -Complex Stability and the K(+) /Na(+) Selectivity by Varying the Lariat-Alkoxy Unit of a Phenylaza[18]Crown-6 Ionophore. *Chemistry, an Asian journal* **2016**, *11* (2), 241–247.
- (153) Dubach, J. M.; Harjes, D. I.; Clark, H. A. Ion-Selective Nano-Optodes Incorporating Quantum Dots. *J. Am. Chem. Soc.* **2007**, *129* (27), 8418–8419.
- (154) Du, X.; Yang, L.; Hu, W.; Wang, R.; Zhai, J.; Xie, X. A Plasticizer-Free Miniaturized Optical Ion Sensing Platform with Ionophores and Silicon-Based Particles. *Anal. Chem.* **2018**, *90* (9), 5818–5824.
- (155) Buck, S. M.; Koo, Y.-E. L.; Park, E.; Xu, H.; Philbert, M. A.; Brasuel, M. A.; Kopelman, R. Optochemical Nanosensor PEBBLEs: Photonic Explorers for Bioanalysis with Biologically Localized Embedding. *Current Opinion in Chemical Biology* **2004**, *8* (5), 540–546.
- (156) Jarolímová, Z.; Vishe, M.; Lacour, J.; Bakker, E. Potassium Ion-Selective Fluorescent and PH Independent Nanosensors Based on Functionalized Polyether Macrocycles. *Chem. Sci.* **2015**, *7* (1), 525–533.
- (157) Carpenter, R. D.; Verkman, A. S. Synthesis of a Sensitive and Selective Potassium-Sensing Fluoroionophore. *Org. Lett.* **2010**, *12* (6), 1160–1163.
- (158) Schröder, C. R.; Weidgans, B. M.; Klimant, I. PH Fluorosensors for Use in Marine Systems. *Analyst* **2005**, *130* (6), 907–916.

- (159) Strobl, M.; Rappitsch, T.; Borisov, S. M.; Mayr, T.; Klimant, I. NIR-Emitting Aza-BODIPY Dyes – New Building Blocks for Broad-Range Optical PH Sensors. *Analyst* **2015**, *140* (21), 7150–7153.
- (160) Vasylevska, A. S.; Karasyov, A. A.; Borisov, S. M.; Krause, C. Novel Coumarin-Based Fluorescent PH Indicators, Probes and Membranes Covering a Broad PH Range. *Anal Bioanal Chem* **2007**, *387* (6), 2131–2141.
- (161) Ahuja, P.; Peshkova, M. A.; Hemphill, B. D.; Gratzl, M. Minimizing Color Interference from Biological Samples in Optode-Based Measurements. *Sensors and Actuators B: Chemical* **2014**, *204*, 319–325.
- (162) Moßhammer, M.; Strobl, M.; Köhl, M.; Klimant, I.; Borisov, S. M.; Koren, K. Design and Application of an Optical Sensor for Simultaneous Imaging of PH and Dissolved O₂ with Low Cross-Talk. *ACS Sens.* **2016**, *1* (6), 681–687.
- (163) Li, Y.; Huszthy, P.; Móczár, I.; Szemenyei, B.; Kunsági-Máté, S. Solvent Effect on the Complex Formation of a Crown Ether Derivative with Sodium and Potassium Ions. Thermodynamic Background of Selectivity. *Chemical Physics Letters* **2013**, *556*, 94–97.
- (164) Solov'ev, V. P.; Strakhova, N. N.; Raevsky, O. A.; Rüdiger, V.; Schneider, H.-J. Solvent Effects on Crown Ether Complexations¹. *J. Org. Chem.* **1996**, *61* (16), 5221–5226.
- (165) Kjær, T. Enzyme Sensor Including a Water-Containing Spacer Layer. US20060275859A1, December 7, **2006**.
- (166) Kjaer, T.; Clausen, L. D. Enzyme Sensor with a Cover Membrane Layer Covered by a Hydrophilic Polymer. WO2006122554A2, November 23, **2006**.
- (167) Thomas, L.; Ansorg, R.; Arndt, T.; Barlage, T. *Labor und Diagnose: Indikation und Bewertung von Laborbefunden für die medizinische Diagnostik*, 6.,; Th-Books: Frankfurt/Main, **2005**.
- (168) Willis, J. B. The Determination of Metals in Blood Serum by Atomic Absorption Spectroscopy—III: Sodium and Potassium. *Spectrochimica Acta* **1960**, *16* (5), 551–558.
- (169) Irnius, A.; Tautkus, S.; Kazlauskas, R.; Kareiva, A. Rapid quantitative determination of metals in blood and liver by FAAS
- (170) PhD, N. R. *Tietz Fundamentals of Clinical Chemistry and Molecular Diagnostics*, 8th ed.; Saunders, **2018**.
- (171) Levy, G. B. Determination of Sodium with Ion-Selective Electrodes. *Clin Chem* **1981**, *27* (8), 1435–1438.
- (172) Worth, H. G. J. A Comparison of the Measurement of Sodium and Potassium by Flame Photometry and Ion-Selective Electrode. *Ann Clin Biochem* **1985**, *22* (4), 343–350.
- (173) Asirvatham, J. R.; Moses, V.; Bjornson, L. Errors in Potassium Measurement: A Laboratory Perspective for the Clinician. *N Am J Med Sci* **2013**, *5* (4), 255–259.
- (174) Klimant, I.; Huber, C.; Liebsch, G.; Neurauter, G.; Stangelmayer, A.; Wolfbeis, O. S. Dual Lifetime Referencing (DLR) — a New Scheme for Converting Fluorescence Intensity into a Frequency-Domain or Time-Domain Information. In *New Trends in Fluorescence Spectroscopy: Applications to Chemical and Life Sciences*; Valeur, B., Brochon, J.-C., Eds.; Springer Series on Fluorescence; Springer: Berlin, Heidelberg, **2001**; pp 257–274.
- (175) Wencel, D.; Abel, T.; McDonagh, C. Optical Chemical PH Sensors. *Anal. Chem.* **2014**, *86* (1), 15–29.

- (176) Tribuser, L.; Borisov, S. M.; Klimant, I. Tuning the Sensitivity of Fluoroionophore-Based K⁺ Sensors via Variation of Polymer Matrix: A Comparative Study. *Sensors and Actuators B: Chemical* **2020**, *312*, 127940.
- (177) Applying ARGET ATRP to the Growth of Polymer Brush Thin Films by Surface-initiated Polymerization <https://www.sigmaaldrich.com/technical-documents/articles/crp-guide/applying-arget-atrp-to-the-growth-of-polymer-brush-thin-films.html> (accessed Mar 25, **2020**).
- (178) Zhao, M.; Zhou, G.; Zhang, L.; Li, X.; Li, T.; Liu, F. Fabrication and Photoactivity of a Tunable-Void SiO₂-TiO₂ Core-Shell Structure on Modified SiO₂ Nanospheres by Grafting an Amphiphilic Diblock Copolymer Using ARGET ATRP. *Soft Matter* **2014**, *10* (8), 1110–1120.
- (179) Niki, E. Action of Ascorbic Acid as a Scavenger of Active and Stable Oxygen Radicals. *Am. J. Clin. Nutr.* **1991**, *54* (6 Suppl), 1119S–1124S.
- (180) Pehlivan, F. E. Vitamin C: An Antioxidant Agent. *Vitamin C* **2017**.
- (181) Peter Warneck. Chemistry of the Natural Atmosphere, Volume 71 - 2nd Edition
- (182) Krupa, S. V. Effects of Atmospheric Ammonia (NH₃) on Terrestrial Vegetation: A Review. *Environmental Pollution* **2003**, *124* (2), 179–221.
- (183) Oudendag, D. A.; Luesink, H. H. The Manure Model: Manure, Minerals (N, P and K), Ammonia Emission, Heavy Metals and the Use of Fertiliser in Dutch Agriculture. *Environmental Pollution* **1998**, *102* (1, Supplement 1), 241–246.
- (184) Timmer, B.; Olthuis, W.; Berg, A. van den. Ammonia Sensors and Their Applications—a Review. *Sensors and Actuators B: Chemical* **2005**, *107* (2), 666–677.
- (185) Rhines, T. D.; Arnold, M. A. Determination of Ammonia in Untreated Serum with a Fiber-Optic Ammonia Gas Sensor. *Analytica Chimica Acta* **1990**, *231*, 231–235.
- (186) Widmer, S.; Dorrestijn, M.; Camerlo, A.; Korent Urek, Š.; Lobnik, A.; E. Housecroft, C.; C. Constable, E.; J. Scherer, L. Coumarin Meets Fluorescein: A Förster Resonance Energy Transfer Enhanced Optical Ammonia Gas Sensor. *Analyst* **2014**, *139* (17), 4335–4342.
- (187) Preininger, C.; Mohr, G. J.; Klimant, I.; Wolfbeis, O. S. Ammonia Fluorosensors Based on Reversible Lactonization of Polymer-Entrapped Rhodamine Dyes, and the Effects of Plasticizers. *Analytica Chimica Acta* **1996**, *334* (1), 113–123.
- (188) Preininger, C.; Mohr, G. J. Fluorosensors for Ammonia Using Rhodamines Immobilized in Plasticized Poly(Vinyl Chloride) and in Sol-Gel; a Comparative Study. *Analytica Chimica Acta* **1997**, *342* (2), 207–213.
- (189) Waich, K.; Mayr, T.; Klimant, I. Microsensors for Detection of Ammonia at Ppb-Concentration Levels. *Measurement Science and Technology* **2007**, *18* (10), 3195–3201.
- (190) Strobl, M.; Walcher, A.; Mayr, T.; Klimant, I.; Borisov, S. M. Trace Ammonia Sensors Based on Fluorescent Near-Infrared-Emitting Aza-BODIPY Dyes. *Anal. Chem.* **2017**, *89* (5), 2859–2865.
- (191) Maierhofer, M.; Borisov, S. M.; Mayr, T. Optical Ammonia Sensor for Continuous Bioprocess Monitoring. *Proceedings* **2018**, *2* (13), 1041.
- (192) Moreno, J.; Arregui, F. J.; Matias, I. R. Fiber Optic Ammonia Sensing Employing Novel Thermoplastic Polyurethane Membranes. *Sensors and Actuators B: Chemical* **2005**, *105* (2), 419–424.

- (193) Nakano, N.; Kobayashi, Y.; Nagashima, K. Development of a Monitoring Tape for Ammonia Gas in Air Using Rose Bengal. *Analyst* **1994**, *119* (9), 2009–2012.
- (194) Mills, A.; Wild, L.; Chang, Q. Plastic Colorimetric Film Sensors for Gaseous Ammonia. *Mikrochimica Acta* **1995**, *121* (1–4), 225–236.
- (195) Waich, K.; Borisov, S.; Mayr, T.; Klimant, I. Dual Lifetime Referenced Trace Ammonia Sensors. *Sensors and Actuators B: Chemical* **2009**, *139* (1), 132–138.
- (196) Mayr, T.; Borisov, S. M.; Abel, T.; Enko, B.; Waich, K.; Mistlberger, G.; Klimant, I. Light Harvesting as a Simple and Versatile Way to Enhance Brightness of Luminescent Sensors. *Anal. Chem.* **2009**, *81* (15), 6541–6545.
- (197) Waich, K.; Mayr, T.; Klimant, I. Fluorescence Sensors for Trace Monitoring of Dissolved Ammonia. *Talanta* **2008**, *77* (1), 66–72.
- (198) Schaude, C.; Meindl, C.; Fröhlich, E.; Attard, J.; Mohr, G. J. Developing a Sensor Layer for the Optical Detection of Amines during Food Spoilage. *Talanta* **2017**, *170*, 481–487.
- (199) Werner, T.; Klimant, I.; Wolfbeis, O. S. Ammonia-Sensitive Polymer Matrix Employing Immobilized Indicator Ion Pairs. *Analyst* **1995**, *120* (6), 1627–1631.
- (200) Lobnik, A.; Wolfbeis, O. S. Sol-Gel Based Optical Sensor for Dissolved Ammonia. *Sensors and Actuators B: Chemical* **1998**, *51* (1), 203–207.
- (201) Mohr, G. J.; Nezel, T.; Spichiger-Keller, U. E. Effect of the Polymer Matrix on the Response of Optical Sensors for Dissolved Aliphatic Amines Based on the Chromoreactant ETHT 4001. *Analytica Chimica Acta* **2000**, *414* (1), 181–187.
- (202) Rodríguez, A. J.; Zamarreño, C. R.; Matías, I. R.; Arregui, F. J.; Cruz, R. F. D.; May-Arrijoja, D. A. A Fiber Optic Ammonia Sensor Using a Universal PH Indicator. *Sensors* **2014**, *14* (3), 4060–4073.
- (203) Chen, X.; Dai, Y.; Li, Z.; Zhang, Z.; Wang, X. Optical Rubbery Ormosils Sensor for the Detection of Ammonia. *Fresenius J Anal Chem* **2001**, *370* (8), 1048–1051.
- (204) Duong, H. D.; Rhee, J. I. A Ratiometric Fluorescence Sensor for the Detection of Ammonia in Water. *Sensors and Actuators B: Chemical* **2014**, *190*, 768–774.
- (205) Back, M.; Trave, E.; Ueda, J.; Tanabe, S. Ratiometric Optical Thermometer Based on Dual Near-Infrared Emission in Cr³⁺-Doped Bismuth-Based Gallate Host. *Chem. Mater.* **2016**, *28* (22), 8347–8356.
- (206) Sabnis, R. W. *Handbook of Acid-Base Indicators*; CRC Press, **2007**.
- (207) HydroMed Products
<http://www.advbmaterials.com/products/hydrophilic/hydromed.html>
(accessed May 27, **2020**).
- (208) Sjöback, R.; Nygren, J.; Kubista, M. Absorption and Fluorescence Properties of Fluorescein. *Spectrochimica Acta Part A: Molecular and Biomolecular Spectroscopy* **1995**, *51* (6), L7–L21.
- (209) Deen, G. R.; Gan, L. H. Influence of Amino Group PKa on the Properties of Stimuli-Responsive Piperazine-Based Polymers and Hydrogels. *Journal of Applied Polymer Science* **2008**, *107* (3), 1449–1458.
- (210) Dorozhkin, S. V.; Epple, M. Biological and Medical Significance of Calcium Phosphates. *Angewandte Chemie International Edition* **2002**, *41* (17), 3130–3146.
- (211) Gattuso, J.; Hansson, L. *Ocean Acidification*; Oxford University Press: Oxford ; New York, **2011**.

- (212) Pravina, P.; Sayaji, D.; Avinash, M. Calcium and Its Role in Human Body. **2013**, *4*, 10.
- (213) Orrenius, S.; Zhivotovsky, B.; Nicotera, P. Regulation of Cell Death: The Calcium–Apoptosis Link. *Nat Rev Mol Cell Biol* **2003**, *4* (7), 552–565.
- (214) Berridge, M. J.; Bootman, M. D.; Lipp, P. Calcium - a Life and Death Signal. *Nature* **1998**, *395* (6703), 645–648.
- (215) Rizzuto, R.; Pozzan, T. Microdomains of Intracellular Ca²⁺: Molecular Determinants and Functional Consequences. *Physiological Reviews* **2006**, *86* (1), 369–408.
- (216) Cashman, K. D. Calcium Intake, Calcium Bioavailability and Bone Health. *British Journal of Nutrition* **2002**, *87* (S2), S169–S177.
- (217) Veldurthy, V.; Wei, R.; Oz, L.; Dhawan, P.; Jeon, Y. H.; Christakos, S. Vitamin D, Calcium Homeostasis and Aging. *Bone Res* **2016**, *4* (1), 1–7.
- (218) Berridge, M. J.; Lipp, P.; Bootman, M. D. The Versatility and Universality of Calcium Signalling. *Nat Rev Mol Cell Biol* **2000**, *1* (1), 11–21.
- (219) Berridge, M. J.; Bootman, M. D.; Roderick, H. L. Calcium Signalling: Dynamics, Homeostasis and Remodelling. *Nat Rev Mol Cell Biol* **2003**, *4* (7), 517–529.
- (220) Suzuki, Koji.; Watanabe, Kazuhiko.; Matsumoto, Yukihiro.; Kobayashi, Mitsuru.; Sato, Sayaka.; Siswanta, Dwi.; Hisamoto, Hideaki. Design and Synthesis of Calcium and Magnesium Ionophores Based on Double-Armed Diazacrown Ether Compounds and Their Application to an Ion Sensing Component for an Ion-Selective Electrode. *Anal. Chem.* **1995**, *67* (2), 324–334.
- (221) Aoki, Y.; Umezawa, N.; Asano, Y.; Hatano, K.; Yano, Y.; Kato, N.; Higuchi, T. A Versatile Strategy for the Synthesis of Crown Ether-Bearing Heterocycles: Discovery of Calcium-Selective Fluoroionophore. *Bioorganic & Medicinal Chemistry* **2007**, *15* (22), 7108–7115.
- (222) Levy, L. A.; Murphy, E.; Raju, B.; London, R. E. Measurement of Cytosolic Free Magnesium Ion Concentration by Fluorine-19 NMR. *Biochemistry* **1988**, *27* (11), 4041–4048.
- (223) Otten, P. A.; London, R. E.; Levy, L. A. A New Approach to the Synthesis of APTRA Indicators. *Bioconjugate Chem.* **2001**, *12* (1), 76–83.
- (224) Metten, B.; Smet, M.; Boens, N.; Dehaen, W. Synthesis of APTRA Derivatives as Building Blocks for Low-Affinity Fluorescent Ca²⁺ Indicators. *Synthesis* **2005**, *2005* (11), 1838–1844.
- (225) Basarić, N.; Baruah, M.; Qin, W.; Metten, B.; Smet, M.; Dehaen, W.; Boens, N. Synthesis and Spectroscopic Characterisation of BODIPY® Based Fluorescent off–on Indicators with Low Affinity for Calcium. *Org. Biomol. Chem.* **2005**, *3* (15), 2755–2761.
- (226) Batat, P.; Vives, G.; Bofinger, R.; Chang, R.-W.; Kauffmann, B.; Oda, R.; Jonusauskas, G.; D. McClenaghan, N. Dynamics of Ion-Regulated Photoinduced Electron Transfer in BODIPY-BAPTA Conjugates. *Photochemical & Photobiological Sciences* **2012**, *11* (11), 1666–1674.
- (227) Liu, R.; Cai, X.; Li, Y.; Zhu, S.; Hu, J.; Zhu, H. Highly Efficient and Selective Red-Emitting Ca²⁺ Probe Based on a BODIPY Fluorophore. *Tetrahedron* **2017**, *73* (34), 5091–5095.
- (228) Ji, J.; Rosenzweig, Z. Fiber Optic PH/Ca²⁺ Fluorescence Microsensor Based on Spectral Processing of Sensing Signals. *Analytica Chimica Acta* **1999**, *397* (1), 93–102.

-
- (229) Boens, N.; Leen, V.; Dehaen, W. Fluorescent Indicators Based on BODIPY. *Chem. Soc. Rev.* **2012**, *41* (3), 1130–1172.
- (230) Peter Müller; Heidi Müller-Dolezal; Karl Nützel; Renate Stoltz; Hanna Söll. *Methods of Organic Chemistry*; 4th Edition (**2014**); Houben-Weyl, 2014.
- (231) Ouellette, R. J.; Rawn, J. D. 11 - Carboxylic Acids and Esters. In *Principles of Organic Chemistry*; Ouellette, R. J., Rawn, J. D., Eds.; Elsevier: Boston, **2015**; pp 287–314.
- (232) Würthner, F.; Kaiser, T. E.; Saha-Möller, C. R. J-Aggregates: From Serendipitous Discovery to Supramolecular Engineering of Functional Dye Materials. *Angewandte Chemie International Edition* **2011**, *50* (15), 3376–3410.
- (233) Bricks, J. L.; Slominskii, Y. L.; Panas, I. D.; Demchenko, A. P. Fluorescent J-Aggregates of Cyanine Dyes: Basic Research and Applications Review. *Methods Appl. Fluoresc.* **2017**, *6* (1), 012001.
- (234) Hestand, N. J.; Spano, F. C. Expanded Theory of H- and J-Molecular Aggregates: The Effects of Vibronic Coupling and Intermolecular Charge Transfer. *Chem. Rev.* **2018**, *118* (15), 7069–7163.
- (235) Staudinger, C.; Strobl, M.; Breininger, J.; Klimant, I.; Borisov, S. M. Fast and Stable Optical PH Sensor Materials for Oceanographic Applications. *Sensors and Actuators B: Chemical* **2019**, *282*, 204–217.

9. Curriculum Vitae

Lukas Tribuser

Date of Birth	14.03.1991
Adress	Münzgrabenstraße 170/8, 8010 Graz
Nationality	Austria
E-mail	lukastribuser@gmx.at

Education

2017-2020	PhD student in Technical Chemistry at Graz University of Technology Topic: "Synthesis of Fluoroionophores and its Applications for Optical Ion Sensors" at Institute for Analytical Chemistry and Food Chemistry Supervisor: Klimant, Ingo, Univ.-Prof. Dipl.-Chem. Dr.rer.nat. and Borisov Sergey M., Assoc.Prof.kand
2014-2017	Master program of Technical Chemistry; Graz University of Technology, Topic: "Synthesis of New Fluorescent Indicator Dyes and Receptors for Optical Ion Sensors" at Institute for Analytical Chemistry and Food Chemistry Supervisor: Borisov Sergey M., Assoc.Prof.kand. and Klimant, Ingo, Univ.-Prof. Dipl.-Chem. Dr.rer.nat.
2010-2014	Bachelor program of Chemistry; Graz University of Technology and Karl-Franzens University Graz (NAWI project) Bachelor thesis at Institute for Organic Chemistry Supervisor: Klempier, Norbert, Ao.Univ.-Prof.i.R. Dr.phil.
2005-2009	Sport-Realgymnasium key course element: competitive sport (Nordic combined), Saalfelden

List of Publications

Tribuser, L.; Borisov, S. M.; Klimant, I. Tuning the Sensitivity of Fluoroionophore-Based K⁺ Sensors via Variation of Polymer Matrix: A Comparative Study. *Sensors and Actuators B: Chemical* 2020, 312, 127940. <https://doi.org/10.1016/j.snb.2020.127940>.

Oral Presentations

Tribuser, L.; Borisov, S.M.; Klimant, I.: Ca²⁺ sensitive fluorescent indicator dyes for optical sensing – 13th ASCS JunganalytikerInnen-Forum, Vienna, 2017

Poster Presentations

Tribuser, L.; Müller, B.J.; Borisov, S.M.; Klimant, I.: Influence of polymers on sensing properties of fluoroionophore-based optodes: a comparative study – Europt(r)ode XIV, Naples, 2018

Tribuser, L.; Müller, B.J.; Borisov, S.M.; Klimant, I.: Ca²⁺ sensitive fluorescent indicator dyes for optical sensing – 13th ASCS JunganalytikerInnen-Forum, Vienna, 2017

Tribuser, L.; Müller, B.J.; Borisov, S.M.; Klimant, I.: Fluorescent Ca²⁺ indicator dyes for optical sensing – 12th International Symposium on Macrocyclic and Supramolecular Chemistry (ISMSC ISACS), Cambridge, 2017

Tribuser, L.; Müller, B.J.; Borisov, S.M.; Klimant, I.: Fluorescent Ca²⁺ indicator dyes for optical sensing – Europt(r)ode XIII, Graz, 2016

10. List of Figures

Figure 2-1: Most important ions for the human body with their main functions.....	6
Figure 2-2: Location of kidneys in the human body with the connection to urinary bladder, for excess ion excretion. Additionally, the function of the Bowman's capsule is illustrated. Within these compartments, ion exchange from blood to urine takes place.....	8
Figure 2-3: Examples of host molecules. a) crown ether b) calixarene c) cyclodextrin.....	12
Figure 2-4: Penta ethylene glycol dimethyl ether (a) and its diol (b). Ca^{2+} ionophore used as a carrier in membranes (c).....	14
Figure 2-5: Examples of a) crown-ether b) aza-crown-ether c) cryptant d) (methoxyethoxyphenyl)aza-crown-ether.....	15
Figure 2-6: Structure of EGTA a) and the developed derivatives, b) and c) by Tsien and coworkers. ⁶³	16
Figure 2-7: a) N-phenyliminodiethoxyacetic acid receptor for selective calcium complexation. b) fluoroionophore derivative of a, synthesized by He et al. ⁶⁴	16
Figure 2-8: Crown-ethers for ion complexation.....	17
Figure 2-9: Jablonski diagram, describing the main phenomena, absorption, fluorescence, delayed fluorescence and phosphorescence. S_0 represents the ground state, S_1 the excited singlet state. T_1 exemplifies the excited triplet state. Intersystem crossing (ISC) describes the transition between excited singlet state S_1 and the triplet state T_1	20
Figure 2-10: Working principle of ion selective electrodes (ISE). An Ag/AgCl reference electrode supplies a constant potential, whereas in this case a liquid membrane changes the potential depending on the activity of a specific target ion. Selectivity of the electrode can be controlled via the choice of ionophores used in the PVC membrane.....	23
Figure 2-11: Principle of IBOS for ion sensing. The PVC sensing membrane is capable for extraction of ions with the use of anionic surfactants. The selective ionophores bind the target ions and promote a proton release to maintain charge neutrality. Since a pH indicator is used for sensing, and internal pH value is changed, e.g. fluorescence can be measured to determine the cation concentration in the sample.....	24
Figure 2-12: Simplified illustration of a polarity sensitive dye (PSD) and the effect of the microenvironment. a) Before complexation of the analyte the indicator is low in its fluorescence intensity. b) After interaction of the analyte the polarity of the complex changes and it can move into another location of the sensing layer. Due to the change in polarity of the surrounding environment the complex is fluorescent.....	25
Figure 2-13: Visualization of PET and ICT upon complexation. a) In PET the absorption spectrum remains unchanged, whereas the emission intensity changes upon analyte interactions. b) In ICT the spectra upon complexation is changed.....	26
Figure 2-14: Illustration of PET. a) Classic photoinduced electron transfer (PET) b) PET-quenching upon complexation of the analyte of interest. Binding events cause a change in the molecular orbitals of the receptor. The indicator in this case is fluorescent.....	28
Figure 2-15: Examples of fluoroionophores a) ¹²¹ , b) ⁷⁰ , c) ¹²² based on the ICT quenching mechanism for cation sensing.....	31
Figure 2-16: Examples of PET fluoroionophores a) ¹²³ , b) ¹²⁴ , c) ¹²⁵ . With increasing ion concentration, the emission intensity is increased, whereas the absorption spectrum remains unchanged.....	32
Figure 2-17: Knife coating illustration for a planar sensing foil. After the hydrogel and the indicator are dissolved in an organic solvent, the remaining sensor cocktail can be knife coated on a sensor support. Immediately after evaporation of the solvent the sensor can be used for measurements in aqueous solutions.....	33
Figure 2-18: Structure of borondipyrrromethene (BODIPY) dyes.....	34
Figure 2-19: Synthesis of meso-substituted BODIPY-dyes via two different synthetic routes.....	35
Figure 2-20: Condensation of pyrrole-carbaldehydes in a one-pot reaction yields to BODIPY dyes.....	35

Figure 2-21: Possible synthetic routes for the introduction of analyte sensitive groups incorporated in BODIPY dyes. Route A results in a PET indicator, while route B yields in a ICT based dye.....	36
Figure 3-1: Chemical structure of the fluoroionophore and schematic illustration of the response mechanism. Via complexation of the analyte the HOMO of the receptor is energetically reduced which enhances the fluorescence emission.....	45
Figure 3-2: a) Emission Spectra of the K ⁺ FI in hydrogel (D4) at different K ⁺ concentrations. Upon protonation with 0.1 M HCl K ⁺ FI is fully "switched on". b) Dynamic response of the indicator in polyurethane hydrogel D4 and PVC/DOS matrix.....	48
Figure 3-3: Dynamic response of hydrogel-immobilized K ⁺ FI to K ⁺ in the absence of Na ⁺ background and with 150 mM Na ⁺ background.....	49
Figure 3-4: a) Chemical structures of the additives and schematic representation of the effect of negatively charged groups. b) Effect of sodium on the sensing properties at different K ⁺ concentrations. c) Dependency of the fluorescence intensity of K ⁺ FI immobilized in D4 and modified D4 on C(K ⁺).....	52
Figure 3-5: a) Dynamic response of K ⁺ FI immobilized in D4, pHEMA and their blends to K ⁺ in the absence of Na ⁺ background and with 150 mM Na ⁺ background. b) Double logarithmic plots of [(I-I _{min})/(I _{max} -I)] vs C(K ⁺) for the sensor materials for determination of K _d	56
Figure 4-1: DLR signal development at low a) and high b) indicator fluorescence emission (blue).....	75
Figure 4-2: a) potassium fluoroionophore b) sodium fluoroionophore c) General sensor composition for the DLR measurements.....	76
Figure 4-3: Potassium sensor calibrated at 23°C and 37°C. An increase in temperature results in a reduced resolution.....	77
Figure 4-4: Calibration of a potassium sensor foil with different amounts of reference, Egyptian blue.....	79
Figure 4-5: Top: Used reagents for the hydrophilization. Bottom: Illustration of the hydrophilization of Egyptian blue.....	80
Figure 4-6: Comparison of an unmodified and a hydrophilized reference, Egyptian blue.....	81
Figure 4-7: Structures of fluoroionophores used for calibrations in different matrices, hydrogel D4 and D1.....	82
Figure 4-8: a) Aggregation of the hydrophilic fluoroionophore in pHEMA in buffer solution over 6 days. The measurements show that pHEMA represents an unstable matrix for this indicator. b) Calibration of the hydrophilic FI in hydrogel D1 with 250 mM sodium background. The 0.1 M HCl represents the fluoroionophores full potential within this matrix. c) Kinetic measurements in D1. The synthesized indicator showed full reversibility. d) Phase angle measurements of the FI in hydrogel D1 at 25°C.....	83
Figure 4-9: Excitation and emission spectrum of Egyptian Blue and the used fluoroionophore.....	84
Figure 4-10: Excitation and emission spectrum of CrGAB and the used fluoroionophore.....	85
Figure 4-11: Two DLR sensor foils with the containing 0.2 w% FI, 40w% CrGAB in hydrogel D4 and a blend of D4/pHPMA 50/50 were calibrated at 37°C. The blended foil reveals a higher phase angle difference, due to higher water uptake of the sensing foil.....	86
Figure 4-12: Calibration using different amounts of fluoroionophore at 1917 and 4000 Hz. a) Phase angle vs. Time. b) Amplitude vs. Time.....	87
Figure 4-13: a) Variation of amount reference used within the sensing foils at a modulation frequency of 1917 Hz. b) Effect of TiO ₂ to the Phase angle difference between 3 and 6 mM K ⁺	88
Figure 4-14: a) Sensing foil containing 0.2 w% FI, 40 w% CrGAB and 100 w% TiO ₂ at different modulation frequencies. b) Phase angle difference between 3 and 6 mM K ⁺ . The modulation frequency behaves linear with the sensing dynamic.....	89
Figure 4-15: Calibration of a potassium sensitive foil containing 5% ascorbic acids, sterilized (red) and unsterilized (black). Concentration vs. a) phase angle and b) amplitude.....	91
Figure 4-16: Calibration of a potassium sensitive foil containing 10% ascorbic acids, sterilized (red) and unsterilized (black). Concentration vs. a) phase angle and b) amplitude.....	92
Figure 4-17: DLR measurements of a sensing foil without ascorbic acid. a) sterilized. b) unsterilized.....	93
Figure 4-18: DLR measurements of a sensing foil with 10% ascorbic acid. a) sterilized. b) unsterilized.....	93
Figure 4-19: a) Phase angle measurements for evaluation of the temperature dependency of a potassium sensor from 30 to 38°C. b) Plot potassium concentration vs. phase angle. The sensor shows a linear	

behavior for all temperatures. c) Phase angle differences in the physiological relevant region against the temperature.....	94
Figure 4-20: Example of a temperature calibration (0.4 w% hydrophilic FI, 40 w% CrGAB, 100 w% TiO ₂ in hydrogel D1) and an extract of the data evaluation for the determination of the temperature coefficients.....	96
Figure 4-21: a) lock-in amplifier (SR830 DSP, Stanford Research) connected with an optical fiber and PMT. b) Visualization of the inlets for optical filters and an example of an optical filter.....	97
Figure 4-22: a) Simplification of the sensing setup used at the fluorolog for determination of background to noise ratios for different excitation wavelength's. b) Measured spectrums from the LED excitation sources used for the measurements.....	98
Figure 4-23: Photobleaching experiment performed at the lock-in amplifier for determination of the photostability of the fluoroionophore at an excitation with blue light.....	100
Figure 4-24: a) calibrations of a foil containing 0.2 w% FI in D4 after 2, 25, 66 and 188 days. b) calibrations of a foil containing 0.2 w% FI and 100 w% TiO ₂ in D4 after 2, 25, 66 and 188 days. c) calibrations of a foil containing 0.2 w% FI and 40 w% CrGAB in D4 after 2, 25, 66 and 188 days. d) calibrations of a foil containing 0.2 w% FI, 40 w% CrGAB and 100 w% TiO ₂ in D4 after 2, 25, 66 and 188 days.....	101
Figure 4-25: Calibration of a foil containing 0.2 w% FI, 40 w% CrGAB and 100 w% TiO ₂ in D4.....	103
Figure 4-26: Synthesis route for the sodium fluoroionophore, Na-FI ₂ gen. The indicator has an elongated sidearm for better sodium complexation.....	105
Figure 4-27: Comparison of the new indicator with the previously used fluoroionophore in D4 and D1.....	106
Figure 4-28: Cross sensitivity of the indicator towards competing ions in hydrogel D4 and D1.....	106
Figure 4-29: a) Loss of sensitivity in pHEMA within 24h. b) aggregation of the indicator in pHEMA within 2 hours.....	107
Figure 5-1: Schematic illustration of the sensor composition (A), spectral properties of the emitters (B) and sensor response to ammonia in the steady state (B) and kinetic (C) modes.....	116
Figure 5-2: Calibrations for fluoroionophore and fluorescein from 0 to 20 mg/L free amine concentration (a,c) and converted plot in total amine concentration (b,d). With the use of the reference the y-axis ((F-F ₀)/F _{ref}) represents comparable and reproducible values.....	118
Figure 5-3: F/F ₀ values for a calibration with 150 mM NH ₃ + different amounts of substituted amines. Both fluorescence emissions were normalized to their 0 mM TAC value. Fluoroionophore does not reveal a significant cross-talk to amines, whereas fluorescein responds to both ammonia and amines.	119
Figure 5-4: Measurements over time at fixed wavelengths and alternating amine concentrations. Plot a) shows the calibrations for the fluoroionophore, plot b) for fluorescein. The fluoroionophore does not reveal cross sensitivity towards substituted amines. The fluorescence intensity of fluorescein shows strong dependency on the concentration of substituted amines. The material was additionally were screened for potential pH dependency between pH 5-8 and interference by 100 mM K ⁺ , showing a robust and reversible sensing system.....	120
Figure 6-1: Structure of Ethylene glycol-bis(2-aminoethylether)-N,N,N,N-tetraacetic acid, EGTA (a) and the developed 1,2-bis(<i>o</i> -aminophenoxy)ethane- <i>N,N,N,N</i> -tetraacetic acid, BAPTA derivatives (b + c) by Tsien and coworkers. ⁶³	129
Figure 6-2: a) N-phenyliminodiethoxyacetic acid (PIDA) receptor for selective calcium complexation. b) fluoroionophore derivative of a, synthesized by He ⁶⁴	130
Figure 6-3: a) Structure of <i>o</i> -aminophenol- <i>N,N,O</i> -triacetic acid (APTRA) ²²² b) BODIPY fluoroionophore using APTRA as a recognition unit for calcium ions ²²⁵ c) APTRA receptor connected to a phenantrenequinone dye. ²²⁴	130
Figure 6-4: Overview of the synthesized fluoroionophores in their protected ethyl ester form (FI-ester), before saponification.....	146
Figure 6-5: a) TLC of the saponification of FI ₅ -ester to FI ₅ . Uncompleted deprotection is seen after 1 h. After 23 h only one spot can be seen via TLC. b) Salt-forms of the FIs, dissolved in water. c) Although the FIs are soluble in D ₂ O, no peaks were found in ¹ H-NMR measurements.....	147
Figure 6-6: pH dependency of the fluorescence intensity in EtOH + universal buffer 1+1 for FI ₁₋₅ . The solutions were measured instantly after preparation and after one day storage. FI 3 and 4 do not show a clear pH-dependency between pH 1 to 9.5. FI ₅ shows an increased fluorescence intensity after one day, more pronounced at higher pH values.....	151

- Figure 6-7: Fluorescence intensity for FI2 upon illumination with UV light for different ethanolic compositions, with and without calcium. With increasing amount of ethanol, the PET is more pronounced. (aqueous buffer: 20 mM HEPES; pH 7.4). At high water content the dye is virtually non-fluorescent even in presence of Ca^{2+} that may be due to aggregation.....152
- Figure 6-8: Fluorescence intensity for FI 1-5 in different ethanolic compositions, with and without 20 mM calcium. With increased amount of ethanol, the PET is in general more pronounced. Aqueous buffer contained 20 mM HEPES; pH 7.4. Ca^{2+} concentration was adjusted to be 20 mM for each calibration solution154
- Figure 6-9: Fluorescence pretests for the fluoroionophores via illumination with a UV-lamp. Solutions contained 20% ethanol and different buffers (TRIS, HEPES, MOPS) to investigate any influences of the derived from the sort of buffer used. After 2 days, solutions were screened again. In most cases the FI precipitates in the solution, indicating an unstable solution composition.155
- Figure 6-10: Fluorescence spectra of FI5 and FI2 in EtOH + ultra-pure water 1+1, with and without 20 mM calcium. The solutions were measured directly after preparation and after 3 days storage. FI5 shows an increased fluorescence after 3 days storage. FI2 shows a decreased fluorescence after 3 days for 20 mM Ca^{2+} , without any signs of aggregation visible in the fluorescence spectrum..... 156
- Figure 6-11: a) Absorption and emission spectrum of FI1 in EtOH + ultra-pure water 9+1. The indicator shows aggregation phenomena indicated in both spectra. b) Absorption and emission spectrum of FI3 in EtOH + ultra-pure water 9+1. The indicator shows formation of J-aggregates with a distinct emission band at 808 nm. c) Fluorescence emission of FI3 in a mixture of THF+EDTA (0.01 mM) + buffer (20 mM HEPES; pH 7.4) 9+1+1; without and with 0.906 mM calcium. d) calibration of FI3 from 0 to 60 μM calcium. Fluorescence intensities start to increase at 10 μM calcium.....157
- Figure 6-12: Calibration of a sensor foil containing 0.2 w% FI3 in hydrogel D7. The sensor shows a fluorescence increase with increased calcium concentration. (left) The sensor does not show any difference by variation of the calcium concentration. (right)..... 159
- Figure 6-13: a) Covalent coupling of a K^+ sensitive BODIPY fluoroionophore on CAP. b) Calibration of an 24 h hydrolyzed (pH 13) CAP-indicator foil and a unhydrolyzed sensor foil, for comparison. c) Effect of hydrolyzation times. (pH 13)161
- Figure S 3-1: contact angle pictures from an unmodified glass slide (a) and modified glass slide (b).59
- Figure S 3-2: FTIR spectrum of the modified and unmodified hydrogel.....59
- Figure S 3-3: a) Dependency of the fluorescence intensity of K^+FI immobilized in hydrogel blends on $C(\text{K}^+)$. b) Dependency of the dissociation constant [K_d] on blend composition..... 61
- Figure S 3-4: a) Schematic representation of the effect of charged additives. b) Dynamic response of K^+FI immobilized in D4 along with different long chain aliphatic sulfates and sulfonates to K^+ in the absence of Na^+ background and with 150 mM Na^+ background. c) Dependency of the fluorescence intensity of K^+FI immobilized in D4 with additives on $C(\text{K}^+)$. d) Effect of sodium on the sensing properties at different concentrations. e) Double logarithmic plots of $[(I-I_{\text{min}})/(I_{\text{max}}-I)]$ vs $C(\text{K}^+)$ for the sensor materials for determination of K_d . Additive $\text{C}_{18}\text{H}_{29}\text{SO}_3^-$ shows the highest binding affinity.....62
- Figure S 3-5: a) Dynamic response of K^+FI immobilized in D4, D4- SO_3^- and a 1:1 w/w blend to K^+ . b) Dependency of the fluorescence intensity of K^+FI immobilized in D4 and D4- SO_3^- on $C(\text{K}^+)$. c) Influence of Na^+ on the sensing properties at different concentrations. d) Intensities of K^+FI in polyurethane hydrogels with and without negatively charged functionalities.63
- Figure S 3-6: Na^+ concentration [mM] vs. intensity at 0 mM K^+ for hydrogel D4, modified hydrogel D4- SO_3^- and the 1:1 blend. All polymers show an intensity increase with increasing Na^+ concentration.....64
- Figure S 3-7: Response of D4, pHPMA and mixtures to K^+ . pHPMA shows low intensities but good binding affinity towards K^+ . Blending of the highly hydrophilic polymer with a copolymer (D4) result in stable material.....64
- Figure S 3-8: normalized emission intensity of D4, pHPMA and pHEMA upon complexation with 500 mM K^+ . pHPMA shows aggregation phenomena visualized by the broader spectrum showing bathochromic shift.....65
- Figure S 3-9: normalized emission intensity of D4, pHPMA and 70% pHEMA in D4 upon complexation with 500 mM K^+ . Aggregation phenomena disappear in polymer blends with hydrogel D4.....65

Figure S 3-10: pHPMA sensor layer in 0 mM buffer solution over 5 minutes. The sensor layer increases its turbidity within minutes. The aggregation phenomena seen by emission spectra cannot be visualized by UV/VIS spectrometry due to increasing turbidity.	66
Figure S 3-11: pHEMA sensor layer in 0 mM buffer solution over 5 minutes. The sensor layer increases its turbidity within minutes.	66
Figure S 5-1: Sensor foil containing 0.66w% fluoroionophore; 0.0033w% fluorescein in hydrogel D1. Buffer contained 500mM BISTRIS with a pH of 6.5.	122
Figure S 5-2: Emission spectra of the NH ₄ ⁺ selective BODIPY fluoroionophore and the phosphor Bi ₂ Ga ₄ O ₉ . Excitation wavelength was chosen to be 430 nm.	122
Figure S 5-3: Sensor response to ammonia for fluorescein and the fluoroionophore, measured in kinetic mode.	123
Figure S 6-1: Absorption, Excitation and Emission spectra of FI1-ester, FI2-ester and FI3-ester.	162
Figure S 6-2: Absorption, Excitation and Emission spectra of FI4-ester and FI5-ester.	163
Figure S 6-3: Calibration of a potassium indicator (in hydrogel D1) for comparison of the spectral properties in section 6.5.2.	163
Figure S 6-4: ¹ H NMR (300Hz), in CDCl ₃ of 1.	164
Figure S 6-5: ¹³ C-APT NMR (76Hz, CDCl ₃) of 1.	164
Figure S 6-6: ¹ H NMR (300Hz), in CDCl ₃ of 2.	165
Figure S 6-7: ¹³ C-APT NMR (76Hz, CDCl ₃) of 2.	165
Figure S 6-8: ¹ H NMR (300Hz), in CDCl ₃ of 3.	166
Figure S 6-9: ¹³ C-APT NMR (76Hz, DMSO-d ₆) of 3.	166
Figure S 6-10: LR-Mass Spectrum of 3 recorded on Advion expression CMS.	167
Figure S 6-11: ¹ H NMR (300Hz), in CDCl ₃ of 4.	167
Figure S 6-12: ¹³ C-APT NMR (76Hz, CD ₂ Cl ₂) of 1.	168
Figure S 6-13: LR-Mass Spectrum of 4 recorded on Advion expression CMS.	168
Figure S 6-14: ¹ H NMR (300Hz), in CDCl ₃ of 5.	169
Figure S 6-15: ¹³ C-APT NMR (76Hz, CDCl ₃) of 5.	169
Figure S 6-16: LR-Mass Spectrum of 5 recorded on Advion expression CMS.	170
Figure S 6-17: ¹ H NMR (300Hz), in CDCl ₃ of 6.	170
Figure S 6-18: ¹³ C-APT NMR (76Hz, CDCl ₃) of 6.	171
Figure S 6-19: LR-Mass Spectrum of 6 recorded on Advion expression CMS.	171
Figure S 6-20: ¹ H NMR (300Hz), in CDCl ₃ of 7.	172
Figure S 6-21: ¹³ C-APT NMR (76Hz, CDCl ₃) of 7.	172
Figure S 6-22: LR-Mass Spectrum of 7 recorded on Advion expression CMS.	173
Figure S 6-23: ¹ H NMR (300Hz), in CDCl ₃ of 8.	173
Figure S 6-24: ¹³ C-APT NMR (76Hz, CDCl ₃) of 8.	174
Figure S 6-25: LR-Mass Spectrum of 8 recorded on Advion expression CMS.	174
Figure S 6-26: ¹ H NMR (300Hz), in DMSO-d ₆ of 9.	175
Figure S 6-27: ¹³ C-APT NMR (76Hz, DMSO-d ₆) of 9.	175
Figure S 6-28: LR-Mass Spectrum of 9 recorded on Advion expression CMS.	176
Figure S 6-29: ¹ H NMR (300Hz), in DMSO-d ₆ of 10.	176
Figure S 6-30: ¹³ C-APT NMR (76Hz, DMSO-d ₆) of 10.	177
Figure S 6-31: LR-Mass Spectrum of 10 recorded on Advion expression CMS.	177
Figure S 6-32: ¹ H NMR (300Hz), in CDCl ₃ of 11.	178
Figure S 6-33: ¹³ C-APT NMR (76Hz, CD ₂ Cl ₂) of 11.	178

Figure S 6-34: LR-Mass Spectrum of 11 recorded on Advion expression CMS.....	179
Figure S 6-35: ^1H NMR (300Hz), in CD_2Cl_2 of 12.....	179
Figure S 6-36: ^{13}C -APT NMR (76Hz, CD_2Cl_2) of 12.....	180
Figure S 6-37: LR-Mass Spectrum of 12 recorded on Advion expression CMS.....	180
Figure S 6-38: LR-Mass Spectrum of 13 recorded on Advion expression CMS.....	181
Figure S 6-39: LR-Mass Spectrum of 14 recorded on Advion expression CMS.....	181
Figure S 6-40: ^1H NMR (300Hz), in CD_2Cl_2 of FI1-ester.....	182
Figure S 6-41: ^{13}C -APT NMR (76Hz, CD_2Cl_2) of FI1-ester.....	182
Figure S 6-42: LR-Mass Spectrum of FI1-ester recorded on Advion expression CMS.....	183
Figure S 6-43: Theoretical isotope pattern (top) of $\text{C}_{57}\text{H}_{60}\text{BFN}_3\text{O}_6$ (FI1-ester - F); Theoretical isotope pattern (middle) of $\text{C}_{57}\text{H}_{60}\text{BF}_2\text{N}_3\text{O}_6\text{Na}$ (FI1-ester + Na); Experimental MALDI-TOF-MS of FI1-ester (bottom).	184
Figure S 6-44: Mass relevant theoretical isotope pattern (top) of $\text{C}_{57}\text{H}_{60}\text{BFN}_3\text{O}_6$ (FI1-ester - F) and theoretical isotope pattern (middle) of $\text{C}_{57}\text{H}_{60}\text{BF}_2\text{N}_3\text{O}_6\text{Na}$ (FI1-ester + Na); Experimental mass relevant range (MALDI-TOF-MS) of FI1-ester (bottom).	185
Figure S 6-45: ^1H NMR (300Hz), in CD_2Cl_2 of FI2-ester.....	186
Figure S 6-46: ^{13}C -APT NMR (76Hz, CD_2Cl_2) of FI2-ester.....	186
Figure S 6-47: LR-Mass Spectrum of FI2-ester recorded on Advion expression CMS.....	187
Figure S 6-48: Theoretical isotope pattern (upper part) of $\text{C}_{53}\text{H}_{46}\text{BCl}_2\text{FN}_3\text{O}_6$ (FI2-ester - F), $\text{C}_{53}\text{H}_{46}\text{BCl}_2\text{F}_2\text{N}_3\text{O}_6\text{H}$ (FI2-ester + H), $\text{C}_{53}\text{H}_{46}\text{BCl}_2\text{F}_2\text{N}_3\text{O}_6$ (FI2-ester). Experimental MALDI-TOF-MS of FI2-ester (bottom).	188
Figure S 6-49: Mass relevant theoretical isotope pattern (upper part) of $\text{C}_{53}\text{H}_{46}\text{BCl}_2\text{FN}_3\text{O}_6$ (FI2-ester - F), $\text{C}_{53}\text{H}_{46}\text{BCl}_2\text{F}_2\text{N}_3\text{O}_6\text{H}$ (FI2-ester + H), $\text{C}_{53}\text{H}_{46}\text{BCl}_2\text{F}_2\text{N}_3\text{O}_6$ (FI2-ester). Experimental mass relevant range (MALDI-TOF-MS) of FI2-ester (bottom).	189
Figure S 6-50: ^1H NMR (300Hz), in CD_2Cl_2 of FI3-ester.....	190
Figure S 6-51: ^{13}C -APT NMR (76Hz, CD_2Cl_2) of FI3-ester.....	190
Figure S 6-52: LR-Mass Spectrum of FI3-ester recorded on Advion expression CMS.....	191
Figure S 6-53: Theoretical isotope pattern (upper part) of $\text{C}_{53}\text{H}_{44}\text{BCl}_2\text{FN}_3\text{O}_7$ (FI3-ester - F), $\text{C}_{53}\text{H}_{44}\text{BCl}_2\text{F}_2\text{N}_3\text{O}_7$ (FI3-ester), $\text{C}_{53}\text{H}_{44}\text{BCl}_2\text{F}_2\text{N}_3\text{O}_7\text{Na}$ (FI3-ester + Na). Experimental MALDI-TOF-MS of FI3-ester (bottom).	192
Figure S 6-54: Mass relevant theoretical isotope pattern (upper part) of $\text{C}_{53}\text{H}_{44}\text{BCl}_2\text{FN}_3\text{O}_7$ (FI3-ester - F), $\text{C}_{53}\text{H}_{44}\text{BCl}_2\text{F}_2\text{N}_3\text{O}_7$ (FI3-ester), $\text{C}_{53}\text{H}_{44}\text{BCl}_2\text{F}_2\text{N}_3\text{O}_7\text{Na}$ (FI3-ester + Na). Experimental mass relevant range (MALDI-TOF-MS) of FI3-ester (bottom).	193
Figure S 6-55: ^1H NMR (300Hz), in CD_2Cl_2 of FI4-ester.....	194
Figure S 6-56: ^{13}C -APT NMR (76Hz, CD_2Cl_2) of FI4-ester.....	194
Figure S 6-57: Theoretical isotope pattern (upper part) of $\text{C}_{65}\text{H}_{68}\text{BCl}_4\text{FN}_3\text{O}_{13}$ (FI4-ester - F), $\text{C}_{65}\text{H}_{68}\text{BCl}_4\text{F}_2\text{N}_3\text{O}_{13}\text{Na}$ (FI4-ester + Na). Experimental MALDI-TOF-MS of FI4-ester (bottom).	195
Figure S 6-58: Mass relevant theoretical isotope pattern (upper part) of $\text{C}_{65}\text{H}_{68}\text{BCl}_4\text{FN}_3\text{O}_{13}$ (FI4-ester - F), $\text{C}_{65}\text{H}_{68}\text{BCl}_4\text{F}_2\text{N}_3\text{O}_{13}\text{Na}$ (FI4-ester + Na). Experimental mass relevant range (MALDI-TOF-MS) of FI4-ester (bottom).	196
Figure S 6-59: ^1H NMR (300Hz), in CD_2Cl_2 of FI5-ester.....	197
Figure S 6-60: ^{13}C -APT NMR (76Hz, CD_2Cl_2) of FI5-ester.....	197
Figure S 6-61: : Theoretical isotope pattern (upper part) of $\text{C}_{77}\text{H}_{81}\text{BCl}_4\text{F}_2\text{N}_4\text{O}_{16}$ (FI5-ester), $\text{C}_{77}\text{H}_{81}\text{BCl}_4\text{F}_2\text{N}_4\text{O}_{16}\text{Na}$ (FI5-ester + Na). Experimental MALDI-TOF-MS of FI5-ester (bottom).	198
Figure S 6-62: Mass relevant theoretical isotope pattern (upper part) of $\text{C}_{77}\text{H}_{81}\text{BCl}_4\text{F}_2\text{N}_4\text{O}_{16}$ (FI5-ester), $\text{C}_{77}\text{H}_{81}\text{BCl}_4\text{F}_2\text{N}_4\text{O}_{16}\text{Na}$ (FI5-ester + Na). Experimental mass relevant range (MALDI-TOF-MS) of FI5-ester (bottom).	199

11. List of Tables

Table 2-1: Normal concentrations of ions in the human body in plasma, urine and cerebrospinal fluid (CSF). ¹⁵	7
Table 2-2: Size of ions and size of different substituted crown-ethers. ^{57,74}	18
Table 3-1: Sensing properties of the K ⁺ FI immobilized into different polyurethane hydrogels.....	50
Table 3-2: Effect of additives on the sensing properties of D4-immobilized K ⁺ FI.....	52
Table 3-3: Sensing properties for the K ⁺ FI immobilized into poly(2-hydroxyalkyl methacrylate) and their blends with hydrogel D4.....	57
Table 4-1: Phase angle differences for a potassium sensor calibrated at 23°C and 37°C.....	78
Table 4-2: Phase angle differences between 0 and 10 mM potassium at different amounts of reference used.....	79
Table 4-3: Phase angle differences of a hydrophilic and hydrophobic reference.....	81
Table 4-4: Summary of the calibrations with varying amounts of fluoroionophore and different modulation frequencies.....	87
Table 4-5: Calculated temperature coefficients for a potassium and sodium sensor.....	95
Table 4-6: Signals from a TiO ₂ foil and a sensor foil for evaluation of the noise to signal ratio.....	98
Table 4-7: Results of the performed background to noise measurements. Excitation of the indicator with a 422 nm Led results in best ratios, for this setup.....	99
Table 4-8: F/F ₀ -values from the calibration containing 0.2 w% FI in D4 after 2, 25, 66 and 188 days.....	101
Table 4-9: F/F ₀ -values from the calibration containing 0.2 w% FI in D4 and 100w% TiO ₂ after 2, 25, 66 and 188 days.....	102
Table 4-10: F/F ₀ -values from the calibration containing 0.2 w% FI in D4 and 40 w% CrGAB after 2, 25, 66 and 188 days.....	102
Table 4-11: F/F ₀ -values from the calibration containing 0.2 w% FI in D4, 40 w% CrGAB and 100 w% TiO ₂ after 2, 25, 66 and 188 days.....	102
Table 4-12: Measured phase angles of different sensor compositions for different potassium concentrations after 2 days storage.....	103
Table 4-13: Measured phase angles of different sensor compositions for different potassium concentrations after 188 days storage.....	103
Table 5-1: Calculated F/F ₀ values for both indicators for the calibrations using emission spectrums and kinetic measurements. From the deviations at the corresponding amine concentration the overall accuracy was calculated.....	120
Table 6-1: Spectral properties of the fluoroionophore precursors, FI-esters.....	149
Table S 3.7-1: measured absolute QY in different solvents.....	60
Table S 3.7-2: Sensing properties for the K ⁺ FI immobilized into blends of hydrogel D1 and D7.....	61
Table S 3.7-3: Effect of additives on the sensing properties of D4-immobilized K ⁺ FI.....	62
Table S 3.7-4: Sensing properties of the polyurethane hydrogel modified with SO ₃ ⁻ groups, in comparison with the unmodified version.....	63

